

UNIVERSIDADE FEDERAL DE SÃO CARLOS  
CENTRO DE CIÊNCIAS BIOLÓGICAS E DA SAÚDE  
PROGRAMA DE PÓS-GRADUAÇÃO EM ECOLOGIA E RECURSOS NATURAIS

BRUNO BECKER KERBER

**PALEOBIOLOGY OF THE ITAJAÍ BASIN (EDIACARAN, SANTA CATARINA, BRAZIL): EVOLUTIONARY, PALEOECOLOGICAL AND TAPHONOMICAL IMPLICATIONS**

PALEOBIOLOGIA DA BACIA DE ITAJAÍ (EDIACARANO, SANTA CATARINA, BRASIL): IMPLICAÇÕES EVOLUTIVAS, PALEOECOLÓGICAS E TAFONÔMICAS

SÃO CARLOS – SP  
2020

BRUNO BECKER KERBER

PALEOBIOLOGY OF THE ITAJAÍ BASIN (EDIACARAN, SANTA CATARINA,  
BRAZIL): EVOLUTIONARY, PALEOECOLOGICAL AND TAPHONOMICAL  
IMPLICATIONS

Tese apresentada ao Programa de Pós-Graduação em Ecologia e Recursos Naturais, da Universidade Federal de São Carlos, para obtenção do título de doutor em Ciências, área de concentração em Ecologia e Recursos Naturais.

Orientador: profa. Dra. Mírian Liza Alves Forancelli Pacheco

Coorientador: prof. Dr. Paulo Sergio Gomes  
Paim

São Carlos-SP

2020



# UNIVERSIDADE FEDERAL DE SÃO CARLOS

Centro de Ciências Biológicas e da Saúde  
Programa de Pós-Graduação em Ecologia e Recursos Naturais

---

## Folha de Aprovação

---

Defesa de Tese de Doutorado do candidato Bruno Becker Kerber, realizada em 04/06/2020.

### Comissão Julgadora:

Profa. Dra. Mírian Liza Alves Forancelli Pacheco (UFSCar)

Prof. Dr. Marcelo Adorna Fernandes (UFSCar)

Profa. Dra. Odete Rocha (UFSCar)

Prof. Dr. Abderrazak El Albani (UP)

Profa. Dra. Alessandro Marques de Oliveira (UEMG)

Homologado(a) pela CGC  
565<sup>o</sup> reunião 17/06/2020  
C.P. - EPN/UFSCar

O presente trabalho foi realizado com apoio da Coordenação de Aperfeiçoamento de Pessoal de Nível Superior - Brasil (CAPES) - Código de Financiamento 001.

O Relatório de Defesa assinado pelos membros da Comissão Julgadora encontra-se arquivado junto ao Programa de Pós-Graduação em Ecologia e Recursos Naturais.

*In dedication to my parents, Elaine Becker Kerber and Gilmar Kerber*

## ACKNOWLEDGEMENTS

This work had the fundamental support of the “Fundação de Amparo à Pesquisa do Estado de São Paulo” (FAPESP) within the projects: 2016/01827-4 e 2018/21886-0. It also had the support of Conselho Nacional de Desenvolvimento Científico e Tecnológico (CNPq) during the initial months of the doctorate.

As it is for almost every scientific endeavor, the results presented here are a consequence of an intense and productive scientific collaboration that I had the opportunity to realize with several great scientists.

I am profoundly grateful to my mentor and scientific inspiration, Mírian Liza Alves Forancelli Pacheco. A lot of this work, and of what I have learned throughout these years, would not have happened without her teachings, her support and her dedication as a scientist and as an advisor.

I am also thankful to my co-advisor Paulo Sergio Gomes Paim (UNISINOS) for all that I learned about geology and the Itajaí Basin; and to Ana Zucatti, the pioneer in Itajaí Basin paleontology; both great scientists and friends that I was lucky to meet.

I am grateful for all the institutions that provided the necessary infrastructure for the development of this work, including: the Brazilian Synchrotron Light Laboratory, under the SR- $\mu$ XRF (20170438, 20171031, 20180327) and  $\mu$ -CT (IMX 20180137) projects; the Brazilian Nanotechnology National Laboratory, under the SEM/EDS (21836 e 23684) and  $\mu$ -CT (20415). I thank very much the support of the laboratory of thin section preparation at UNISINOS, which provided dozens of thin sections for this work. I also thank the thin section laboratory of the Geosciences Institute at UNESP (Rio Claro) and the professor Luiz Sergio Amarante Simões.

I am deeply grateful to prof. Abderrazak El Albani, for receiving and advising me during the BEPE period at the Université de Poitiers (France), and for all the opportunities I had during my stay in his lab. I am also grateful to prof. Alain Meunier, for the collaboration, as well as for everything I learned about clays from him. I would like to thank Kurt Konhauser for his helpful and detailed insights in the work about the preservation of the Itajaí Basin fossils. I also thank very much Marc Laflamme for all the prodigious help in the work about the filamentous structures.

I am extremely grateful to my dear friend Ahmed Abd Elmola, for the amazing scientific collaboration, and for the good friendship that we were able to develop during my stay in France.

I would like also to thank Claude Fontaine for all his help with the x-ray diffraction analyses. I thank also all the technical support of Arnaud Mazurier, Julien Brunet, Claude Laforest, and Celine Boissard.

I am grateful to Milene Figueiredo for all her help and kindness during the palynological investigation developed in collaboration with Petrobras, as well as to the technical help of Igor Augusto Nascimento de Almeida and Gilton Braz de Aquino Filho.

I am profoundly grateful to the professors and the student representatives of the postgraduation commission of the PPGERN, which supported the development of my sandwich doctorate, in special to prof. Ana Lombardi, prof. Marcelo Adorna, Roberta Freitas and Raphael Machado.

I am profoundly thankful to my longtime friends Gustavo Prado and Gabriel Ladeira Osés, with whom I had many essential scientific discussions; and to my friend Gabriel Barros for the great scientific collaboration, and for all the trajectory we shared within the paleontological world. I thank also all the help of Ilana Lehn during the experiments at the Brazilian synchrotron. I am also grateful to my brother Pedro Becker Kerber, and to my sister Bianca Becker Kerber, for all their help in some steps of this work.

I am eternally grateful to the unrestricted support of my parents throughout all these years. I own much of my formation as a scientist and as a person to them, my father Gilmar Kerber, and my mother Elaine Becker Kerber.

At last, but not least, I would like to thank all the citizens of Apiúna (SC) that helped me in one way or another during the time-consuming field works.

## **AGRADECIMENTOS**

Este trabalho teve o apoio fundamental da Fundação de Amparo à Pesquisa do Estado de São Paulo (FAPESP) dentro dos projetos: 2016/01827-4 e 2018/21886-0. Também teve o apoio do Conselho Nacional de Desenvolvimento Científico e Tecnológico (CNPq) durante os primeiros meses do doutorado.

Como é para quase todo trabalho científico, os resultados apresentados aqui são frutos também de uma intensa e produtiva colaboração científica que eu tive a oportunidade de realizar com diversos ótimos cientistas.

Sou profundamente grato à minha mentora e inspiração científica Mírian Liza Alves Forancelli Pacheco. Muito desse trabalho, e do que aprendi ao longo dos anos, não teria acontecido sem os seus ensinamentos, seu apoio e sua dedicação como cientista e orientadora.

Agradeço também a toda a ajuda do meu coorientador prof. Paulo Sergio Gomes Paim (UNISINOS), por tudo que aprendi sobre geologia e sobre a Bacia de Itajaí; e à Ana Zucatti, pioneira na paleontologia da Bacia de Itajaí; ambos grandes cientistas e amigos que tive a sorte de conhecer.

Sou grato a todas as instituições que forneceram a infraestrutura necessária para o desenvolvimento deste trabalho, incluindo: Laboratório Nacional de Luz Síncrotron (LNLS), dentro dos projetos SR-XRF (20170438, 20171031, 20180327), e  $\mu$ -CT (IMX 20180137); Laboratório Nacional de Nanotecnologia (LNNano), projetos MEV/EDS (21836 e 23684) e  $\mu$ -CT (proposal 20415). Sou muito grato também ao laboratório de preparação de lâminas delgadas da UNISINOS, o qual providenciou dezenas de lâminas delgadas para este trabalho. Também agradeço ao laboratório de preparação de lâminas do Instituto de Geociências da UNESP (Rio Claro) e ao professor Luiz Sergio Amarante Simões.

Sou imensamente grato ao prof. Abderrazak El Albani por me receber e me orientar durante o período BEPE na Université de Poitiers (França), e por todas as oportunidades que tive durante minha estadia em seu laboratório. Também agradeço profundamente ao prof. Alain Meunier por ter aberto a oportunidade de desenvolver esse trabalho em conjunto com o prof. Abderrazak, assim como por tudo que aprendi

sobre argilas. Eu gostaria de agradecer a Kurt Konhauser pelos seus úteis e detalhados insights no trabalho sobre a preservação dos fósseis da Bacia de Itajaí. Eu também sou muito grato a Marc Laflamme por toda a prodigiosa ajuda no trabalho sobre as estruturas filamentosas.

Sou extremamente grato ao meu amigo Ahmed Abd Elmola por toda a incrível colaboração científica e pela ótima amizade que pudemos desenvolver ao longo da minha estadia na França.

Agradeço a Claude Fontaine, por toda a ajuda que me ofereceu durante as análises de difração de raios-X. Agradeço também a Arnaud Mazurier, Julien Brunet, Claude Laforest, e Celine Boissard, por todo o apoio técnico que recebi na Université de Poitiers.

Agradeço à Milene Figueiredo por toda a ajuda e gentileza durante as análises palinológicas desenvolvidas em colaboração com a Petrobrás, assim como ao apoio técnico de Augusto Nascimento de Almeida e Gilton Braz de Aquino Filho.

Sou extremamente grato aos professores e representantes discentes da comissão de pós-graduação do PPGERN, que apoiaram a possibilidade de desenvolver o doutorado sanduíche, em especial à profa. Ana Lombardi, prof. Marcelo Adorna, Roberta Freitas e Raphael Machado.

Aos meus amigos de longa data e ótimos cientistas Gustavo Prado e Gabriel Ladeira Osés, com os quais muitas discussões foram de grande ajuda para o desenvolvimento deste trabalho. Agradeço também a Gabriel Barros, por toda a ajuda e ótima colaboração científica que pudemos desenvolver ao longo da nossa trajetória dentro da paleontologia. Eu agradeço também a ajuda de Ilana Lehn durante os experimentos no Síncrotron. Sou grato também ao meu irmão Pedro Becker Kerber, e minha irmã Bianca Becker Kerber, pela ajuda em determinadas etapas deste trabalho.

Sou eternamente grato ao apoio irrestrito dos meus pais ao longo de todos esses anos. Devo muito da minha formação como cientista e como pessoa a eles, meu pai Gilmar Kerber, e minha mãe Elaine Becker Kerber.

Por fim, gostaria de agradecer a todos os cidadãos de Apiúna que de alguma forma ajudaram nos longos trabalhos de campo.

*"We are here because one odd group of fishes had a peculiar fin anatomy that could transform into legs for terrestrial creatures; because the earth never froze entirely during an ice age; because a small and tenuous species, arising in Africa a quarter of a million years ago, has managed, so far, to survive by hook and by crook. We may yearn for a "higher" answer--but none exists. This explanation, though superficially troubling, if not terrifying, is ultimately liberating and exhilarating. We cannot read the meaning of life passively in the facts of nature. We must construct these answers ourselves--from our own wisdom and ethical sense. There is no other way."*

Stephen Jay Gould, Life Magazine, 1988

## SUMMARY

### ABSTRACT

<b>1. INTRODUCTION .....</b>	16
1.1. THE EDIACARAN PERIOD.....	16
1.2 THE PRESERVATION STYLES OF THE EDIACARAN BIOTA.....	19
1.3 THE EDIACARAN MACROFOSSILS OF SOUTH AMERICA.....	20
<b>2. GOALS .....</b>	22
<b>3. ARTICLE 1 – THE OLDEST RECORD OF EDIACARAN MACROFOSSILS IN GONDWANA (~563 MA, ITAJAÍ BASIN, BRAZIL) .....</b>	23
<b>4. ARTICLE 2 – <i>BEGGIATOA</i>-LIKE <i>IN SITU</i> COMMUNITIES FROM THE EDIACARAN ITAJAÍ BASIN (~563 MA) – THE EXPANSION OF SULPHIDE OXIDIZING BACTERIA IN THE EDIACARAN PERIOD.....</b>	61
<b>5. ARTICLE 3 – THE ROLE OF VOLCANIC-DERIVED CLAYS IN THE PRESERVATION OF EDIACARAN BIOTA.....</b>	80
<b>6. FINAL CONSIDERATIONS.....</b>	127
<b>REFERENCES.....</b>	128

## ÍNDICE

### RESUMO

<b>1. INTRODUÇÃO .....</b>	<b>16</b>
1.1. THE EDIACARAN PERIOD.....	16
1.2 THE PRESERVATION STYLES OF THE EDIACARAN BIOTA.....	19
1.3 THE EDIACARAN MACROFOSSILS OF SOUTH AMERICA.....	20
<b>2. OBJETIVOS .....</b>	<b>22</b>
<b>3. ARTIGO 1 – THE OLDEST RECORD OF EDIACARAN MACROFOSSILS IN GONDWANA (~563 MA, ITAJAÍ BASIN, BRAZIL) .....</b>	<b>23</b>
<b>4. ARTIGO 2 – BEGGIA TOA-LIKE <i>IN SITU</i> COMMUNITIES FROM THE EDIACARAN ITAJAÍ BASIN (~563 MA) – THE EXPANSION OF SULPHIDE OXIDIZING BACTERIA IN THE EDIACARAN PERIOD.....</b>	<b>61</b>
<b>5. ARTIGO 3 – THE ROLE OF VOLCANIC-DERIVED CLAYS IN THE PRESERVATION OF EDIACARAN BIOTA.....</b>	<b>80</b>
<b>6. CONSIDERAÇÕES FINAIS.....</b>	<b>127</b>
<b>REFERÊNCIAS.....</b>	<b>128</b>

## ABSTRACT

New studies on the geologic history of Earth are increasingly revealing the complex relationships among evolutionary patterns, diversification of major groups, and environmental changes. In the fossil record of the Ediacaran Period (635–541 Ma), the appearance of macroscopically complex organisms and animals resulted in major modifications in the environment, setting the stage for the subsequent “Cambrian explosion” and the development of Phanerozoic-style ecosystems. The Ediacaran biota can be found in several localities throughout the world, and researchers on this subject are able now to divide it in mainly three Assemblages: Avalon, White Sea and Nama. Compared to other deposits around the world, studies on South American Ediacaran fossils are still in their early stages, but already show a great potential to understand the evolution of early complex life. In this context, this work aimed to investigate the taxonomy, taphonomy and age of the poorly known fossils from the Itajaí Basin (Santa Catarina, southern Brazil), as well as its relationships to other coeval fossiliferous strata. For that, a multi-approach investigation was conducted, using diverse techniques, such as: stereomicroscopic investigation; petrography; U/Pb radiometric dating (SHRIMP); scanning electron microscopy (SEM) and dispersive energy spectroscopy (EDS); computerized microtomography ( $\mu$ CT); and Raman and infrared spectroscopy. The results of this work are presented here in three main published and/or submitted articles regarding: [I] the description of the Itajaí Biota and its age; [II] the taphonomic characteristics of the ‘Ediacaran-style’ preservation at the Itajaí Basin; and [III] the nature of microbial filaments. In Article 1, it is reported the presence of Ediacaran soft-bodied organisms, such as *Palaeopascichnus*, discoidal forms (*Aspidella* and *Nimbia*), as well as abundant microbial mat features (e.g., reticulated tufts, Arumberia, and wrinkles). Moreover, the age of the Itajaí Basin is further constrained by U/Pb radiometric dating of volcanic tuffs, giving a depositional age ca. 563 Ma and setting this Ediacaran biota as one of the oldest in Gondwana. In Article 2, it is presented a detailed investigation on the microbial filaments and their possible affinities with giant filamentous sulfide-oxidizing bacteria, such as the modern *Beggiatoa*. This has great implications for understanding the biotic and geochemical context during Ediacaran times. In Article 3, it is provided a model to the fossilization mechanisms of the Itajaí Basin, in which the micro and macrofossils would have been

preserved by volcanic and microbial activity. This work shows for the first time robust evidences for the role of clay authigenesis in the early diagenesis of fossils. In sum, this thesis provides a comprehensive take on the paleobiology, taphonomy, and age of the Ediacaran Itajaí Biota, showing that these deposits are of key importance in studies on early macroscopic complex lifeforms of the fossil record.

**Key words:** Avalon Assemblage. Ediacaran Biota. Discoidal Fossils. Pseudofossils. Microbially Induced Sedimentary Structures (MISS). Taphonomy. Clay authigenesis. Illite

## RESUMO

Novos estudos sobre a história geológica da Terra estão cada vez mais revelando as relações complexas que existem entre padrões evolutivos, diversificação dos principais grupos de organismos, e mudanças ambientais. No registro fóssil do Período Ediacarano (635–541 Ma), o aparecimento de organismos macroscópicos complexos e animais resultaram em grandes modificações no ambiente, preparando o palco para a subsequente “explosão Cambriana” e o desenvolvimento de ecossistemas típicos do Fanerozoico. A biota ediacarana pode ser encontrada em várias localidades globalmente, e agora os pesquisadores do tema são capazes de dividi-la em três principais assembleias: Avalon, White Sea e Nama. Mesmo assim, comparado com outros depósitos globalmente, estudos sobre fósseis ediacaranos na América do Sul ainda estão em suas fases iniciais, mas já mostram um grande potencial para a compreensão da evolução inicial de organismos complexos. Este trabalho teve como objetivo investigar a taxonomia, tafonomia e idade dos fósseis da Bacia de Itajaí (Santa Catarina, Brasil), assim como suas possíveis relações com outros estratos fossilíferos contemporâneos. Para tanto, uma investigação de abordagem múltipla foi conduzida, usando diversas técnicas, como: estereomicroscopia; petrografia; datação radiométrica por U/Pb (SHRIMP); microscopia eletrônica de varredura (MEV) e espectroscopia de energia dispersiva (EDS); microtomografia computadorizada ( $\mu$ CT); e espectroscopia Raman e de infravermelho. Os resultados deste trabalho estão apresentados aqui em três artigos publicados e/ou submetidos, considerando: [I] a descrição e idade da biota de Itajaí; [II] os processos tafonômicos da preservação do ‘tipo Ediacarana’ na Bacia de Itajaí; e [III] a natureza dos filamentos micrométricos. No Artigo 1, é reportada a presença de organismos de corpo mole, como *Palaeopascichnus*, formas discoides (*Aspidella* e *Nimbia*), assim como abundantes texturas de esteiras microbianas (e.g., *tufts* reticulados, *Arumberia* e *wrinkles*). Além disso, a idade da Bacia de Itajaí é melhor restringida por datação radiométrica U/Pb de tufo vulcânico, resultando numa idade de deposição de ca. 563 Ma e definindo esta biota ediacarana como uma das mais antigas do Gondwana. No Artigo 2, é apresentada uma detalhada investigação sobre os filamentos microbianos encontrados e suas possíveis afinidades com bactérias filamentosas gigantes oxidantes de enxofre, como o moderno gênero *Beggiatoa*.

Estes resultados trazem implicações para a compreensão do contexto biótico e geoquímico durante o Ediacarano. No Artigo 3, é fornecido um modelo sobre os mecanismos de fossilização na Bacia de Itajaí, no qual micro e macrofósseis teriam sido preservados por meio de atividade vulcânica e microbiana. Este trabalho mostra pela primeira vez evidências robustas para o papel da autigênese de argilominerais na diagênese inicial de fósseis. Em resumo, esta tese fornece uma visão ampla sobre a paleobiologia, tafonomia e idade da bacia ediacarana de Itajaí, mostrando que estes depósitos são de importância chave para estudos sobre as primeiras formas de vida macroscópicas e complexas do registro fóssil.

**Palavras-chave:** Assembleia Avalon. Biota Ediacarana. Fósseis Discoides. Pseudofósseis. Estruturas Sedimentares Microbialmente Induzidas (MISS). Tafonomia. Autigênese de Argila. Ilita.

## 1 INTRODUCTION

### 1.1 THE EDIACARAN PERIOD

The organisms that appear in the fossil record of the Ediacaran Period (636–539 Ma) have often been considered as the prelude to the so-called “Cambrian explosion”. However, several studies are now showing the paleobiological peculiarities of the Ediacaran assemblages, changing our views about early animal evolution, and the dawn of macroscopic and complex organisms (Xiao and Laflamme, 2009; Ding et al., 2019; Dunn and Liu, 2019; Ivantsov et al., 2019). During this time, a diverse and global biota of soft-bodied organisms of unknown affinity developed in benthic ecosystems that set the stage for major subsequent biotic transformations (Fig. 1).



**Fig. 1.** Artistic reconstruction of an Ediacaran seafloor (White Sea Assemblage) containing some of the typical and enigmatic Ediacaran soft-bodied organisms. Art by Julia Soares d’Oliveira.

The Ediacaran Period is broadly interspaced between two large events: the end of the Marinoan glaciation, marked by the deposition of the cap carbonates (~635 Ma); and the Cambrian biological radiation, or the ‘Cambrian explosion’. The limit of the Ediacaran/Cambrian is still discussed, but it is usually regarded as the first appearance of the ichnofossil *Treptichnus pedum*, ca. 541 Ma (Buatois, 2018).

Although there is the traditional delimitation of the Ediacaran in three main assemblages (Waggoner, 2003; Narbonne, 2005) (see below), still there are no formal subdivisions for this time period that allow detailed correlations between geologic units throughout the world (Narbonne et al., 2012). Other attempts to create a biostratigraphic framework for the Ediacaran have mostly relied on acritarch biozones. For example, Grey (Grey, 2005) defined five acritarch biozones for the Ediacaran successions of Australia, while other researchers suggested two biozones for the Ediacaran deposits of China: a lower biozone dominated by *Tianzhushania spinosa*; and an upper biozone defined by *Tanarium conoideum* – *Hocosphaeridium scaberfacium* – *H. anozos* (McFadden et al., 2009; Liu et al., 2013b; Xiao et al., 2014). However, although these biozones are useful for regional correlations, their use for understanding the global biostratigraphy of the Ediacaran still need to be further investigated.

Despite this lack of biostratigraphic zonations, the Ediacaran Period presents taxonomic, ecological, and taphonomic characteristics that are singular in the fossil record (Shen et al., 2008; Xiao and Laflamme, 2009). As pointed out above, these biotic events are evidenced in three assemblages: the Avalon, White Sea and Nama clusters. Other important fossiliferous deposits include those from the Doushantuo Formation of China, with the embryo-like fossils (Yin et al., 2016), and the Lantian Formation, with the diverse macroalgae and putative metazoans (Yuan et al., 2011; Wan et al., 2016).

The Avalon localities (~570–559 Ma) record the appearance of the first macroscopic complex soft-bodied organisms in deep-marine settings, supposedly bellow the photic zone (Liu et al., 2015). The rise of these early ecosystems has been linked to increasing levels of oxygen (Canfield et al., 2007), and some works revealed that this biotic event can be characterized by an explosion of morphospace (Shen et

al., 2008). The Avalonian communities were dominated by sessile benthic macroorganisms characterized by frondose morphologies (e.g., rangeomorphs and arboreomorphs) of unknown affinities, but largely considered as stem-group metazoans. Other more elusive macrofossils also occur, including putative sponges (e.g., *Thectardis* (Sperling et al., 2011); but see (Antcliffe et al., 2014)) and cnidarians (e.g., *Haootia quadriformis* (Liu et al., 2014); but see (Miranda et al., 2015)), as well as possible ichnofossils. Microbial mat features are observed, but are uncommon in the deep settings of the Avalonian deposits (Droser et al., 2017), where, instead, dense fabric of submillimeter- to millimeter-sized filaments are present (Liu et al., 2016a). Some of these filaments were recently observed to connect the holdfast of frondose taxa, which led the authors to interpreted them as stolonic connections of the macroorganisms (Liu and Dunn, 2020). However, other interpretations may also apply to similar filamentous fossils (see Article 3 of this thesis).

The younger White Sea paleocommunities (~558–550 Ma) developed mostly on photic and shallower settings, compared to the Avalonian ones (Grazhdankin, 2004, 2014). During this time, further evolutionary and ecologic innovations occurred. Especially, it is in the White Sea deposits that abundant evidences of motility can be observed, as showed by the horizontal trace fossils and the feeding traces of mobile organisms. Dickinsoniomorphs, erniettomorphs, kimberellomorphs, and other enigmatic forms also appear for the first time during the White Sea. Of special interest for studies on early animal evolution is the fossil *Kimberella*, one of the few Ediacaran taxa usually considered as a crown-group metazoan, probably a mollusk (Fedonkin et al., 2007). This bilateral form is frequently associated with scratch-marks on bedding planes that are interpreted as their feeding traces (Ivantsov et al., 2019). The White Sea localities also bear abundant evidence for the development of microbial mats, a feature uncommon and controversial in the previous Avalon ecosystems.

The Nama paleocommunities (550–539 Ma) marked the final stage of the Ediacaran biota, where the ecosystems seem to have suffered a significant loss in diversity (Darroch et al., 2015a). This biota also presents rangeomorphs and erniettomorphs, but it is mainly characterized by the appearance of several tubular animals ('Wormworld fauna'), including mineralized metazoans, and increasingly complex ichnofossils (Schiffbauer et al., 2016; Wood, 2018). Finally, the Ediacaran/Cambrian transition shows the demise of this Ediacaran biota, with only

some proposed surviving taxa in Cambrian deposits (Jensen et al., 1998; Hagadorn et al., 2000).

## 1.2 THE PRESERVATION STYLES OF THE EDIACARAN BIOTA

Although there are reports of Ediacaran fossils preserved by kerogenization (Xiao et al., 2002), pyritization (Cai and Hua, 2007; Cai et al., 2010; Guan et al., 2017), and, possibly, aluminosilicification (Anderson et al., 2011; Cai et al., 2012; MEYER et al., 2012), the Ediacaran Period is widely recognized by the common preservation of the soft-bodied macro-organisms as molds and casts in siliciclastic rocks. This ‘Ediacaran-style’ preservation can be further divided in the ‘Conception’ (positive relief under ash layers), ‘Flinders’ (positive and negative epirelief), and ‘Nama-styles’ (three-dimensionally within sandstones).

The Conception style is basically defined by the preservation of the macro-organisms in positive epirelief bellow ash-fall deposits (Seilacher, 1992; Narbonne, 2005). This type of fossilization is observed in the deep-marine Avalon paleocommunities of Newfoundland and England. However, recent works (Liu, 2016) have suggested that, instead of volcanic burial, the most likely mechanism for their fossilization was the ‘death-mask’ model.

The ‘death mask’ hypothesis was firstly proposed by Gehling (Gehling, 1999) to explain the moldic preservation of the ‘Flinders-style’. In this model, the author suggested that the presence of microbial mats stabilized the seafloor, limited the diffusion of ions, and (after a burying event) led to the precipitation of iron sulfides as a result of microbial metabolism, forming an early diagenetic sole veneer that replicated the buried macro-organisms and microbial mats. Although recent works supported the death mask model for Avalon and White Sea localities (Liu, 2016; Liu et al., 2019), still this taphonomic scenario remains contentious to other researchers.

Other hypotheses were also raised for the ‘Ediacaran-style’ preservation. Tarhan et al. (Tarhan et al., 2017) suggested that silica-rich oceans would have promoted an early silica cementation of the fossil-bearing deposits. On the other hand, Bobrovskiy et al. (2019a) provided evidence for the rheological model initially raised by Wade (Wade, 1968), where the different properties (e.g., viscosity) of sediments

(over- and underlying decaying organisms) were essential to their positive epirelief preservation.

### 1.3 THE EDIACARAN MACROFOSSILS OF SOUTH AMERICA

Ediacaran fossiliferous deposits are known to occur in several localities worldwide. However, despite the presence of several Ediacaran-age geologic units in South America, only few fossil taxa were reported until now. This more likely reflects the lack of more studies (compared to other Ediacaran deposits) than a true paleontological phenomenon. Nonetheless, the importance of the South America ediacaran record has been increasingly demonstrated by recent works.

The most known Ediacaran localities in South America are those bearing the Nama-type organisms of the latest Ediacaran. These are exemplified by a number of carbonate and siliciclastic successions, such as: the Corumbá and Bambuí Groups in Brazil (Warren et al., 2014; Becker-Kerber et al., 2017); the Tagatiya Guazu Formation in Paraguay (Warren et al., 2011); the Arroyo del Soldado Group in Uruguay (Gaucher et al., 2003); and possibly the Sierras Bayas Group in Argentina (Gaucher et al., 2005). One of the main things these units have in common is the presence of the biomineralized genus *Cloudina*, often regarded as a terminal Ediacaran index taxon. Other macrofossils include: *Corumbella* (Tamengo, Sete Lagoas, and Tagatiya Guazu formations) (Warren et al., 2014, 2017; Pacheco et al., 2015); *Paraconularia* (Tamengo Formation) (Van Iten et al., 2014); *Namacalathus* (Tagatiya Guazu Formation) (Warren et al., 2017); the putative tubular fossils *Soldadotubulus* and *Waltheria* (Yerbal Formation) (Gaucher, C., Sprechmann, 1999); and the algae *Vendotaenia* (Tamengo Formation), *Eoholynia* and *Tawuia* (Guaicurus Formation) (Gaucher et al., 2003). The reported *Vendotaenia* from the Cerradinho and Bocaina Formations (see (Gaucher et al., 2003)), recovered by acid macerations, are highly fragmented and poorly preserved, and their identification within this genus is considered here as controversial.

Soft-bodied Ediacaran fossils are rare in South America successions, and as discussed in the first article of this thesis, they are highly problematic. Yet, it is worthy to mention the proposed presence of *Nemiana* from the (Cambrian?) Puncoviscana Formation in Argentina (Aceñolaza and Aceñolaza, 2007; Aceñolaza, 2012); putative *Aspidella* discs from the Cerro Negro Formation in Argentina (Arrouy et al., 2016) (but

see (Inglez et al., 2019)); and possible *Aspidella*, *Inrites*, and *Sekwia* from the Camaquã Basin in Brazil (Netto, 2012).

Apart from these occurrences, some preliminary works reported the supposed presence of Ediacaran soft-bodied organisms in the Itajaí Basin (IB – southern Brazil) (Rosa, 2005). Although most of the works on the paleontology of the Itajaí basin remained unpublished until now, they showed the great potential of this basin for studies on the early evolution of complex large organisms.

In this thesis, I bring a new look into the paleontology of the poorly known IB, showing the presence of undoubtful soft-bodied ediacarans (e.g., *Palaeopascichnus*), as well as discoidal forms, microbial filaments, pseudofossils and several morphotypes of microbially induced sedimentary structures (MISS). The age of the Itajaí basin is also further refined by new U/Pb radiometric dating of tuff levels (~563 Ma), setting this Ediacaran fossil record as one of the oldest in Gondwana. The high-fidelity preservation found in some of the fossiliferous levels is also addressed and a new model for the ‘Ediacaran-style’ preservation is proposed, where volcanic and microbial activity played major roles during the fossilization of the biota. Finally, it is presented a detailed discussion on the nature of the IB microbial filaments, and their implications for understanding the Ediacaran biological and geochemical evolution.

## 2 GOALS

The aims of this work were:

- A)** To investigate the taxonomic composition of the Itajaí Basin fossil biota;
- B)** To analyze the evolutionary and paleoecological context of this biota;
- C)** To study the paleoenvironment and fossilization context of the macroscopic fossils, with relation to the association with microbially induced sedimentary structures (MISS) and the taphonomic conditions of the early diagenesis;
- D)** To compare the Itajaí biota with other correlate units in Brazil and other places in the world, such as Australia, England and Canada.

### 3 ARTICLE ONE

*Published in Gondwana Research*

#### The oldest record of Ediacaran macrofossils in Gondwana (~563 Ma, Itajaí Basin, Brazil)

**Abstract.** The Avalon biota (Ediacaran Period, 570–559 Ma) marks the first appearance of macroscopic and complex benthic communities in the fossil record. This assemblage is known from a few localities worldwide, mainly in Canada and England. Here, we report for the first time the presence of Ediacaran macrofossils in deposits of similar age from Gondwana (Itajaí Basin, southern Brazil). Our new radiometric date (~563 Ma) indicates that the Itajaí Basin can be chronocorrelated with the classic Avalonian deposits and thus represents one of the oldest records of the Ediacaran biota in Gondwana. We describe the presence of the Ediacaran genus *Palaeopascichnus*, as well as discs (*Aspidella* and *Nimbia*), and other problematic forms. Contrary to the deep-marine macroorganisms of the Avalon Assemblage, the Itajaí fossils are associated with abundant and exceptionally preserved three-dimensional microbial mats and microbially induced sedimentary structures (MISS) in relatively shallow settings (upper slope and distal delta front deposits). In this sense, the Itajaí biota could represent early adaptations of benthic macrobiota to the shallower and more photic environments that characterize the later White Sea Assemblage.

#### 1. Introduction

The first fossil evidence of macroscopic complex life forms is preserved in rocks associated with deep aphotic environments in the middle-late Ediacaran Period (Liu et al., 2015). The appearance of this Ediacaran biota marked the development of macroscopic benthic ecosystems characterized by an “explosion” of morphospace (i.e., Avalon biota) (Shen et al., 2008), including possible stem-group metazoans (Liu et al., 2015). Subsequent biotas include the White Sea and Nama Assemblages, which have distinct biotic compositions and further evolutionary

innovations (e.g., mobility and skeletonized animals, respectively) and were associated with shallow waters and photic zones (Grazhdankin, 2004; Boag et al., 2016).

Despite this knowledge, the mechanisms and biases behind the transitions among these biotas still need to be better understood. It is likely that both biological and environmental changes played a synergic role in ecosystem structuration during the Ediacaran. Specifically, the Avalon and White Sea biotas differ dramatically in the sense that the latter contains the first macroscopically complex organisms that were adapted to shallow waters and were associated with abundant textured organic surfaces (Droser et al., 2017).

Studies on the Avalonian biotas have mostly been restricted to the widely investigated rocks in Canada and England (Ford, 1958; Misra, 1969; Boynton and Ford, 1995; Narbonne and Gehling, 2003; Hofmann et al., 2008; Narbonne et al., 2014; Liu et al., 2015). Therefore, exploring the paleontological potential of other coeval deposits is essential to developing a more complete picture of the early evolution of macroscopic life. To date, Ediacaran units in South America bearing putative soft-bodied taxa have been reported only in deposits near the Ediacaran-Cambrian transition (Gaucher, 2018) and require further investigations regarding their proposed body fossil content (Inglez et al., 2019).

One geologic unit with great potential for studies on Ediacaran biota is the Itajaí Basin (IB). This geologic unit has long been controversial in terms of its paleontological record, mostly due to scarce studies. Previous and mostly unpublished works have suggested the presence of Cambrian (*Chancelloria* and *Choia*) and Ediacaran taxa (*Aspidella*), as well as putative ichnofossils such as *Diplocraterium*, *Helmintidichnites*, and *Oldhamia* (Da Rosa et al., 1997; Leipnitz et al., 1997; Paim et al., 1997). These claims have led to some uncertainty about the age of the basin since radiometric dating suggested an upper Neoproterozoic age (Guadagnin et al. 2010; Basei et al. 2011 and references therein).

This study reports new fossil findings and geochronological data for the Itajaí Group. Here, we show the presence of macroorganisms, as well as putative animals, and abundant microbially induced sedimentary structures (MISS) associated with settings that are shallower than those of other Avalonian deposits. In this sense, the

Itajaí biota can be considered a key locality for understanding the colonization of shallower (and possibly photic) environments by complex Ediacaran organisms.

## 2. Geological context

During the late to post-orogenic stages of the Pan-African-Brasiliano Orogeny (~ 600 – 540 Ma), several sedimentary basins formed as a result of the collision of the Rio de la Plata, Congo and Kalahari cratons (Gresse et al., 1996). They include the Itajaí (Guadagnin et al., 2010; Basei et al., 2011), Camaquã (Paim et al., 2000; Netto, 2012), Arroyo del Soldado (Gaucher, 2000; Blanco et al., 2009) and Nama (Saylor et al., 1995; Grotzinger et al., 1995) basins (Supplementary Fig. 1), among others, and the IB is the focus of this work.

The E-NE-elongated IB is interpreted as a foreland basin (Rostirolla, 1991; Rostirolla et al., 1992; Gresse et al., 1996; Guadagnin et al., 2010) related to the Dom Feliciano Belt (DFB) in Santa Catarina State (Supplementary Fig. 1). The DFB comprises, from east to west, the Florianópolis Magmatic Arc, the metavolcano-sedimentary Brusque Complex and the foreland IB. To the northwest, the IB covers the Santa Catarina Granulite Complex, a tectonically stable area related to the Luis Alves Microplate (Guadagnin et al., 2010; Basei et al., 2011) (Fig. 1). The IB contains a thick siliciclastic succession, with minor volcaniclastic strata, that was deposited between 572 and 549 Ma (Guadagnin et al., 2010). This succession includes alluvial, deltaic and shallow- to deep-marine strata organized into five depositional sequences (adapted from (Fonseca, 2004) and (Teixeira et al., 2004) (Fig. 1)).

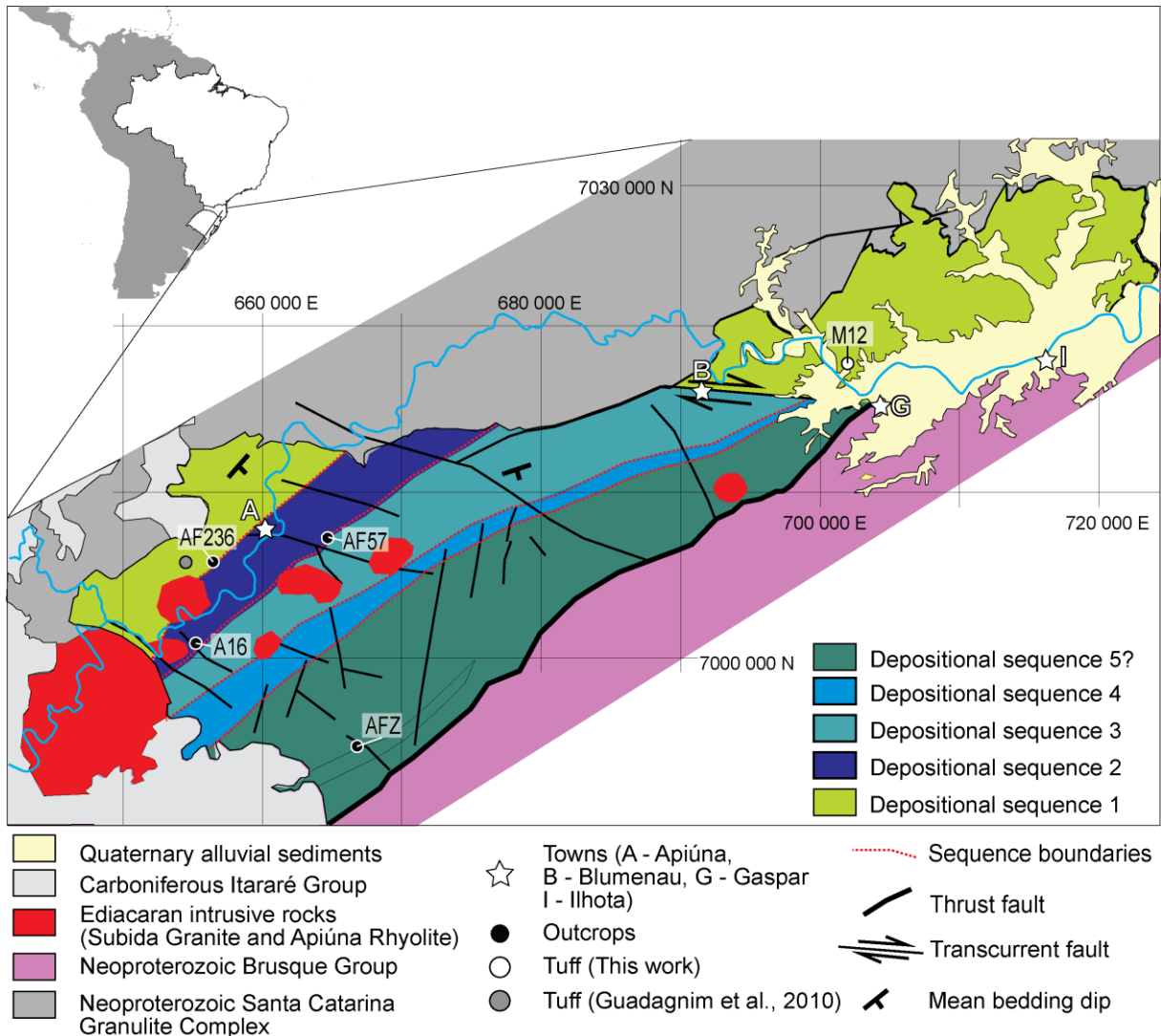


**Fig. 1.** Simplified geological map of the Itajaí Basin showing the main depositional sequences (DS) (modified after Fonseca, 2004 and Teixeira et al., 2004) and main fossiliferous outcrops.

Depositional sequence 1 (DS1) encompasses a transgressive systems tract characterized by alluvial conglomerates and sandstones followed by deltaic to shallow-marine sandstones to siltstones and rarer shales (Figs. 1, 2). The alluvial and delta plain facies include trough cross-bedded, fining-upward lenses of clast-supported conglomerates and sandstones related to braided streams. The trough cross-bedded sets are bounded by low-angle, down-current dipping surfaces related to the frontal accretion of fluvial braid bars. The shallow-marine deposits are composed of fine- to medium-grained, well-sorted sandstone lenses displaying swaley and hummocky cross-bedding and rarer wave ripples associated with wave-dominated coastal areas.

Finally, the delta front and prodelta facies encompass coarsening- and thickening-upward packages of thin-bedded siltstones and rarer shales and fine- to very fine-grained, massive or climbing ripple sandstones (distal delta front to prodelta) overlain by massive, meter-scale sandstone lenses (proximal delta front).

A relatively deep-marine succession (DS2), mostly composed of high-density, channelized to unconfined turbidites (Apiúna Turbidite Complex) and fine-grained, slope to basinal facies, unconformably overlies the previous units and represents a succeeding lowstand systems tract. Turbidite channels comprise meter- to a few tens of meters-wide and several meters-thick lenses composed of matrix-supported conglomerates and/or very coarse- to coarse-grained, massive sandstones. The turbidite channel fill usually exhibits fining-upward trends and abundant rip-up clasts near their erosional bases and are surrounded by thin-bedded, fine-grained slope deposits. Slumped beds are rare. Unconfined, more distal turbidite deposits are tabular and composed of decimeter-scale beds of fine- to very fine-grained, massive to planar-bedded sandstones (turbidite lobe) and centimeter-scale couplets of fine- to very fine-grained sandstone and siltstone (lobe fringe). The transition between channelized and nonchannelized turbidite facies is gradual.

An erosional, subaerial unconformity highlighted by fluvial facies resting immediately above the slope strata of the previous depositional sequence delineates the base of the subsequent succession (DS3), which is mostly composed of deltaic to shallow-marine deposits that display features similar to those of DS1. The subsequent depositional sequence (DS4) repeats the previous sequence, including the presence of fluvial strata above a subaerial unconformity scoured into marine deposits of DS3. However, DS4 includes a larger proportion of fluvial and proximal, wave-influenced delta front sandstones than DS3. Above the fourth depositional sequence, a thick, strongly deformed, and partially inverted package (DS5) containing turbidite, delta front to prodelta, and alluvial strata occurs. However, its actual stratigraphic position is still uncertain. Whereas Rostirolla (1991), Fonseca (2004), and Guadagnin et al. (2010) describe it as the youngest sequence of the IB, Basei et al. (2011) suggest that this unit has been overthrust onto the underlying units. The turbiditic, delta front to prodelta, and alluvial facies are similar to those described in more detail in DS1 and DS2.

The studied fossils and MISS were found in shallow- to relatively deep-marine strata (Figs. 1–3, and Supplementary Fig. 2), including the fine-grained, distal delta front facies of DS1 (e.g., outcrops AF236 and M12) and the upper slope facies (fine-grained, thin-bedded turbidites) close to the subaerial unconformity that delineates the DS2 upper boundary (e.g., outcrop A16). The fossils occur in millimetric rhythmites of clay, silt and fine-grained sand. Body fossils and/or microbial mats were not found in the deeper facies of DS2. No true palynomorphs were recovered from palynological macerations, but artifacts of particulate organic material were observed during the investigation (Supplementary Text 1).

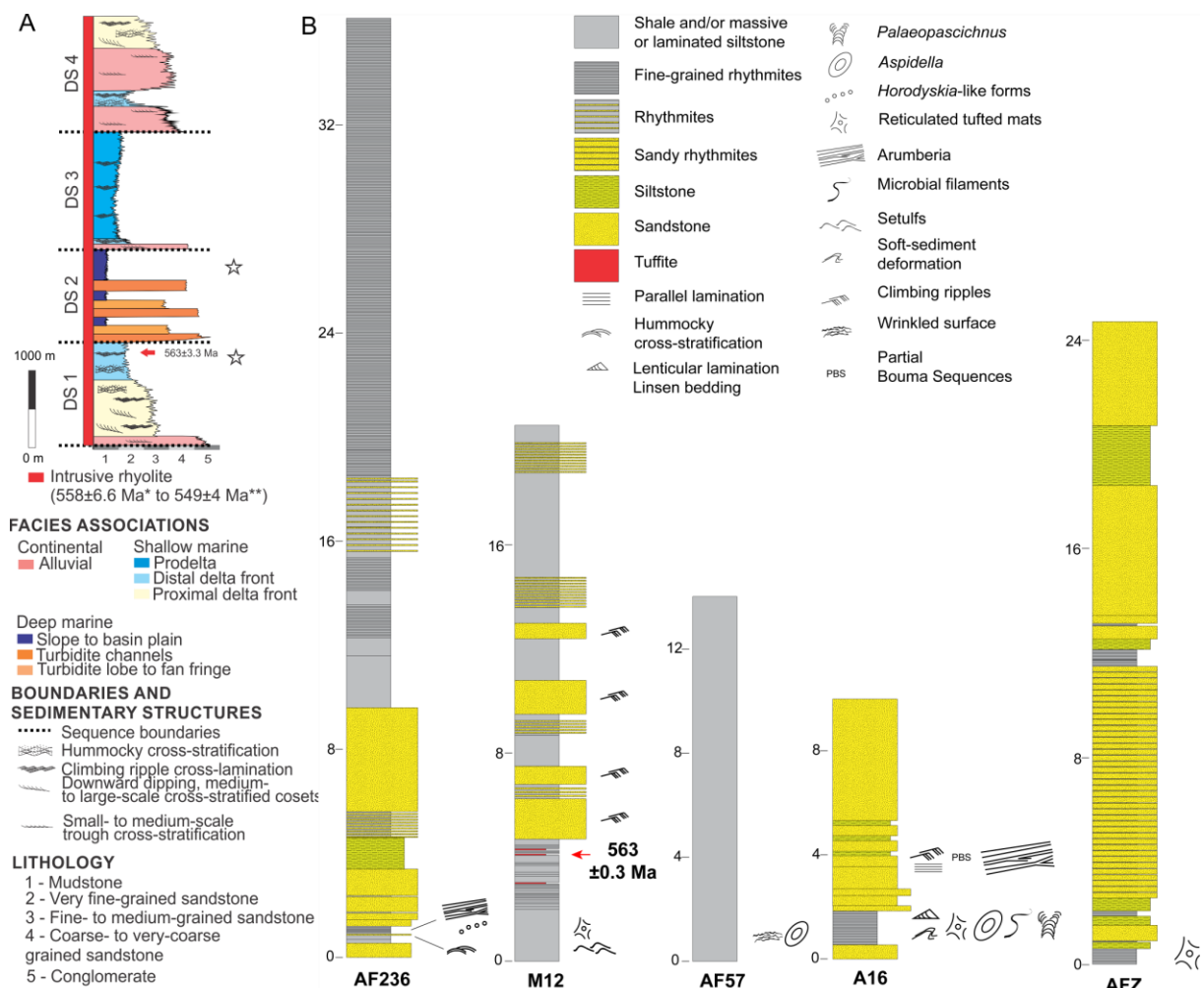


**Fig. 2.** A) Simplified composite column displaying depositional sequences DS1 to DS4, facies associations, related grain size trends, main sedimentary structures, estimated positions of fossil horizons (stars), and dated tuff layer (red arrow) (based on Fonseca (2004)); B) Profiles of the studied sections. \*After Basei et al. (2011). \*\*After Guadagnin et al. (2010).

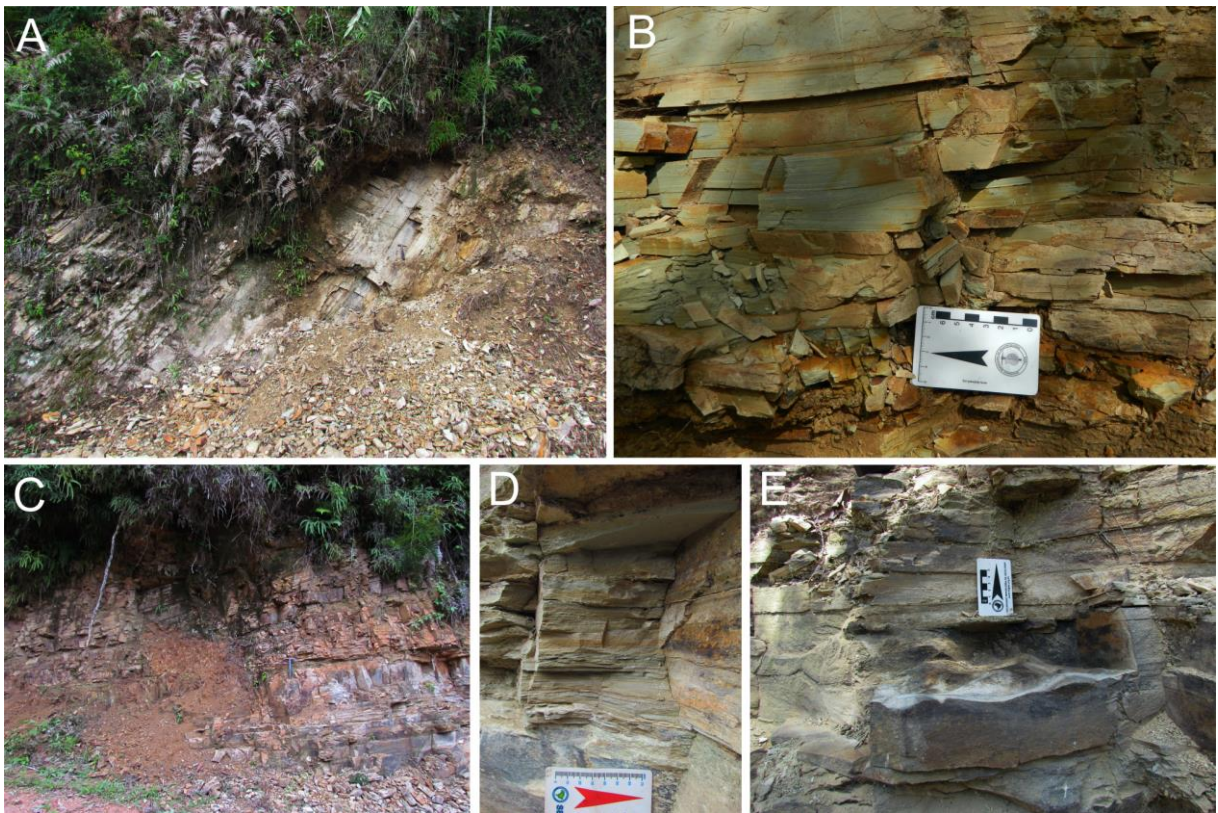


**Fig. 3.** Photographs of the main fossiliferous localities. A–B) Outcrop A16 (depositional sequences 2–3); B) Detail of the fossiliferous fine-grained rhythmites present in A16; C–E) Outcrop AF236 (depositional sequence 1); D) Detail of the fossiliferous horizon characterized by fine-sandstone/mudstone intercalations; E) Wave-rippled sandstone at the same locality.

### 3. Material and methods

#### 3.1. Samples and localities

We prospected approximately 234 outcrops (Supplementary Fig. 2, Supplementary Table) throughout the basin during field work, but the majority of samples were collected in the more prolific localities AF236, M12, A16, AF57, and AFZ (Figs. 1, 2). The samples were collected *in situ*, except for sample CAP/1A–558, which was found in the float. All hand samples, including body fossils and MISS ( $n = 295$ ), analyzed here have been deposited in the “Coleção Arqueológica e Paleontológica” (CAP-549–582 and CAP-877–1019) at the Universidade Federal de São Carlos (Sorocaba, Brazil).

### *3.2. Macroscopic and petrographic investigation*

Polished sections parallel and transverse to the bedding plane were made to examine the biological and sedimentary features under a SteREO Discovery V20 stereomicroscope coupled with an Axiocam camera at the Laboratório de Ecologia at the Universidade Federal de Mato Grosso do Sul. Thin sections were prepared at the Programa de Pós-Graduação em Geologia da Universidade do Vale do Rio dos Sinos (UNISINOS – São Leopoldo) and at the Setor de Laminação of the UNESP (Rio Claro). The thin sections were analyzed under a Leica microscope at the Instituto de Geociências of Universidade de São Paulo (IGc-USP).

### *3.3. Scanning electron microscopy and $\mu$ X-ray fluorescence*

Scanning electron microscopy (SEM) analyses were performed using Quanta 650FEG and FEI Inspect F50 microscopes at the Brazilian National Laboratory of Nanotechnology (LNNano/CNPEM), both in high-vacuum mode and with a current tension of 15 kV. Synchrotron radiation  $\mu$ X-ray fluorescence (SR- $\mu$ XRF) mapping was performed at the Brazilian Synchrotron Light Laboratory (LNLS), and measurements were made using polychromatic excitation in microbeam mode and filtering with Fe foils. The FlyScan mode was used with 500 ms of count time per point. The data were later treated with PyMCA software.

### *3.4. U-Pb geochronology*

Zircon grains were separated from a felsic tuff layer (sample T2A1M12; Figs. 1, 2) after crushing and milling using a jaw crusher and ring mill apparatus. Heavy and light minerals were separated using heavy liquids and a Frantz® magnetic separator after concentration of minerals by manual panning. Handpicked zircon crystals were mounted in an epoxy disc, ground and polished. Reflected light photomicrographs of samples were obtained, and images were produced using a scanning electron microscope for backscattered electron (BSE) and cathodoluminescence (CL) imaging. In situ laser ablation inductively coupled plasma mass spectrometry (LA-ICP-MS) U-Pb zircon dating was carried out at the Isotope Geology Laboratory of Universidade Federal de Ouro Preto (Brazil) using a Photon-machines ArF excimer laser 193

coupled to a high-resolution sector field inductively coupled plasma mass spectrometer (HR-SF-ICP-MS, Element 2). A laser spot size of 30 µm was used, and data were acquired in peak jumping mode during a 20-s background measurement followed by a 20-s sample ablation. To evaluate the accuracy and precision of the laser ablation results, the zircon reference materials BB-1 (Santos et al., 2017), Plešovice (Sláma et al., 2008) and GJ-1 (Jackson et al., 2004) were also analyzed. The obtained ages agreed within the experimental errors:  $563.8 \pm 3.2$  Ma ( $n = 14$ ) for BB-1,  $601.3 \pm 2.8$  Ma ( $n = 12$ ) for GJ-1 and  $338.4 \pm 2.2$  Ma ( $n = 12$ ) for Plešovice. The raw data were corrected for background signal, and laser-induced elemental fractional and instrumental mass discriminations were corrected by the reference zircon BB-1. The common Pb correction was based on the measured  $^{204}\text{Pb}$  composition (of the sample) following the model of Stacey and Kramers (Stacey and Kramers, 1975). The decay constant values used were from Jaffey et al. (1971). The data were corrected and reduced using the software Glitter (Van Actherbergh et al., 2001), and Isoplot-Ex (Ludwig, 2003) was used for age calculation. Uncertainty propagation was applied to the obtained data according to Horstwood et al. (2016).

#### 4. Age

To constrain the age of the studied succession, U-Pb zircon dating was carried out on a tuff sample (Figs. 1, 2) by LA-ICP-MS. This rock is interlayered with distal delta front rhythmites in the upper portion of DS1, the basal unit of the IB (Figs. 1, 2). The tuff occurs near strata with MISS in outcrop M12 (Fig. 2). Approximately 70- to 250-µm-long zircon grains ( $n = 35$ ) with prismatic and euhedral habits and sector zoning were extracted (Fig. 4A), following the work of (Corfu et al., 2003). Juvenile igneous zircons (31 of 35 dated grains) were recognized, yielding a concordant age of  $563 \pm 3.3$  Ma (95% confidence, MSWD=1.6) (Fig. 4B), which corresponds to the magmatic crystallization age of the tuff.

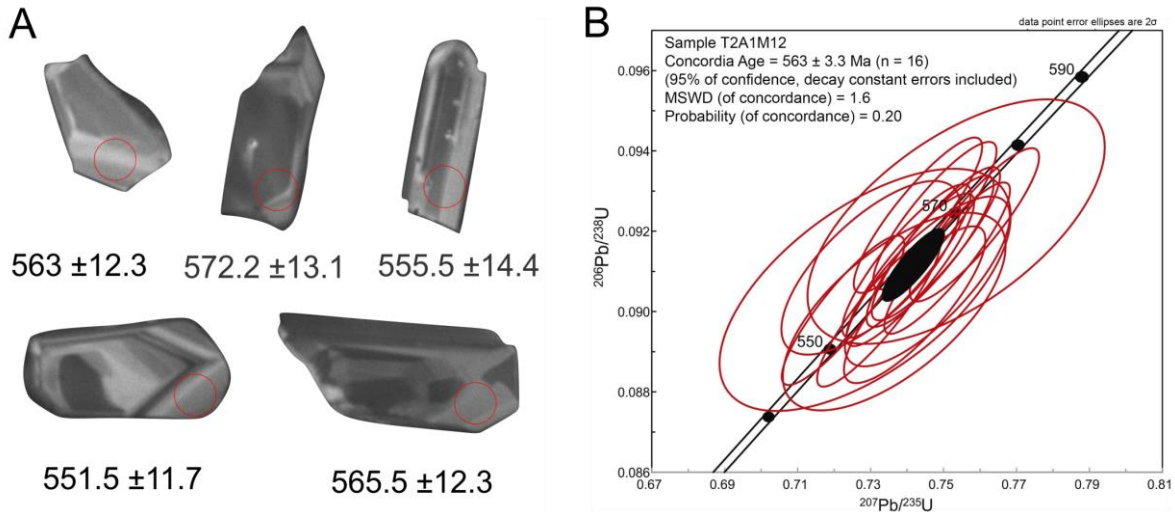


**Fig. 4.** A) Zircon morphologies obtained from the tuff investigated for radiometric U-Pb dating; B) Concordia diagram and concordia age obtained from the in situ LA-ICP-MS U-Pb zircon analyses.

These results broadly correlate this succession to the Avalon Assemblage (~570 – 557 Ma) (Schmitz, 2012; Noble et al., 2015; Pu et al., 2016) and mark the Itajaí Group as one of the earliest records of macroscopic life in Gondwana. The radiometric dating presented here is in accord with previously reported ages (Guadagnin et al., 2010), setting a minimal depositional age of  $563 \pm 3$  Ma. Upper age limits given by the dating of the intrusive rhyolites that cross-cut the entire basin (ca. 558 Ma – 549 Ma; Basei et al. (2011), Guadagnin et al. (2010)) also corroborate an Avalonian age.

## 5. Body fossils

The body fossil assemblage includes *Palaeopascichnus*, *Aspidella*, *Nimbia*, and other problematic forms. These fossils were recovered from thin-bedded rhythmites related to upper slope (*Palaeopascichnus* and *Aspidella*) and distal delta front (*Aspidella* and *Nimbia*) depositional settings (Figs. 2, 3). The rhythmites are characterized by millimetric intercalations of clay and silt (Fig. 3B). The body fossils occur in association with abundant surface structures related to microbial mat growth in both slope and delta depositional environments. Additionally, neither body fossils nor MISS were found in the deeper facies (slope rise to basin plain).

*Palaeopascichnus* ( $n = 27$ ) occurs as impressions comprising a series of straight to curved segments (i.e., chambers) and are abundantly preserved in some layers of mudstones in the thin-bedded rhythmite from outcrop A16 (Fig. 5). The chamber thickness varies from 0.1–0.3 mm, while the width varies from 0.3–1 mm. Some specimens show evidence of branching (Fig. 5A–B). The series width increases slightly in the direction of growth but diminishes after branching.

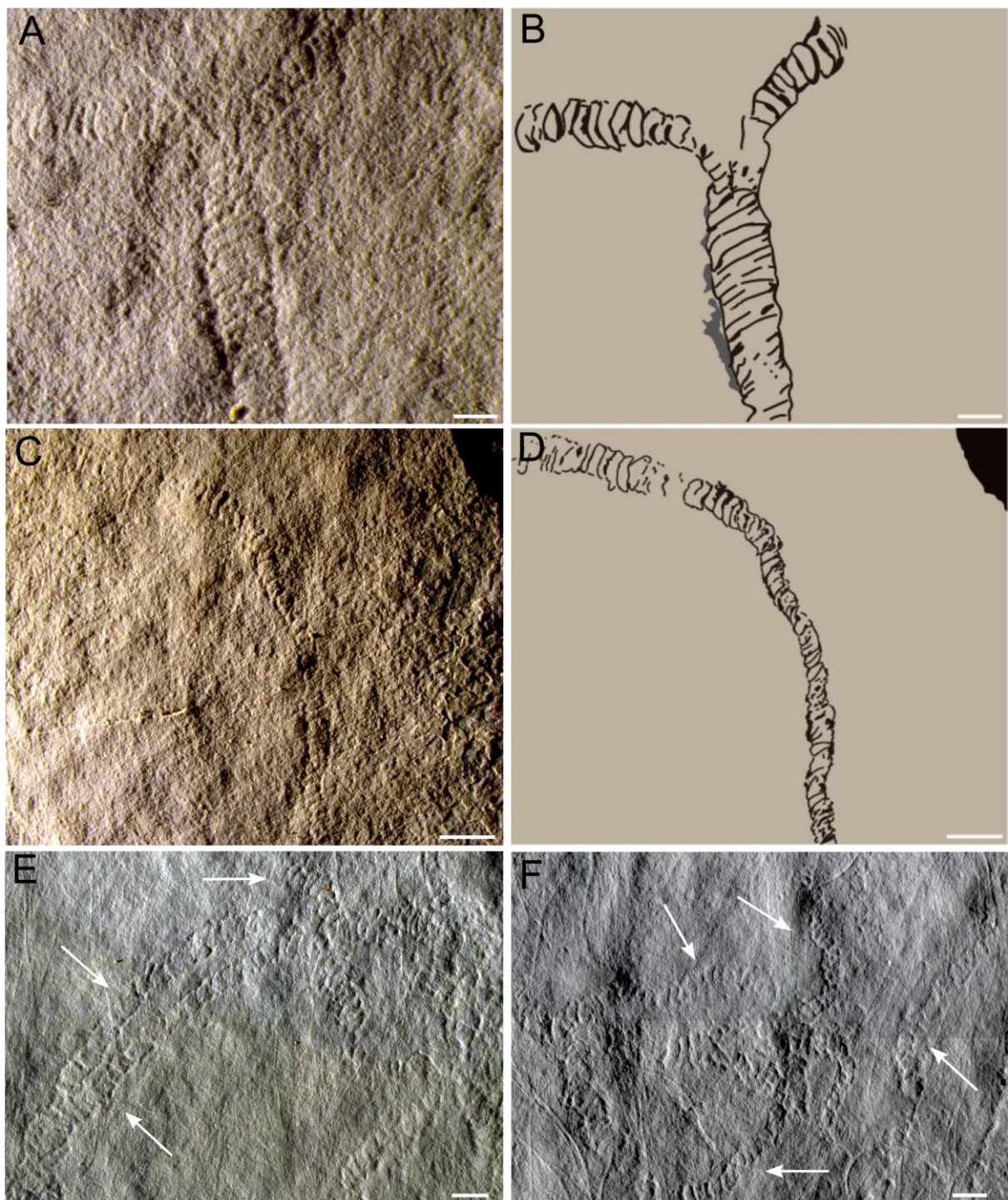


**Fig. 5.** *Palaeopascichnus* from the Itajaí Basin (CAP/1A–556). A) Specimen in positive epirelief showing bifurcation and a subsequent decrease in width; B) Interpretative drawing of A; C) Positive epirelief with *Palaeopascichnus* showing a gradual increase in width; D) Interpretative drawing of C. E-F) Several individuals occurring at the same level together with microbial filaments. Scales: 1 mm (A, B, E-F); 2 mm (C, D).

*Palaeopascichnus* is still considered to have unclear biological affinities, but it is well established as a body fossil (Antcliffe et al., 2011). Its chambered morphology has prompted previous comparisons with the modern group of giant protists Xenophyophora (Seilacher et al., 2003; Kolesnikov et al., 2018). Interestingly, this fossil is a long-ranging and, possibly, generalist organism (Kolesnikov et al., 2018), a common constituent of both the Avalon and White Sea Assemblages (Muscente et al., 2018), but also reported from deposits near the Ediacaran/Cambrian transition (Kolesnikov and Bobkov, 2019). Recent works have suggested that it may also represent one of the earliest skeletal (agglutinated) organisms (Kolesnikov et al., 2018). The presence of this fossil not only corroborates an Ediacaran age for the IB but also extends the paleobiogeographic range of this important taxon.

*Aspidella* specimens ( $n = 11$ ) are preserved in negative to flat epirelief. These fossils mainly exhibit two morphotypes: convex and type morphs (following Gehling et al., 2000). The first morphotype is represented by convex ellipsoidal discs ( $n = 4$ ) in positive hyporelief, with maximum diameters of ~10–14 mm and minimum diameters of ~9–12 mm. These forms present fine concave edges delimiting the convex disc. At the center, the disc shows a convex circular region (central boss) also delimited by a fine concave ring (Fig. 6A–B). One sample shows two conjoined specimens of the convex morph (Fig. 6C), while another presents an attached stalk-like structure (Fig. 6F–G). This morphotype was found within the thin-bedded rhythmite of outcrop A16 (upper slope setting). The type morphs ( $n = 4$ ) were found in delta front and upper slope deposits and are preserved in negative epirelief; they are defined by an ellipsoidal disc (5–14 mm in diameter) with a concave external zone cut by radial lines that converge into a central ridge (Fig. 6D–E, H). Two of these specimens (Fig. 6H) were previously described as *Parvancorina* (Rosa, 2005). Additionally, two discs, similar to the intermediate forms described by Burzynski and Narbonne (2015), are

characterized by faint ellipsoidal impressions with maximum diameters of 15–22 mm and minimum diameters of 10–17 mm (e.g., Fig. 6I).

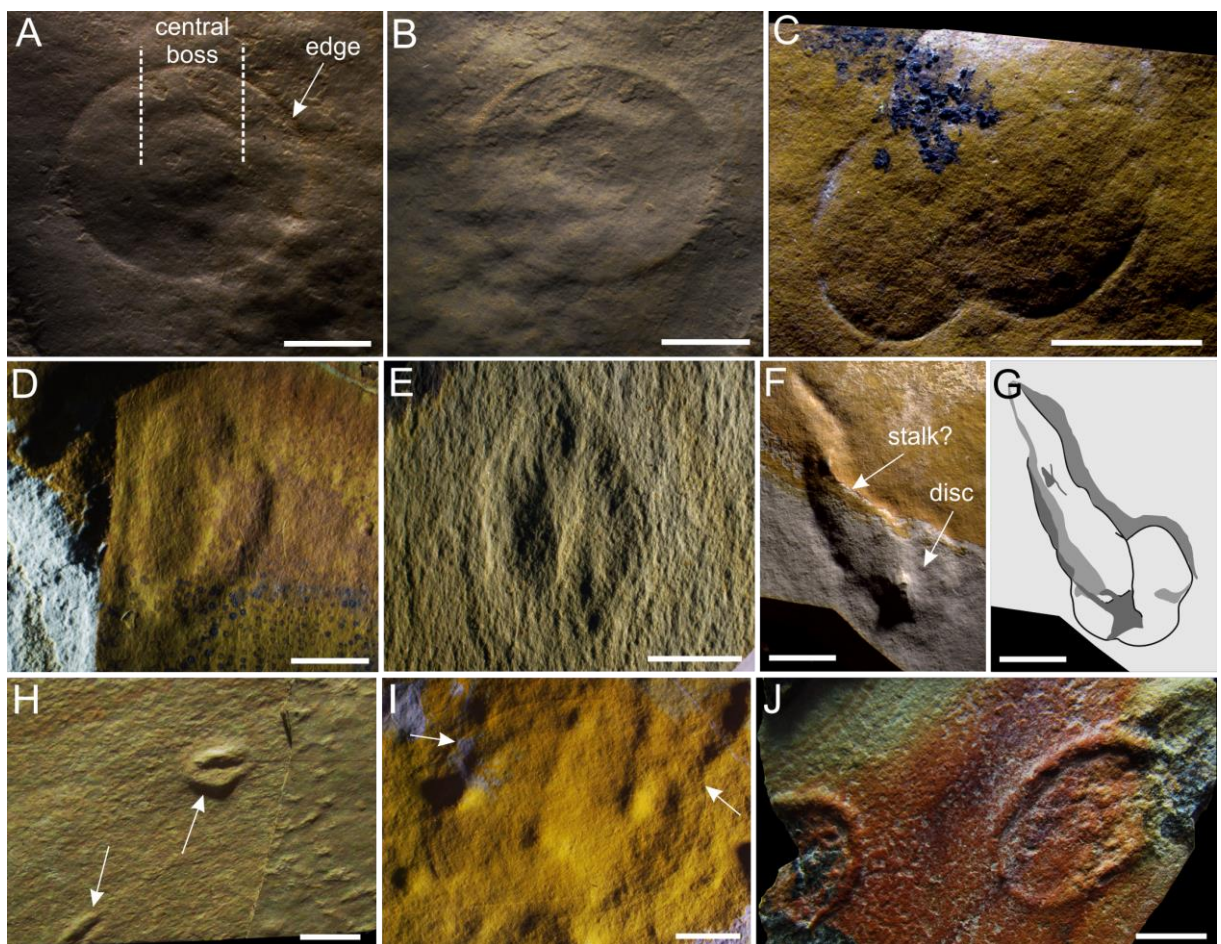


**Fig. 6.** Discoidal fossils from the Itajaí Basin. A) The convex morph of *Aspidella* in positive hyporelief, showing the central boss and concave edges (CAP/1A–549); B) counterpart of sample in (A). C) Conjoined specimens of the convex morph (CAP/1A–550); D–E) The type morph of *Aspidella* (arrows) from upper slope (D) and delta front deposits (E, H) (CAP/1A–878; CAP/1A–551); F) A disc (white arrow) in positive epirelief with possible attached stalk (black arrow) (CAP/1A–877); G) A schematic drawing of (F); H) Possible type morph of *Aspidella*, previously interpreted as *Parvancorina* (CAP/1A–552); I) Faint impression of a discoidal morphology (CAP/1A–555); J) *Nimbia* specimens from distal delta front deposits (CAP/1A–553). Scales: 5 mm (A–F, G, I); 10 mm (H, J, K).

Discoidal forms are one of the most common morphotaxa found in Ediacaran rocks, but there are also reports of similar fossils in rocks of different ages (Nagovitsin

et al., 2008; Burzynski et al., 2020). Although usually regarded as the holdfasts of Ediacaran fronds (Gehling et al., 2000; Tarhan et al., 2015), other interpretations, including microbial colonies and fluid escape structures, have been made for some occurrences (Grazhdankin and Gerdes, 2007; Menon et al., 2016). Thus, studies dealing with discoidal impressions should evaluate these different possibilities. However, distinguishing the origin of these structures can be difficult, and several occurrences may still be considered problematic (e.g., Inglez et al., 2019).

In the IB, at least for the *Aspidella* morphs, our results showed that these fossils could be related to the basal portions of complex macroscopic forms (e.g., frondose organisms). For instance, one specimen preserved in positive epirelief showed an attached stalk-like structure (Fig. 6F–G) that could represent the stalk of a macroscopic frond-like organism. This structure greatly differs from the filamentous fossils described below, both by its larger size and tapered nature. Tool marks are an unlikely origin, since the observed feature is preserved in positive epirelief. Additionally, load casts were not seen in these beds, and their usual mode of occurrence (positive features on the sole of beds) differs from our case. Alternatively, another possibility is the formation by rolled-up mats, which could explain the positive epirelief of the structure. However, it is intriguing that this form appears to be associated with a disc.

Polished sections of *Aspidella* showed no evidence for fluid escape structures (Fig. 7). In some samples, convolute laminations are present, but an undisrupted layer of fine-grained sand just below the fossil suggests that the soft-sediment deformation had no influence on the morphology of the disc (Fig. 7C–D). Thus, it is unlikely that these forms represent fluid/gas escape features or abiotic geologic features. It is also questionable whether the fossils could represent microbial colonies, since they lack several concentric rings, sharp radially arranged furrows and filaments, all of which have been suggested to be evidence for a microbial colony origin (Grazhdankin and Gerdes, 2007).

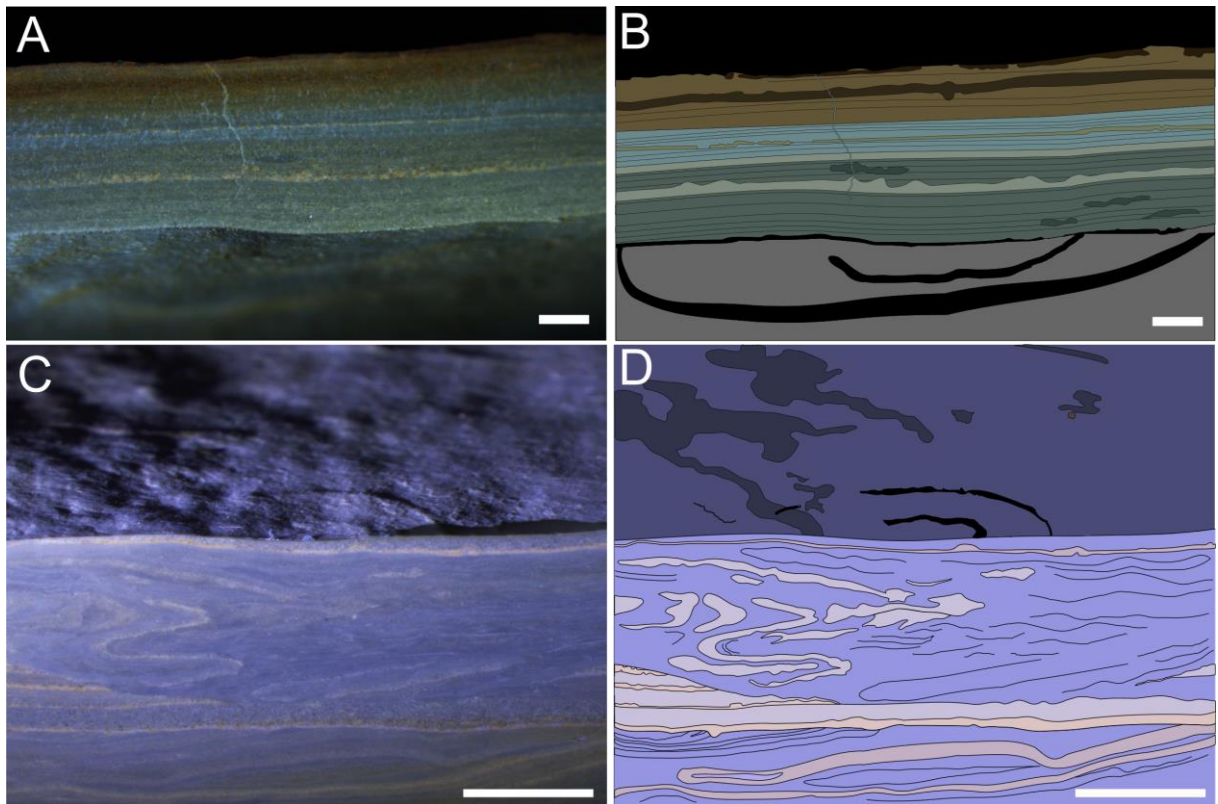


**Fig. 7.** Polished sections of *Aspidella*. A) Vertical section through positive hyporelief showing undisturbed laminations above the specimen; B) Schematic drawing of A; C) Section of epirelief demonstrating an undisturbed sandy layer below the specimen; D) Schematic drawing of C. Scales: 1 mm (A, B), 5 mm (C, D).

In contrast to *Aspidella*, *Nimbia* ( $n = 18$ ) is found only in the distal delta front deposits (outcrop AF236). These discoidal impressions are characterized by ellipsoidal rings in positive epirelief (Fig. 6J). The discs present major axes of 24–30 mm and minor axes of 16–19 mm, with annular ring widths of 1.5–3 mm. The annular ring surrounds a nearly flat surface, which presents only faint circular protrusions (Fig. 6J). One sample separated for thin sectioning did not exhibit fluid escape features or wavy-crinkly lamination.

Recent work (Liu et al., 2013a) has suggested a microbial origin for *Nimbia*, an acceptable interpretation based on its similarity to modern ring structures constructed by the cyanobacteria *Lyngbya aestuarii* at Laguna Mormona (compare our Fig. 6J to Fig. 4E of Horodyski (1977)).

## 6. Three-dimensional microbial mats and MISS

### 6.1. Reticulated tufted mats

Most of the occurrences of microbially related structures represent reticulated tufted mats, which consist of millimetric pinnacles (or cones) connected by ridges (Fig. 8A–B). The centers of the pinnacles are circular to elliptical in horizontal sections (Fig. 8B, D), with a mean width of 1.7 mm ( $n = 37$ ). The ridges present a mean width of 0.4 mm ( $n = 37$ ) and are slightly larger in the proximities of the pinnacles and gradually decrease in width farther from them. These well-preserved tufted mats often co-occur with micrometric microbial filaments (Fig. 8E–F).

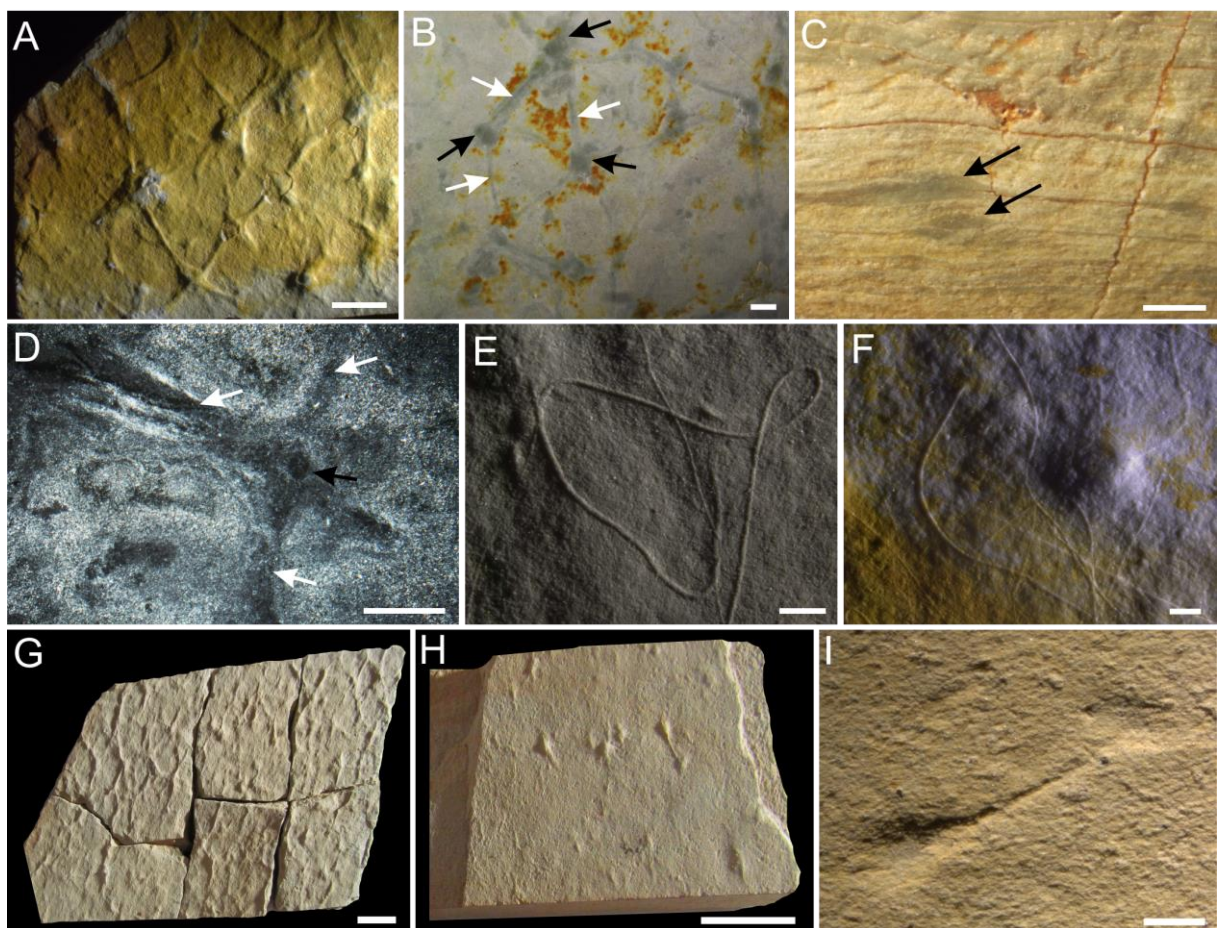


**Fig. 8.** Hand samples and thin sections of microbial tufted mats. A) Bedding plane views of three-dimensional microbial tufts (CAP/1A–559); B) Hand sample polished parallel to the bedding plane, revealing the preservation of the microbial mats by an argillaceous material darker than the surrounding rock (CAP/1F–03). Note the sectioned pinnacles (black arrows) and the ridges connecting them (white arrows) (CAP/1F–03); C) Transverse section of a hand sample, indicating the presence of

small elevations that correspond to the cones of the mat (arrows) (CAP/1A–560); D) Thin sections made parallel to the bedding plane, highlighting the three-dimensional morphology of the microbial mats, with ridges (white arrows) and pinnacles (black arrows) (CAP/1F–03). (E–F) Micrometric filaments often found associated with the first stages of formation of the tufted mats (CAP/1A–561; CAP/1A–555). (G–I) Reticulated tufts preserved as simple surface morphologies (CAP/1A–570; CAP/1A–571). Scales: 5 mm (A); 1 mm (B–C, E–F, I); 0.5 mm (D); 10 mm (G, H)

This type of microbial mat is abundant in the thin-bedded rhythmites (upper slope), where *Aspidella* and *Palaeopascichnus* also occur (outcrop A16), as well as in the distal delta front deposits. Specifically, in the upper slope facies, these fossilized tufted mats are three-dimensionally preserved, a feature clearly evident in polished and thin sections (Fig. 8B, D). The presence of Si, Al, K, Fe and Ti demonstrated by SR- $\mu$ XRF point analysis (Supplementary Fig. 3) points to an aluminosilicate composition with associated titanium phases. In contrast, the tufted morphologies in the distal delta front deposits (Fig. 8G–I) are preserved only as impressions and are thus similar to the typical preservation of MISS.

Samples also show different degrees of interconnection of the centers. Small domes with incipient connections (Fig. 9A–B) gradually transition to more reticulated and interconnected mats (Fig. 10).

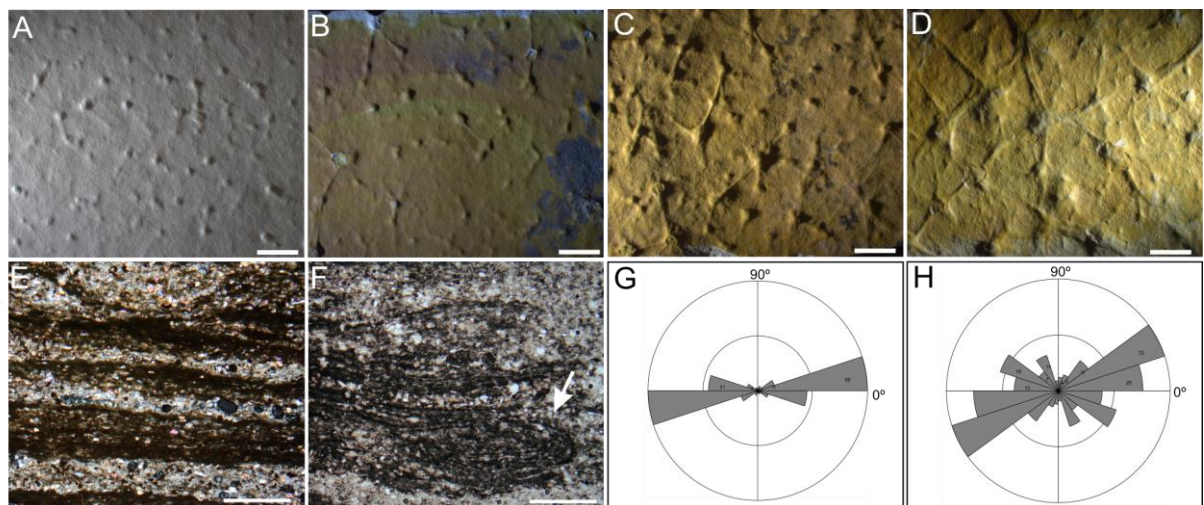


**Fig. 9.** A–B) Different stages of formation of tufted microbial mats (CAP/1A–567; CAP/1A–568; CAP/1A–569; CAP/1A–559). E–F) Wavy-crinkly lamination with abundant floating grains (CAP/1F–08), and evidence of soft deformation (B) (CAP/1F–

09); G) Orientation of grains inside microbial laminae ( $n = 125$ ); H) Orientation of grains in the siltstone-sandstone layers ( $n = 130$ ). Scales: 5 mm. (A–E); 1 mm (E–F).

Wavy-crinkly laminae with evidence of cohesive behavior and disrupted laminations are also found associated with these tufts in thin sections (Fig. 9E–F). Horizontally oriented floating grains are observed within the wavy-crinkly laminations (Fig. 9G–H).

The three-dimensional preservation of the Itajaí Group reticulated mats has yielded good retention of the original morphology, apparently showing different degrees of developmental growth, from isolated domes through more interconnected samples to a fully established reticulated tufted mat (Fig. 9). Similar formative processes have been observed in recent photosynthetic reticulated mats (Shepard and Sumner, 2010). For instance, studies have associated the genesis of tufts and reticulated patterns with gradients in oxygen (Sim et al., 2012) and undirected filament gliding and collision, followed by their alignment and clumping (Shepard and Sumner, 2010). Conspicuously, the afore mentioned processes of the origin and development of tufted mats (Walter et al., 1972, 1976; Flannery and Walter, 2012) may also account for the morphologies recorded in the Itajaí biota (Figs. 8–9). Additionally, it is worth noting that IB tufts are very similar to modern microbial tufts (see Fig. 2-1-4 in Schieber et al. (2007)) constructed by filamentous cyanobacteria, such as *Lyngbya aestuarii* (Horodyski, 1977) and *Microcoleus chthonoplastes* (Schieber et al., 2007).

Likely due to the peculiar three-dimensional preservation (Fig. 8) of the tufted mats, these morphologies were first thought to represent the preserved remains of *Chancelloria* (Da Rosa et al., 1997; Leipnitz et al., 1997; Paim et al., 1997). However, the resemblance is only superficial since the IB structures do not present any boundaries related to a body outline, and the “sclerites” (i.e., pinnacles and ridges) lack the regular morphology observed in true *Chancelloria* sclerites. In contrast, these features cover the whole bedding plane surface and are irregular in the number of ridges that depart from the pinnacle.

Some variations in the morphology of these tufted mats can generate a false dumbbell appearance, which led to the interpretation of these features as the ichnogenus *Diplocraterion* (Netto and Rosa, 1997). However, we observed that these

structures are characterized by millimetric domes interconnected by more than two strands (Fig. 10) and are similar in size to the reticulated microbial mats described above. Micro-computed tomography ( $\mu$ CT) analysis demonstrated no deformation in the laminations beneath the structures (Fig. 10C). This absence of *spreiten* morphologies in microtomographic investigations (Fig. 10C), combined with the interconnection of more than two spherical structures (Fig. 10D–E), suggests a network of interconnected tuft pinnacles and not a true dumbbell morphology related to a vertical shift in sediment.

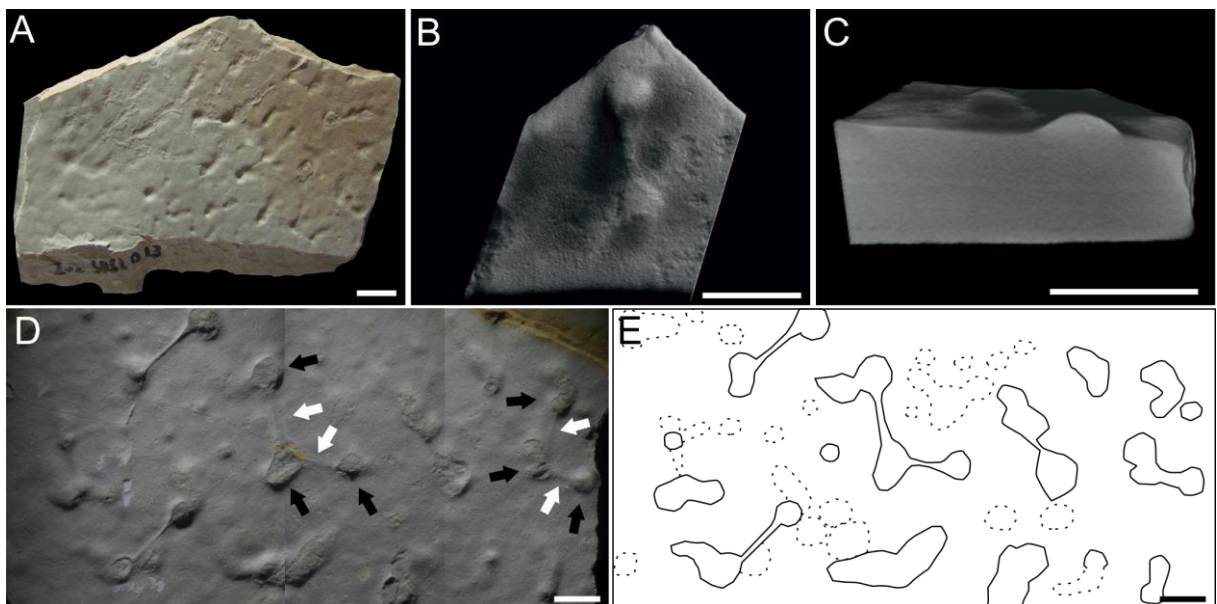


**Fig. 10.** Tufted microbial mats resembling dumbbell morphologies (CAP/1A–579). A) Hand sample with interconnected dumbbell forms; B)  $\mu$ CT image of the surface of a sample with a dumbbell shape; C) Transverse section of the  $\mu$ CT reconstruction; D) Hand sample demonstrating the presence of more than two spherical structures (black arrows) interconnected by strands (white arrows); E) Schematic representation of D. Scales: 10 mm (A); 5 mm (B–E).

The filamentous impressions occasionally occurring associated with the reticulated mats were also previously interpreted as trace fossils (i.e., *Helminthoidichnites*; Netto, 2012). Instead, our observations suggest that these fossils represent exquisitely preserved microbial filaments. Their body fossil nature is evident by the overlap of individuals (Fig. 8E–F), instead of a cross-cutting interaction that would be expected in horizontal trace fossils. For the same reason, these filaments are

unlikely to be tectographs (e.g., Seilacher et al., 2000). Therefore, no strong evidence indicates the presence of ichnofossils in the IB – a situation that is similar to other deposits with analogous ages (but see references Liu et al., 2010 and Liu et al., 2015 for putative trace fossils in the Avalonian biota). Abundant and undisputable trace fossils appear later in the White Sea Assemblage (Droser et al., 2006).

## 6.2. *Arumberia*-type microbial mats

Another type of 3-D preservation of microbial mats in the Itajaí Group is *Arumberia* (Fig. 13). This fossil consists of an almost parallel series of filamentous structures arranged horizontally on the bedding planes (Fig. 11A–C). Lateral connections are observed. The width of the filaments can vary along stratigraphic levels, but they occur mainly in two size ranges: 0.5–0.8 mm (mean = 0.52, n = 16) and 0.9–3 mm (mean = 1.6, n = 40). Extremities are not observed, but dichotomous ramifications of the filaments are more abundant in the smaller type than in the larger one. Most of the structures are three-dimensionally preserved in a manner similar to that described above for the reticulated tufts (Fig. 11D), and thin sections indicate that the filaments exhibit ellipsoidal or domal outlines with convex tops in cross-section (Fig. 11D). The base of the mats presents a more horizontal surface than the top, apparently following the bedding plane (Fig. 11D). *Arumberia* appears both in the distal delta front and upper slope settings. Orientation measurements of *Arumberia* crests in the first depositional setting show a preferential direction (Supplementary Fig. 4) that is comparable to previously reported paleocurrent readings for the same depositional sequence (Fonseca, 2004).

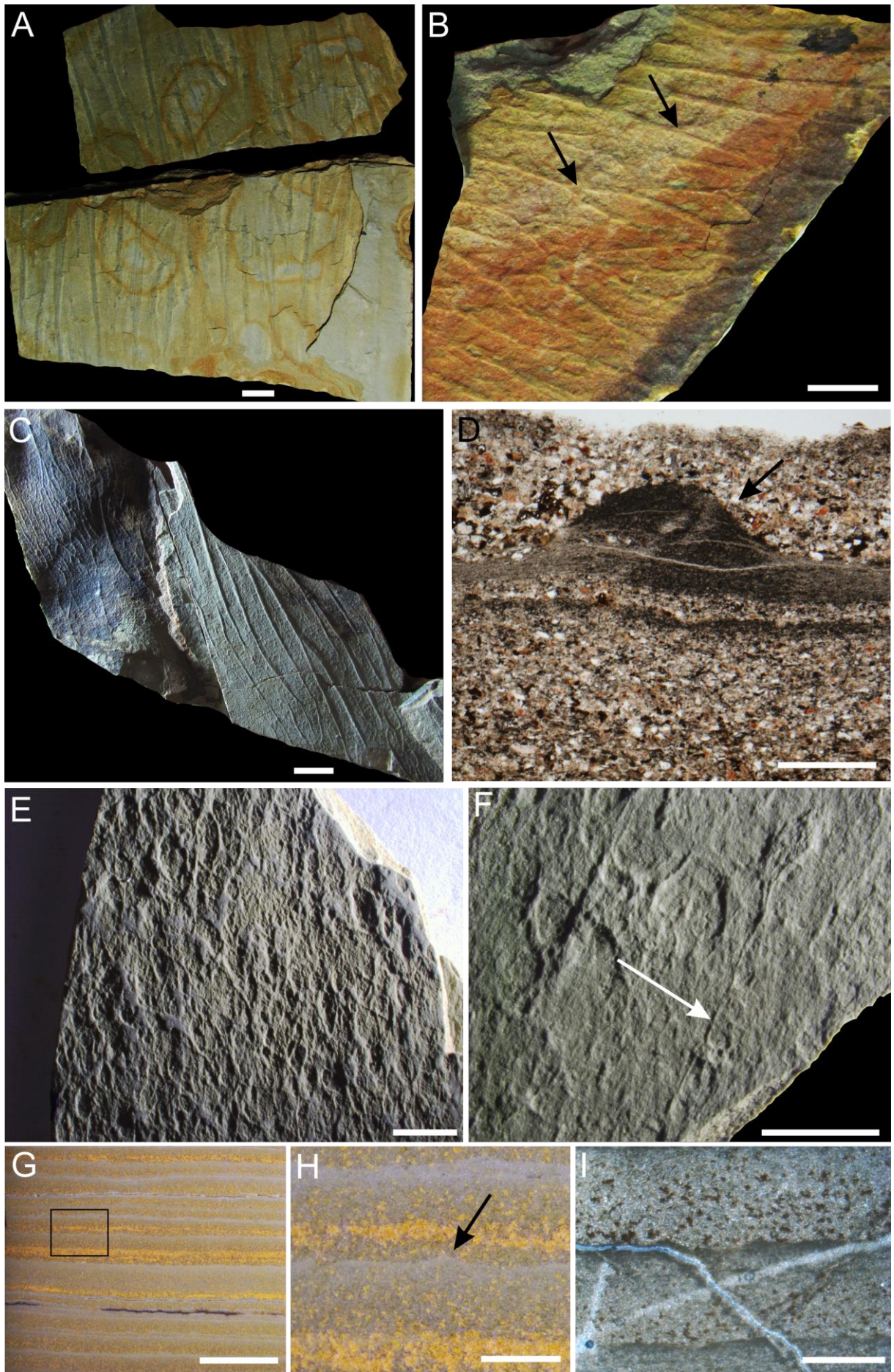


**Fig. 11.** Arumberia mats and simple wrinkled surfaces. A–C) 3-D preserved specimens on a bedding plane (as viewed from above) exhibiting abundant linear crests and common ramifications (arrows) (CAP/1A–563; CAP/1A–564; CAP/1A–566); D) Thin section (in transmitted light) of a 3-D preserved Arumberia in transverse sections showing the domal outline of the crest and the lateral connections (CAP/1F–05). E–F) Hand samples with wrinkles on top of the beds (CAP/1A–572; CAP/1A–575). The white arrow highlights a filamentous structure; G) Transverse section and polished surface of a hand sample with wrinkles (CAP/1A–576); H) Enlargement of the rectangle in (G), presenting a ridge in cross-section (arrow); I) Thin section of wrinkles demonstrating little variation in grain size (mostly clay and fine silt) between the laminae. Scales: 10 mm (A–C); 0.5 mm (D); 5 mm (E–G); 1 mm (H–I).

The biological affinity of Arumberia is still considered controversial (Davies et al., 2016) since it has been interpreted as a body fossil (Glaessner and Walter, 1975), an abiogenic structure resulting from turbid flow (Brasier, 1979), and the product of scouring currents on a microbial mat surface (McIlroy and Walter, 1997). Our three-dimensional specimens preserved by aluminosilicates presenting laterally continuous connections in perpendicular sections corroborate a mat morphology, thus supporting the third interpretation.

Remarkably, the similar orientations between the crests of Arumberia (Supplementary Fig. 4) and sedimentary structures (Fonseca, 2004) in the delta front deposits of the IB indicate that currents indeed could have played a role in the formation of this peculiar morphology. Additionally, its occurrence in the delta front deposits suggests that this structure most likely represents the growth of photosynthetic microbial communities. Arumberia-like mats have recently been observed in modern photosynthetic mats (Kolesnikov et al., 2017).

### 6.3. Simple wrinkled surfaces

Simple wrinkles are the most common surface structures in the delta front and prodelta sediments of the IB (Fig. 11E–I). They are defined by simple reticulated textures formed by a network of intertwined convex ridges (0.2 – 1.8 mm). In contrast to the tufts, these wrinkles do not present either pinnacles or a more organized reticulated fabric. Some samples display rare associated submillimetric filaments (Fig.

11F). The hyporelief of the reticulated structures is characterized by convex bulbous polygons and narrow concave depressions, similar to the so-called elephant-skin texture. In transverse sections and thin sections, the wrinkles appear as crinkly laminations alternating with iron oxide-rich laminae (Fig. 11G–I). There are no significant changes in the grain size between the laminations.

These wrinkles are interpreted to represent surface sedimentary features related to mat growth, as evidenced by the crinkly laminae in thin sections and their resemblance to biolaminites in vertical sections (Fig. 11G–I). The origin by loading can be ruled out by the homogeneous grain size (mostly clay to fine-grained silt) at the interfaces where the wrinkles occur (Fig. 11I). Additionally, their association with putative microbial filaments (Fig. 11F) further supports a microbial mat interpretation. These simple wrinkles differ from the reticulated tufts by their more irregular arrangement and lack of pinnacles. It is unlikely that they represent a taphonomic variation of the latter because gradational morphologies were not observed and the presence of fine structures such as filaments suggests that some surfaces were relatively well preserved.

#### *6.4. Small discoidal structures*

Simple and abundant discoidal protrusions were observed on top of the beds (positive epirelief) in outcrop AF236 and near the Arumberia level, although the two are seldom seen in the same bedding plane. These ‘pimples’ exhibit circular to ellipsoidal outlines, millimetric diameters (1.2 – 3.7 mm), and heights of ca. 0.5 mm (Fig. 12). Some specimens show circular depressions in the center of the pimple (Fig. 12D), which is due to unequal partitioning of part and counterpart, leaving portions of the structure on the hyporelief (Fig. 12F). The counterparts (sole of the beds) are characterized by negative hyporelief circular impressions (Fig. 12F–G, K). Transverse sections of hand samples show no pipe or fluid escape structures, but some pimples present higher concentrations of clay minerals in the upper portion of the structure (Fig. 12H–I) or even in the whole pimple (Fig. 12I).

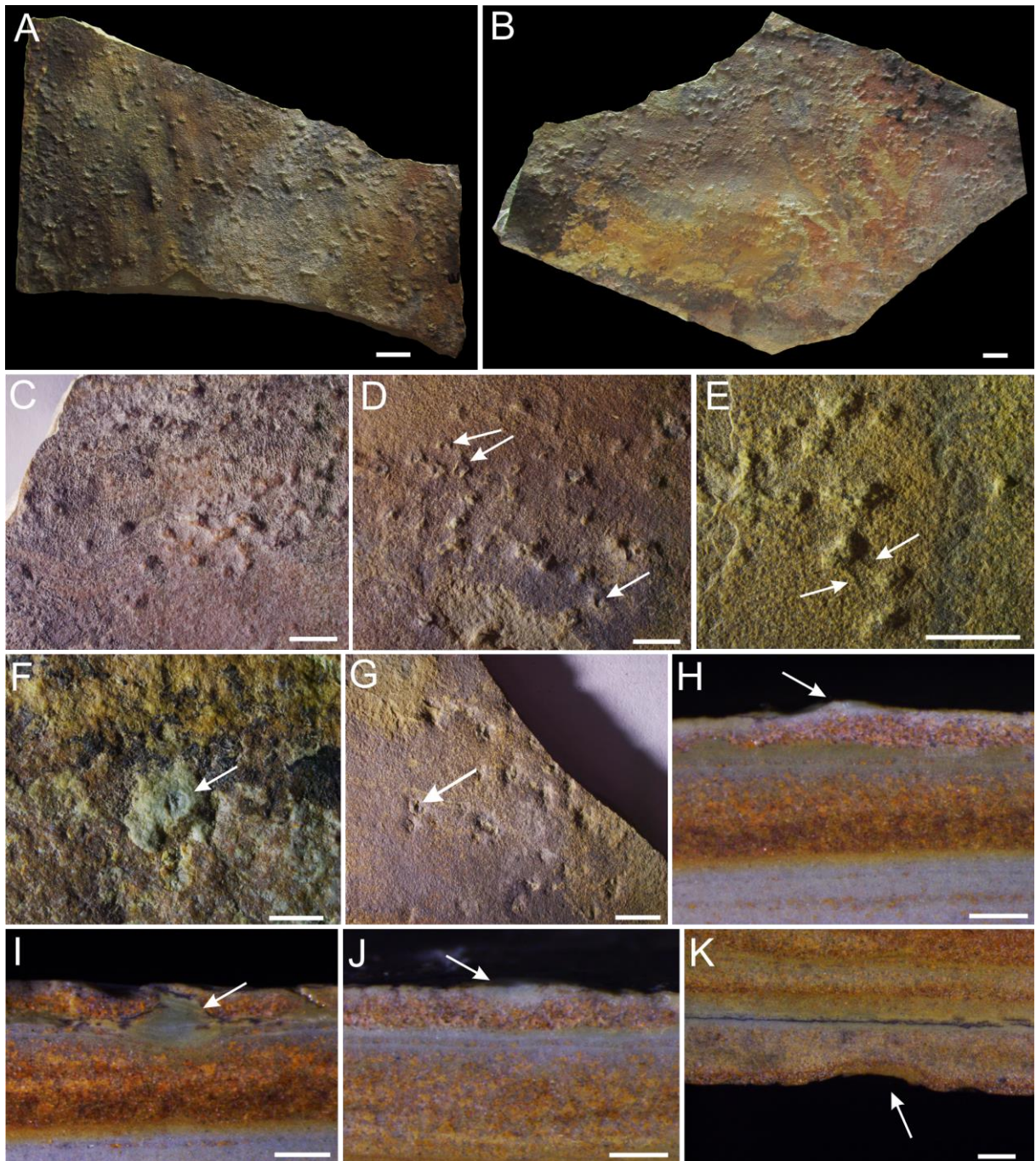


**Fig. 12.** Pimples from the Itajaí Basin. A–B) Hand samples with a profusion of specimens on top of the beds (positive epirelief) (CAP/1A–577; CAP/1A–578); C–E) Close-up of the structures in epirelief, showing depressions at the centers of some individuals (white arrows in D) and connecting ridges (white arrows in E) (CAP/1A–578); F) Portion of a pimple left on the bottom of the bed (CAP/1A–578); G) Hyporelief with small pits, corresponding to the counterpart of the pimple (CAP/1A–578). The white arrow marks the presence of portions of the pimple left behind after separation of the sample; H–J) Transverse sections of the pimples in epirelief (CAP/1A–577). Note

the concentrations of argillaceous white material (white arrows). K. Transverse section of hyporelief (CAP/1A–577). Scales: 10 mm (A, B); 5 mm (C–E, G); 0.5 mm (F); 1 mm (H–K).

Simple and small discoidal structures are commonly observed in Meso-Neoproterozoic deposits (McIlroy et al., 2005; Callow et al., 2011; Menon et al., 2016), and a variety of taxonomic names (e.g., *Beltanelliformis brunsae*, *B. minutae*, *Inrites punctatus*, *Medusinites* aff. *asteroides*, and *Rameshia rampurensis*; see McIlroy et al. 2005 and Kumar and Pandey 2008) or descriptive terms (e.g., small discoidal forms, mounds, domes, and pimples; see Menon et al. 2016 and Callow et al. 2011) have been used to encompass morphological variations of these forms. Thus, following the same pattern as for other discoidal impressions, controversies arise regarding their biological affinities. Recent works have presented strong evidence that some are the result of fluid escape and subordinate load structures, which occurred in a substrate dominated by microbial mats (Menon et al., 2016). In terms of morphology and size, IB small discs are more similar to the pimples reported by Menon et al. (2016) and Callow et al. (2011).

However, regarding the IB pimples, we did not observe pipes or disturbed laminations (Fig. 12H–K). Furthermore, they are preserved in positive epirelief, similar to the 1 Ga. pimples reported by Callow et al. (2011) but unlike the Ediacaran negative epirelief pimples of Menon et al. (2016). Strand connections observed between some IB specimens also argue against a fluid escape origin, suggesting similarities between the pimples and the stages of formation of microbial tufted mats. It is interesting to note that Arumberia is commonly reported to co-occur with small round impressions in positive epirelief (e.g., Bland, 1984; Callow et al., 2011; Kumar and Ahmad, 2014; Kumar and Pandey, 2008), as is the case in the IB. Therefore, we suggest that these forms represent different stages of formation of microbial surfaces and/or microbially bound surfaces under different energetic systems.

## 7. Problematic forms

### 7.1. Linearly arranged pits

These structures are characterized by impressions of serially arranged pits on the sole of the bed (negative hyporelief) (Fig. 13A–B). Each pit has a subrounded outline, and the diameter varies between 1 and 1.5 mm ( $n = 10$ ). The distances between the centroids of each pit vary between 2.4 and 4.7 mm ( $n = 8$ ). The specimen in Fig. 13A shows faint strings connecting the beads. One sample (CAP/1A-558) exhibits specimens preserved in three dimensions, possibly by iron oxides, as indicated by the higher intensities of Fe in the fossils than in the host matrix (Fig. 13D–G). In addition, there is displacement of sediment around one of the beads (Fig. 13C), suggesting formation prior to the lithification of the rock.

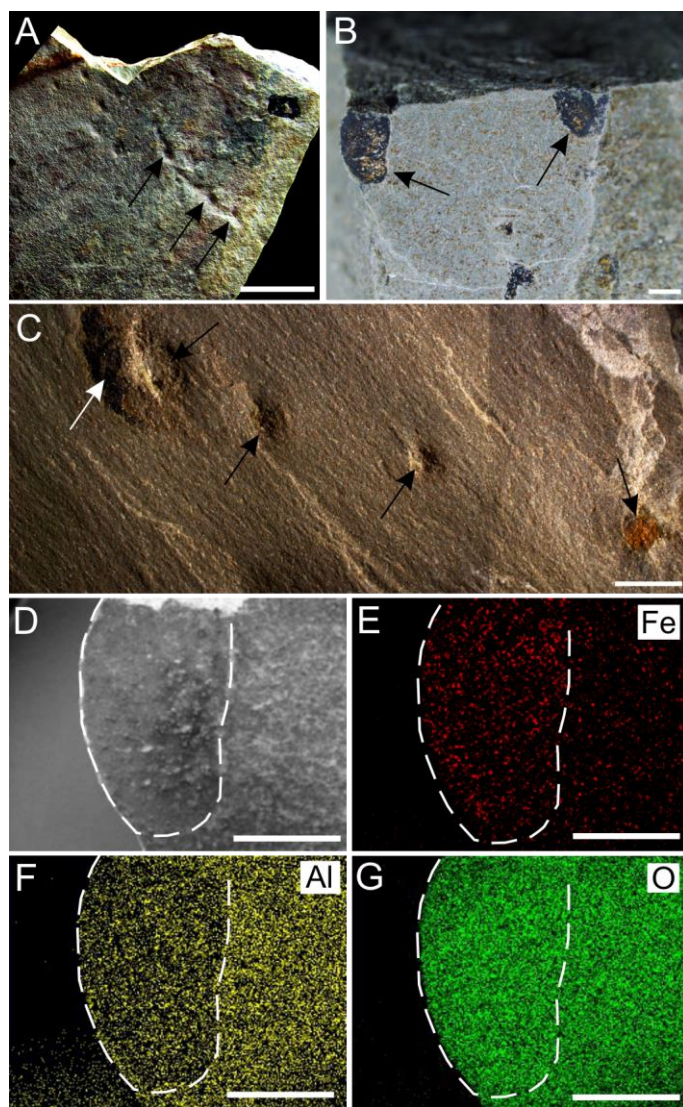


**Fig. 13.** Hand samples and energy-dispersive X-ray spectroscopy (EDS) maps of linearly arranged beads. (A) An impression of negative hyporelief of serially arranged pits (arrows) from the delta front deposits (CAP/1A-553). Note the presence of possible strings in the specimen; B–C) 3-D preservation of beads in transverse section

(C) and in bedding plane view (D) (CAP/1A–558); D–G) Electron image (D) and EDS maps (E–G) of the specimen in (B). Scales: 10 mm (A); 1 mm (B, D–G); 5 mm (C).

In contrast to other body fossils described here, the specimens described as linearly arranged pits are less discernable morphologically. However, their arrangement and the presence of strings connecting some of the circular structures (Fig. 13A) favor a biogenic origin. The morphology and size resemble those observed in the fossil *Horodyskia*. This taxon was defined as impressions of strings of beads, sometimes presenting connecting strands (Grey and Williams, 1990; Calver et al., 2010). However, *Horodyskia* has mostly been reported from Mesoproterozoic deposits, and Ediacaran occurrences, such as those in China (Shen et al., 2007; Dong et al., 2008) and India (Mathur and Srivastava, 2004), are considered controversial (Calver et al., 2010).

Alternatively, these linearly arranged pits could represent a different taphomorph of the pimples, in which bottom currents produced a linear arrangement of the structures. This could be the case for the sample illustrated in Fig. 13A but seems more unlikely for the 3-D forms considering their morphologies. In this sense, these two types of structures may exhibit distinct origins. The preservation by iron oxide also suggests that pyritization may have been the pathway for three-dimensional preservation. Nevertheless, due to an insufficient number of samples and poor preservation, no further interpretations about these structures can be made at present.

## 7.2. Stellate discs

Millimetric discs with submillimetric radial lines (Fig. 14) are present in two different preservation modes: as low relief molds and as flat yellow discs. In the first type, we observed displacement of sediment near the border of one of the discs. Stereomicroscopy and SEM investigations of the yellow discs showed the presence of cubic pseudomorphs of pyrite (Fig. 14G) and submicrometric star-shaped crystals, respectively (Fig. 15). EDS mapping demonstrated that the intensities of Fe are higher in the discoidal form than in the host rock (Fig. 14J–N).

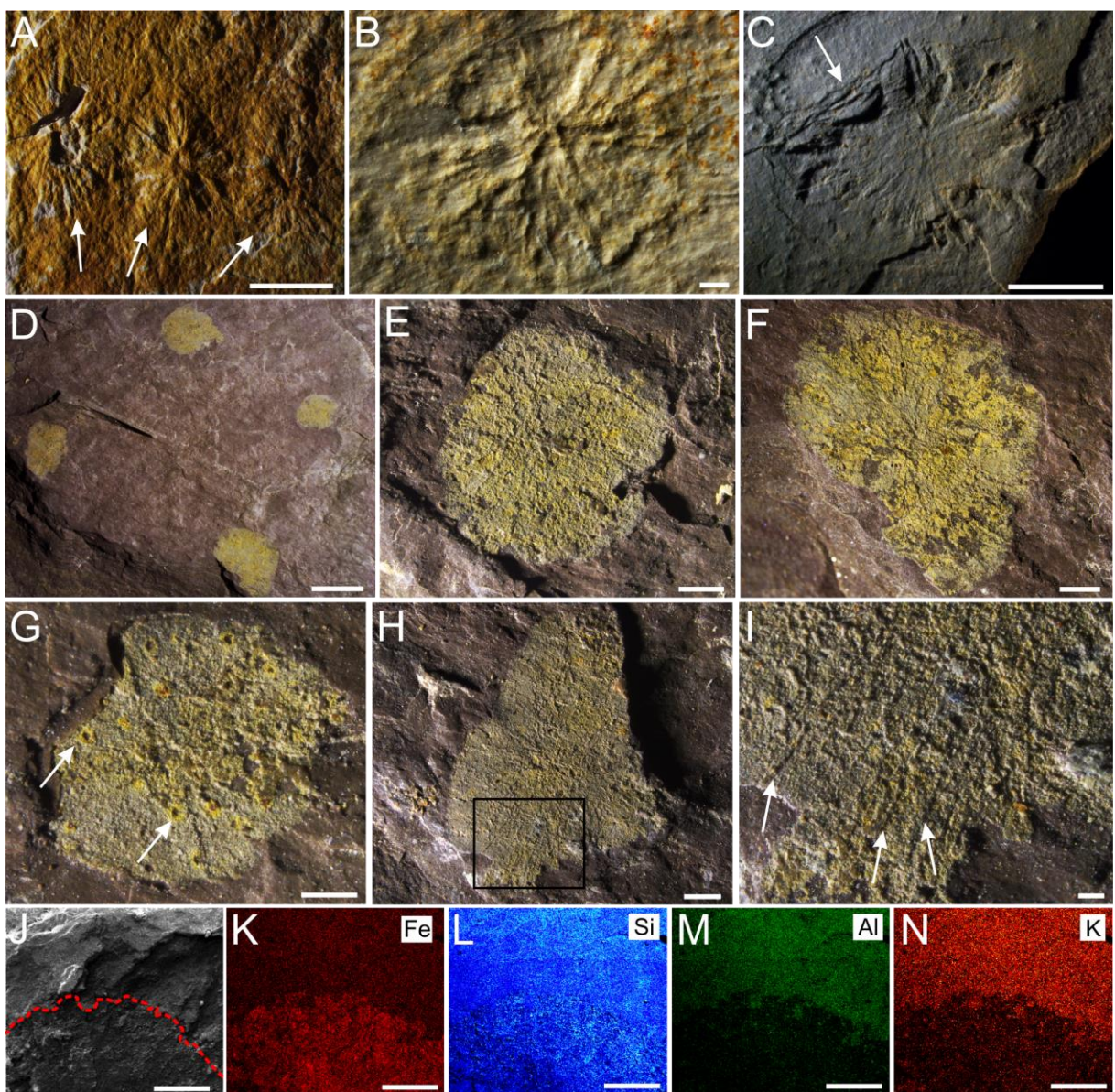


**Fig. 14.** Enigmatic discs from the IB. A. Three juxtaposed specimens of discs with radial lines (positive hyporelief) (CAP/1A–580). B. Radial disc with almost flat relief (CAP/1A–581). C. Irregular outline of one radial disc, with evidence of sediment displacement (white arrows) (CAP/1A–582). D–I. Flat, yellow discs with scarce radial crests (white arrows in I) and cubic crystals (white arrows in G) (CAP/1A–583). J–N. Electron image and EDS maps of a yellow disc (below the red line) (CAP/1A–584). Scales: 1 mm (B, E, F, H); 5 mm (A, C–D); 0.5 mm (G); 0.2 mm (I); 0.4 mm (J–N).

Stellate discs similar to those in Fig. 14A–C were putatively interpreted as body fossils of the Cambrian taxon *Choia* (see Becker-Kerber et al., 2015; Rosa, 2005). However, the similarity of these forms with discoidal inorganic minerals (e.g.,

Seilacher, 2001) makes a biotic origin unlikely. For example, the displacement of sediment near the border of one of the specimens (Fig. 14C) is comparable to the structures that arise from the displacive growth of crystals (Seilacher, 2001). Additionally, the lobed arrangement of the radial grooves in our samples is also similar to the morphology of pyrite (or marcasite) discs (see Fig. 11a, b of Seilacher, 2001), also known as pyrite rosettes (Cloud, 1973), although other minerals can generate similar morphologies. Therefore, these IB discs are considered pseudofossils.

The yellow flat discs are even more likely to represent pseudomorphs after pyrite dissolution (Fig. 14D–I). These discs are similar to those preserved as molds in terms of their size and presence of radially oriented ridges and lobed edges. However, the yellow discs differ from the other forms by their flat nature and iron oxide composition (Fig. 15J–N). The nanometric star-shaped and acicular crystals found in SEM investigations (Fig. 15) corroborate this interpretation since these crystal habits are found in goethite and hematite (Cornell and Schwertmann, 2003). For instance, star-shaped crystals of goethite after marcasite and needles of the latter mineral have been reported filling the chambers of microfossils originally filled with organics (Soliman, 2001). The presence of submillimetric cubes associated with some specimens may also attest to a pyritic origin, as previously noted for other pseudofossils (Cloud, 1973). Hence, in the case of the stellate discs, the originally precipitated marcasite may have been pseudomorphosed into iron oxyhydroxides later in diagenesis. The same mechanism may account for the *Choia*-like molds, but in this case, the original mineral left no discernible geochemical traces.

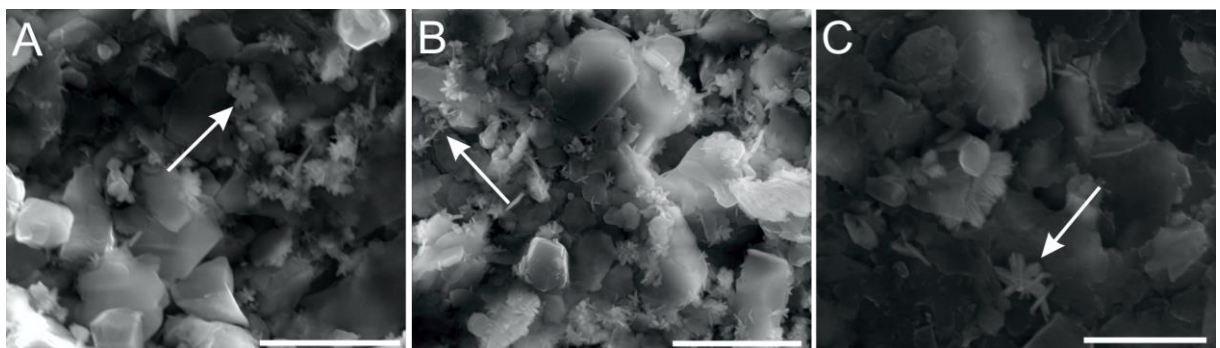


**Fig. 15.** A–B. Nanometric star-shaped and acicular crystals (white arrows) found in great abundance in the yellow discs from the IB (CAP/1A–584). C. Rare star-shaped crystals (white arrow) are also found in the rock matrix. Scales: 5 µm (A, B); 1 µm (C).

The IB discs might have resulted from the activities of sulfate-reducing bacteria using some source of C<sub>org</sub> and subsequently yielded the conditions for pyrite and/or marcasite precipitation (Southam et al., 2001). However, we acknowledge that at best, this interpretation is speculative since the validation of a microbial origin would require the study of isotopic fractionation in undissolved fresh discs.

Interestingly, the size, shape, and preservation of the yellow discs are quite similar to problematic circular remains reported from tillite beds of the Neoproterozoic Maikhanuul Formation (Serezhnikova et al., 2014), albeit the latter have been interpreted as being related to microbial colonies. This hypothesis is based mainly on the fact that the disc diameters are normally distributed and the discs are enriched in titanium and iron and bear nanometric particles that the authors described as “bacteriomorph structures” (Serezhnikova et al., 2014). However, it seems that some of the “bacteriomorph structures” represent the same crystal habit observed in the star-shaped nanocrystals reported here. Considering their Fe composition and similarity to the crystal habits of iron oxides, the Maikhanuul star-shaped submicrometric forms are also more parsimoniously interpreted as small crystals of goethite and/or hematite.

## 8. Discussion

### 8.1. The Ediacaran soft-bodied fossil record in South America

Deposits of Avalonian age bearing Ediacaran macrofossils are usually rare. Specifically, in South America, the Itajaí Group represents one of the earliest records of such a biota. Other Ediacaran fossil assemblages are generally more recent. For example, *Nemiana* was reported from the siliciclastic deposits of the Puncoviscana Formation in Argentina (Aceñolaza and Aceñolaza, 2007; Aceñolaza et al., 2009), but detailed studies employing polished sections to test other possible origins for these simple discs are lacking. In addition, Escayola et al. (2011) proposed an early Cambrian age for this unit, coeval with 540–535 Ma volcanic activity.

Discoidal structures assigned to *Aspidella* have also been reported from the Cerro Negro Formation in Argentina (Arrouy et al., 2016), but these structures occur above deposits containing *Cloudina* fossils (Gaucher et al., 2005); hence, they are

likely to be late Ediacaran to early Cambrian in age. Their interpretation as body fossils also requires further investigation (Inglez et al., 2019).

In Brazil, putative Ediacaran soft-bodied organisms have been described in siliciclastic rocks in the Jaibaras Basin (Barroso et al., 2014). However, later reinterpretations of the geology and fossil content showed that the studied sections are part of the Silurian Ipu Formation (Parnaíba Basin, NE Brazil) (Barroso, 2016; Inglez et al., 2019). Consequently, these fossils are no longer considered to represent Ediacaran taxa (Barroso, 2016).

Finally, possible body fossils (*Aspidella*, *Intrites*, and *Sekwia*) have been described in the Camaquã Basin (southern Brazil), mostly in the ~559–540 Ma Santa Barbara Allogroup (Netto, 2012), with a maximum depositional age of  $566 \pm 6.9$  Ma (Bicca et al., 2013). However, a microbial mat-influenced origin, such as that described by Menon et al. (2016), cannot be ruled out.

Therefore, the fossil assemblage reported here can be considered the oldest known Ediacaran biota in Gondwana and is associated with indisputable Ediacaran taxa. Although simple discoidal impressions in Ediacaran deposits do not always represent the holdfasts of large macroorganisms, the presence of *Palaeopascichnus* strongly corroborates the Ediacaran age of the deposits, broadening even further the paleobiogeographic occurrence of this important taxon.

## 8.2. The Itajaí Basin in the context of Ediacaran ecosystems

With the exception of a few claims of a shallow paleoenvironment for the Avalon biota (Retallack, 2016), several works have noted that these biological communities developed in deep-marine settings, well below the photic zone (Mason et al., 2013). This conclusion agrees with the scarcity of well-developed MISS in these deposits (Droser et al., 2017). The association of Ediacaran organisms with abundant MISS is well known in the younger White Sea and Nama Assemblages (Gehling and Droser, 2009; Droser et al., 2017), and they may even be involved in the moldic preservation of Ediacaran organisms, according to the death mask model (Gehling, 1999; Liu, 2016).

In contrast to the Avalonian record (Droser et al., 2017), the Itajaí biota occurs within strata that represent shallower conditions (delta front and upper slope deposits) and are also associated with abundant microbially influenced surfaces (Figs. 8–11). In particular, fossils of *Palaeopascichnus* and *Aspidella* found in thin-bedded rhythmites ascribed to an upper slope setting (outcrop A16) occur in association with abundant reticulated tufted mats (Figs. 8, 9). Moreover, it is important to note that both body fossils and microbial surfaces are absent in the deep basin plain deposits in the IB studied thus far. In this sense, the IB may help to understand the early colonization of shallower (distal delta front and upper slope) – possibly photic (abundant microbial tufted mats and MISS) – settings.

Some long-lasting taxa of Ediacaran macroscopic organisms, such as *Palaeopascichnus*, occur in Avalonian and White Sea deposits. This taxon not only had a widespread geographical distribution but possibly also adapted to very different environments: deep-marine and aphotic settings vs shallower and photic settings. Thus, understanding the ecological changes and/or bias in the geological record of the Ediacaran is fundamental to the development of a better picture of the early evolution of macroscopic life and its relation to environmental conditions. The IB offers a unique perspective regarding its age and depositional environments, with a macroscopic biota that, although depauperate, can record the early adaptations to shallower settings by probably generalist organisms such as *Palaeopascichnus*.

## 9. Conclusions

The IB can help to answer important open questions regarding the early evolution of macroscopic benthic communities during the Ediacaran Period. The IB fossil record provides evidence of the first steps of the colonization of shallower environments, possibly within the photic zone. The body fossil assemblage occurs in upper slope and distal delta front deposits associated with abundant and exquisitely preserved microbial mats, including the well-known Arumberia morphology. This situation differs from that observed in the deep-marine Avalonian deposits of Canada and England, where MISS are rarer. The discoidal impressions identified within the *Aspidella* plexus suggest the presence of frond-like macroorganisms. The remarkable presence of the indisputable Ediacaran taxon *Palaeopascichnus* further correlates the

IB with the other Ediacaran deposits and, together with the radiometric dating (ca. 563 Ma), marks this unit as the oldest known occurrence of Ediacaran body fossils in Gondwana.

### Acknowledgments

The authors are grateful for the support of the Fundação de Amparo à Pesquisa do Estado de São Paulo (FAPESP - Grant 2016/01827-4 and Grant 2018/21886-0), the Programa de Pós-Graduação em Ecologia e Recursos Naturais (PPGERN – UFSCar), and the Programa de Pós-Graduação em Geologia (PPGeo – UNISINOS). This work was also supported by La Région Nouvelle Aquitaine. We acknowledge C. Fontaine, C. Laforest for laboratory support at the University of Poitiers. The authors would like to thank the Brazilian Synchrotron Light Laboratory (LNLS-CNPEM) and the Brazilian Nanotechnology National Laboratory (LNNano-CNEPM) for their technical support and for providing infrastructure for the SR- $\mu$ XRF (proposal 20170438; 20171031), SEM/EDS (proposal 21836 and 23684) and  $\mu$ -CT (proposal 20415) analyses. We also thank Petrobras Research Centre (CENPES) for all of their support with the palynological preparation, as well as the technical help of Igor Augusto Nascimento de Almeida and Gilton Braz de Aquino Filho. The authors are also grateful to Laboratório de Ecologia (UFMS), Alan Eriksson and Alêny Lopes Francisco Batista for enabling the stereomicroscope investigation. We thank the Laboratório de Preparação de Lâminas Delgadas of UNISINOS and the Setor de Laminação of UNESP (Rio Claro) for thin section preparation. We thank Fabiano Emmanuel Montoro for assistance with the SEM/EDS, and Gabriel Baréa Barros and Bianca Becker Kerber for their support in field activity. Finally, we would like to gratefully acknowledge all of the help we received from the citizens of Apiúna city during field investigations.

**Supplementary information for “The oldest record of Ediacaran macrofossils in Gondwana (~563 Ma, Itajaí Basin, Brazil)”**

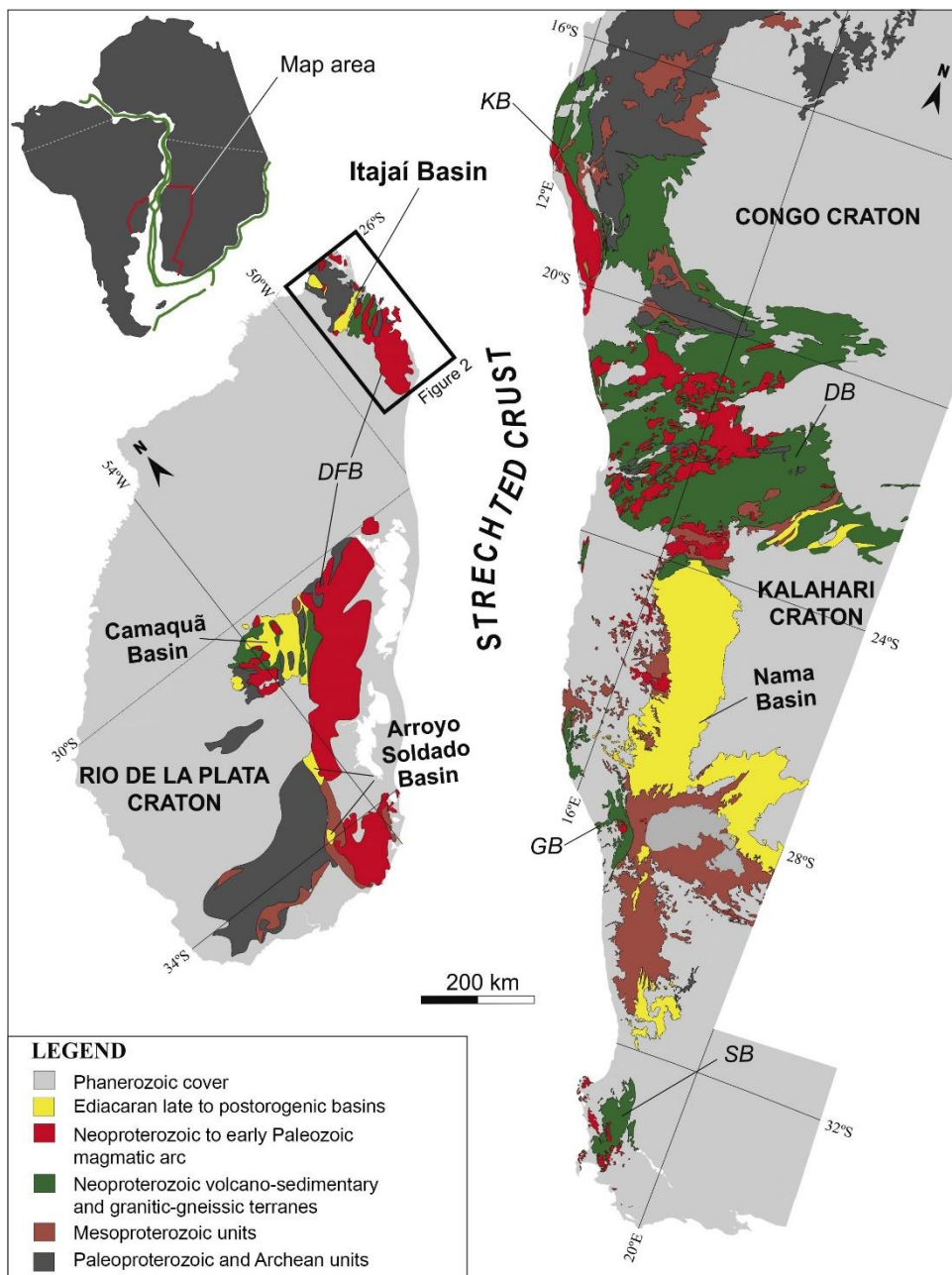


**Figure S1.** Paleogeographic reconstruction of Neoproterozoic belts. The basins with described Ediacaran biota are indicated (modified after Guadagnin et al. 2010). DFB – Don Feliciano Belt; KB – Kaoko Belt; DB – Damara Belt; GB – Gariep Belt; SB – Saldania Belt.

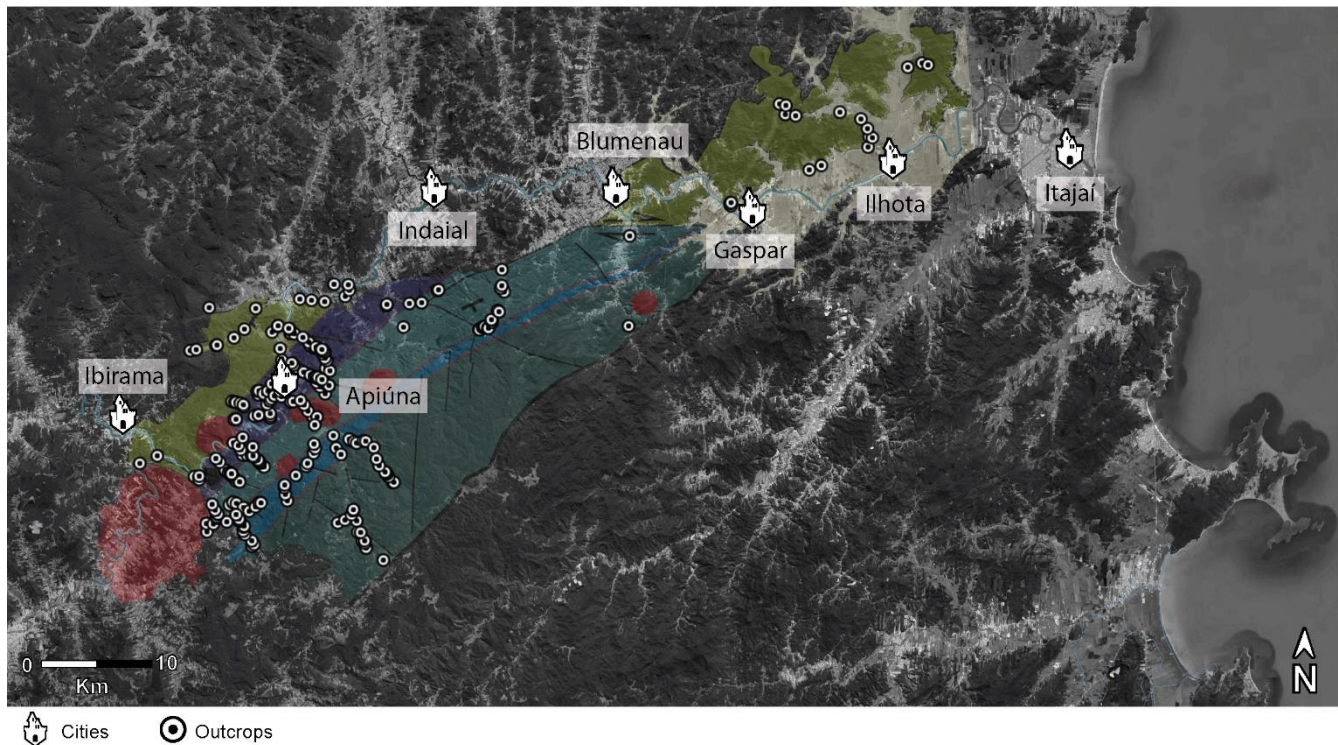


**Figure S2.** Geologic map and localization of all the outcrops prospected during field investigations.

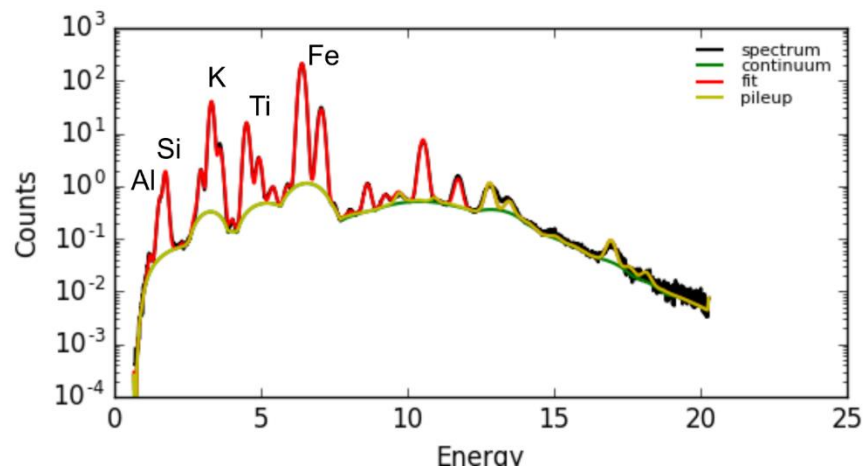


**Figure S3.** SR- $\mu$ XRF point analysis of three-dimensional reticulate mats showing the presence of Al, Si, K, Fe and Ti.

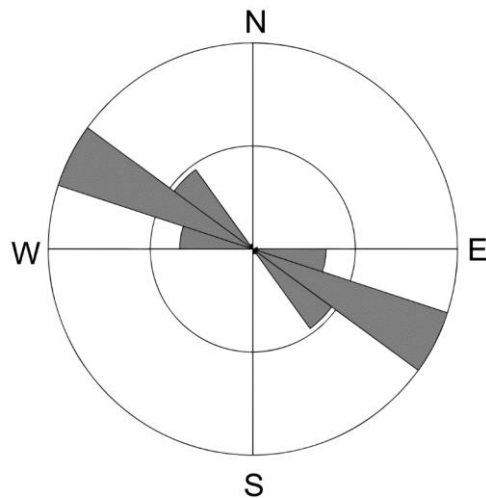


**Figure S4.** Measured orientations of *Arumberia* crests ( $n = 79$ ) recovered in the outcrop AF236.

#### Supplementary Text 1 – Palynological artifacts

Attempts to recover palynomorphs through acid maceration procedures did not yield discernible microfossils, but only putative organic spheres. Through the acid maceration of 128 samples from 15 outcrops using the method of Grey (2005) and a modified version that included filters at every step to maximize recovery, we were able to find organic remains in only one level of an outcrop in DS2 (Fig. 19). These carbonaceous structures present a spherical morphology with a granular appearance (“sponge-like”) and great variation in size (from 20 to 560  $\mu\text{m}$  in diameter). Some more elongated and conjoined specimens were also observed. Bubbles were visible inside some of the specimens (Fig. 19A, D, G, I).

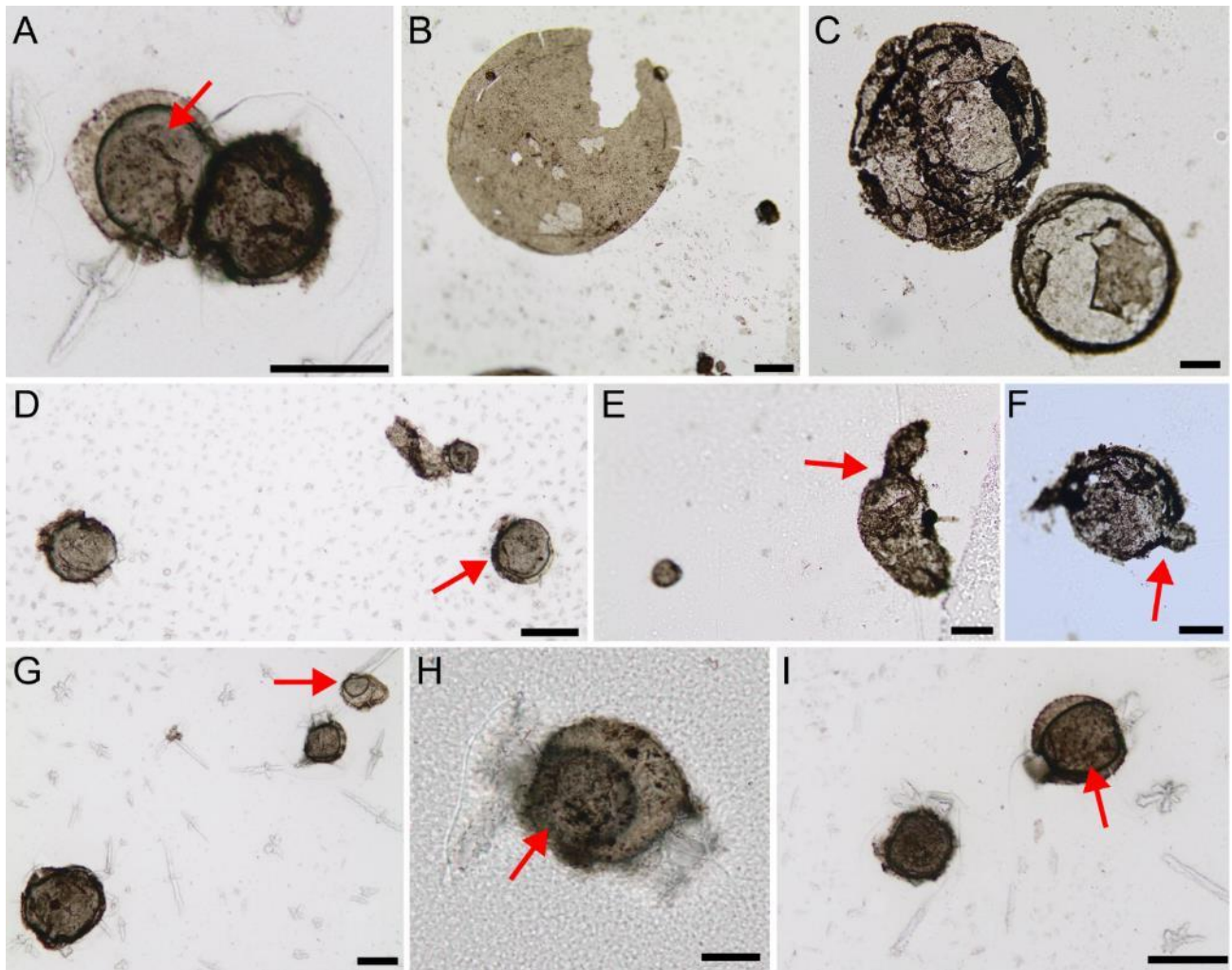


**Figure S5.** Palynological artifacts created after acid maceration of samples from the Itajaí Group that are rich in finely dispersed organic matter (CAP/1F-06, CAP/1F-07); note bubbles inside some of the organic spheres (red arrows). Scales: 50 µm (A, C–G, I), 100 µm (B), 10 µm (H).

These organic spheres present a remarkable resemblance to leiospherid acritarchs, but their granular texture, presence in the first steps of acid dissolution as supernatants, wide variations in size, conjoined forms and the occurrence of bubbles inside some of the vesicles (Fig. 19) suggest an origin by flocculation of finely disseminated organic matter, similar to those observed and interpreted by Grey (2005) as artifacts. Strikingly, the presence of bubbles inside the structures may suggest that they originated by aggregation of organic particles around gas bubbles of silicon tetrafluoride ( $\text{SiF}_4$ ), released during the HF reaction with silicates. In fact, Fuxing and Qiling (1982) gave similar interpretations when studying the behavior of finely

disseminated organic substances during acid maceration. These authors were able to show that this process can indeed create spherical pseudofossils that can be confused with true microfossils.

The apparent absence of true organic microfossils in the IB can reflect some diagenetic alteration and/or weathering of the rocks in the exposed outcrops studied here. Nevertheless, the observation that palynological artifacts can easily occur highlights the caution necessary when dealing with simple organic vesicles from Precambrian rocks, especially regarding the morphological group of the leiospherids.

## 4 ARTICLE TWO

### ***Beggiatoa*-like *in situ* communities from the Ediacaran Itajaí Basin (~563 Ma) – the expansion of sulphide oxidizing bacteria in the Ediacaran Period**

#### **Abstract.**

Precambrian filamentous microfossils are common and diverse. Nevertheless, their taxonomic assignment can be difficult due to their overall simple shapes typically lacking in diagnostic features. Here, we report *in situ* communities of well-preserved, large filamentous impressions from the Ediacaran Itajaí Basin (ca. 563 Ma) of Brazil. The filaments are uniserial (unbranched) and can reach up to 200 µm in width and up to 44000 µm in length. They occur as both densely packed or sparsely populated surfaces, and typically show a consistent orientation. Although simple in shape, their preferred orientation suggests they were tethered to the seafloor, and their overall flexibility (e.g. bent, folded, and twisted) supports a biological (rather than sedimentary) affinity. Biometric comparisons with modern filamentous groups further support their biological affinity, suggesting links with either large sulphide-oxidizing bacteria (SOB) or eukaryotes. Their association with other complex macrobiota (e.g. frondose organisms, *Palaeopascichnus*) suggest that they likely played an important role in the ecological dynamics of these early benthic communities by providing firm substrates for metazoans to inhabit. It is further hypothesized that the dynamic redox condition in the latest Ediacaran, with the non-continuous rise in oxygen concentration and periods of hypoxia, may have created ideal conditions for sulphide-oxidizing bacteria to thrive.

**Keywords:** Filamentous Fossils, Ediacaran Ecosystems, Avalon Assemblage, Itajaí Basin, *Beggiatoa*, Sulphide-Oxidizing Bacteria.

## 1. Introduction

Simple, relatively large (ca. >30 µm) unbranched filamentous (UF) microfossils are common in the Precambrian fossil record (Knoll, 1982; Knoll et al., 1991; Butterfield et al., 1994; Javaux and Knoll, 2017). Depending on their size and morphological complexity, these filaments are typically interpreted as either cyanobacteria or eukaryotes (Tynni and Donner, 1980; Nyberg and Schopf, 1984; Butterfield et al., 1994; Butterfield, 2015; Sergeev et al., 2016; Bengtson et al., 2017). These fossils are usually investigated by means of palynological maceration or thin sections of cherts and phosphatic rocks. However, in rare circumstances, filamentous organisms can be preserved as carbonaceous compressions (Cohen et al., 2009; Tang et al., 2015) or even as casts and moulds in siliciclastic rocks (Callow and Brasier, 2009b; Liu et al., 2016b; Liu and Dunn, 2020), the latter making them difficult to differentiate from trace fossils (Droser et al., 2005; Jensen et al., 2005, 2007; Sappenfield et al., 2011).

Nevertheless, even when a body fossil origin is corroborated, the possibility that some of these occurrences represent the remains of large filamentous sulphur-oxidizing bacteria (LFSOB), similar to the modern *Beggiatoa* and *Thioploca*, is poorly explored. Modern LFSOB are ubiquitous in marine and freshwater environments where H<sub>2</sub>S and oxygen geochemical gradients are prevalent (e.g. environments at the interface of euxinic and oxic conditions; (Jørgensen et al., 2015; Strohl, 2015b). Yet, only few studies have suggested the presence of SOBs in the fossil record (Peckmann et al., 2004; Bailey et al., 2013; Pierre et al., 2015). This is due, in part, to their simple morphology and overall morphological similarities with cyanobacteria (Larkin and Strohl, 1983; Strohl, 2015a).

Here, we report exceptionally preserved *in situ* communities of large unbranched filamentous microorganisms from the Ediacaran of the Itajaí Basin (IB) of Brazil (~563 Ma, Becker-Kerber et al., 2020). Based on morphological and ecological comparisons with modern analogues, these fossils are interpreted as the remains of large filamentous sulphur-oxidizing bacteria (LFSOB). Their presence in Ediacaran (Avalonian-Assemblage; Boag et al., 2016) deposits from Brazil (this report), Newfoundland (Liu and Dunn, 2020) and England (Callow and Brasier, 2009b) suggest that they were important components of these earliest complex macroscopic ecosystems.

## 2. Morphology and ecology

Over 1,600 individual specimens (Fig. 1) were investigated as part of this study (see methods). Filament size range from 33  $\mu\text{m}$  to 193  $\mu\text{m}$  wide (mean =  $68.9 \pm 0.43 \mu\text{m}$ , n = 1636), and from 1270  $\mu\text{m}$  to 44000  $\mu\text{m}$  long (mean =  $11000 \pm 717.8 \mu\text{m}$ , n = 117). All filaments have remarkably consistent widths from one extremity to another, varying only ~13  $\mu\text{m}$  (on average). In many cases, their extremities occur as blunt (or slightly tapered) terminations. Filament surfaces are typically smooth, lacking any discernible ornamentation (although see Fig. 1c, 2b) (Becker-Kerber et al. submitted). Despite the high number of individuals investigated, we found no evidence for differentiated cell-types such as attachment and/or rhizoid-like structure, or possible reproductive bodies. Filaments can be either sparsely or densely concentrated on bedding planes (Fig. 1, 2, Supplementary Figure 1–3). Some of the densest surfaces showcase up to 50 individuals/cm<sup>2</sup>.

Although simple in form, the filaments can be differentiated from abiogenic structures. For example, the absence of vertical continuity or vertical disruption of sediments below or above the filaments (as seen in polished sections) is particularly helpful in refuting some abiogenic structures such as fractures, syneresis cracks, and petee structures. Furthermore, the non-linear nature of many specimens, including examples that are curved, bent, overlapping, and even looping (Fig. 1) also supports a biological affinity. Additionally, their preservation in positive epirelief (on the tops of beds) rules out an abiotic origin by tool marks. Moreover, the overlapping nature of some specimens (e.g. Fig. 1c–d), including examples that are highly interwoven (Fig. 2a–b), combined with the absence of cross-cutting relationships and preferential orientation of the filaments (Fig. 2e), all supports a body fossil, rather than a trace fossil or a tectograph (see ref. Becker-Kerber et al., 2020) interpretation.

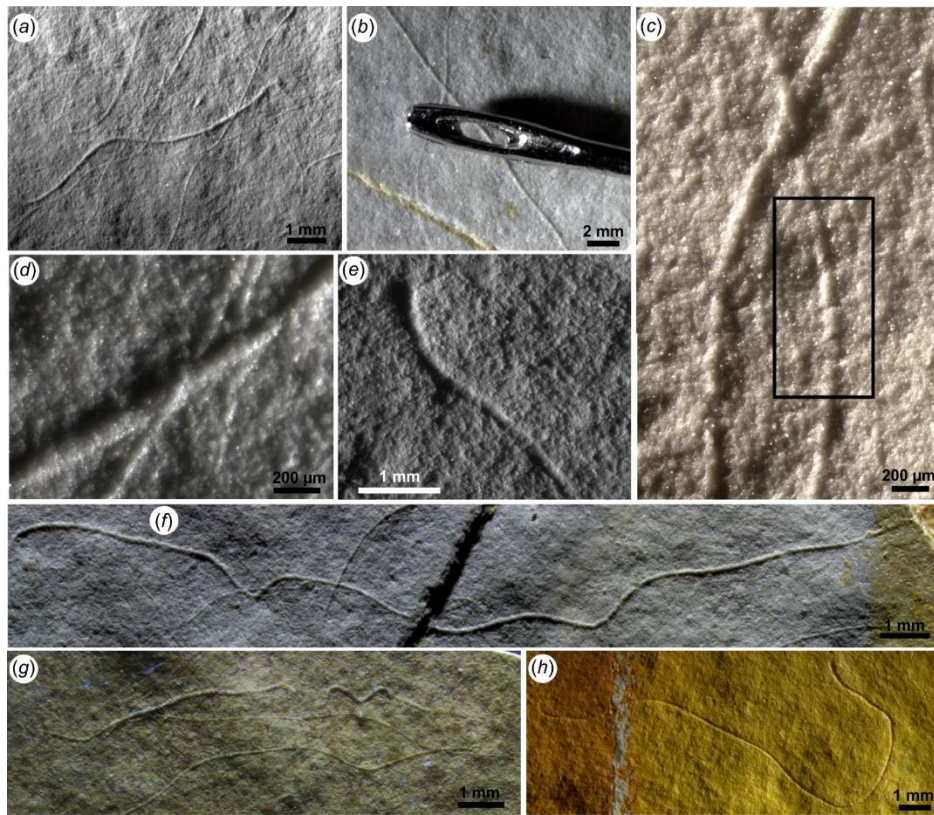


**Figure 1. Filamentous fossils from the Itajaí Basin (a-h).** Note possible cell-like arrangement in (c), overlapping (not cross-cutting) relationships in (d), blunt terminations in (e), and the long and sinuous nature of the filaments (f-h).

The filaments are interpreted as being originally composed of soft tissues, given that they were capable of bending, folding, and twisting plastically without breaking (Fig. 2a, b). Several specimens display sinuosity (Fig. 1, 2) and even a high degree of interlacing with other filaments (Fig. 2a–b). Interestingly, the latter is more common on less populated surfaces, indicating that this arrangement is not a consequence of dense assemblages.

Formerly buried extremities (Fig. 2c) and specimen alignment (Fig. 2e, Supplementary Fig. 1–3) suggest *in situ* preservation and a benthic habit. The oriented populations also suggest the influence of gentle bottom-water currents that did not disarticulate or detach the specimens from the substrate prior to fossilization. Given the absence of evidence for strong sediment reworking and/or storm deposits, the filament orientation agrees with the interpretation (Becker-Kerber et al., 2020) of an upper slope setting dominated by millimetre-scale intercalations of siltstones and claystones. In rare cases, filament overlapping patterns can even allow for inference of the likely sequence of filament superposition prior to burial (Fig. 2f, Supplementary

Fig. 4). This further corroborates the *in situ* nature of these populations, as well as suggesting a potential vertical mode of life, with basal portions of the filament likely buried or attached to the substrate.

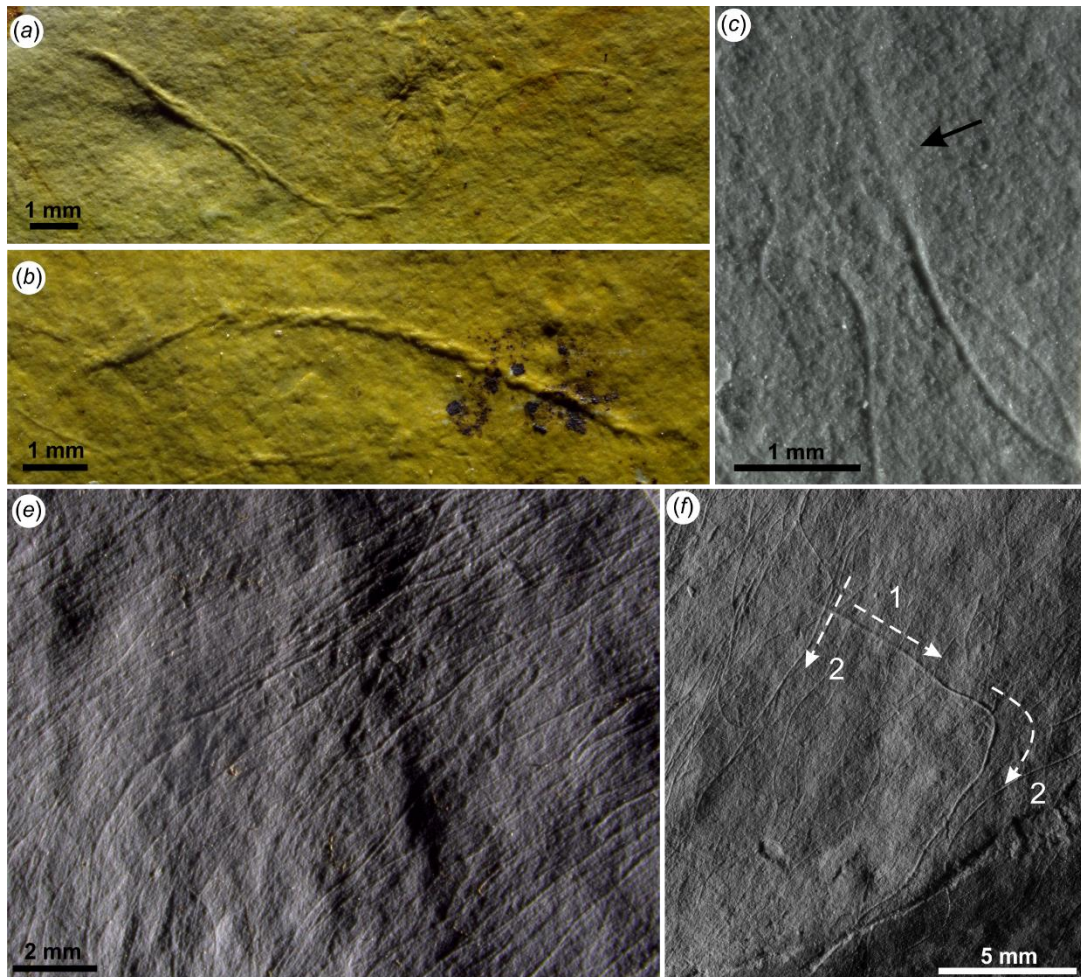


**Figure 2. Disposition of the filaments on the bedding plane.** Highly interwoven individuals (a-b), partially buried extremities (c), densely populated surfaces with preferential orientation (e), and sequentially orientated specimens (f).

Interestingly, it may be possible to interpret the original life position of the microbial filaments based on their surficial expression. As seen in figure 3, a single bedding plane showcases two distinct regions: a region with a high density of filaments next to a slightly raised section that has a pustular (“old elephant skin” of Runnegar and Fedonkin (1992) texture and lacks filaments altogether. In planar view, these two regions are divided by a straight to sinuous positive-relief ridge (Fig. 3). Since the bedding plane is smooth and continuous between both regions, it is unlikely that this feature represents a fracture (or a different bedding plane altogether), and we therefore interpret this as an original surface. Filaments that extend from the high-density region

apparently disappear into the low-density surface once they reach the ridge (Fig. 3c–d), rarely leaving more than a faint impression. In this sense, we interpret the pustular low-density region as the remains of a microbial mat cover (Microbially-Induced Sedimentary Structures [MISS] of Noffke (2001) that overlay the filament-rich layer. The exposure of the filamentous under-mat surface likely resulted from the overlying microbial mat being torn-off by a rare high-energy bottom-current. Sedimentary structures interpreted as “rolled-up” microbial mats (Supplementary Fig. 5) are common in the region, and suggest that a significant portion of the filaments resided within the substrate and/or microbial mats prior to burial.

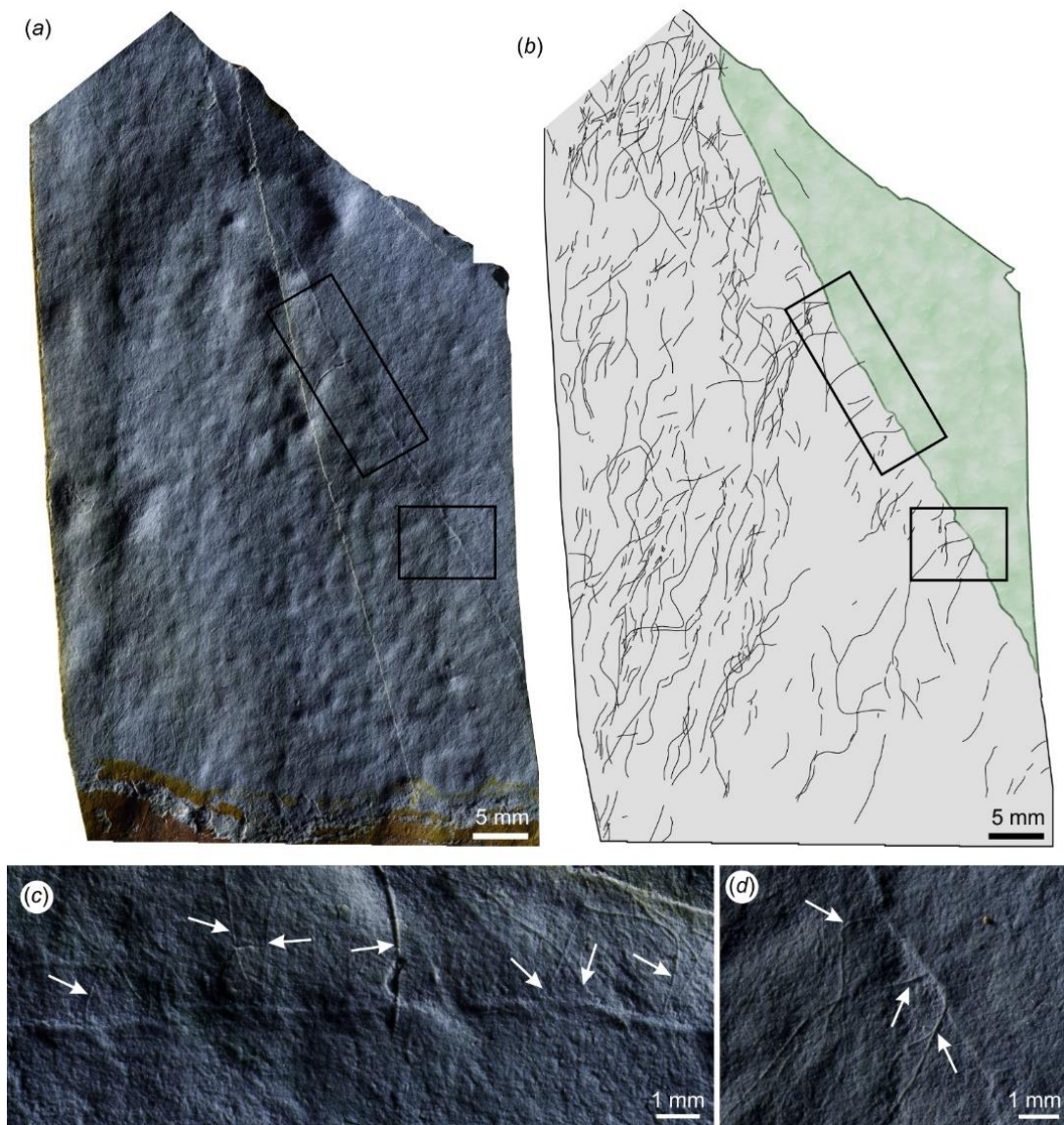


**Figure 3. Sample showing original bedding plane with an exposed, filament-rich lower surface.** (a-b) Bedding plane photograph (a) and interpretive drawing (b) showing the filaments and the positive-relief ridge between the lower and upper

surfaces. (c-d) Close-up of (a) displaying the filaments disappearing at the positive ridge.

To better constrain the comparisons with modern filamentous groups, we created a database with size ranges of unbranched filamentous organisms (cyanobacteria, LFSOB, and eukaryotes) (See references in Supplementary Table 1). The results suggest that the Itajaí Basin filaments exhibit values closer to those observed for sulphur-oxidizing bacteria (e.g. *Beggiatoa*) and eukaryotes rather than cyanobacteria (Fig. 4). This is also the case for the calculated biovolume ( $\pi/4 \times W^2 \times L$ ) of these groups (Fig. 4).

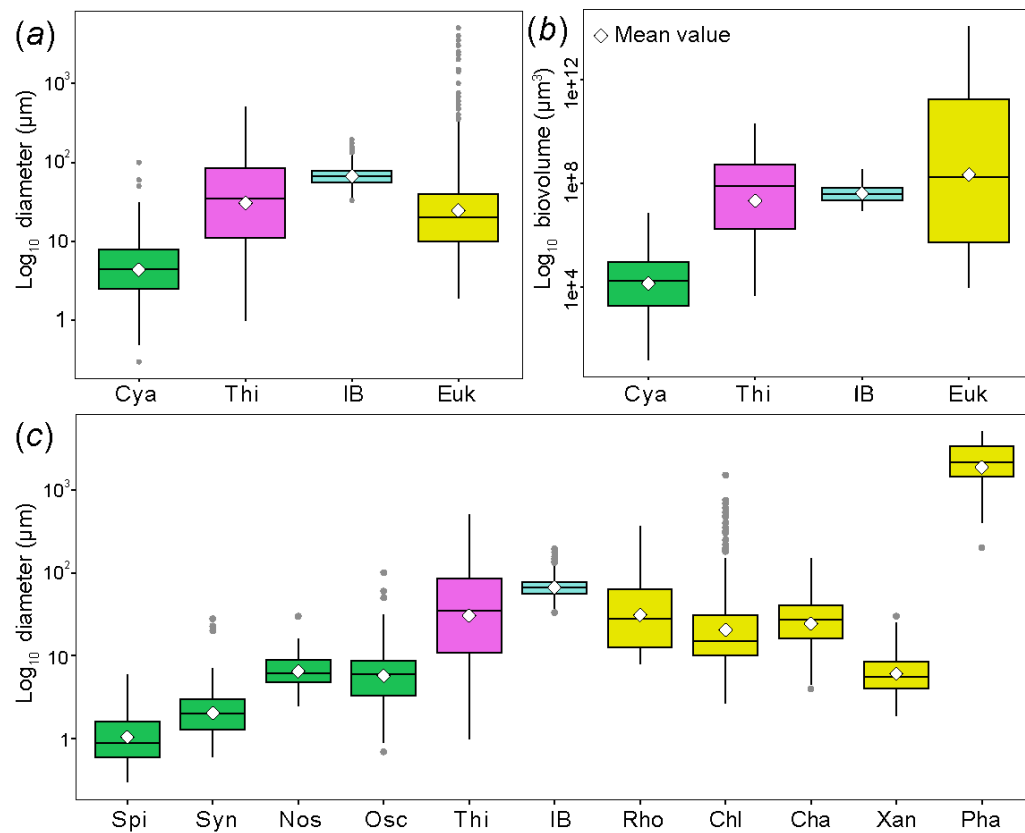


**Figure 4. Biometric comparison of the IB filaments and modern groups of unbranched filamentous organisms.** Box plots for the diameters (a) and estimated biovolumes (b) of major groups and IB filaments, and box plot of the diameters of the same groups divided in their main taxa (c). Green boxes = Cyanobacteria, purple = Thiotrichales, light blue boxes = Itajaí Basin (IB) filaments, yellow: eukaryotes. Cya = Cyanobacteria; Thi = Thiotrichales; IB = Itajaí Basin filaments; Euk = Eukarya; Spi = Spirulinales; Syn = Synechococcales; Nos = Nostocales; Osc = Oscillatoriales; Rho =

Rhodophyta; Chlorophyta; Cha = “Charophyta”; Pha = Phaeophyceae. Data from Supplementary Table 1.

### 3. Biological affinities

Interpreting the biological affinities of morphologically simple filaments by shape alone is difficult and is only confounded when applied to fossil data. Yet, large datasets based on *in situ* communities, when combined with ecological characterization derived from sedimentary facies analyses, can allow for hypotheses concerning the likely biological relationships of these forms, or even help elucidate the likely mode of life of such organisms.

The large filaments herein described from the Itajaí Basin of Brazil exhibit comparable size ranges to both LFSOB and eukaryotes, but they differ from most of the reported size-ranges of modern cyanobacteria (Fig. 4). Indeed, the diameter of filamentous cyanobacteria is typically < 100 µm (Fig. 4), while the largest IB filaments reported here can reach widths of nearly 200 µm (Supplementary Fig. 6). On the other hand, modern filamentous sulphide-oxidizing bacteria can attain exceptionally large dimensions: populations of the filamentous genus *Beggiatoa* were found with individuals measuring up to 200 µm in diameter (Larkin and Henk, 1996). In fact, the largest bacteria known is *Thiomargarita*, a SOB that can reach up to 750 µm in diameter (Schulz, 2006). The lengths observed for the IB filaments, as well as the calculated biovolumes, are also akin to the values observed in large LFSOB and eukaryotes (Fig. 4).

Given the simplicity of the filamentous fossils reported here, especially considering the lack of any diagnostic characters such as specialized anchoring structures, it is difficult to make a more robust palaeobiological interpretation of their affinities. However, the consistent width of the IB filaments suggests a closer affinity with modern large LFSOB than with unbranched filamentous eukaryotes. For instance, modern unbranched filamentous eukaryotes are rarely uniform along their entire length, and typically exhibit a complex set of specialized cellular characters. For example, *Bangia* shows clear variations in filament width towards the apex (uniseriate to multiseriate thalli), rhizoid attachments, and specialized reproductive structures (Sutherland et al., 2011). Chlorophytes with similar sizes to the IB filaments (e.g., *Chaetomorpha*, *Urospora*) typically show a pronounced morphological complexity, including differentiated holdfasts, constricted septa (i.e., *Chaetomorpha*), and

distinctive distal tapering (Lokhorst and Trask, 1981; Blair, 1983; Vahedi and Pasbakhsh, 2015). Given the number of filaments (>1600) investigated from IB deposits and their exceptional preservation, it is most parsimonious that additional morphological characters are in fact absent (rather than not preserved) from the external morphology of the filaments.

Finally, the *in situ* preservation of the filaments from the Itajaí Basin allows a unique opportunity to understand aspects of their palaeoecology and perhaps even their preferred metabolic pathway. Their benthic vertical mode of life (Fig. 5), partially prostrate, and perhaps even partially buried, is remarkably similar to the ecology of modern LFSOB (Jørgensen et al., 2015; Strohl, 2015b). Indeed, large filamentous sulphide-oxidizing bacteria can colonize extensive seafloor areas in dysoxic settings, building large communities that live attached and/or partially buried in the substrate (Schulz et al., 1996). Some species, like *Beggiatoa* and *Thioploca*, can even show motility through gliding and the capacity to adjust their positions accordingly to local geochemical variations (Teske and Nelson, 2006). The presence of sequential orientations (Fig. 2f, Supplementary Fig. 4) in the IB filaments shows that these organisms were able to return to a partial vertical position following an event that felled them. This suggests some degree of control in their position at the sediment-water interface, possibly reflecting some type of gliding motility.



**Figure 5.** Artistic reconstruction of the possible life habits of the Itajaí Basin filaments.

In addition to the Itajaí Group, large filaments have been reported from the Longmyndian Supergroup (~567-556 Ma) of England (Callow and Brasier, 2009b, 2009a), and in the Trepassey Formation (~565-560 Ma) of Newfoundland, Canada (Liu et al., 2016b). Other possible sulphur-oxidizing bacteria were observed in phosphorites of the Doushantuo Formation (Bailey et al., 2013).

Recently Liu and Dunn (2020) reinterpreted the large filaments of Newfoundland as stolon-like structures connecting frondose organisms. However, among the thousands of filaments investigated on 38 surfaces by the authors, only a handful of cases of thicker ( $\geq 1$  mm) and much longer (up to 4 meters) filaments were observed to cross-cut (or terminate at) frondose organisms. The “typical” filament size reported varied between 100 to 1000  $\mu\text{m}$  wide and 2 to 40 cm long, values that are not far from the dimensions of LFSOB (see Supplementary Table 1; e.g. *Thioploca*, Jørgensen and Gallardo, 1999). Thus, we propose that these filamentous impressions of Newfoundland (and elsewhere) may represent remains of LFSOB, however the stolonic interpretation may remain valid specifically for the larger filaments found adjacent to the fronds (especially given the large range in sizes reported (Liu and Dunn, 2020).

#### **4. Sulphide oxidizers, Ediacaran macrobiota and dynamic oxygen levels in the Ediacaran**

The chemoautotrophic metabolism of LFSOB relies on sulphides (e.g.,  $\text{H}_2\text{S}$ ) as electron donors and oxygen or nitrate as electron acceptors (Teske and Nelson, 2006). Therefore, they are adapted to live in settings with significant geochemical gradients (Nelson et al., 1986; Teske and Nelson, 2006), more specifically, at the interface between sulphidic and low oxygenated zones. During the late Neoproterozoic, the non-continuous and episodic oxygenation of the oceans (Bowyer et al., 2017) could have created favourable micro-oxic conditions ideal for SOB metabolism. Indeed, recent works (Sperling et al., 2015; Tostevin et al., 2016; Bowyer et al., 2017) propose that Ediacaran oceans were marked by dynamic redox conditions, with persistent and frequent low-oxygen levels. Consequently, this scenario would be highly favourable for a widespread development of SOB in a range of different settings.

If correctly interpreted, the widespread distribution (both temporally and geographically) of filamentous SOB would have played an important role in mitigating the biogeochemical cycles of the late Neoproterozoic. For example, because these organisms also use and accumulate nitrate (as an alternative electron acceptor) (Fossing et al., 1995; Zopfi et al., 2001), their metabolism could have impacted the nitrogen cycle (and fixation) in the Ediacaran oceans, increasing primary productivity and/or leading to eutrophication (Sayama, 2001; Teske and Nelson, 2006). Likewise, their metabolic activities may have contributed to the S and C cycles of marine ecosystems (Jørgensen, 1977; Fossing et al., 1995), and would have contributed to the growing sulphate concentrations of Ediacaran oceans (Kunzmann et al., 2017). In fact, recent studies have shown that biologically-driven sulphide oxidation rates can be three (or more) orders of magnitude higher than abiotic rates (Luther et al., 2011).

If we are correct, the increasing oxygen levels of the late Neoproterozoic and early Phanerozoic would have acted as a double-edged sword for SOB. First off, the rise of oxygen would have created widespread hypoxic conditions that favoured the development of chemosynthetic microorganisms and associated macrobiota. However, further oxygenation would have restricted sulphur-based communities and may have affected biotic events throughout the middle-late Ediacaran (Darroch et al., 2015b; Muscente et al., 2018, 2019), such as the changes in the taxonomic composition and ecology of the Avalon and White Sea assemblages. Meanwhile, new adaptations to increasingly oxygenated environments may have promoted the colonization of shallower settings by the typical biota of the White Sea. The diversification of more metabolically active (and more complex) macro-organisms prior to the Ediacaran/Cambrian transition may have played a role in shaping the evolutionary novelties of the Cambrian radiation event (Darroch et al., 2015b; Muscente et al., 2019).

It is also interesting to speculate on the ecological and evolutionary impacts of this SOB expansion during the early evolution of complex macroscopic life. If correct, their ubiquitous presence in deep-water, Avalonian-age deposits (Callow and Brasier, 2009b, 2009a; Liu et al., 2016b) suggests that they were relatively common in the early benthic communities at this time as chemosynthetic bacteria are an important primary producer in modern deep-water ecosystems (Felbeck and Somero, 1982). Moreover, as high levels of sulphide are typically toxic to aquatic invertebrates (Grieshaber and Völkel, 1998), the dominance of LFSOB could have served not only as a food source,

but also as a detoxification mechanism exploited by macroscopic organisms. Symbiotic relationships between Ediacaran organisms and chemosynthetic bacteria have been proposed (McMenamin, 1998; Dufour and McIlroy, 2017), and should continue to be investigated as an alternative to Osmotrophy (Laflamme et al., 2009). Finally, based on comparisons with the strict ecology of recent sulphur-oxidizing bacteria, another implication of the widespread presence of SOB in Avalonian deposits is that the Ediacaran organisms possibly evolved in oligotrophic environments, near the interface between hypoxic and sulfidic conditions, where these bacteria can maintain their metabolism.

## 5. Conclusions

Here we present a new association of large filaments from the Ediacaran of the Itajaí Basin. These well-preserved structures bear morphological and ecological similarities with large sulphide-oxidizing bacteria such as *Beggiatoa*. The apparent widespread occurrence of such organisms during the middle-late Ediacaran suggests that they likely contributed to the biogeochemical patterns of the N and S cycles. Moreover, the association of SOB with Ediacara biota suggests that they may have been important components of these early ecosystems, possibly playing important roles in the food chain, or in close ecological interactions with the Ediacaran biota.

## Methods

**Sampling.** Samples were recovered from upper slope, fine-grained rhythmites of the Depositional Sequence 2 of the Itajaí Basin (see Becker-Kerber et al., submitted, and references therein). These rhythmites comprise a millimetric intercalation of claystone and fine- to coarse-grained siltstone. These fossiliferous surfaces are associated with volcaniclastic and pyroclastic sediments, which likely played a major role in the high-fidelity fossilization observed in these beds (Becker-Kerber et al., submitted).

**Stereomicroscope and biometry.** We used the high magnification SteREO Discovery.V20 stereomicroscope coupled with an Axiocam camera at the Laboratório de Ecologia in the Universidade Federal de Mato Grosso do Sul. To ensure better characterizations of the microbial-rich surfaces and to avoid measuring the same specimen more than once, we imaged the entire surface by using consecutive snapshots that were later joined through image processing. We then selected

appropriate specimens and used the ZEN software to make all width measurements ( $n = 1636$ ). When investigating original length, possible changes in the diameter, and biovolume calculations, we choose only complete (both extremities visible) specimens ( $n = 117$ ; measuring each sample three times). For the biometric comparison, we compiled data from published articles (see Supplementary Table). We considered the reported size for the entire unbranched filamentous structure (including sheath if applicable). We considered both lower and upper size limits of each taxon for diameter comparison. We used the formula  $\pi/4 \times W^2 \times L$  for the biovolume calculation (Hillebrand et al., 1999). This allows for an estimation of the real value since: [1] we had to use only the upper size limit of the diameter and length because most of the works only reported the upper limit for the latter, and [2] taxa that are tapered can result in slightly overestimated values. The final database was processed with the R-studio software version 1.2.1335, with the ggplot2 package.

**Ethics.** This work has not involved any living subjects and conforms to the Ethics guidelines of the National Mining Agency (ANA, Brazil).

**Data accessibility.** Data available in this manuscript and its Supplementary Material

#### **Authors' contributions**

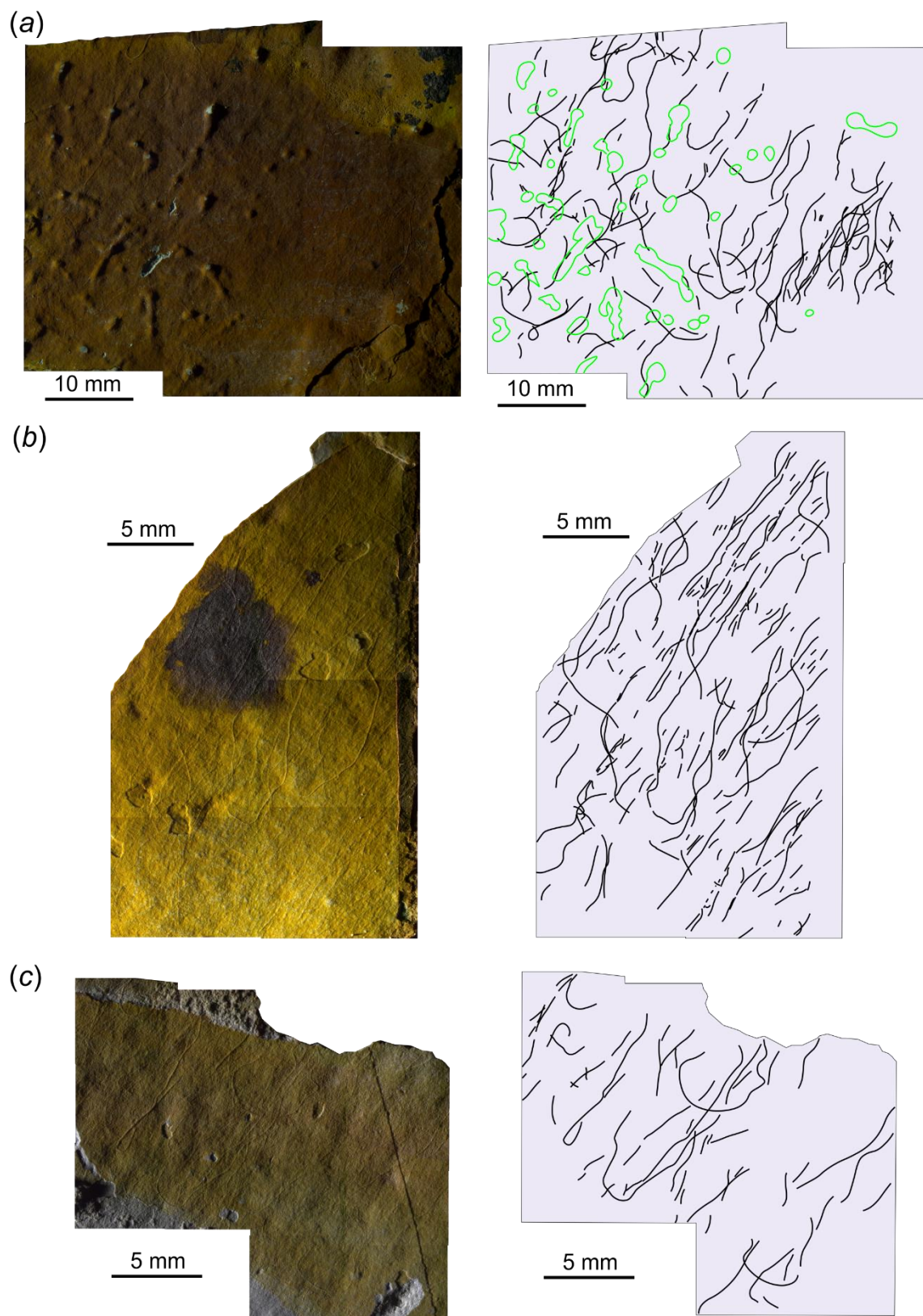
B.B-K. and P.S.G.P. designed the study; B.B-K., P.S.G.P. and A.L.Z.R. collected the material; B.B-K. and G.E.B.B carried out the morphological description and database compilation; all authors contributed to the interpretations of the results. B.B-K. drafted the manuscript, with significant contributions from M.L., P.S.G.P., A.E.A., G.M.E.M.P., G.L.O, and G.E.B.B.; all authors gave final approval for publication.

**Funding.** This work was funded by the Fundação de Amparo à Pesquisa do Estado de São Paulo under the proposal grants 2016/01827-4 and 2018/21886-0.

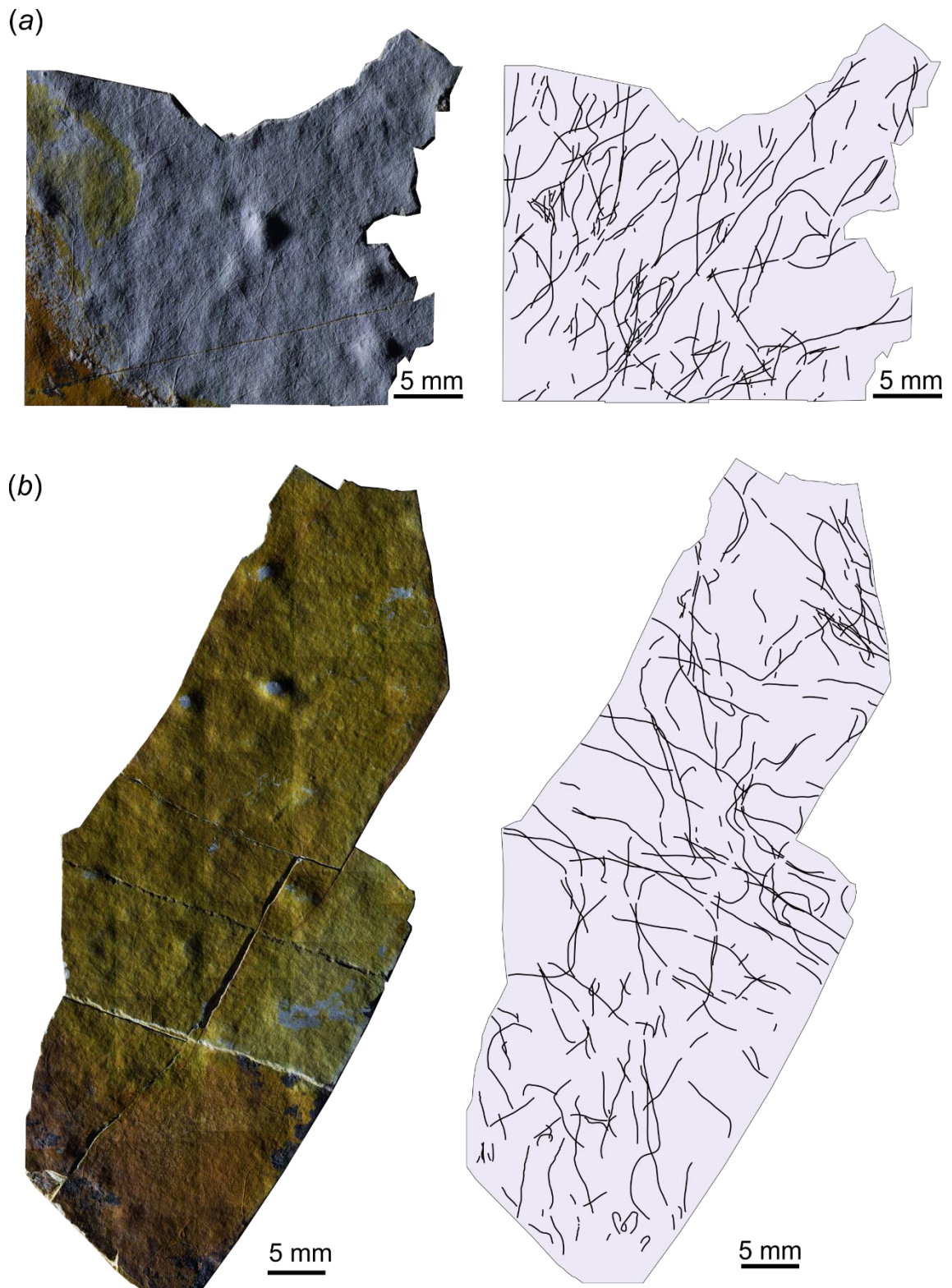
**Acknowledgements.** The authors thank the Fundação de Amparo à Pesquisa do Estado de São Paulo (FAPESP - Grant 2016/01827-4 and Grant 2018/21886-0), the Programa de Pós-Graduação em Ecologia e Recursos Naturais (PPGERN – UFSCar), and the Programa de Pós-Graduação em Geologia (PPGeo – UNISINOS). This work was also supported by La Région Nouvelle Aquitaine. B.B-K. and PSGP would like to thank for the support from the Conselho Nacional de Desenvolvimento Científico e Tecnológico (CNPq). The artistic representation was made by Júlia Soares d’Oliveira.

**Supplementary Information**

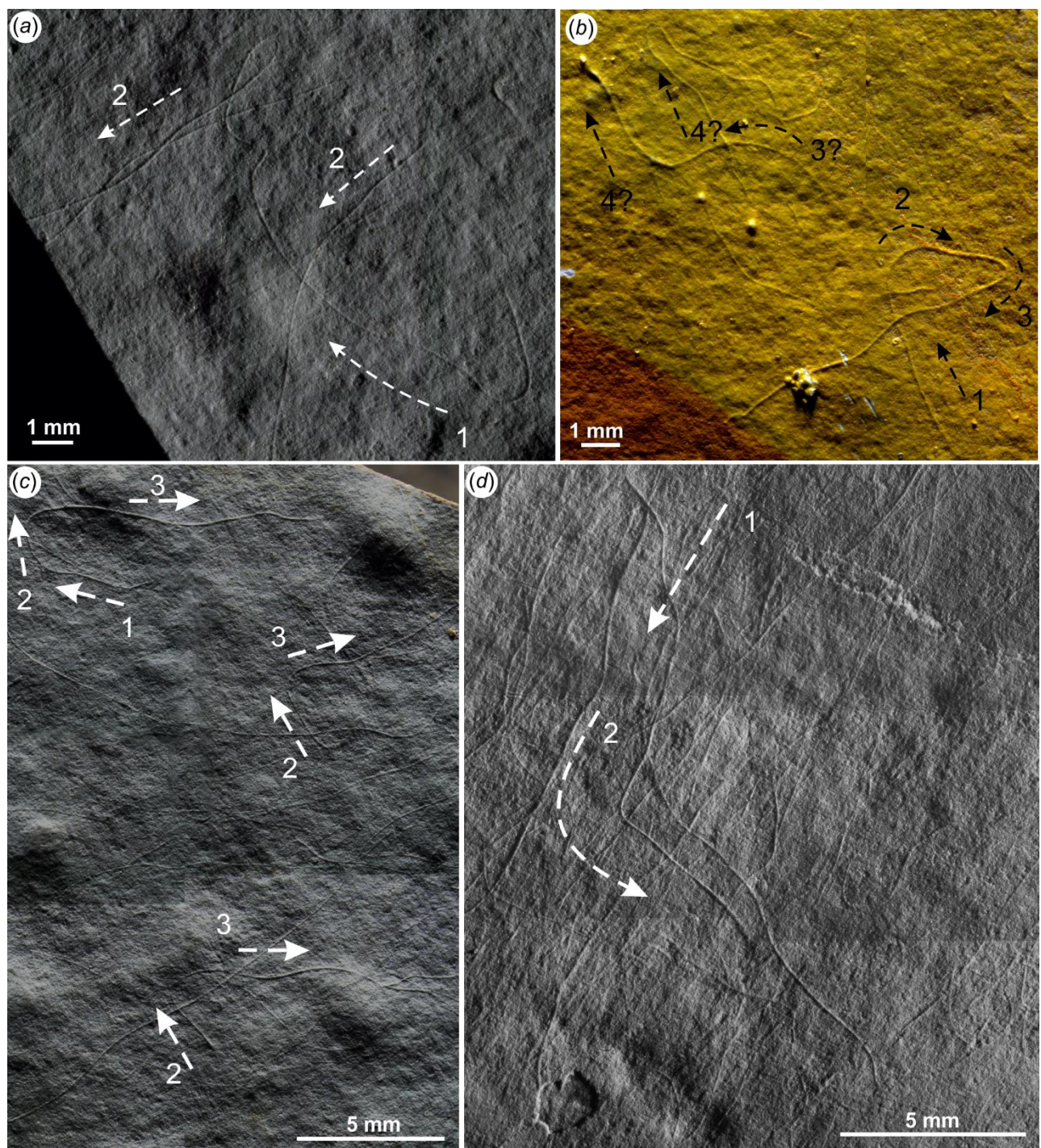
**Supplementary Figure 1.** Schematic drawing of a densely populated surface. Note the general orientation of the filaments towards the upper-left and bottom-right.



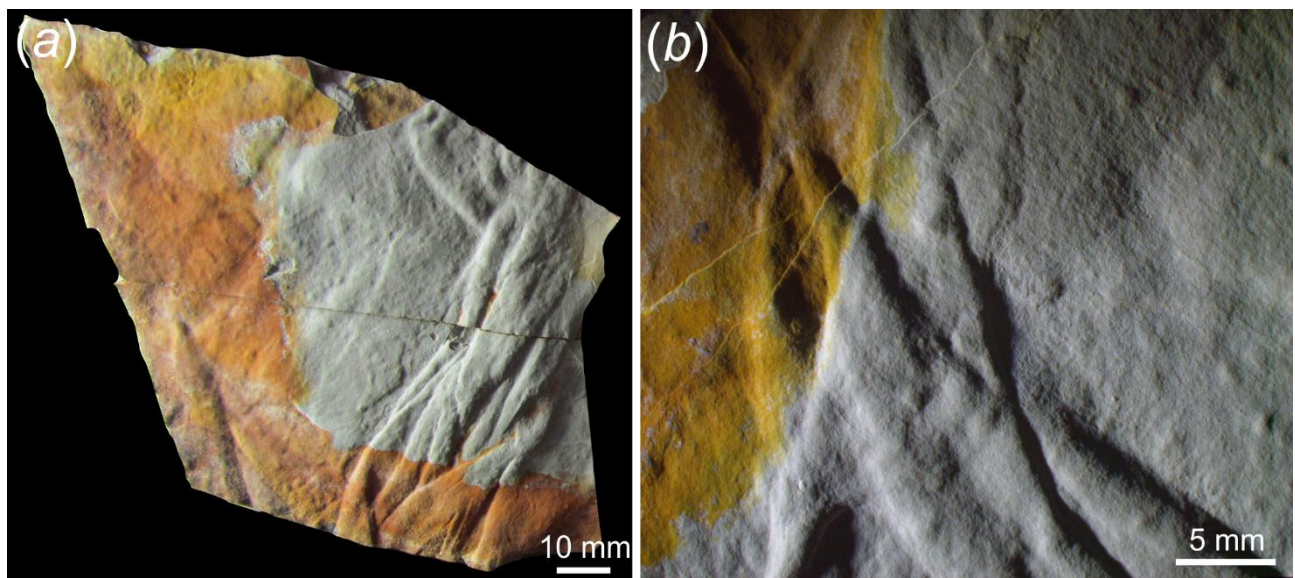
**Supplementary Figure 2.** Imaging of the entire surface with visible filaments and their respective schematic drawing. Note the association of the filaments with the pustular surface in (a), and several oriented individuals in (b) and (c).



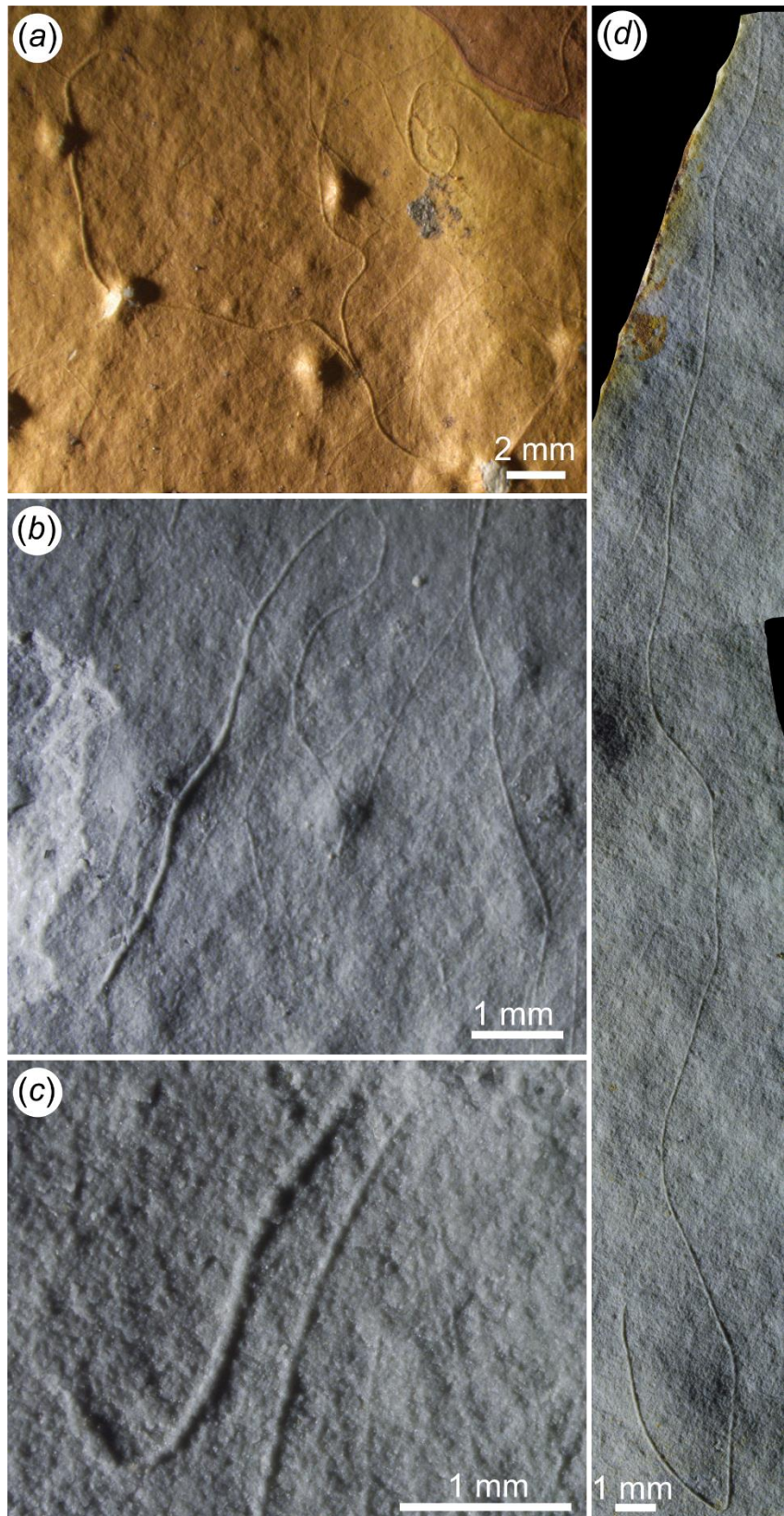
**Supplementary Figure 3.** Oriented specimens associated with pustular surface.



**Supplementary Figure 4.** Sequentially oriented filaments. The order of orientation can be revealed by the pattern of superposition of the filaments.



**Supplementary Figure 5.** Rolled up microbial mats (positive epirelief) with highly folded morphologies.



**Supplementary Figure 6.** Some of the largest filaments (in width [a,b,c,] and length [d]) recorded for the Itajaí Basin.

## 5 ARTICLE THREE

### The role of volcanic-derived clays in the preservation of Ediacaran biota

#### Abstract

The early evolution of metazoans has been reconstructed by studies on exceptionally preserved molds in siliciclastic rocks from the Ediacaran Period. However, there remains considerable controversy regarding the formation mechanisms of this unusual ‘Ediacaran-style’ preservation. Proposed hypotheses usually include early authigenesis of minerals, but evidences for this are scarce. In a recently discovered Ediacaran biota in Brazil, we show that the moldic preservation can also be related to clay mineral authigenesis. Specifically, these clays originated from microbial alteration of original pyroclastic sediments, leading to early illitization and morphological templating of the fossiliferous surfaces on an almost cellular level. Such high-fidelity preservation was made possible by the rapid burial during volcanic events and the in-situ templating of tissue by clays via microbially-mediated biomimetic mineralization. This newly described *Lagerstätten* demonstrates that a number of minerals can facilitate preservation, and that perhaps ‘Ediacaran-style’ preservation is in and of itself only unique by the age of the specific fossils preserved, not the mechanisms.

#### Introduction

The typical moldic preservation of soft-bodied organisms in the Ediacaran Period (635–539 Ma) (Gehling, 1999; Tarhan et al., 2016; Liu, 2016; Bobrovskiy et al., 2019b), in particular the positive epirelief type where the fossils protrude up from the surface (Bobrovskiy et al., 2019b), has few parallels in other periods of geologic time, hence the term “Ediacaran-style preservation.” One explanation points to rheological differences amongst the sediments (Wade, 1968), a hypothesis that has received recent support (Bobrovskiy et al., 2019b). Gehling (1999) also proposed the so-called ‘death-mask’ model for this preservation, in which microbial mats stabilized the sediments and produced a veneer of authigenic pyrite ( $\text{FeS}_2$ ) that replicated the morphology of the organisms. Evidence in favor of this hypothesis comes from the presence of iron oxide and pyrite concentrations along fossiliferous bedding planes in certain localities (Liu, 2016; Liu et al., 2019). Other hypotheses include episodic event

deposition (Seilacher, 1992), early cementation by quartz ( $\text{SiO}_2$ ) in silica-rich oceans (Tarhan et al., 2016), and burial by volcanic ash – the so-called “Conception-style” preservation (Narbonne, 2005).

It is similarly possible that multiple mechanisms could produce this type of moldic fossilization and/or that taphonomic factors varied according to the geologic setting. In this regard, the Itajaí Basin (da Silva et al., 2002; Guadagnin et al., 2010; Basei et al., 2011) (ca. 563 Ma, Brazil) appears to be a promising locality in which to study the possible mechanisms of preservation operating during the Ediacaran Period due to the high-fidelity preservation of the fossils. In a recent paper, Becker-Kerber et al.(Becker-Kerber et al., 2020) described the Itajaí biota, reporting the presence of *Palaeopascichnus*, discoidal forms, microbial filaments, Arumberia and fossilized microbial tufts. In this work, we apply a diverse array of techniques to address the fossilization processes of this new Ediacaran locality. More specifically, we demonstrate the close association of body fossils and microbial mats with volcanic sediments. We then provide a mechanism for the morphological preservation of tissue on an almost cellular level that includes the rapid formation of authigenic clays during early diagenesis as a result of the alteration of volcanic materials and microbial activity.

## Results

The Itajaí biota is composed of the well-known chambered taxon *Palaeopascichnus*, the discoidal forms *Aspidella* and *Nimbia*, and micron-sized microbial filaments (Becker-Kerber et al., 2020) (Fig. 1). Well-preserved reticulated and Arumberia-type microbial mats have also been observed (Fig. 1b). We detected three modes of preservation: (1) impressions in positive epirelief (*Palaeopascichnus*, *Aspidella*, and microbial filaments); (2) impressions in negative epirelief (*Aspidella*); and (3) three-dimensionally preserved microbial mats (Fig. 1). Investigations by microtomography ( $\mu\text{-CT}$ ) corroborated the moldic preservation of the filaments as well as the unusual 3D nature of the microbial mats (Supplementary Fig. 1, and Movie 1). Remarkably, very small filaments (c. 30  $\mu\text{m}$  in width) are preserved as impressions, and some individuals even seem to bear cellular structures (Fig. 1e). This minute detail indicates a level of morphological retention in molds that is unprecedented in the fossil record because filamentous microfossils with cellular structures are usually permineralized or occur as palynomorphs (Schopf and Klein, 1992). Additionally, to our knowledge, this is the first

case of three-dimensional preservation of microbial mats in siliciclastic settings in the geological record.

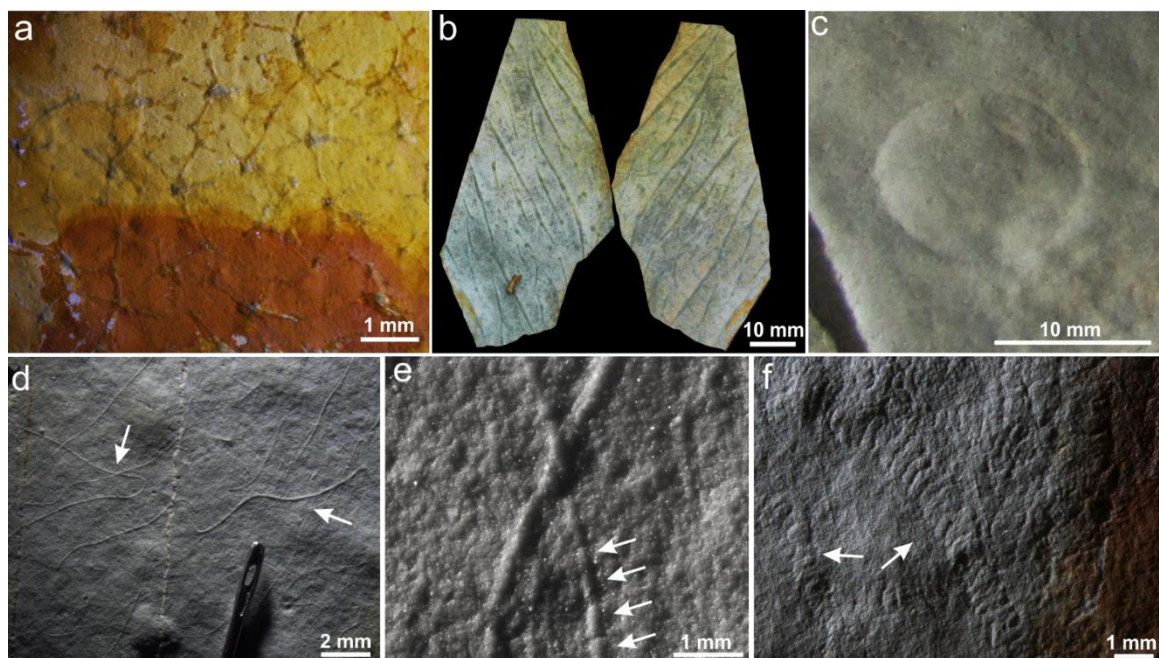


**Figure 1. Typical fossils and preservation styles in the Itajaí Basin.** (a) Three-dimensionally preserved tufted microbial mats (CAP-879). (b) 3D Arumberia-type microbial mats (CAP-880). (c) *Aspidella* in positive hyporelief (CAP-549). (d) Microbial filaments in positive epirelief (CAP-881). (e) Exquisite preservation of microbial filaments bearing cellular structures (arrows) (CAP-866). (f) *Palaeopascichnus* in positive epirelief.

The fossiliferous levels mostly occur in pale-gray millimeter-scale rhythmites of mud and silt that were deposited in an upper slope setting subjected to rhyolitic volcaniclastic input (Supplementary Text 1, Supplementary Figs. 2, 3). These layers additionally display abundant evidence of microbial mat development. The fossil impressions are located in clay-rich laminations characterized by opaque and microcrystalline clay minerals (Supplementary Fig. 4). This material also forms the unique three-dimensional microbial mats (Fig. 1d–e, Supplementary Figs. 4, 5). Exquisitely preserved microbial mats are also present in distal delta-front deposits (e.g., Arumberia; Supplementary Fig. 2) associated with reworked volcaniclasts and impressions of *Nimbia*.

The upper slope fossiliferous beds, which yielded the majority of samples, are represented by ash-fall pyroclasts, including elongate, cuspatate, angular and blocky devitrified vitric clasts; euhedral phenocrysts (some broken); accretionary pellets

(*sensu* Brown et al. (2012); ash clusters; and coated particles (Fig. 2, Supplementary Figs. 6, 7g–j). Coarse-grained silt laminae interbedded with the fossiliferous horizons also contain volcaniclasts, which likely represent a mix of primary and reworked ash-fall deposits (Supplementary Figs. 2, 7a–f, k–o). These clasts exhibit devitrification features with formation of clay minerals (Supplementary Fig. 8), as well as clay rims and fluid and/or melt inclusions (Supplementary Figs. 7n–o, 8g).

Fine layers of altered ash were observed directly covering well-preserved microbial filaments (Fig. 2d, Supplementary Fig. 6). In thin section, these surfaces are characterized by localized concentrations of very fine clays (Supplementary Fig. 6g–h). In some layers, early-formed fractures developed mainly following these bedding surfaces. These layers were filled by fibrous radial micaceous crystallites (sericite) and later by quartz (Fig. 2l–m, Supplementary Fig. 6i–l). The formation of this fibrous sericite seems to have occurred before the lithification of the deposits given their molding relationship with the surrounding sediments (Fig. 2m). The early-filled fractures are observed in some instances to crosscut the clay-mineralized fossiliferous surfaces, implying an early origin for the fossil-bearing clays.

Other outcrops, mostly restricted to the southwestern portion of the basin, also show evidence of volcanic activity. In particular, abundant and well-preserved glass shards and glass spheres (*i.e.*, acneliths) occurring in silicified tuffites in one fossiliferous outcrop display devitrification to clay minerals similar to those described above (Fig. 2n, o, Supplementary Fig. 9). It is interesting to note that these acneliths have peculiar morphologies with spheroidal, ellipsoidal and tear-drop shapes, many bearing spiny projections that resemble modern Pelle's tears (Heiken, 1972). This configuration indicates that the Itajaí Basin also had pyroclastic sediments derived from basaltic volcanism.

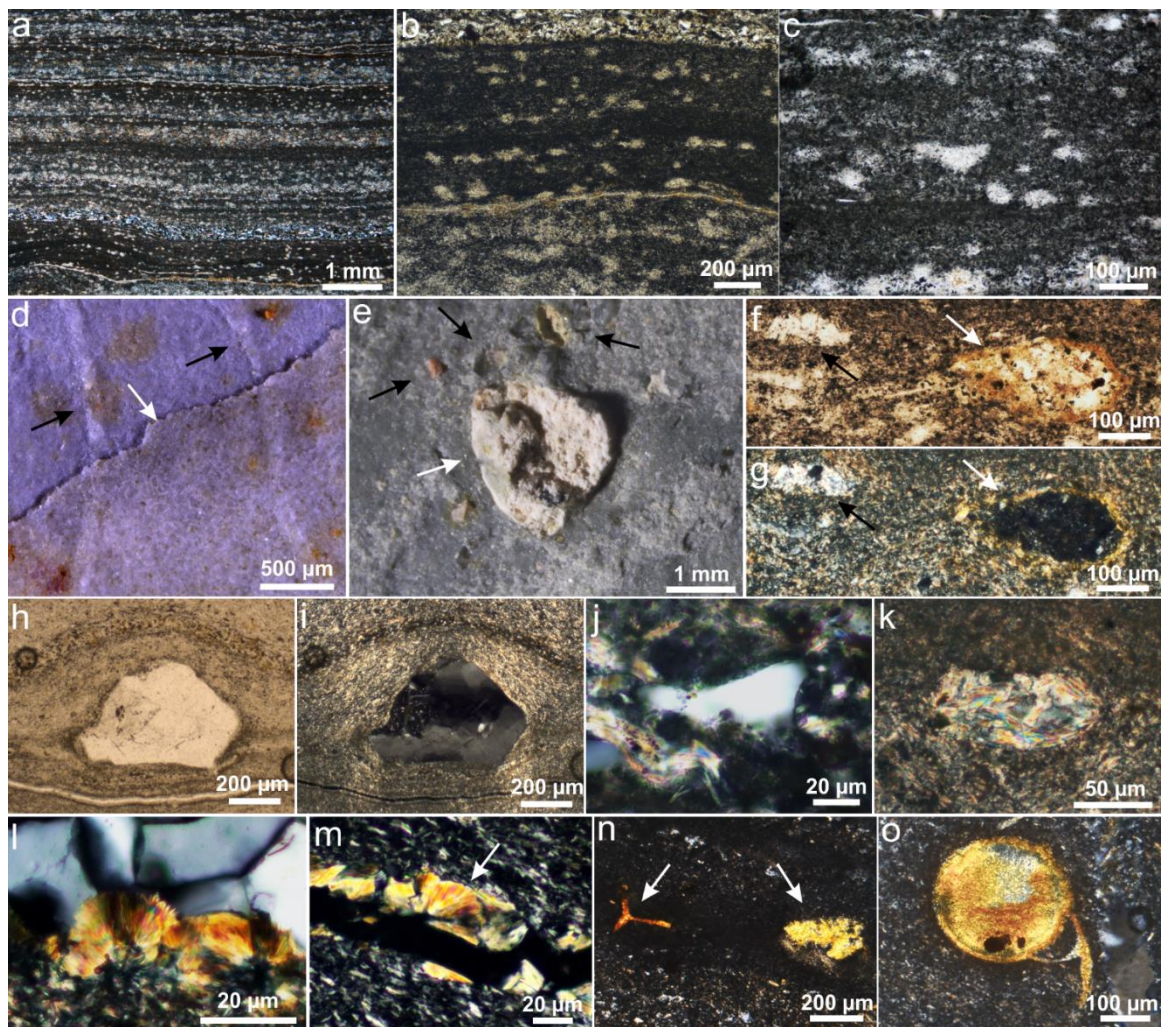


**Figure 2. Pyroclasts from the fossiliferous horizons of the Itajaí Basin.** (a) Vertical thin section through different clay (darker) and silt (whitish) laminations with several devitrified pyroclasts (small scattered white clasts); crossed nicols. (b) Closer view of the same texture, with devitrified pyroclasts following the bedding plane; plane-polarized light. (c) Pyroclasts devitrified to microcrystalline quartz. (d) Microbial filaments covered by a thin layer of altered ash. (e) Accretionary pellet (white arrow) and scattered phenocrysts (black arrows). (f-g) Thin sections of a small accretionary pellet (white arrow) and devitrified pyroclast (black arrow); plane-polarized light (f) and crossed nicols (g). (h-i) Large lithic phenocryst with an equant shape. (j) Cuspate shard, crossed nicols. (k) Euhedral clast devitrified to sericite. (l-m) Fibrous radial sericite in early-formed fractures. Note the molding relationship (m) with the host rock. (n-o) Devitrified glass shards (n) and glass spheres (o) in cherty tuffite.

X-ray diffraction (XRD) patterns and mid-infrared (MIR) and near-infrared (NIR) spectra further reveal that the fossil-bearing clays (clay-rich fossiliferous surfaces and

clay-mineralized microbial mats; hereafter FBCs) are mineralogically similar to the volcanic sediments (volcaniclastic laminae - VL, tuffs and tuffites) but differ from other facies throughout the basin that do not show abundant volcaniclasts or clay mineralized fossils (see Supplementary Text 2, Figs. 10–19, Dataset 1). The FBCs and clays from the volcanic-derived sediments show a predominance of illite (1M polytype) and ordered illite-smectite mixed-layer minerals (R3 I-S MLMs), as suggested by the shoulder on the left side of the illite peak (at 10 Å) and further confirmed by NEWMOD modelling (Supplementary Figs. 14, 15). At higher resolution, the XRD data show that the FBCs exhibit a higher proportion of illite than the clays from the adjacent VL of the same beds, as well as from the tuffs and tuffites (Supplementary Figs. 13, 14). By contrast, the clay assemblages from facies with no fossil-bearing clays are represented by smectite and randomly ordered R0 I/S MLMs (Fig. 3h, Extended Text 2, and Supplementary Figs. 10–19).

Interestingly, in the MIR region between 3000 and 2800 cm<sup>-1</sup>, spectra from both the FBCs and the volcanic material show higher intensities in the absorption bands related to the CH<sub>3</sub> and CH<sub>2</sub> stretching vibrations of aliphatic compounds than those found in samples without fossil-bearing authigenic clays (Supplementary Fig. 18). This finding reinforces the interpretation that volcanic sediments played a role in improving the preservation of the remaining organic material.

In agreement with the results above, scanning electron microscopy with energy dispersive X-ray spectrometry (SEM-EDS) and synchrotron radiation micro-X-ray fluorescence spectroscopy (SR- $\mu$ XRF) analyses showed that the FBCs have high concentrations of K, Al, Fe, Ti, and Mg (Fig. 3), while the host rock contains high concentrations of elements related to the nature of the clasts and cements (e.g., Si, Na, and Fe). The higher concentrations of Al and K, and slightly higher concentrations of Mg in the FBCs than in the host rock, are related to their illitic composition, as confirmed by the oxide weight% results of EDS point analyses (Dataset 2). These illite-rich crystals have the following average composition: (Si<sub>3.56</sub>,Al<sub>0.44</sub>)O<sub>10</sub>(Al<sub>1.63</sub>,Mg<sub>0.11</sub>,Fe<sub>0.20</sub>)(OH)<sub>2</sub>(K<sub>0.61</sub>,Na<sub>0.01</sub>). Raman spectroscopy of the 3D clay-mineralized microbial mats additionally reveals the characteristic peaks of illite (ca. 200 cm<sup>-1</sup>, 264 cm<sup>-1</sup>, 396 cm<sup>-1</sup>, 464 cm<sup>-1</sup>, and 703 cm<sup>-1</sup>) (Fig. 3e, Dataset 3). The results from the fitting of several spectra demonstrate that illite is indeed more concentrated in the FBCs than the cement/matrix (Supplementary Text 3, Supplementary Fig. 21).

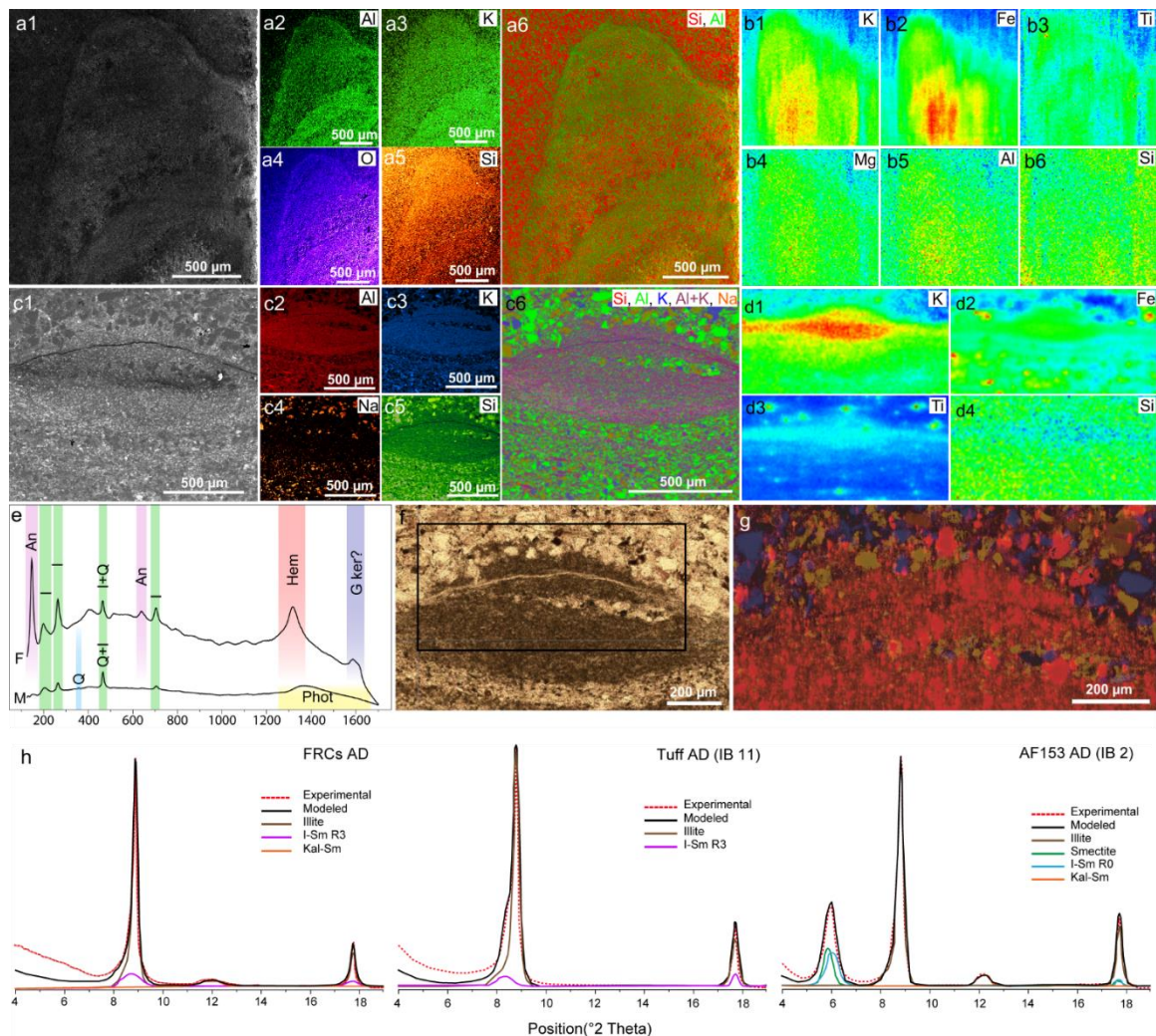


**Figure 3. Geochemical analyses of the fossil-related clays (FBCs) in three-dimensionally preserved microbial mats. (a)** SEM image and EDS maps of a region diagonally crosscutting a 3D preserved tufted microbial mat (see Supplementary Fig. 5), highlighting the concentration of Al and K in the biogenic structure. **(b)** SR- $\mu$ XRF maps of the same region, showing increased intensities of K, Fe, Ti, Mg and Al in the fossil-bearing clays. **(c)** SEM image and EDS maps of a cross-section through a 3D preserved Arumberia-type microbial mat (see Supplementary Fig. 5), revealing relatively higher intensities of Al and K in the fossil. **(d)** SR- $\mu$ XRF of the same region as in (c), showing enrichments and spatial relations of K, Fe and Ti with the microbial mat. **(e)** Representative Raman spectra of FBCs (F) and rock matrix (M). An – anatase, I – illite, Q – quartz, Hem – disordered hematite, G ker – possible G band of kerogen, Phot – artifact of photoluminescence from the glass. **(f-g)** Raman mapping of anatase, quartz and plagioclase of the Arumberia sample. Note the concentration of disseminated and fine-grained anatase in the fossil. **(h)** XRD patterns (air-dried) and

NEWMOD modeling of the FBCs, the tuff sample, and a distal delta-front mudstone sample.

Raman spectroscopy reveals that anatase ( $TiO_2$ ) is the Ti-bearing phase in the 3D clay mineralized microbial mats (Fig. 3e–g, Dataset 4). Anatase is formed of micrometer- to submicrometer-sized crystals (Fig. 3g, Supplementary Fig. 22). Anatase is especially concentrated in the microbial mats, while the matrix also contains a high proportion of another  $TiO_2$  mineral, rutile (Supplementary Text 3, Dataset 3).

## Discussion

The alteration of unstable volcanic glass is well known to promote the formation of new silicate phases(Fisher and Schmincke, 1984; Kawano and Tomita, 1992, 1997, 2002; Ghiara et al., 1993; Kawano et al., 1997; De La Fuente et al., 2000; Konhauser et al., 2002). Their instability is due to nonbridging silicate sites, which allow easy alteration at low temperatures(Kawano et al., 1997). In fact, both experimental and field-based studies have shown the formation of smectite and R0 I-S MLMs from the alteration of volcanic glass occurring at low temperature(Kawano and Tomita, 1992, 1997; Ghiara et al., 1993; De La Fuente et al., 2000). For instance, Kawano & Tomita(Kawano and Tomita, 2002) demonstrated that bacterially influenced alteration of pyroclastic sediments can lead to smectite formation through an allophane precursor, while Konhauser et al.(Konhauser et al., 2002) showed the formation of smectite directly on the cell surfaces of bacteria colonizing basaltic tephra. According to our results, in the FBCs and volcanic sediments of the Itajaí Basin, smectite and/or I-S MLMs were likely the mineral phases derived from the alteration of volcanic sediments. In the Itajaí Basin, the alteration of volcanic sediments, supported by microbial activity, resulted in microenvironments enriched in cations, such as  $K^+$ ,  $Al^{+3}$ , and  $Na^+$ , and then to the precipitation of newly formed clay minerals.

The higher amount of illite in the FBCs than in the adjacent VL and tuffs suggests a link between the presence and activity of microbial communities, and the processes of early diagenetic illitization that resulted in fossil preservation. It is hypothesized here that this higher illitization could then have occurred via two mechanisms: [1] further enrichment in  $K^+$  resulting from microbial metabolism and/or [2] dissimilatory iron reduction (DIR) of  $Fe^{3+}$  in smectite. The former hypothesis is similar to the one proposed for the microbial mats of the Paleoproterozoic Francevillian

Group (Aubineau et al., 2019), where the presence and/or metabolism of ancient microbial mats served as the source of K<sup>+</sup> for the illitization of these microbially related surfaces. Unlike the Francevillian case, in the Itajaí Basin, K-feldspar grains are common in volcaniclastic sediments and likely contributed to posterior diagenetic illitization. However, their presence does not account for the higher illitization of the FBCs than the clays in the VL and tuffs. The second mechanism (DIR) is related to the dissolution of smectite layers during the illitization process. This process could also account for the presence of disordered hematite in the FBCs (see Kim (2012). Furthermore, Zhang et al. (2007) demonstrated that illitization by DIR can be enhanced by an external supply of Al and K, which in the Itajaí Basin could have come from volcaniclastic material. The release of dissolved iron may have also contributed to the adsorption of this element by the extracellular surfaces of bacterial cells, as observed in modern examples (Konhauser et al., 1993). This process can subsequently result in the formation of sites prone to the nucleation of clay mineral phases (Konhauser et al., 1993, 1998; Konhauser and Urrutia, 1999). Several other studies also supported the role of microbes and extracellular polymeric substances (EPS) in providing sites for the nucleation and growth of clay and silicate phases (Ferris et al., 1987, 1991; Tazaki, 1997; Ueshima and Tazaki, 2001).

Interestingly, the enrichment in anatase (as well as disordered hematite, Fe<sub>2</sub>O<sub>3</sub> – Fig. 3e) inside the microbial mats suggests another role for the microbial metabolism in defining the microenvironmental conditions. Studies with modern cases have shown that Fe and Ti can be released in the microenvironment through the bioleaching of ilmenite (FeTiO<sub>3</sub>) by Fe(II)-oxidizing and/or iron-scavenging bacteria (i.e., those that produce siderophores) (Navarrete et al., 2013), thus creating conditions for the precipitation of new phases, such as anatase. Furthermore, experiments with photosynthetic microbial mats have shown the influence of biological activity on the precipitation of anatase when ilmenite was added to the medium (Bower et al., 2015, 2017). In the Itajaí Basin, Fe-Ti oxide grains (e.g., ilmenite and titanomagnetite - now altered to leucoxene; Supplementary Fig. 22) are common in the volcaniclastic sediments, and are a likely source of anatase and Fe enrichment in the ancient mats.

We hypothesize that a combination of abundant and easily-altered volcanic particles - in addition to microbial activity - were the essential conditions necessary for the preservation of the Itajaí biota. This complex interplay between volcanic sediments and microbial activity culminated in the formation of abundant early diagenetic clays

(Fig. 4), resulting in templating the fossil-bearing surfaces with clay precipitates, and preserving the external morphologies of macro-organisms and microbial filaments. In this sense, the Itajaí fossilization pathway could be regarded as a connecting model between the death-mask and the conception-style hypotheses, where both microbial and volcanic activity were essential to the ‘Ediacaran-style’ fossilization by authigenic minerals.



**Figure 4.** Artistic representation of the volcanic and microbial influences on the preservation of Itajaí organisms.

The role of volcanic material in the preservation of certain Ediacaran assemblages has been previously proposed for the conception-style preservation (Narbonne, 2005). However, details explaining this mechanism have not been provided to support this hypothesis, and until now, no authigenic minerals have been associated with this model. In this sense, without further evidence, one could consider the ‘conception-style’ preservation observed in Newfoundland as resulting simply from event deposition, as previously noted (Seilacher, 1992). Moreover, recent studies have even extended the death-mask model to these deposits, where pyritization would have played a major role in the moldic fossilization (Liu, 2016). Our work shows that, at least for some basins, the fossilization of the Ediacaran macroscopic communities was the result of the interconnected processes related to volcanic and microbial activity.

Volcanic activity has often been considered one of the main causes of biotic events during the history of life on Earth, and here we demonstrated unequivocally that volcanism also played an important role in preserving the information of ancient ecosystems. Other examples are also known from the fossil record (Jefferson, 1982; Hay, 1986; Scott, 1990; Briggs et al., 1996; Orr et al., 2000; Sutton et al., 2005; Jiang et al., 2011; Cantrill et al., 2013) and show that volcanism was not only important for exceptional preservation throughout the geologic record but also diverse in terms of processes and composition of the precursor material.

## **Materials and Methods**

**Macroscopic and petrographic investigation.** Macroscopic features of hand samples were analyzed using a Stereomicroscope ZEISS SteREO Discovery V20 coupled with an Axiocam camera at the Laboratório de Ecologia at the Universidade Federal de Mato Grosso do Sul. The preparation of thin sections was carried out in the Programa de Pós-Graduação em Geologia da Universidade do Vale do Rio dos Sinos (UNISINOS – São Leopoldo). Approximately 119 thin sections of the fossiliferous levels, tuffites, tuffs, and other facies were prepared in order to compare the petrographic data with the mineralogical results from the other techniques. Representative thin sections were polished for a better characterization of the volcaniclasts and devitrification features. We used Zeiss microscopes at the UNINOS and Université de Poitiers (France).

**X-ray diffraction and NEWMOD modeling.** Whole-rock powder and clay mineral fractions (<2 µm) from 24 samples were analyzed with a Panalytical Xpert Pro diffractometer at the University of Poitiers using Cu ( $K\alpha = 1.541874 \text{ \AA}$ ) radiation, with the following configuration: Xcelerator detector; geometry  $\square/\square$  (Bragg-Brentano) ; goniometer of 240 mm radius; wavelength filter of Ni (0.3 mm thick); anti-divergence slit of  $1/8^\circ 2\text{\AA}$ , anti-diffusion slit of  $1/4^\circ 2\text{\AA}$ ; mask of 10 mm in diameter; soller slit of 0.04 rd spacing; and fixed sample holder. The analyses were performed with a voltage of 40 kV and current of 40 mA in the angular range of 2 to  $65^\circ 2\text{\AA}$  (powder) and from 2 to  $35^\circ 2\text{\AA}$  (oriented preparation).

Twenty-two samples originated from different levels (fossiliferous and nonfossiliferous) throughout the basin, while the fossil clays and the intercalated coarse-grained laminae were carefully selected and removed from the fossiliferous

beds. These fossiliferous samples were first prepared using air abrasive processes to grossly clean and remove surrounding matrix from the 3D clay-mineralized microbial mats. Then, we extracted the clays from the selected structures and laminae (fossilized microbial mats and intercalated coarse-grained laminae) under a stereomicroscope using a scalpel. All samples were ground in a mortar and separated for powder analysis. Later, we extracted the clay size fraction ( $<2\text{ }\mu\text{m}$ ) for the oriented preparation. These clay size fractions were then Ca saturated and mounted on glass slides for analysis in air-dried ethylene glycol and after thermal treatment (i.e.,  $350^{\circ}\text{C}$  and  $550^{\circ}\text{C}$ ).

For the characterization of the I-S MLMs we used NEWMOD simulation to model the Reichweite ordering parameter ( $R$ ), which can range from randomly interstratified ( $R = 0$ ) to long-range ordered MLMs ( $R = 1, 2$ , and  $3$ ).

**Scanning electron microscopy.** We used a Quanta 650FEG and FEI Inspect F50 microscopes (project SEM-21836 and SEM-23684) at the Brazilian National Laboratory of Nanotechnology (LNNano/CNPEM) and a JEOL JSM IT500 scanning electron microscope, equipped with secondary electron, backscatter electron detectors and coupled with a Bruker lynxeye Energy Dispersive X-ray Spectrometer (EDX) at the IC2MP laboratory of the Université de Poitiers. Analyses were conducted in high-vacuum mode and with a current tension of 15 Kv. Quantitative SEM point analyses were performed for clay minerals and the corresponding structural formulas were calculated from the total oxides weight percent.

**SR- $\mu$ XRF.** The SR- $\mu$ XRF investigation was performed at the Brazilian Synchrotron Light Laboratory (LNLS) under proposals 20171031 and 20180327. We used polychromatic excitation in microbeam mode and filtering with Fe foils for the measurements. For the FlyScan mode we applied 500 ms of count time per point. For data treatment we used the PyMCA software.

**Raman spectroscopy.** We used a Renishaw InVia microRaman with 785 nm lasers and 17 mW total power (attenuated). The spectra acquisition for all the points in the clays was performed using the same configuration: 785 nm laser; 1s of exposure time; 100 accumulations; laser power of 50%; static acquisition with center in 750; and objective of 100x. This approach yielded robust data for the statistical comparisons of

the fossil clays, matrix and detrital micas. These spectra were obtained in two different time periods and thus compared separately regarding peak position since small variations can occur in the equipment. Both groups of data presented the same pattern of results (see Supplementary Fig. 2). The Raman spectra of the Ti-oxides were realized using the same configuration, with the exception of laser power (5% in this case). Baseline subtraction and fitting were performed using WiRE 4.1. Raman maps were obtained using the streamline method.

**Mid-infrared and near-infrared (MIR, NIR).** We used the clay fractions of the samples for the MIR and NIR investigation. For the MIR, we prepared KBr discs with 1 mg of sample and 149 mg of KBr. The mixture was ground and then pressed under 8 tons during 5 minutes to create the discs. Then, the samples were analyzed by a Nicolet iS50 Fourier transform infrared spectrometer using a DTGS KBr detector with a resolution of  $4\text{ cm}^{-1}$  and accumulation of 100 scans in the range of  $4000\text{-}400\text{ cm}^{-1}$ . The NIR was performed in a Nicolet 6700 Fourier transform infrared spectrometer. All spectra were processed using the OMNIC software.

**$\mu$ -CT.** The X-ray microtomographic analysis was performed at the PLATINA platform of the IC2MP (University of Poitiers) with the RX-Solutions EasyTom XL Duo device. We used a microfocus X-ray source (Hamamatsu L8121-03) coupled with a flat panel imager (Varian PaxScan 2520 DX). The acquisition parameters were as follows: 120 kV voltage,  $200\text{ }\mu\text{A}$  current, 1 mm Al filter, stack acquisition with 2880 projections in 2 turns to acquire the whole sample, 8 frames per second, average of 10 frames per projection, with anti-ring shift procedure and a spatial resolution of  $18.3\text{ }\mu\text{m}$ . The data reconstructions were computed using XAct (RX Solutions) and virtual sections: 3D rendering and movies were produced using AVIZO v.2019.2 (Thermo FisherTM-FEI). X-ray microtomography was also performed at the Brazilian Synchrotron Light Laboratory (LNLS) in the IMX beamline in the energy range of 5 keV to 20 keV with average flux of  $8.1 \times 10^{13}$  photons/s/mm<sup>2</sup> using the white beam. We used a Si filter of 350  $\mu\text{m}$ . The sample was rotated in  $180^\circ$ , and the time of exposition varied according to the intensity of the transmitted beam. The images were reconstructed with the pyRaft62 algorithm. We then processed the reconstructed images using the software AMIRA 6.2 and AVIZO 9.1.

## Acknowledgments

The authors thank the Fundação de Amparo à Pesquisa do Estado de São Paulo (FAPESP - Grant 2016/01827-4 and Grant 2018/21886-0), the Programa de Pós-Graduação em Ecologia e Recursos Naturais (PPGERN – UFSCar), and the Programa de Pós-Graduação em geologia (PPGeo – UNISINOS). This work was also supported by La Région Nouvelle Aquitaine. BB-K and PSGP thanks the Conselho Nacional de Desenvolvimento Científico e Tecnológico (CNPq) for the support. We thank the Brazilian Synchrotron Light Laboratory (LNLS-CNPEM) and the Brazilian Nanotechnology National Laboratory (LNNano-CNEPM), which provided the facilities for the SR- $\mu$ XRF (proposals 20170438; 20171031; 20180327), SEM/EDS (proposals 21836 and 23684) and  $\mu$ -CT (IMX proposal 20180137) analyses. The Laboratório de Preparação de Lâminas Delgadas of UNISINOS provided the thin section preparation. The authors are also grateful to Laboratório de Ecologia (UFMS), Alan Eriksson and Alêny Lopes Francisco Batista for providing access to Stereomicroscope SteREO Discovery V20. We are thankful for the scientific advice from H-U Schminke. We acknowledge J. Brunet, B. Gregoire, C. Laforest, and C. Boissard for all the support during the analyses at the University of Poitiers. The artistic reconstruction was made by J. S. d’Oliveira.

## Author Contributions

BBK, MLAfp and AEA conceived the project. BBK wrote the article with significant contributions from all authors. BBK and CF conducted the clay analyses; interpretations of these results were made by BBK, AEA, KK, AAE, CF, and AMe. AMA performed the  $\mu$ CT analyses and reconstructions at the Université of Poitiers and BBK carried out the  $\mu$ CT analyses at LNLS. AAE performed the structural formula calculations and the Newmod modelling. Field work was performed by BBK, MLAfp, PSGP, ALZR, and TRF. Geologic interpretations were performed by PSGP. Petrographic study was carried out by BBK, with contribution of PSGP and TRF. SR- $\mu$ XRF was conducted by BBK, GMEMP, and GLO. SEM analyses were performed by BBK, GMEMP and GLO. Raman investigations of the clays were made by BBK, and Raman analyses of the Ti-oxides were realized by PBK and DG.

## Competing Interests statement

The authors declare no competing interest.

## Extended Data for “The role of volcanic-derived clays in the preservation of Ediacaran biota”

### **Supplementary Text 1 – Geologic setting**

The Itajaí Group is interpreted as a foreland basin composed of four or five depositional sequences with occasional volcaniclastic input (Rostirolla, 1991; Rostirolla et al., 1992, 1999; Guadagnin et al., 2010; Basei et al., 2011) (DS1–5) (Supplementary Fig. 2, 3). However, there remains controversies regarding the stratigraphic position of the possible DS 5, and for that reason it was excluded from our generalized stratigraphic column (Supplementary Fig. 2). Some authors interpret the DS5 deposits as a repetition of the previous units due to overthrusting. Zircon radiometric dating of tuff levels of the DS1 revealed sedimentation ages of  $563 \pm 3$  Ma (Becker-Kerber et al., 2020), agreeing with previous reported ranges for the deposition of the Itajaí Basin (572–549 Ma; see ref (Guadagnin et al., 2010))

At the base, the DS 1 is characterized by alluvial deposits grading to deltaic-shallow marine settings. The overlying DS2 is composed by turbidite deposits, and upsection by upper-slope sediments. DS3 is defined mainly by shallow marine and prodelta deposits. DS4 is also characterized by shallow marine settings, but in this case with more influence of fluvial and proximal delta sediments. The possible DS5 repeats the facies observed in the previous sequences, being composed of turbidites and deltaic deposits. Further discussion on the stratigraphy, depositional environments and tectonic setting of the basin can be found in Rostirolla (Rostirolla, 1991), Rostirolla et al. (Rostirolla et al., 1992), Gresse et al. (Gresse et al., 1996), Fonseca (Fonseca, 2004), Teixeira et al. (Teixeira et al., 2004), Guadagnin (Guadagnin et al., 2010), Basei et al. (Basei et al., 2011). Here we follow the approach of Becker-Kerber et al. (Becker-Kerber et al., 2020) in adapting the depositional sequences defined by Fonseca (Fonseca, 2004) and Teixeira et al. (Teixeira et al., 2004).

### **Supplementary Text 2 – Clay assemblage of the Itajaí Basin**

XRD patterns, MIR and NIR spectra of distinct facies from the Itajaí Basin show that the content of smectite and R0 illite–smectite mixed layer minerals (I–S MLMs) increases towards shallower and proximal settings of the delta deposits, while

fossiliferous horizons display similarities with tuffs and tuffites (Supplementary Figs. 9–19, Dataset 1). The similarities of fossiliferous beds and volcanic sediments (i.e., the higher illite content) in the IR absorption bands are clearer in the Si-O-Si stretching region near  $1030\text{ cm}^{-1}$ , in the OH stretching band near  $3622\text{ cm}^{-1}$  and in the  $2\nu(\text{OH})$  overtone in the NIR region near  $7072\text{ cm}^{-1}$ . It is interesting to note also that the absorption bands related to the presence of Mg in octahedral sheets seems to be more intense in the fossiliferous levels and volcanic sediments, corroborating the data from the elemental analyses (main text).

The smectite enrichment in proximal facies likely reflects river-borne sediments, similar to those observed in modern cases (Meunier, 2005). Conversely, the random occurrence of kaolinite–smectite MLMs, as well as its disordered and iron-rich nature (Supplementary Fig. 9–12, 15–18), suggests a later formation stage by acidic alteration of original clay minerals and/or other minerals (e.g. feldspars, micas), as seen in thin sections (data not shown). Interestingly, the turbidite complex of the depositional sequence 2 (DS2) also showed an increase in smectite content, which likely reflects the reworking of the previous deltaic deposits. Chlorite–smectite MLMs are also present in some samples and its concentration increases in localities closer to intruding rhyolite bodies or to the basin border. This suggests that this Chl–S MLMs results from the later alteration of smectite-rich rocks near these zones.

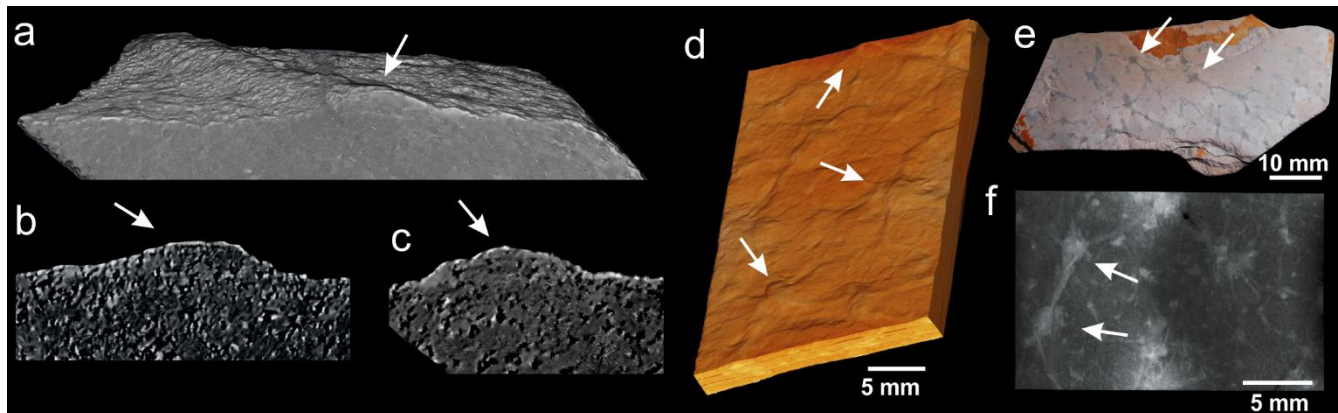
In sum, the results show a complex clay assemblage for the Itajaí Basin, related to sedimentological and diagenetic processes. Importantly, we corroborate the genetic association of the authigenic clays in the fossils and in the volcanic sediments, ruling out other hypotheses for clay enrichment in the fossiliferous surfaces and structures.

### **Supplementary Text 3 - Raman spectroscopy results**

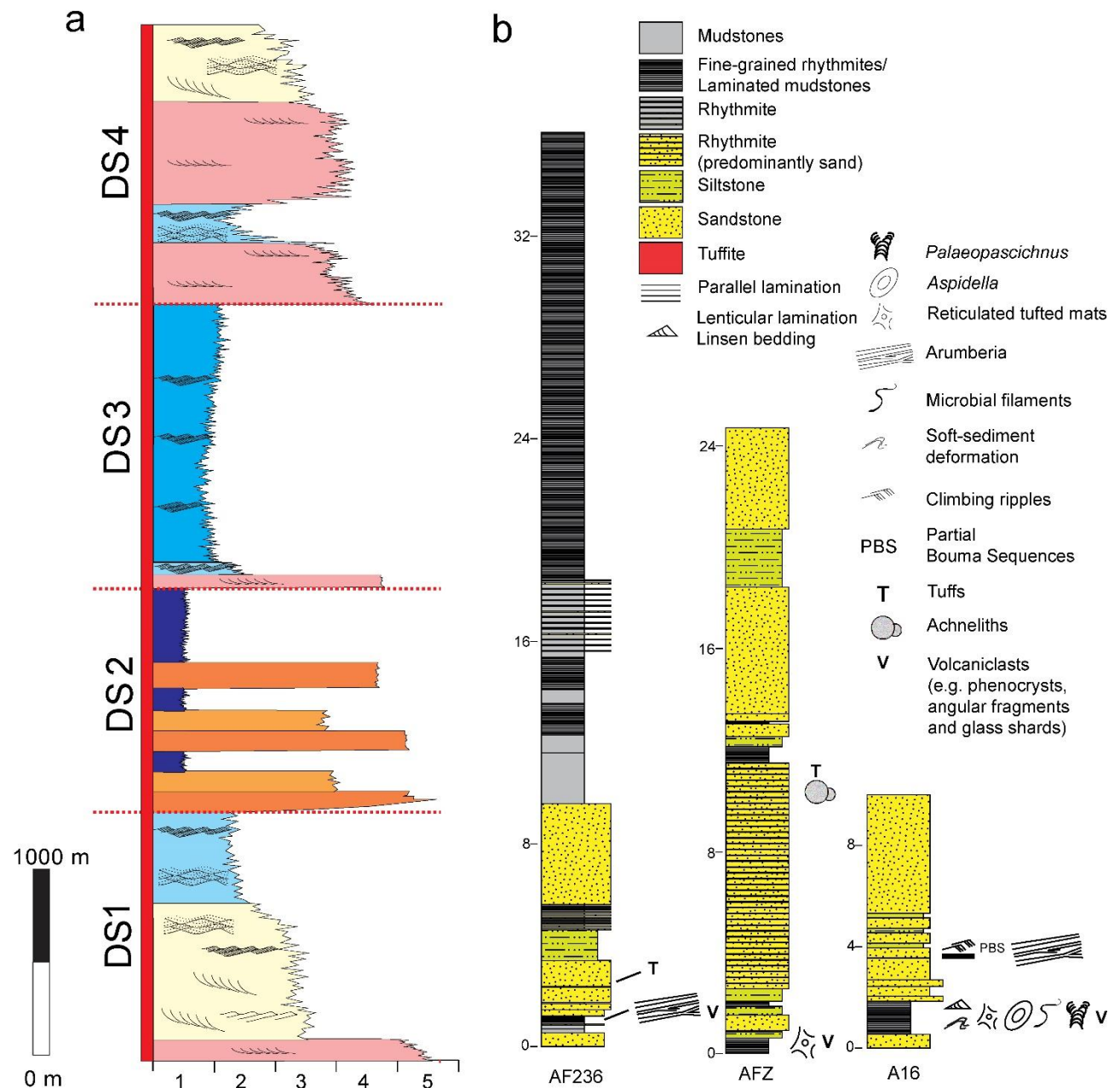
Statistical comparisons of the values obtained by the fitting of the Raman point analyses (Dataset S3) showed that bands of illite are more prevalent in FRCs than in the matrix/cement. Despite that the spectra from the matrix/cement also showed illite, the higher presence of quartz is evident by the common appearance of the weak quartz band near  $355\text{ cm}^{-1}$ . The concentration of clay minerals in the fossils is further evidenced by the higher ratios of  $700\text{ cm}^{-1}/464\text{ cm}^{-1}$  peak area (Supplementary Fig. 21). Higher full width at half maximum (FWHM) values and lower positions of the peak near  $464\text{ cm}^{-1}$  also differentiate the fossils from the matrix (Supplementary Fig. 21). These features are related to the higher influence of the illite band near  $464\text{ cm}^{-1}$ ,

instead of the one representing quartz (Supplementary Fig. 21). When compared to detrital micas, the peak at  $700\text{ cm}^{-1}$  from both the FRCs and matrix clays show similar positions and higher FWHM variation, reflecting not only different mineralogy from the detrital micas, but also a less crystallized clay mineral of authigenic origin.

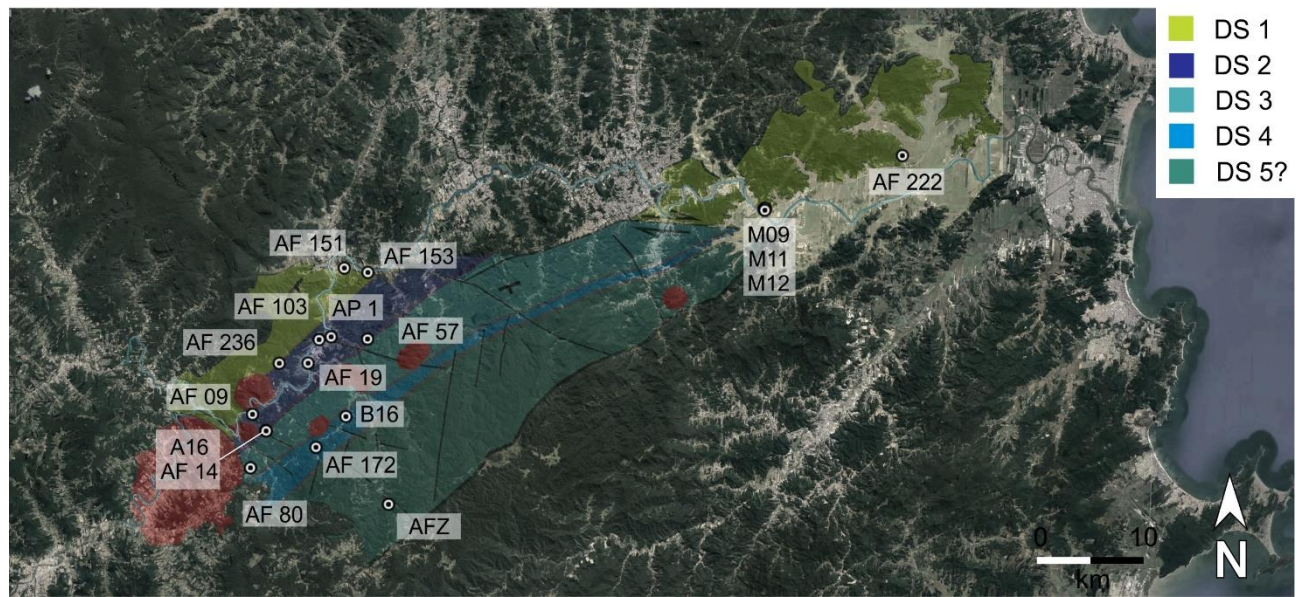
Raman point analyses in randomly chosen  $\text{TiO}_2$  crystals showed a higher proportion of anatase (ca.  $147\text{ cm}^{-1}$ ,  $399\text{ cm}^{-1}$ ,  $639\text{ cm}^{-1}$ ) (compared to rutile) in the FRCs (87.9%; n = 66) than the host rock (66.1%; n = 65) (Dataset S4). Moreover, the point analyses in the clay minerals demonstrated the elevated presence of disseminated fine-grained anatase (Fig. 3e) in the fossils (98.8%, n = 81) compared to the points in the matrix/cement (39.8%, n = 93) (Dataset S3, 4).



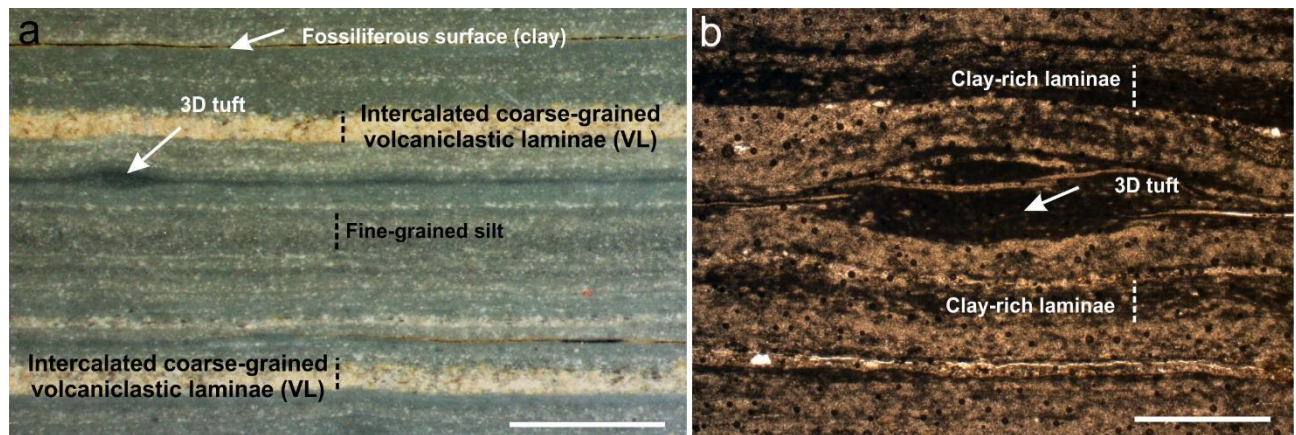
**Supplementary Figure 1.  $\mu$ CT of microbial filaments and 3D microbial tufts.** (a) 3D reconstruction of microbial filaments and sectional views. (b-c) The same clastic texture in the fossils as in the matrix. (d) 3D view of the surface of a sample containing preserved tufts that can be distinguished from the surrounding rock in polished (e) and microtomographic sections (f).



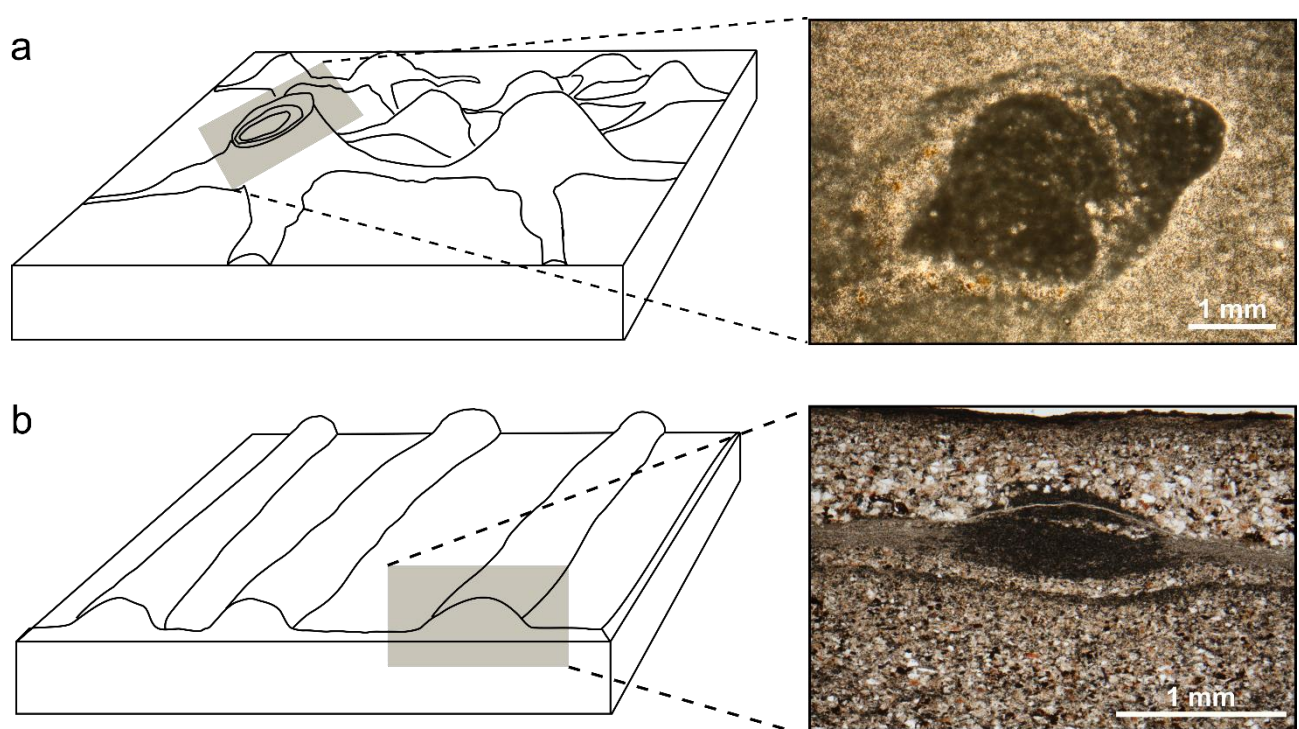
**Supplementary Figure 2. Stratigraphic framework of the Itajaí Basin.** (a) A generalized stratigraphic column of the basin, with the main depositional sequences: DS1; DS2; DS3; and DS4. Depositional Sequence 5 was omitted due to its uncertain stratigraphic relationship. (b) Stratigraphic logs of the main fossiliferous outcrops: AF236; AFZ; and A16.



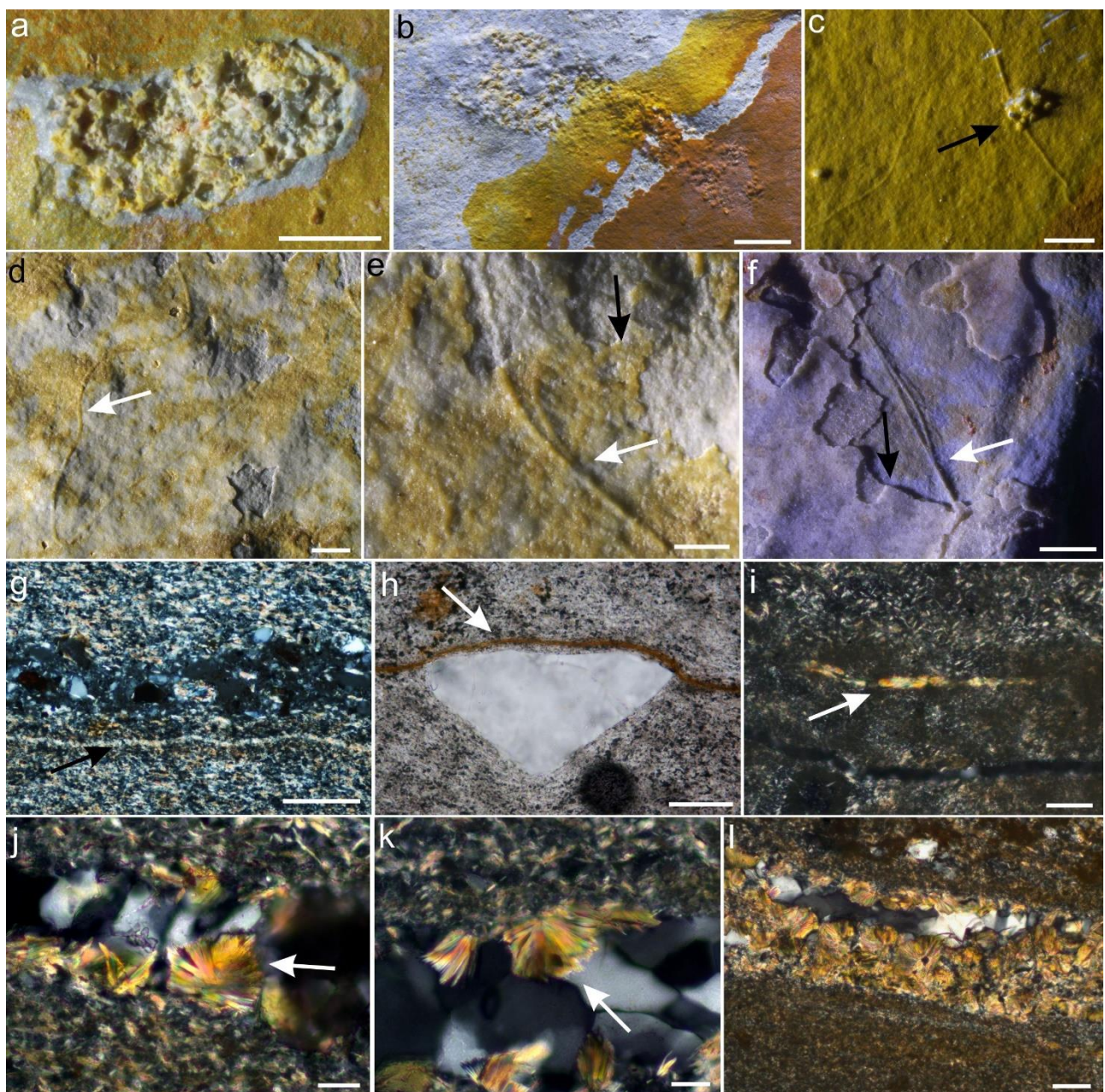
**Supplementary Figure 3. Geographic localization of the outcrops investigated in this study.** The depositional sequences occur from northwestern to southeastern as from base to top, being: DS1, DS2, DS3, DS4, and DS5.



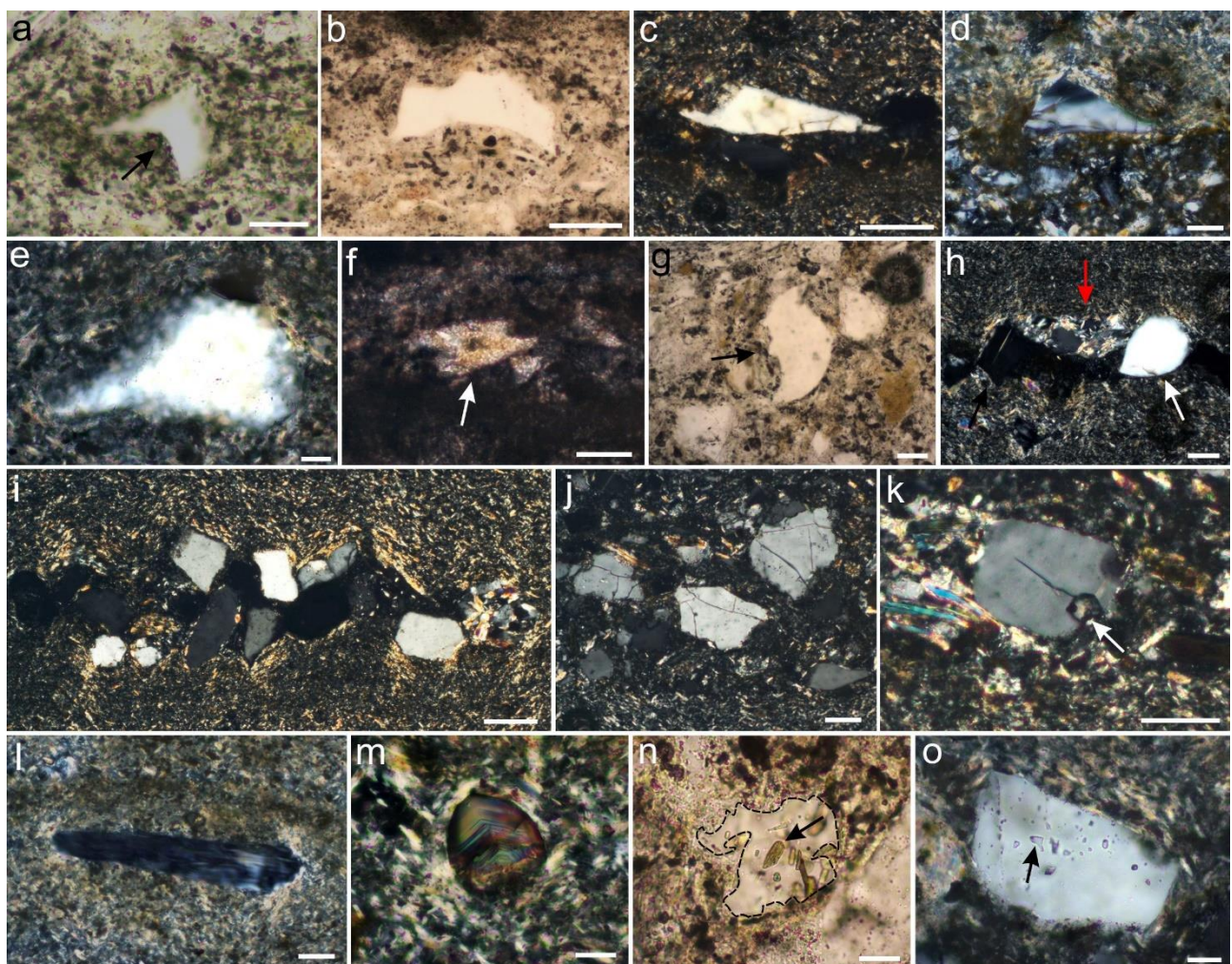
**Supplementary Figure 4. Sedimentary laminae.** (a) Polished cross-section of a hand sample showing the millimeter-scale laminations comprising clay, fine-grained silt and coarse-grained volcaniclastic silt (VL), and the clays preserving the three-dimensional microbial mats. (b) Thin section in plane-polarized light of a similar sample showing the opaque clay-rich laminae intercalated with very fine silt. Scale: 2 mm (a); 1 mm (b).



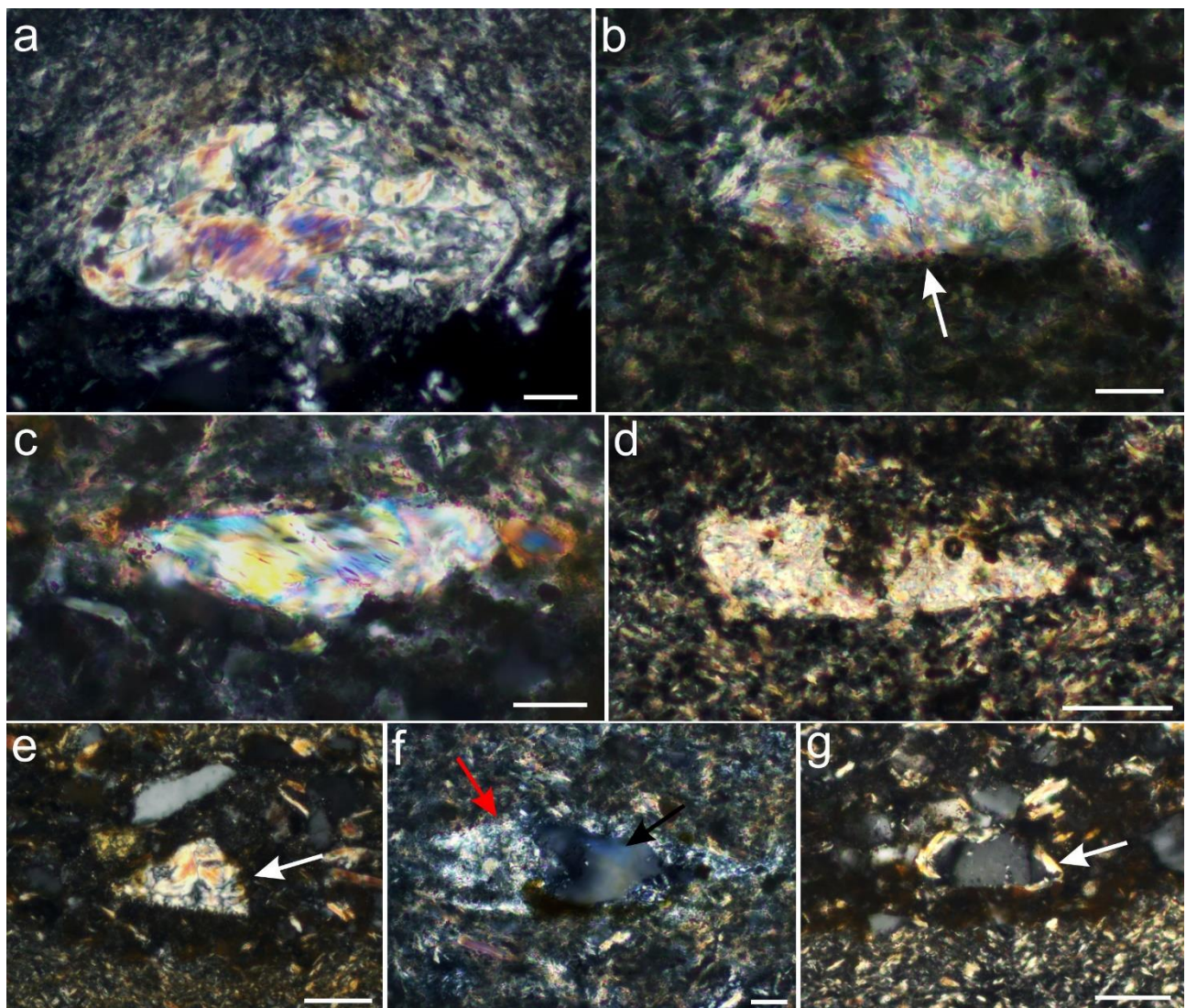
**Supplementary Figure 5. Three-dimensionally preserved microbial mats.** **(a)** Reticulated mats. **(b)** Arumberia-like mats. Insets showing the specific orientations of the thin sections figured to the right.



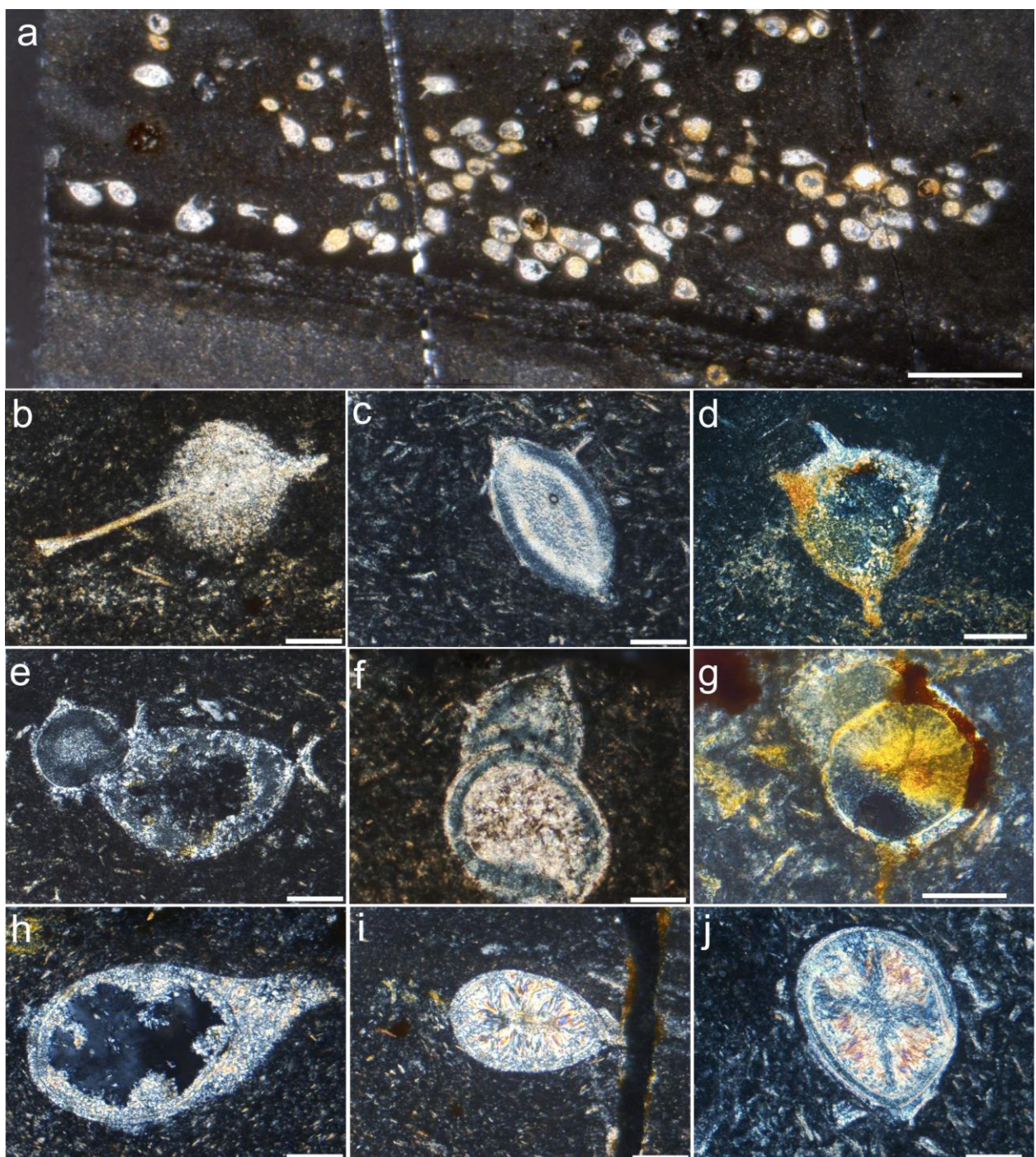
**Supplementary Figure 6. Ash layers and associated features.** (a, b) Slightly reworked accretionary pellets composed of euhedral pyroclasts. (c) Ash cluster associate with fossils. (d-f) Altered ash layers covering filamentous microfossils. (g) Fine-grained ash layer in thin section, similar to those in the hand samples (d, e). (h) Altered fine-grained ash layer covering large euhedral clast. (i) Initial development of fibrous sericite following bedding planes. (j-l) Early-formed fractures filled with fibrous radial sericite and quartz. Scales: 1 mm (a, c, d, f); 2 mm (b); 0.5 mm (e); 100  $\mu\text{m}$  (g); 50  $\mu\text{m}$  (h, i, l); 20  $\mu\text{m}$  (j, k).



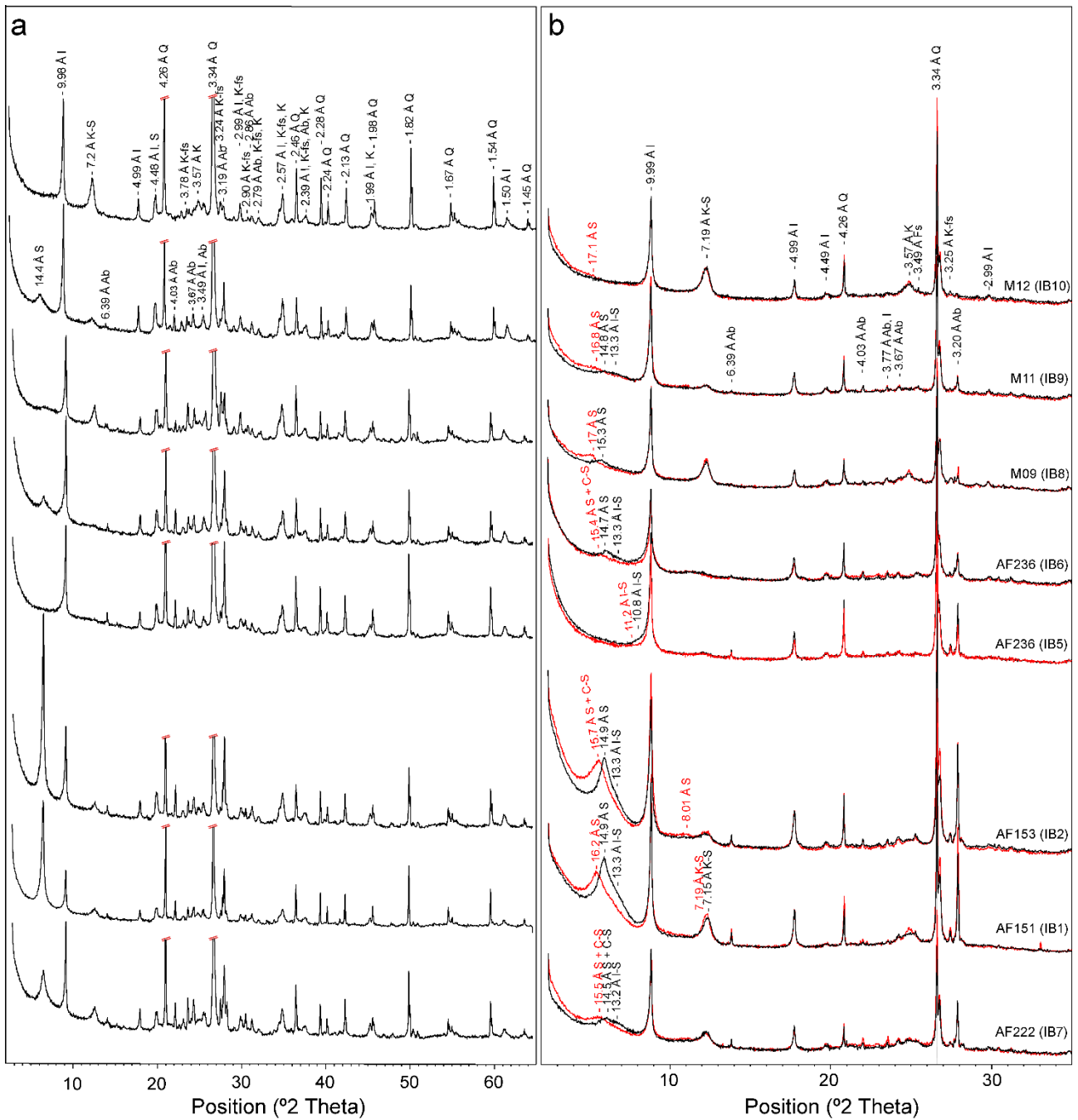
**Supplementary Figure 7. Glass shards and other pyroclasts.** (a–f) Vitric clasts and possible glass shards found associated with the fossiliferous surfaces. (g–h) Smooth shards with fluidal shapes. (i–j) Thin section of accretionary pellets, showing large euhedral phenocrysts, some of which are broken. (k) Phenocryst with vesiculated surface. (l) Phenocryst of perthite. (m) A zircon clast. (n) Apparently dissolved vitric clast with melted inclusions. (o) A vitric clast with fluid inclusions. Scales: 20 µm (a, e, m–o); 50 µm (b, d, f–h, j–l); 100 µm (c, i).



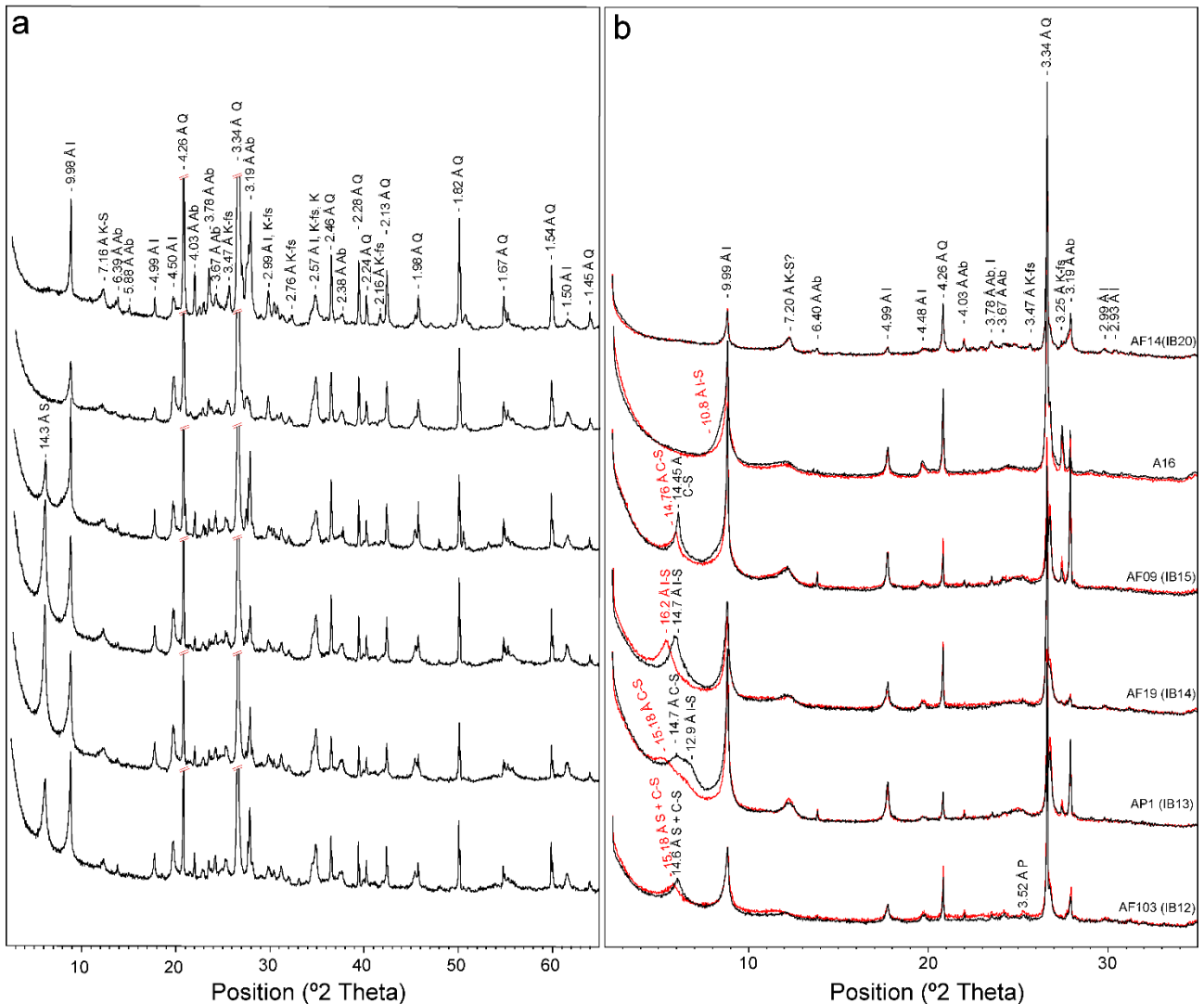
**Supplementary Figure 8. Devitrified glass shards, glassy fragments and clay rims.** (a–d) Devitrified glassy clasts with angular or rounded morphologies. (e) Devitrified euhedral pyroclast. (f) Glass shard devitrified to clay minerals on the exterior and to quartz in the central region. (g) euhedral phenocryst with clay rims. Scales: 20  $\mu\text{m}$  (a–c, f); 50  $\mu\text{m}$  (d, e, g).



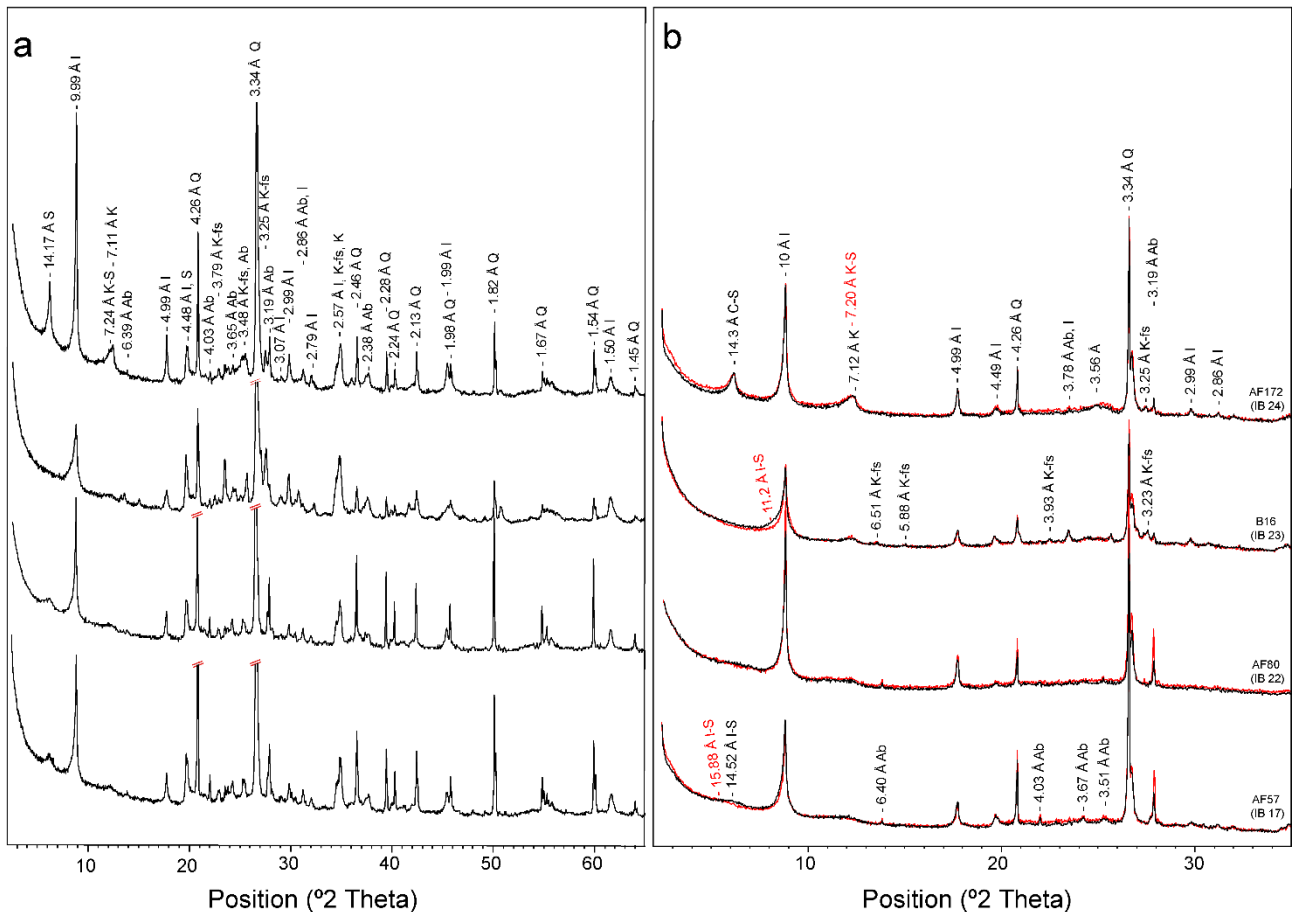
**Supplementary Figure 9. Glass spheres in cherty tuffites of the AFZ outcrop.** (a) Large concentration of slightly transported glass spheres. (b–d) Spheroidal to ellipsoidal shapes with spiny projections. (e–g) Conjoined spheres suggesting subaerial origin by impact. (h) A glass sphere with morphology analogous to vase-shaped microfossils. (i–j) Ellipsoidal glass spheres with clear devitrification features. Scales: 1 mm (a); 100 µm (b–f, h–j); 50 µm (g).



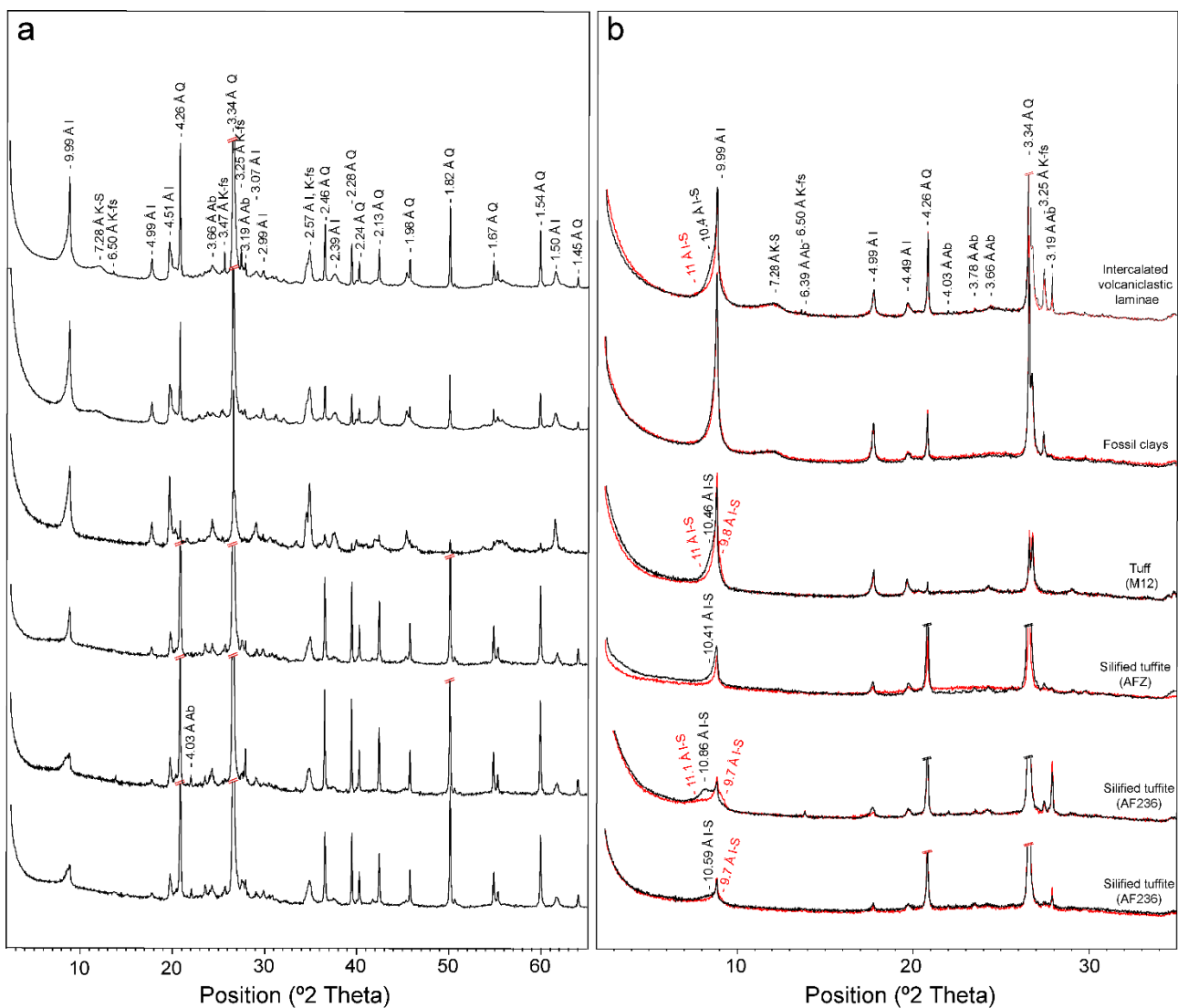
**Supplementary Figure 10. XRD patterns of representative samples from the depositional sequence 1.** Graphs are organized by their relative stratigraphic position in the DS1. **(a)** Bulk powder and **(b)** clay size-fractions ( $<2 \mu\text{m}$ ). Note the higher content of smectite and/or smectite-rich I-S MLMs in the lower sections (more proximal depositional settings). I – Illite; S – Smectite; Q – Quartz; K-fs – K-feldspar; Ab – Albite; K – Kaolinite; I-S – Illite-Smectite mixed layer; C-S – Chlorite-Smectite mixed layer; K-S – Kaolinite-Smectite mixed layer.



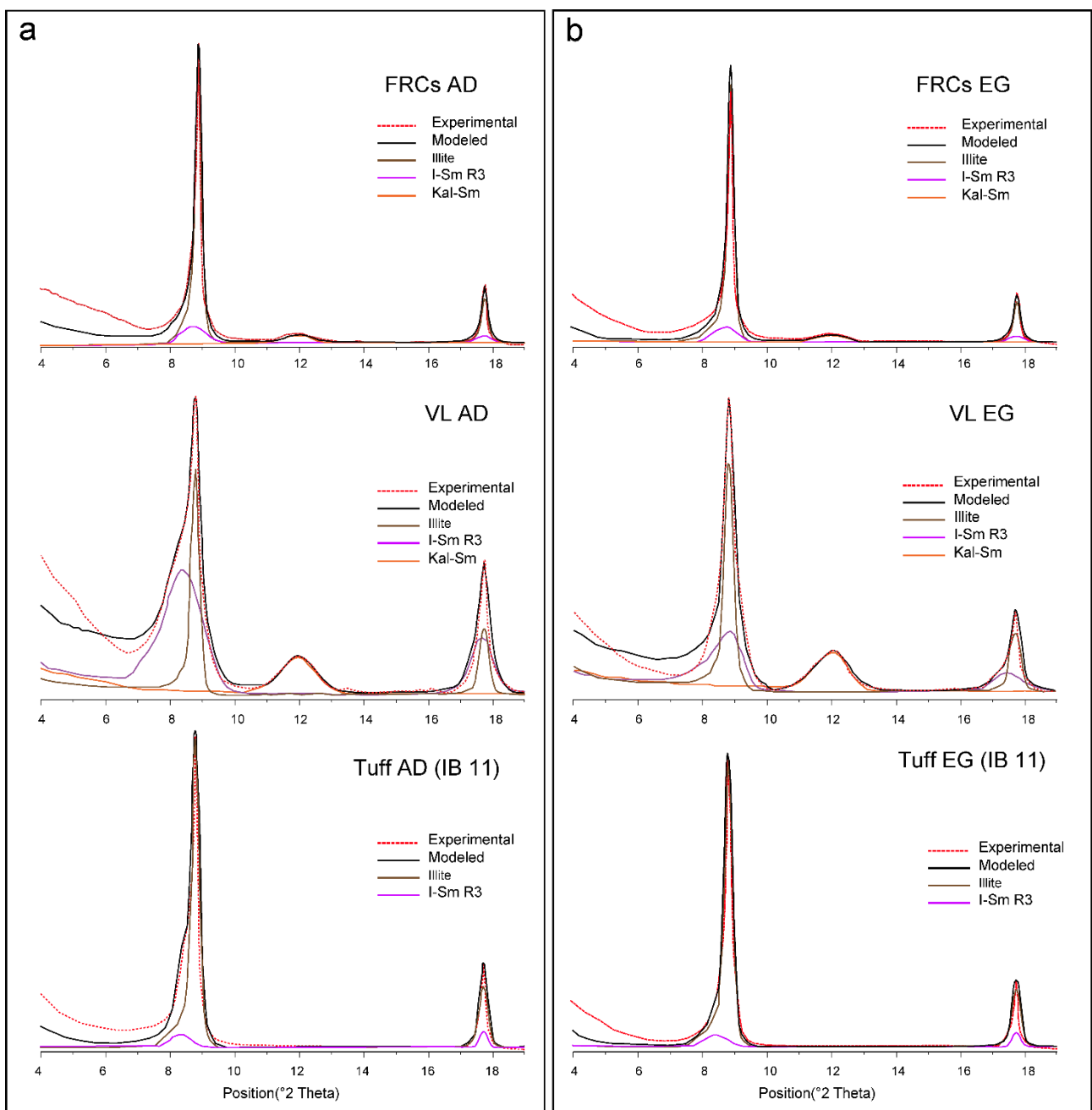
**Supplementary Figure 11. XRD patterns of representative samples from the depositional sequence 2.** Graphs are organized by their relative stratigraphic position in the DS2. **(a)** bulk powder and **(b)** clay fractions (< 2  $\mu$ m). Note the higher smectitic content in the turbiditic complex of the DS2 (IB 12–15). Sample A16, which represents the fossiliferous outcrop, presenting R3 I–S MLMs. I – Illite; S – Smectite; Q – Quartz; K-fs – K-feldspar; Ab – Albite; K – Kaolinite; I-S – Illite-Smectite mixed layer; C-S – Chlorite-Smectite mixed layer; K-S – Kaolinite-Smectite mixed layer.



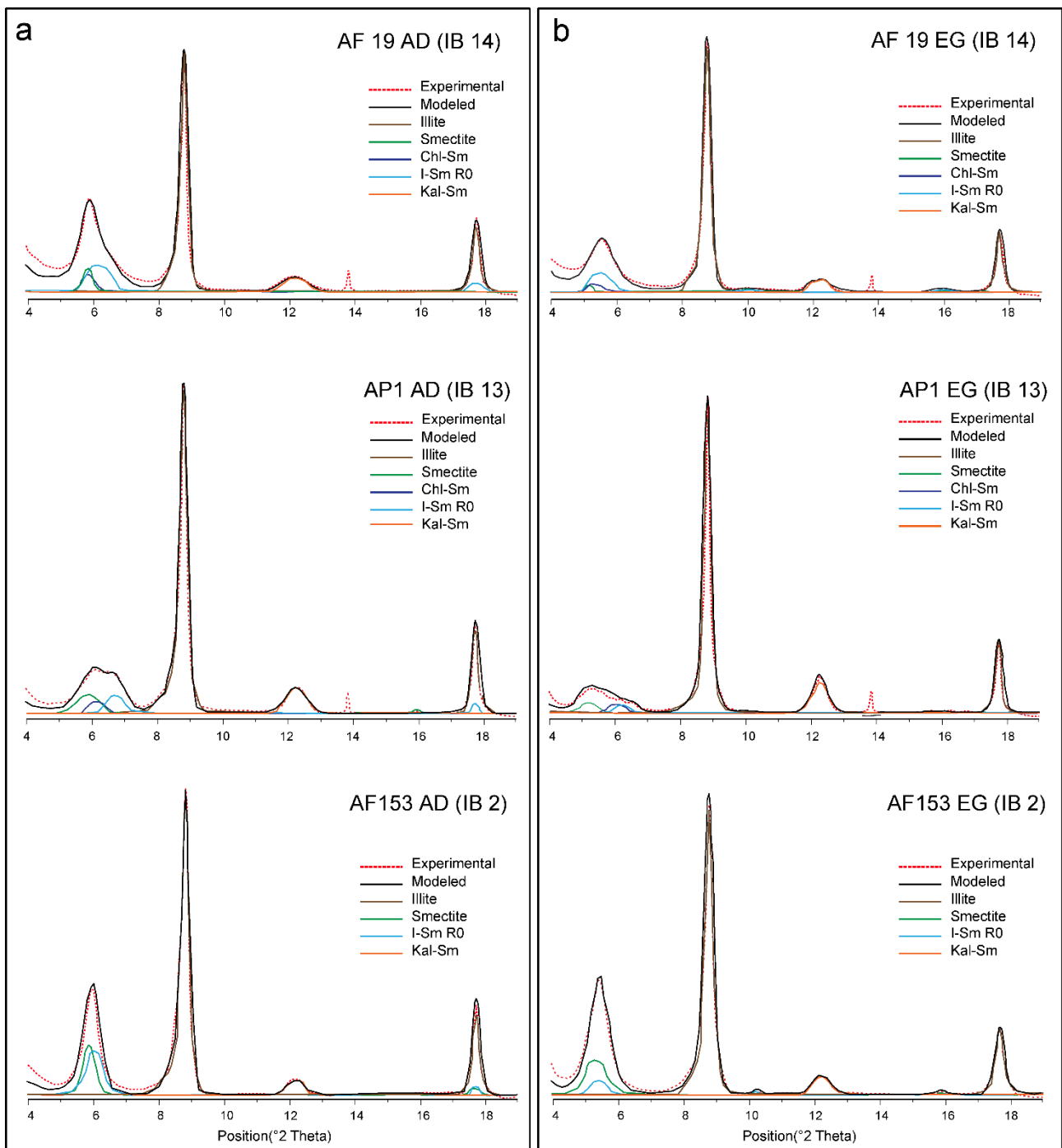
**Supplementary Figure 12. XRD patterns of representative samples from the depositional sequence 3 (distal settings of AF57; B16) and 4 (proximal settings of AF172). (a) bulk powder and (b) clay fractions (< 2  $\mu$ m). Sample B16 represents a fossiliferous outcrop. Note the presence of illite-rich I-S MLMs in B16. I – Illite; S – Smectite; Q – Quartz; K-fs – K-feldspar; Ab – Albite; K – Kaolinite; I-S – Illite-Smectite mixed layer; C-S – Chlorite-Smectite mixed layer; K-S – Kaolinite-Smectite mixed layer.**



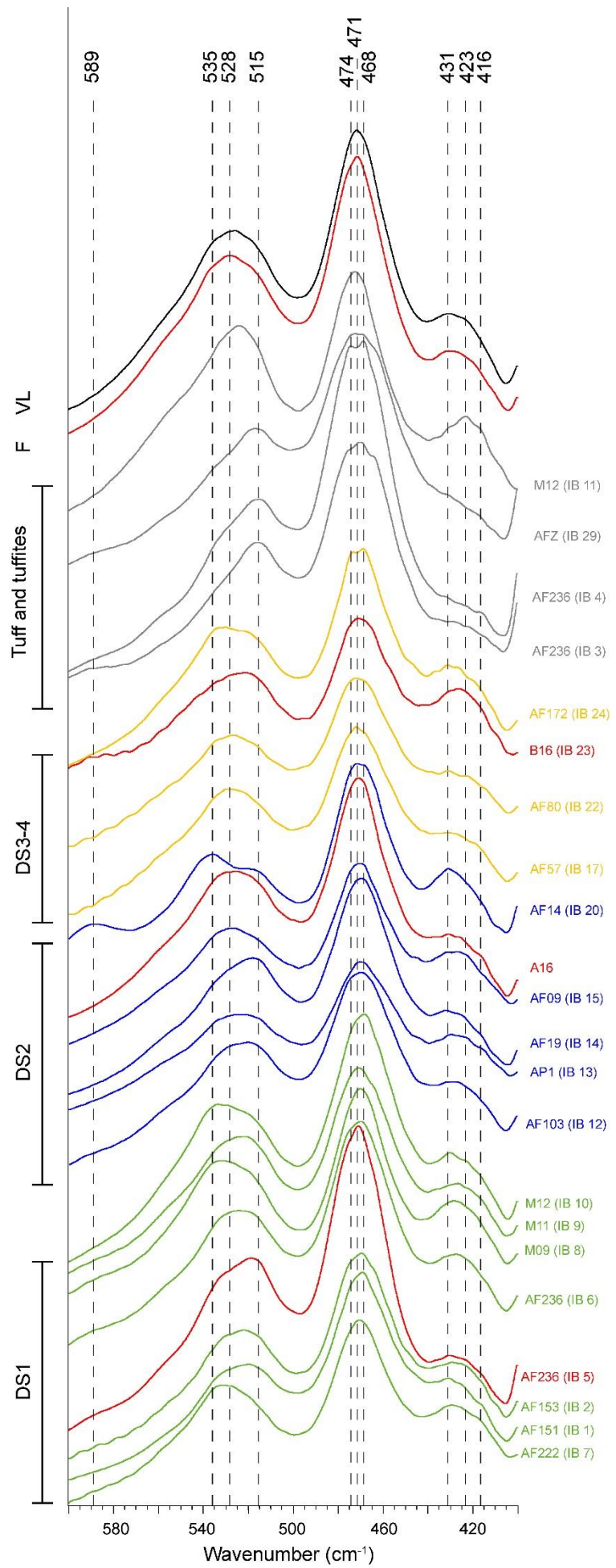
**Supplementary Figure 13.** XRD patterns from the tuff (M12), tuffites (AF236, AFZ), fossil clays, and intercalated volcanoclastic coarse-grained laminae (VL). **(a)** bulk powder and **(b)** clay fractions ( $< 2 \mu\text{m}$ ). Note illite-rich I-S MLMs in all samples except those extracted from the fossil lamina. I – Illite; S – Smectite; Q – Quartz; K-fs – K-feldspar; Ab – Albite; K – Kaolinite; I-S – Illite-Smectite mixed layer; C-S – Chlorite-Smectite mixed layer; K-S – Kaolinite-Smectite mixed layer.



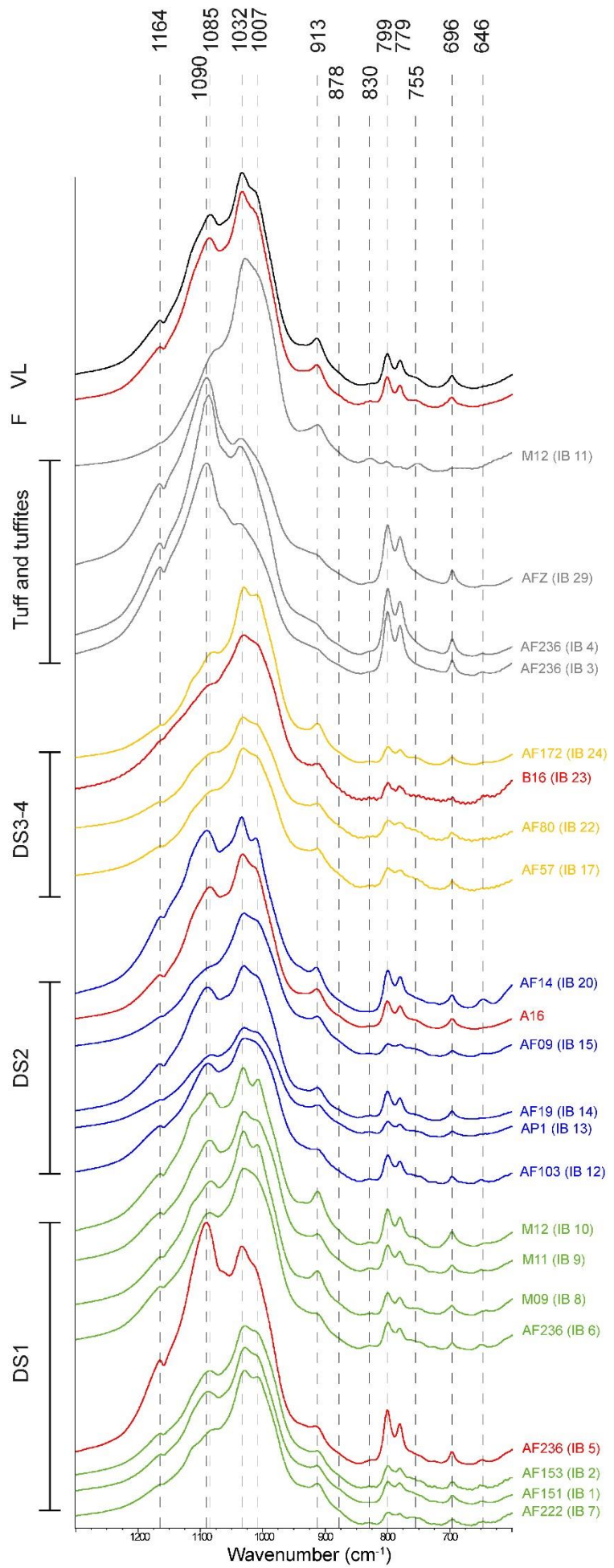
**Supplementary Figure 14. Experimental (dashed lines) and modeled (continuous lines) XRD profiles by Newmod of fossil clays (FRCs), volcanoclastic laminae (VL) and tuff clays, showing the R3 I-S MLMs ordering. (a) After air-dried preparation (AD) and (b) after ethylene-glycol saturation (EG).**



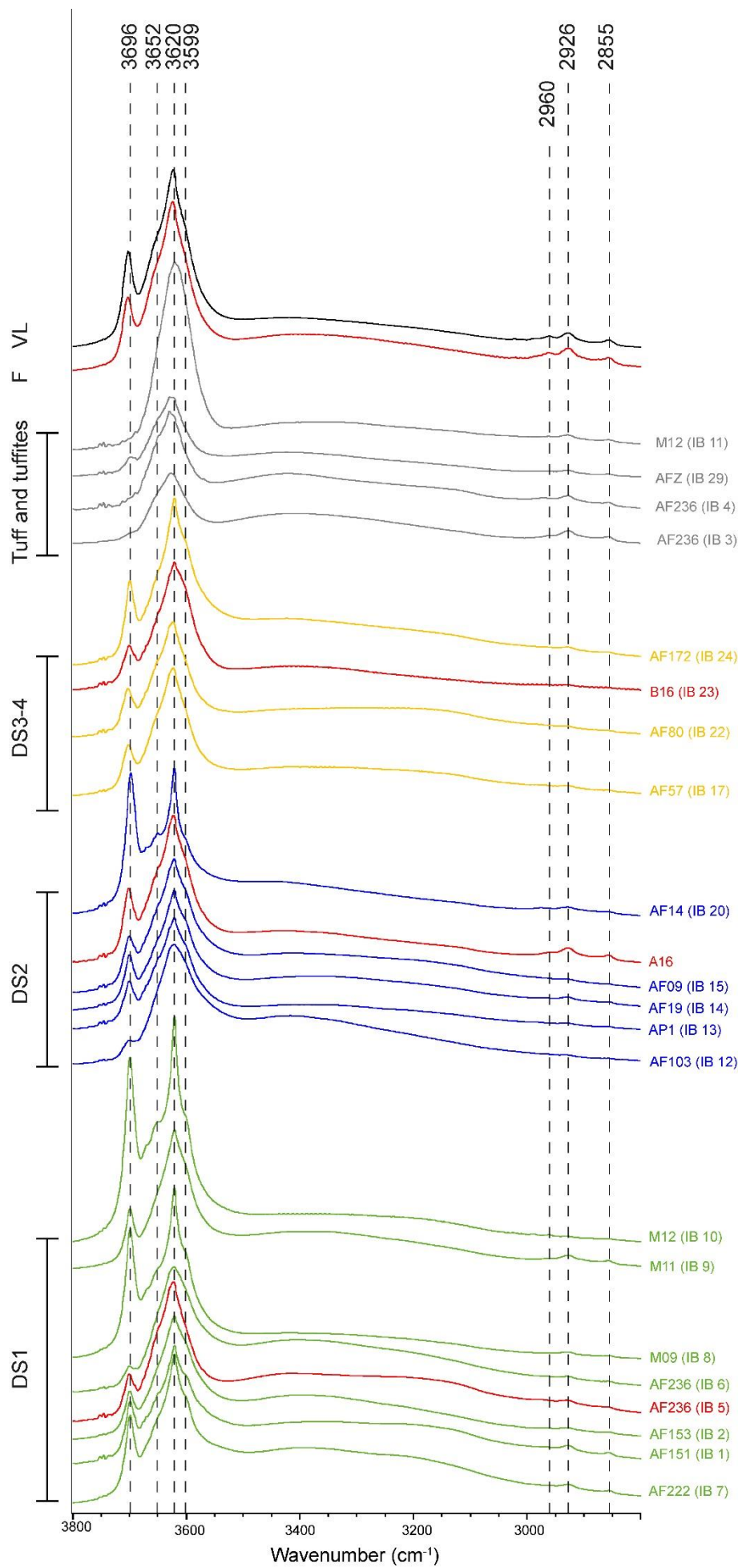
**Supplementary Figure 15. Experimental (dashed lines) and modeled (continuous lines) XRD profiles by Newmod of representative samples from smectite-rich facies, showing the R0 I-S MLMs ordering. (a) After air-dried preparation (AD) and (b) after ethylene-glycol saturation (EG).**



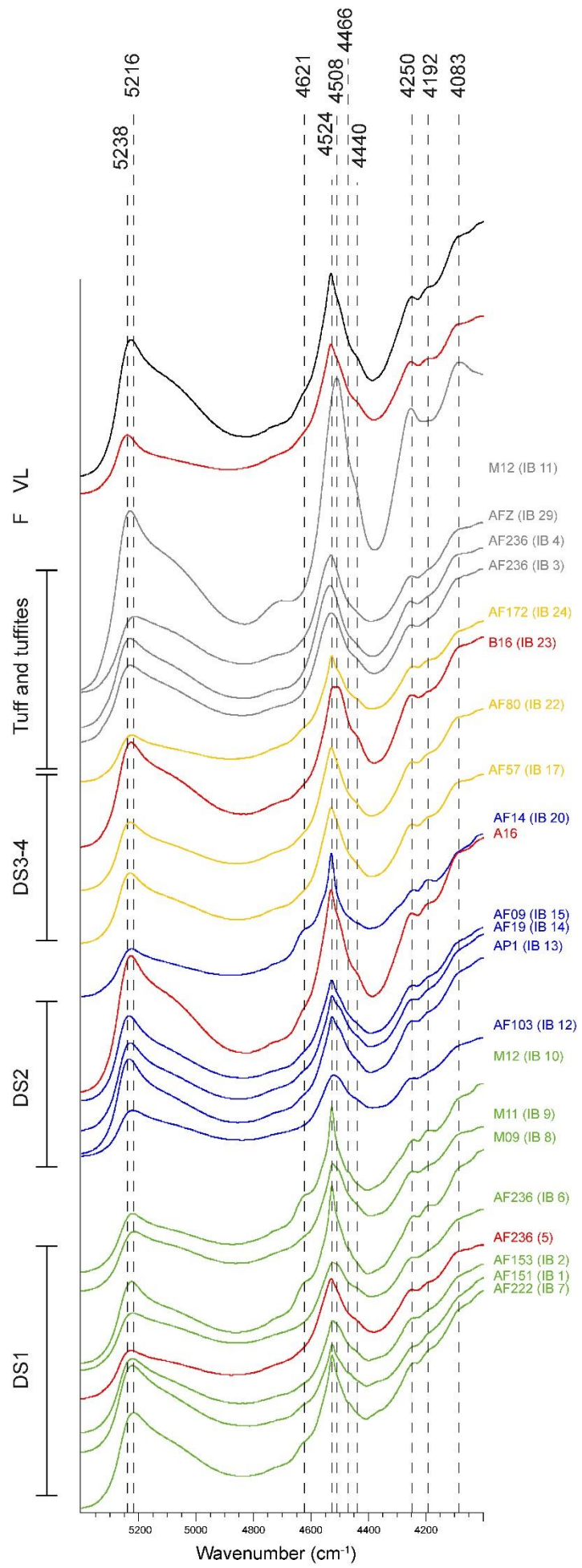
**Supplementary Figure 16. Infrared spectra of the clay fractions in the 600-400 cm<sup>-1</sup> region.** The bands between 420 and 431 cm<sup>-1</sup> are a mixture of the bands of illite (ca. 426 cm<sup>-1</sup>) and kaolinite (ca. 431 cm<sup>-1</sup>). The band near 470 cm<sup>-1</sup> can be assigned to the Si–O–Si bending, and shifts to higher frequencies (471–472 cm<sup>-1</sup>) can be also related to illite or kaolinite bands, while lower frequencies (469 cm<sup>-1</sup>) are more similar to some reported values of smectite (Russell and Fraser, 1994). The bands between 515 cm<sup>-1</sup> and 535 cm<sup>-1</sup> can be assigned to the Si–O–Al<sup>VI</sup> bending vibration (Farmer, 1974). Higher frequencies (~532 cm<sup>-1</sup>) could be related to kaolinite bands, while intermediate (~529 cm<sup>-1</sup>) and lower frequencies (~520 cm<sup>-1</sup>) are closer to illite and smectite values, respectively. Bands around ~589 cm<sup>-1</sup> are attributed to albite(Russell and Fraser, 1994). For details see Dataset S1.



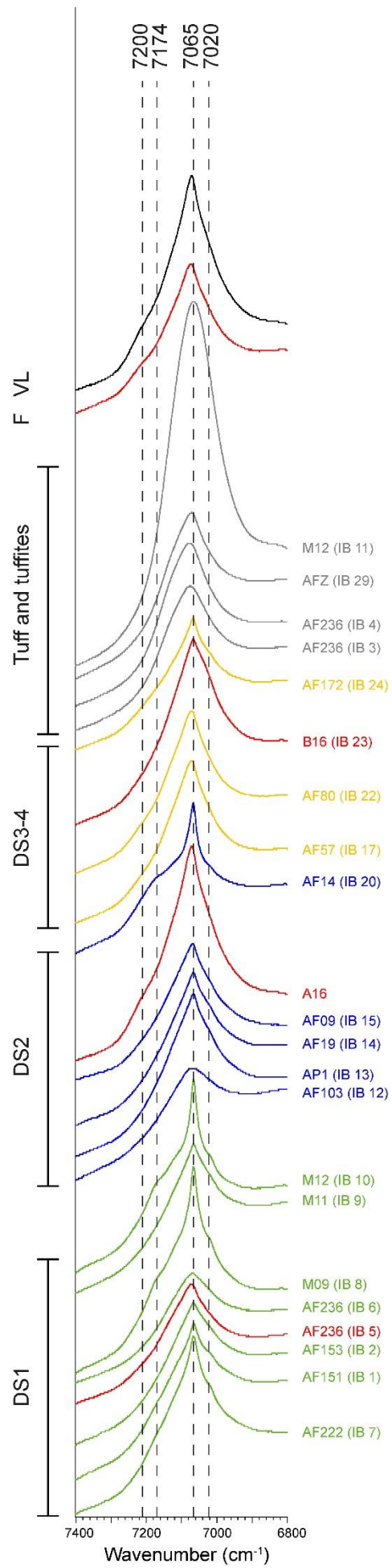
**Supplementary Figure 17. Infrared spectra of the clay fractions in the 1300–600 cm<sup>-1</sup> region.** The broadening of the band near 1028 cm<sup>-1</sup> can be attributed to the Si–O–Si stretching vibrations in samples with higher smectite content. In samples with a higher illite composition, the Si–O–Si stretching vibration appear towards higher frequencies (1032 cm<sup>-1</sup>), and the two strong bands near 1031 cm<sup>-1</sup> and 1008 cm<sup>-1</sup> can be attributed to the kaolinite Si–O–Si stretching vibrations. A weak band near 830 cm<sup>-1</sup> can be assigned to the Al<sup>IV</sup>–O out of plane vibration or AlMgOH bending vibrations of illite (Farmer, 1974; Zviagina et al., 2015), and the band near 913 cm<sup>-1</sup> to the AlOHAl bending of illite, smectite or kaolinite. A weak inflexion near 878 cm<sup>-1</sup> can be related to the δ(AlFe<sup>3+</sup>OH) vibrations in kaolinite (Mendelovici et al., 1979; Petit and Decarreau, 1990). The typical absorption bands of quartz appear at 779 cm<sup>-1</sup>, 799 cm<sup>-1</sup>, and near 1085 cm<sup>-1</sup> and 1163 cm<sup>-1</sup>. DS1 = Depositional Sequence 1; DS2 = Depositional Sequence 2; DS3-4 = Depositional Sequence 3 and 4; F = Fossil clays; VL = intercalated coarse-grained volcaniclastic laminae. For details see Dataset S1.



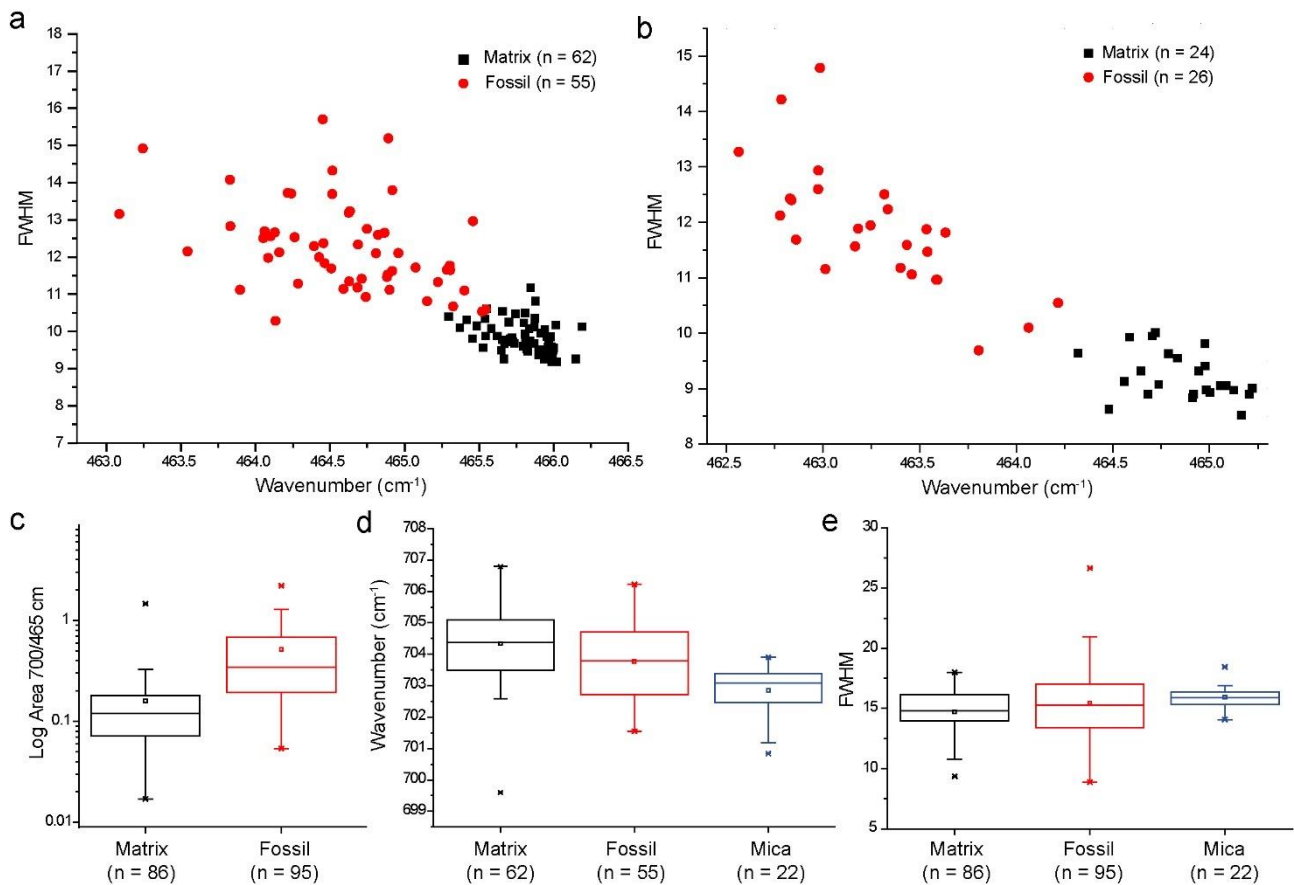
**Supplementary Figure 18. Infrared spectra of the clay fractions in the OH stretching region.** Absorption bands at 3696, 3620, ca. 3669 and ca. 3650  $\text{cm}^{-1}$  are typical of disordered kaolinite, and shoulders near 3600  $\text{cm}^{-1}$  can be attributed to  $\text{Fe}^{3+}$  in their octahedral sheets ( $\text{vAlFeOH}$ ). The broadening of the band near 3620  $\text{cm}^{-1}$  can be related to the presence of the OH-stretching of montmorillonite in the samples higher in smectite content, as seen by XRD patterns. The broadening at the same region also can be related to illite in the illite-rich samples. The broad band near 3420  $\text{cm}^{-1}$  in the smectite-rich samples can be related to the OH stretching of absorbed  $\text{H}_2\text{O}$ , which were not released upon heating. A weak shoulder near 3568  $\text{cm}^{-1}$  in few samples shows that nontronite can also be present in small quantities. Absorption bands between 3000–2800  $\text{cm}^{-1}$  reveal the presence of aliphatic hydrocarbons, relatively more intense in the fossiliferous substrates and volcanic rocks, but small peaks are present throughout almost all examined samples. These bands can be assigned to symmetric  $\text{CH}_3$  stretching (near 2960  $\text{cm}^{-1}$ ), asymmetrical  $\text{CH}_2$  stretching (near 2926  $\text{cm}^{-1}$ ) and symmetrical  $\text{CH}_2$  stretching (near 2855  $\text{cm}^{-1}$ ). For details see Dataset S1.



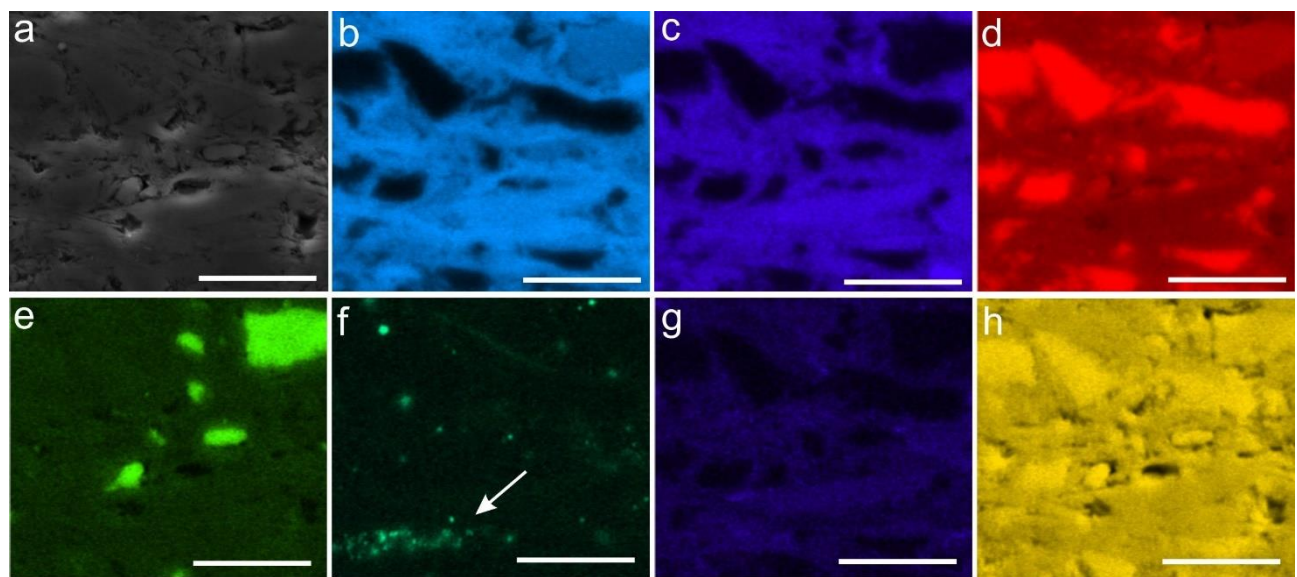
**Supplementary Figure 19. Near-Infrared spectra of the clay fractions in the 5300–4100 cm<sup>-1</sup> region.** The narrow band near 4527 cm<sup>-1</sup> can be attributed to kaolinite, as well as the weaker band near 4621 cm<sup>-1</sup>. The broadening of the region near 4524 cm<sup>-1</sup> is observed in the smectite-rich samples, and can represent the combination bands of montmorillonite. The shoulder near 4466 cm<sup>-1</sup> can be correlated with the absorption band of AlFe<sup>3+</sup>OH and the shoulder near 4440 cm<sup>-1</sup> to (v+δ) AlMgOH (Madejová et al., 2017). Interestingly, the last shoulder is more pronounced in the fossiliferous samples and in the tuff, corroborating the previous presence of montmorillonite, which was later illitized. The shoulder near 4500 cm<sup>-1</sup> could be related to the structural OH in illite. The broad band near 5220 cm<sup>-1</sup> is assigned to the combination modes of the vibrations of water molecules (Madejová et al., 2017). For details see Dataset S1.



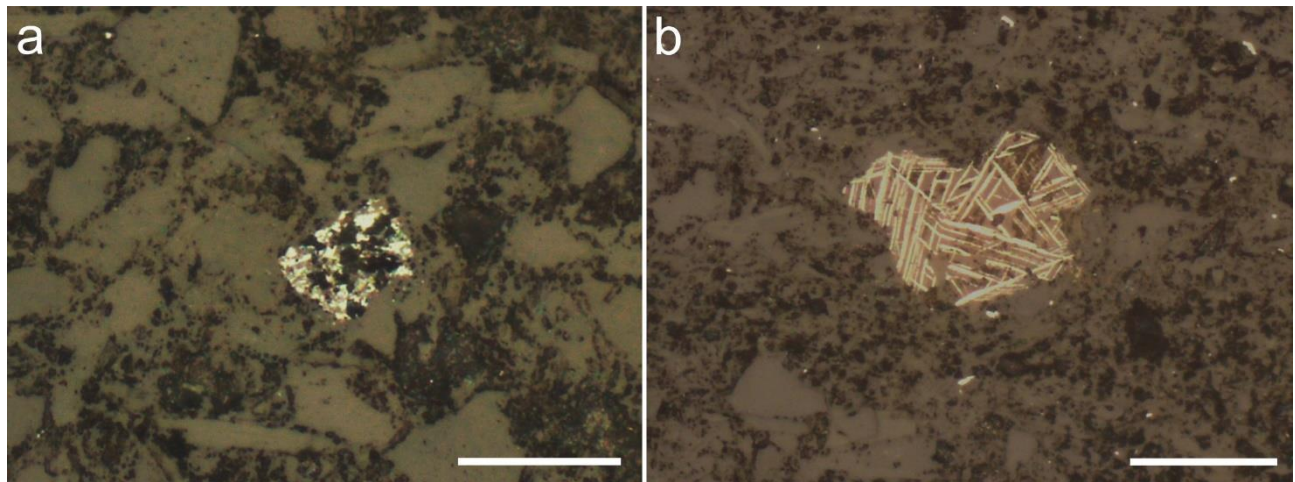
**Supplementary Figure 20. Near-Infrared spectra of the clay fractions in the first overtone region (7400–6800 cm<sup>-1</sup>).** The narrow band at 7065 cm<sup>-1</sup> is attributed to the 2vAl<sub>2</sub>OH overtone of the OH stretching modes (3620 cm<sup>-1</sup>) of kaolinite (Petit et al., 1999), and the shoulder near 7170 cm<sup>-1</sup> corresponds to the first overtone of the 3669 cm<sup>-1</sup> band of kaolinite (Madejová et al., 2017). Changes to higher positions near 7071 cm<sup>-1</sup> likely reflects the 2v(OH) overtone of illite, present in most of the fossiliferous samples and tuffs. The shoulder near 7020 cm<sup>-1</sup> could be related to the overtone of the band at 3598 cm<sup>-1</sup> (vA1OHFe<sup>3+</sup>) of kaolinites with Fe<sup>3+</sup> substitutions. However, the presence of this shoulder seems to correlate with the presence of kaolinite. For details see Dataset S1.



**Supplementary Figure 21. Statistical comparison of Raman fitting results from fossil clays (red), matrix clays (black) and detrital mica (blue).** (a) Scatter plot showing the relationship of full width at half maximum and peak position of fossil and matrix clays. Note that fossil clays present higher FWHM values and lower peak positions, due to the presence of bands of illite (and sometimes quartz) in this region. (b) Same as (a), but results from investigations realized in a different day. (c) Box plot of the 700/465 cm<sup>-1</sup> area ratio, showing higher proportion of area of the peak near 700 cm<sup>-1</sup> (characteristic of phyllosilicates) in the fossils. (d) Box plot of the position of the peak near 700 cm<sup>-1</sup> for the clays in the matrix and the fossils, as well as for micas. Note similar values for fossils and matrix clays. (e) FWHM of the peak near 700 cm<sup>-1</sup> for each type of clay. Note higher FWHM in the spectra from fossil clays and lower values of FWHM for micas, suggesting higher and lower degrees of crystallinity respectively.



**Supplementary Figure 22. EDS maps of a small region inside a three-dimensionally preserved Arumberia-type microbial mat.** (a) electron image. Elemental maps of (b) aluminum, (c) potassium, (d) silicon, (e) sodium, (f) titanium, highlighting fine-grained anatase concentrations (e.g. arrow), (g) iron, and (h) oxygen. Scale: 10  $\mu\text{m}$ .



**Supplementary Figure 23. Leucoxene grains.** (a) Leucoxene after Fe-Ti oxide mineral (probably ilmenite). (b) Leucoxene after titanomagnetite, presenting characteristic trellis texture. Scales: 50  $\mu\text{m}$ .

**Movie 1 (separate file).** Microtomographic movie composed of horizontal sections (bedding plane) of a sample with 3D clay mineralized microbial tufts.

**Dataset 1 (separate file).** Infrared absorption bands of the selected samples (clay fraction)

**Dataset 2 (separate file).** Oxide wt% results and calculated structural formula of illite crystals from fossils

**Dataset 3 (separate file).** Raman fitting results for the fossil and cement/matrix (C/M) clay minerals, and detrital micas

**Dataset 4 (separate file).** Raman spectroscopy polymorph identification in randomly chosen TiO<sub>2</sub> crystals from fossils (3D Arumberia mats) and sedimentary matrix

## 6 FINAL CONSIDERATIONS

The Itajaí Basin provides a unique view on the first benthic communities of macroscopic complex organisms from the fossil record. The new radiometric dating for this occurrence suggests that it can be regarded as one of the oldest in Gondwanan deposits. Despite relatively depauperate in its taxonomic composition, the Itajaí biota yields well-known Ediacaran taxa, such as *Palaeopascichnus*. Other forms are also present, such as discoidal morphologies, diverse microbially-related structures, and well-preserved microbial filamentous forms.

Moreover, the filaments are here interpreted as the impressions of large sulphur-oxidizing bacteria, similar to the modern genus *Beggiatoa*. The common occurrence of these filaments with the Ediacaran biota suggest that they could have been important components of these benthic communities. It is possible that they also contributed to the biogeochemical cycles of N, S and C, during Ediacaran times.

The exceptional preservation of the Itajaí biota sheds new light on the 'Ediacaran-style' moldic fossilization. In this case, it shows how the complex interplay between volcanic sediments and microbial activity can play a major role in the preservation of the external morphology of soft-bodied organisms. This occurred through an early formation of clays that templated the external surfaces of the Ediacaran organisms.

Finally, this work highlights the great potential of the Itajaí Basin for the studies on the early evolution of complex macroorganisms and animals. Future studies can focus in expanding the now known fossil composition, as well as prospecting other portions of the basin. Importantly, volcanoclastic and pyroclastic sediments can also reveal other exceptionally preserved assemblages in this unity. At the same time, the common occurrence of such deposits provides a good opportunity to improve the age constraints of the basin by U/Pb radiometric dating.

## REFERENCES

- ACEÑOLAZA, F.G., 2012, Biodiversity of the Ediacaran-early Cambrian transition in northwestern Argentina and related areas: *Revue de Paleobiologie*, v. 31, p. 299–309.
- ACEÑOLAZA, G., and ACEÑOLAZA, F., 2007, Insights in the Neoproterozoic-Early Cambrian transition of NW Argentina: Facies, environments and fossils in the proto-margin of western Gondwana: *Geological Society Special Publication*, v. 286, p. 1–13, doi: 10.1144/SP286.1.
- ACEÑOLAZA, G.F., GERMS, G.J.B., and ACEÑOLAZA, F.G., 2009, Chapter 9.3 Trace Fossils and the Agronomic Revolution at the Neoproterozoic-Cambrian Transition in Southwest Gondwana: *Developments in Precambrian Geology*, v. 16, p. 339–347, doi: 10.1016/S0166-2635(09)01624-7.
- VAN ACTHERBERGH, E., RYAN, C.G., JACKSON, S.E., and GRIFFIN, W.L., 2001, Data reduction software for LA-ICP-MS, in Sylvester, P.J., ed., *Laser Ablation-ICP-Mass Spectrometry in the Earth Sciences: Principles and Applications*: Mineralogical Association of Canada Short Course Series, Ottawa.
- ANDERSON, E.P., SCHIFFBAUER, J.D., and XIAO, S., 2011, Taphonomic study of Ediacaran organic-walled fossils confirms the importance of clay minerals and pyrite in Burgess Shale-type preservation: *Geology*, v. 39, p. 643–646, doi: 10.1130/G31969.1.
- ANTCLIFFE, J.B., CALLOW, R.H.T., and BRASIER, M.D., 2014, Giving the early fossil record of sponges a squeeze: *Biological Reviews*, v. 89, p. 972–1004, doi: 10.1111/brv.12090.
- ANTCLIFFE, J.B., GOODAY, A.J., and BRASIER, M.D., 2011, Testing the protozoan hypothesis for Ediacaran fossils: A developmental analysis of *Palaeopascichnus*: *Palaeontology*, v. 54, p. 1157–1175, doi: 10.1111/j.1475-4983.2011.01058.x.
- ARROUY, M.J., WARREN, L. V., QUAGLIO, F., POIRÉ, D.G., SIMÕES, M.G., ROSA, M.B., and PERAL, L.E.G., 2016, Ediacaran discs from South America: Probable soft-bodied macrofossils unlock the paleogeography of the Clymene Ocean: *Scientific Reports*, v. 6, p. 1–10, doi: 10.1038/srep30590.

- AUBINEAU, J., EL ABANI, A., BEKKER, A., SOMOGYI, A., BANKOLE, O.M., MACCHIARELLI, R., MEUNIER, A., RIBOULLEAU, A., REYNAUD, J.Y., and KONHAUSER, K.O., 2019, Microbially induced potassium enrichment in Paleoproterozoic shales and implications for reverse weathering on early Earth: *Nature communications*, v. 10, p. 2670, doi: 10.1038/s41467-019-10620-3.  
<http://dx.doi.org/10.1038/s41467-019-10620-3>.
- BAILEY, J. V., CORSETTI, F.A., GREENE, S.E., CROSBY, C.H., LIU, P., and ORPHAN, V.J., 2013, Filamentous sulfur bacteria preserved in modern and ancient phosphatic sediments: Implications for the role of oxygen and bacteria in phosphogenesis: *Geobiology*, v. 11, p. 397–405, doi: 10.1111/gbi.12046.
- BARROSO, F.R.G., 2016, Invertebrados fósseis da Formação Ipu (Siluriano), Grupo Serra Grande, Bacia do Parnaíba: Universidade Federal de Pernambuco, 107 p.
- BARROSO, F.R.G., VIANA, M.S.S., DE LIMA FILHO, M.F., and AGOSTINHO, S.M.O., 2014, First Ediacaran fauna occurrence in Northeastern Brazil (Jaibaras Basin, ? Ediacaran-Cambrian): Preliminary results and regional correlation: *Anais da Academia Brasileira de Ciencias*, v. 86, p. 1029–1042, doi: 10.1590/0001-3765201420130162.
- BASEI, M.A.S., DRUKAS, C.O., NUTMAN, A.P., WEMMER, K., DUNYI, L., SANTOS, P.R., PASSARELLI, C.R., NETO, M.C.C., SIGA, O., and OSAKO, L., 2011, The Itajaí foreland basin: A tectono-sedimentary record of the Ediacaran period, Southern Brazil: *International Journal of Earth Sciences*, v. 100, p. 543–569, doi: 10.1007/s00531-010-0604-4.
- BECKER-KERBER, B., PACHECO, M.L.A.F., RUDNITZKI, I.D., GALANTE, D., RODRIGUES, F., and LEME, J.D.M., 2017, Ecological interactions in Cloudina from the Ediacaran of Brazil: Implications for the rise of animal biomineralization: *Scientific Reports*, v. 7, p. 1–11, doi: 10.1038/s41598-017-05753-8.
- BECKER-KERBER, B., PAIM, P.S.G., CHEMALLE JUNIOR, F., GIRELLI, T.J., DA ROSA, A.L.Z., ALBANI, A. El, OSÉS, G.L., PRADO, G.M.E.M., FIGUEIREDO, M., SIMÕES, L.S.A., and PACHECO, M.L.A.F., 2020, The oldest record of Ediacaran macrofossils in Gondwana (~563 Ma, Itajaí Basin, Brazil): *Gondwana Research*, v. 84, p. 211–228, doi: 10.1016/j.gr.2020.03.007.  
<https://linkinghub.elsevier.com/retrieve/pii/S1342937X20301210>.

- BECKER-KERBER, B., ROSA, A.L.Z. da, PAIM, P.S.G., and PACHECO, M.L.A.F., 2015, Choia-like impressions in ediacaran rocks (Itajaí Basin, Brazil) - Ecosystem engineers in shallow waters?, *in* Astrobiology Science Conference - Habitability, Habitable Worlds, and Life: Chicago.
- BENGTSON, S., SALLSTEDT, T., BELIVANOVA, V., and WHITEHOUSE, M., 2017, Three-dimensional preservation of cellular and subcellular structures suggests 1.6 billion-year-old crown-group red algae: 1–38 p.
- BICCA, M.M., CHEMALE, F., JELINEK, A.R., DE OLIVEIRA, C.H.E., GUADAGNIN, F., and ARMSTRONG, R., 2013, Tectonic evolution and provenance of the Santa Bárbara Group, Camaquã Mines region, Rio Grande do Sul, Brazil: Journal of South American Earth Sciences, v. 48, p. 173–192, doi: 10.1016/j.jsames.2013.09.006. <http://dx.doi.org/10.1016/j.jsames.2013.09.006>.
- BLAIR, S.M., 1983, Taxonomic treatment of the Chaetomorpha and Rhizoclonium species (Cladophorales: Chlorophyta) in New England: Rhodora, v. 85, p. 175–211.
- BLANCO, G., RAJESH, H.M., GAUCHER, C., GERMS, G.J.B., and CHEMALE, F., 2009, Provenance of the Arroyo del Soldado Group (Ediacaran to Cambrian, Uruguay): Implications for the paleogeographic evolution of southwestern Gondwana: Precambrian Research, v. 171, p. 57–73, doi: 10.1016/j.precamres.2009.03.003.
- BLAND, B.H., 1984, Arumberia Glaessner & Walter, a review of its potential for correlation in the region of the Precambrian-Cambrian boundary: Geological Magazine, v. 121, p. 625–633, doi: 10.1017/S0016756800030776.
- BOAG, T.H., DARROCH, S.A.F., and LAFLAMME, M., 2016, Ediacaran distributions in space and time: Testing assemblage concepts of earliest macroscopic body fossils: Paleobiology, v. 42, p. 574–594, doi: 10.1017/pab.2016.20.
- BOBROVSKIY, I., KRASNOVA, A., IVANTSOV, A., LUZHNAIA (SEREZHNIKOVA), E., and BROCKS, J.J., 2019a, Simple sediment rheology explains the Ediacara biota preservation: Nature Ecology and Evolution, v. 3, p. 582–589, doi: 10.1038/s41559-019-0820-7. <http://dx.doi.org/10.1038/s41559-019-0820-7>.
- BOBROVSKIY, I., KRASNOVA, A., IVANTSOV, A., LUZHNAIA (SEREZHNIKOVA), E., and BROCKS, J.J., 2019b, Simple sediment rheology explains the Ediacara biota

- preservation: *Nature Ecology and Evolution*, doi: 10.1038/s41559-019-0820-7.  
<http://dx.doi.org/10.1038/s41559-019-0820-7>.
- BOWER, D.M., HUMMER, D.R., and STEELE, A., 2017, An experimental look at the taphonomy of cyanobacterial mats in siliciclastic sediments: *PALAIOS*, v. 32, p. 725–738, doi: 10.2110/palo.2017.016.  
<https://pubs.geoscienceworld.org/palaios/article-lookup?doi=10.2110/palo.2017.016>.
- BOWER, D.M., HUMMER, D.R., STEELE, A., and KYONO, A., 2015, The Co-Evolution of Fe-Oxides, Ti-Oxides, and Other Microbially Induced Mineral Precipitates In Sandy Sediments: Understanding the Role of Cyanobacteria In Weathering and Early Diagenesis: *Journal of Sedimentary Research*, v. 85, p. 1213–1227, doi: 10.2110/jsr.2015.76.
- BOWYER, F., WOOD, R.A., and POULTON, S.W., 2017, Controls on the evolution of Ediacaran metazoan ecosystems: A redox perspective: *Geobiology*, v. 15, p. 516–551, doi: 10.1111/gbi.12232.
- BOYNTON, H.E., and FORD, T.D., 1995, Ediacaran fossils from the Precambrian (Charnian Supergroup) of Charnwood Forest, Leicestershire, England: *Mercian Geologist*, v. 13, p. 165–182.
- BRASIER, M.D., 1979, The Cambrian radiation event, in House, M.R., ed., *The Origin of the Major Invertebrate Groups*: Academic Press, London, p. 103–159.
- BRIGGS, D.E.G., SIVETER, D.J., and SIVETER, D.J., 1996, Soft-bodied fossils from a Silurian volcaniclastic deposit: *Nature*, v. 382, p. 248–250, doi: 10.1038/382248a0.
- BROWN, R.J., BONADONNA, C., and DURANT, A.J., 2012, A review of volcanic ash aggregation: *Physics and Chemistry of the Earth*, v. 45–46, p. 65–78, doi: 10.1016/j.pce.2011.11.001. <http://dx.doi.org/10.1016/j.pce.2011.11.001>.
- BUATOIS, L.A., 2018, *Treptichnus pedum* and the Ediacaran-Cambrian boundary: Significance and caveats: *Geological Magazine*, v. 155, p. 174–180, doi: 10.1017/S0016756817000656.
- BURZYNSKI, G., DECECCHI, T.A., NARBONNE, G.M., and DALRYMPLE, R.W., 2020, Cryogenian Aspidella from northwestern Canada: *Precambrian Research*, v.

- 336, p. 105507, doi: 10.1016/j.precamres.2019.105507.  
<https://doi.org/10.1016/j.precamres.2019.105507>.
- BURZYNSKI, G., and NARBONNE, G.M., 2015, The discs of Avalon: Relating discoid fossils to frondose organisms in the Ediacaran of Newfoundland, Canada: *Palaeogeography, Palaeoclimatology, Palaeoecology*, v. 434, p. 34–45, doi: 10.1016/j.palaeo.2015.01.014. <http://dx.doi.org/10.1016/j.palaeo.2015.01.014>.
- BUTTERFIELD, N.J., 2015, Proterozoic photosynthesis - a critical review: *Palaeontology*, v. 58, p. 953–972, doi: 10.1111/pala.12211.
- BUTTERFIELD, N.J., KNOLL, A.H., and SWETT, K., 1994, Paleobiology of the Neoproterozoic Svanbergfjellet Formation, Spitsbergen: *Lethaia*, v. 27, p. 76–76, doi: 10.1111/j.1502-3931.1994.tb01558.x. <http://doi.wiley.com/10.1111/j.1502-3931.1994.tb01558.x>.
- CAI, Y., and HUA, H., 2007, Pyritization in the Gaojiashan Biota: *Chinese Science Bulletin*, v. 52, p. 645–650, doi: 10.1007/s11434-007-0080-9.
- CAI, Y., HUA, H., XIAO, S., SCHIFFBAUER, J.D., and LI, P., 2010, Biostratinomy of the Late Ediacaran Pyritized Gaojiashan Lagerstatte From Southern Shaanxi, South China: Importance of Event Deposits: *Palaios*, v. 25, p. 487–506, doi: 10.2110/palo.2009.p09-133r.
- CAI, Y., SCHIFFBAUER, J.D., HUA, H., and XIAO, S., 2012, Preservational modes in the Ediacaran Gaojiashan Lagerstätte: Pyritization, aluminosilicification, and carbonaceous compression: *Palaeogeography, Palaeoclimatology, Palaeoecology*, v. 326–328, p. 109–117, doi: 10.1016/j.palaeo.2012.02.009. <http://dx.doi.org/10.1016/j.palaeo.2012.02.009>.
- CALLOW, R.H.T., BATTISON, L., and BRASIER, M.D., 2011, Diverse microbially induced sedimentary structures from 1Ga lakes of the Diabaig Formation, Torridon Group, northwest Scotland: *Sedimentary Geology*, v. 239, p. 117–128, doi: 10.1016/j.sedgeo.2011.06.002.
- CALLOW, R.H.T., and BRASIER, M.D., 2009a, A solution to Darwin's dilemma of 1859: Exceptional preservation in Salter's material from the late Ediacaran Longmyndian supergroup, England: *Journal of the Geological Society*, v. 166, p. 1–4, doi: 10.1144/0016-76492008-095.

- CALLOW, R.H.T., and BRASIER, M.D., 2009b, Remarkable preservation of microbial mats in Neoproterozoic siliciclastic settings: Implications for Ediacaran taphonomic models: *Earth-Science Reviews*, v. 96, p. 207–219, doi: 10.1016/j.earscirev.2009.07.002.
- CALVER, C.R., GREY, K., and LAAN, M., 2010, The “string of beads” fossil (*Horodyskia*) in the mid-Proterozoic of Tasmania: *Precambrian Research*, v. 180, p. 18–25, doi: 10.1016/j.precamres.2010.02.005.  
<http://dx.doi.org/10.1016/j.precamres.2010.02.005>.
- CANFIELD, D.E., POULTON, S.W., and NARBONNE, G.M., 2007, Late-Neoproterozoic deep-ocean oxygenation and the rise of animal life: *Science*, v. 315, p. 92–95, doi: 10.1126/science.1135013.
- CANTRILL, D.J., BAMFORD, M.K., WAGSTAFF, B.E., and SAUQUET, H., 2013, Early Eocene fossil plants from the Mwadui kimberlite pipe, Tanzania: Review of Palaeobotany and Palynology, v. 196, p. 19–35, doi: 10.1016/j.revpalbo.2013.04.002.
- CLOUD, P., 1973, Pseudofossils: A Plea for Caution: *Geology*, v. 1, p. 123, doi: 10.1130/0091-7613(1973)1<123:PAPFC>2.0.CO;2.  
<https://pubs.geoscienceworld.org/geology/article/1/3/123-127/203333>.
- COHEN, P.A., BRADLEY, A., KNOLL, A.H., GROTZINGER, J.P., JENSEN, S., ABELSON, J., HAND, K., LOVE, G., METZ, J., McLOUGHLIN, N., MEISTER, P., SHEPARD, R., TICE, M., and WILSON, J.P., 2009, Tubular Compression Fossils from the Ediacaran Nama Group, Namibia: *Journal of Paleontology*, v. 83, p. 110–122, doi: 10.1666/09-040r.1.
- CORFU, F., HANCHAR, J.M., HOSKIN, P.W.O., and KINNY, P., 2003, Atlas of Zircon Textures: *Reviews in Mineralogy and Geochemistry*, v. 53, p. 469–500, doi: 10.2113/0530469. <https://pubs.geoscienceworld.org/rimg/article/53/1/469-500/87484>.
- CORNELL, R.M., and SCHWERTMANN, U., 2003, The Iron Oxides: Structure, Properties, Reactions, Occurrences and Uses: Wiley, Weinheim.
- DARROCH, S.A.F., SPERLING, E.A., BOAG, T.H., RACICOT, R.A., MASON, S.J., MORGAN, A.S., TWEEDT, S., MYROW, P., JOHNSTON, D.T., ERWIN, D.H., and LAFLAMME, M.,

- 2015a, Biotic replacement and mass extinction of the Ediacara biota: Proceedings of the Royal Society B: Biological Sciences, v. 282, doi: 10.1098/rspb.2015.1003.
- DARROCH, S.A.F., SPERLING, E.A., BOAG, T.H., RACICOT, R.A., MASON, S.J., MORGAN, A.S., TWEEDT, S., MYROW, P., JOHNSTON, D.T., ERWIN, D.H., and LAFLAMME, M., 2015b, Biotic replacement and mass extinction of the Ediacara biota: Proceedings of the Royal Society B: Biological Sciences, v. 282, doi: 10.1098/rspb.2015.1003.
- DAVIES, N.S., LIU, A.G., GIBLING, M.R., and MILLER, R.F., 2016, Resolving MISS conceptions and misconceptions: A geological approach to sedimentary surface textures generated by microbial and abiotic processes: Earth-Science Reviews, v. 154, p. 210–246, doi: 10.1016/j.earscirev.2016.01.005.  
<http://dx.doi.org/10.1016/j.earscirev.2016.01.005>.
- DING, W., DONG, L., SUN, Y., MA, H., XU, Y., YANG, R., PENG, Y., ZHOU, C., and SHEN, B., 2019, Early animal evolution and highly oxygenated seafloor niches hosted by microbial mats: Scientific Reports, v. 9, p. 1–11, doi: 10.1038/s41598-019-49993-2.
- DONG, L., XIAO, S., SHEN, B., and ZHOU, C., 2008, Silicified Horodyskia and Palaeopascichnus from upper Ediacaran cherts in South China: Tentative phylogenetic interpretation and implications for evolutionary stasis: Journal of the Geological Society, v. 165, p. 367–378, doi: 10.1144/0016-76492007-074.
- DROSER, M.L., GEHLING, J.G., and JENSEN, S.R., 2006, Assemblage palaeoecology of the Ediacara biota: The unabridged edition? Palaeogeography, Palaeoclimatology, Palaeoecology, v. 232, p. 131–147, doi: 10.1016/j.palaeo.2005.12.015.
- DROSER, M.L., GEHLING, J.G., JENSEN, S., and BRIGGS, D.E.G., 2005, Ediacaran trace fossils: true and false, *in* Briggs, D.E.G., ed., Evolving Form and Function: Fossils and Development: Peabody Museum of Natural History, New Haven, p. 125–138.
- DROSER, M.L., TARHAN, L.G., and GEHLING, J.G., 2017, The Rise of Animals in a Changing Environment: Global Ecological Innovation in the Late Ediacaran:

- Annual Review of Earth and Planetary Sciences, v. 45, p. 593–617, doi: 10.1146/annurev-earth-063016-015645.
- DUFOUR, S.C., and McILROY, D., 2017, Ediacaran pre-placozoan diploblasts in the Avalonian biota: The role of chemosynthesis in the evolution of early animal life: Geological Society Special Publication, v. 448, p. 211–219, doi: 10.1144/SP448.5.
- DUNN, F.S., and LIU, A.G., 2019, Viewing the Ediacaran biota as a failed experiment is unhelpful: *Nature Ecology and Evolution*, v. 3, p. 512–514, doi: 10.1038/s41559-019-0815-4. <http://dx.doi.org/10.1038/s41559-019-0815-4>.
- ESCAVOLA, M.P., VAN STAAL, C.R., and DAVIS, W.J., 2011, The age and tectonic setting of the Puncoviscana Formation in northwestern Argentina: An accretionary complex related to Early Cambrian closure of the Puncoviscana Ocean and accretion of the Arequipa-Antofalla block: *Journal of South American Earth Sciences*, v. 32, p. 438–459, doi: 10.1016/j.jsames.2011.04.013. <http://dx.doi.org/10.1016/j.jsames.2011.04.013>.
- FARMER, V.C., 1974, The Infrared Spectra of Minerals (V. C. Farmer, Ed.): Mineralogical Society of Great Britain and Ireland, London. <https://pubs.geoscienceworld.org/books/book/1871/>.
- FEDONKIN, M.A., SIMONETTA, A., and IVANTSOV, A.Y., 2007, New data on Kimberella, the Vendian mollusc-like organism (White Sea region, Russia): Palaeoecological and evolutionary implications: Geological Society Special Publication, v. 286, p. 157–179, doi: 10.1144/SP286.12.
- FELBECK, H., and SOMERO, G.N., 1982, Primary production in deep-sea hydrothermal vent organisms: roles of sulfide-oxidizing bacteria: *Trends in Biochemical Sciences*, v. 7, p. 201–204, doi: 10.1016/0968-0004(82)90088-3. <https://linkinghub.elsevier.com/retrieve/pii/0968000482900883>.
- FERRIS, F.G., FYFE, W.S., and BEVERIDGE, T.J., 1991, Bacteria as Nucleation Sites for Authigenic Minerals: Elsevier Science Publishers B.V., 319–325 p. <http://dx.doi.org/10.1016/B978-0-444-88900-3.50035-7>.
- FERRIS, F.G., FYFE, W.S., and BEVERIDGE, T.J., 1987, Bacteria as nucleation sites for authigenic minerals in a metal-contaminated lake sediment: *Chemical Geology*,

- v. 63, p. 225–232, doi: 10.1016/0009-2541(87)90165-3.
- FISHER, R. V., and SCHMINCKE, H.-U., 1984, Alteration of Volcanic Glass, *in* Pyroclastic Rocks: Springer Berlin Heidelberg, Berlin, Heidelberg, p. 312–345. [http://link.springer.com/10.1007/978-3-642-74864-6\\_12](http://link.springer.com/10.1007/978-3-642-74864-6_12).
- FLANNERY, D.T., and WALTER, M.R., 2012, Archean tufted microbial mats and the Great Oxidation Event: New insights into an ancient problem: Australian Journal of Earth Sciences, v. 59, p. 1–11, doi: 10.1080/08120099.2011.607849.
- FONSECA, M.M., 2004, Sistemas deposicionais e estratigrafia de sequências da Bacia do Itajaí, SC e detalhamento do Complexo Turbidítico de Apiúna:UNISINOS.
- FORD, T.D., 1958, Pre-cambrian fossils from Charnwood Forest: Proceedings of the Yorkshire Geological Society, v. 31, p. 211–217, doi: 10.1144/pygs.31.3.211.
- FOSSING, H., GALLARDO, V.A., JØRGENSEN, B.B., HÜTTEL, M., NIELSEN, L.P., SCHULZ, H., CANFIELD, D.E., FORSTER, S., GLUD, R.N., GUNDERSEN, J.K., KÜVER, J., RAMSING, N.B., TESKE, A., THAMDRUP, B., et al., 1995, Concentration and transport of nitrate by the mat-forming sulphur bacterium Thioploca: Nature, v. 374, p. 713–715, doi: 10.1038/374713a0. <https://www.nature.com/articles/374713a0>.
- FUXING, W., and QILING, L., 1982, Precambrian acritarcha: A cautionary note: Precambrian Research, v. 16, p. 291–302, doi: 10.1016/0301-9268(82)90065-1. <https://linkinghub.elsevier.com/retrieve/pii/0301926882900651>.
- GAUCHER, C., SPRECHMANN, P., 1999, Upper Vendian skeletal fauna of the Arroyo del Soldado Group, Uruguay: Beringeria, v. 23, p. 55–91.
- GAUCHER, C., 2000, Sedimentology, palaeontology and stratigraphy of the Arroyo del Soldado Group (Vendian to Cambrian, Uruguay): Beringeria, v. 26, p. 1–120.
- GAUCHER, C., 2018, The Ediacaran-Early Cambrian Fossil Record in Southwest Gondwana, *in* Geology of Southwest Gondwana: Springer International Publishing, p. 543–560. [http://link.springer.com/10.1007/978-3-319-68920-3\\_20](http://link.springer.com/10.1007/978-3-319-68920-3_20).
- GAUCHER, C., BOGGIANI, P.C., SPRECHMANN, P., SIAL, A.N., and FAIRCHILD, T., 2003, Integrated correlation of the Vendian to Cambrian Arroyo del Soldado and Corumbá Groups (Uruguay and Brazil): Palaeogeographic, palaeoclimatic and

- palaeobiologic implications: Precambrian Research, v. 120, p. 241–278, doi: 10.1016/S0301-9268(02)00140-7.
- GAUCHER, C., POIRE, D.G., GOMEZ PERAL, L., and CHIGLINO, L., 2005, Litoestratigrafia, Bioestratigrafia y Correlaciones De Las Sucesiones Sedimentarias Del Neoproterozoico-Cambrico Del Craton Del Rio De La Plata (Uruguay y Argentina): Latin American Journal of Sedimentology and Basin Analysis, v. 12, p. 145–160.
- GEHLING, J.G., 1999, Microbial Mats in Terminal Proterozoic Siliciclastics: Ediacaran Death Masks: Palaios, v. 14, p. 40, doi: 10.2307/3515360.
- GEHLING, J.G., and DROSER, M.L., 2009, Textured organic surfaces associated with the Ediacara biota in South Australia: Earth-Science Reviews, v. 96, p. 196–206, doi: 10.1016/j.earscirev.2009.03.002.  
<http://dx.doi.org/10.1016/j.earscirev.2009.03.002>.
- GEHLING, J.G., NARBONNE, G.M., and ANDERSON, M.M., 2000, The first named Ediacaran body fossil, Aspidella Terranovica: Palaeontology, v. 43, p. 427–456, doi: 10.1111/j.0031-0239.2000.00134.x. <http://doi.wiley.com/10.1111/j.0031-0239.2000.00134.x>.
- GHIARA, M.R., FRANCO, E., PETTI, C., STANZIONE, D., and VALENTINO, G.M., 1993, Hydrothermal interaction between basaltic glass, deionized water and seawater: Chemical Geology, v. 104, p. 125–138, doi: 10.1016/0009-2541(93)90146-A.
- GLAESSNER, M.F., and WALTER, M.R., 1975, New Precambrian fossils from the Arumbera Sandstone, Northern Territory, Australia: Alcheringa: An Australasian Journal of Palaeontology, v. 1, p. 59–69, doi: 10.1080/03115517508619480.  
<http://www.tandfonline.com/doi/abs/10.1080/03115517508619480>.
- GRAZHDANKIN, D., 2004, Patterns of distribution in the Ediacaran biotas: facies versus biogeography and evolution: Paleobiology, v. 30, p. 203–221, doi: 10.1666/0094-8373(2004)030<0203:podite>2.0.co;2.
- GRAZHDANKIN, D., 2014, Patterns of Evolution of the Ediacaran Soft-Bodied Biota: Journal of Paleontology, v. 88, p. 269–283, doi: 10.1666/13-072.
- GRAZHDANKIN, D., and GERDES, G., 2007, Ediacaran microbial colonies: Lethaia, v. 40, p. 201–210, doi: 10.1111/j.1502-3931.2007.00025.x.

- [http://doi.wiley.com/10.1111/j.1502-3931.2007.00025.x.](http://doi.wiley.com/10.1111/j.1502-3931.2007.00025.x)
- GRESSE, P.G., CHEMALE, F., DA SILVA, L.C., WALRAVEN, F., and HARTMANN, L.A., 1996, Late- to post-orogenic basins of the Pan-African - Brasiliano collision orogen in southern Africa and southern Brazil: Basin Research, v. 8, p. 157–171, doi: 10.1046/j.1365-2117.1996.01504.x. <http://doi.wiley.com/10.1046/j.1365-2117.1996.01504.x>.
- GREY, K., 2005, Ediacaran palynology of Australia: Memoir of the Association of Australasian Palaeontologists, v. 31, p. 439.  
<http://trove.nla.gov.au/work/14832209?q&versionId=46618761>.
- GREY, K., and WILLIAMS, I.R., 1990, Problematic bedding-plane markings from the Middle Proterozoic Manganese Subgroup, Bangemall Basin, Western Australia: Precambrian Research, v. 46, p. 307–327, doi: 10.1016/0301-9268(90)90018-L.
- GRIESHABER, M.K., and VÖLKEL, S., 1998, Animal adaptations for tolerance and exploitation of poisonous sulfide: Annual Review of Physiology, v. 60, p. 33–53, doi: 10.1146/annurev.physiol.60.1.33.  
<http://www.annualreviews.org/doi/10.1146/annurev.physiol.60.1.33>.
- GROTZINGER, J.P., BOWRING, S.A., SAYLOR, B.Z., and KAUFMAN, A.J., 1995, Biostratigraphic and Geochronologic Constraints on Early Animal Evolution: Science, v. 270, p. 598–604, doi: 10.1126/science.270.5236.598.  
<http://www.sciencemag.org/cgi/doi/10.1126/science.270.5236.598>.
- GUADAGNIN, F., CHEMALE, F., DUSSIN, I.A., JELINEK, A.R., DOS SANTOS, M.N., BORBA, M.L., JUSTINO, D., BERTOTTI, A.L., and ALESSANDRETTI, L., 2010, Depositional age and provenance of the Itajaí Basin, Santa Catarina State, Brazil: Implications for SW Gondwana correlation: Precambrian Research, v. 180, p. 156–182, doi: 10.1016/j.precamres.2010.04.002.
- GUAN, C., WANG, W., ZHOU, C., MUSCENTE, A.D., WAN, B., CHEN, X., YUAN, X., CHEN, Z., and OUYANG, Q., 2017, Controls on fossil pyritization: Redox conditions, sedimentary organic matter content, and Chuaria preservation in the Ediacaran Lantian Biota: Palaeogeography, Palaeoclimatology, Palaeoecology, v. 474, p. 26–35, doi: 10.1016/j.palaeo.2016.05.013.  
<http://dx.doi.org/10.1016/j.palaeo.2016.05.013>.

- HAGADORN, J.W., FEDO, C.M., and WAGGONER, B.M., 2000, Early Cambrian Ediacaran-type fossils from California: *Journal of Paleontology*, v. 74, p. 731–740, doi: 10.1666/0022-3360(2000)074<0731:ECETFF>2.0.CO;2.  
<http://www.bioone.org/doi/abs/10.1666/0022-3360%282000%29074%3C0731%3AECETFF%3E2.0.CO%3B2>.
- HAY, R.L., 1986, Role of tephra in the preservation of fossils in Cenozoic deposits of East Africa: *Geological Society Special Publication*, v. 25, p. 339–344, doi: 10.1144/GSL.SP.1986.025.01.28.
- HEIKEN, G., 1972, Morphology and Petrography of Volcanic Ashes: *Geological Society of America Bulletin*, v. 83, p. 1961–1988.
- HILLEBRAND, H., DÜRSELEN, C.D., KIRSCHTEL, D., POLLINGHER, U., and ZOHARY, T., 1999, Biovolume calculation for pelagic and benthic microalgae: *Journal of Phycology*, v. 35, p. 403–424, doi: 10.1046/j.1529-8817.1999.3520403.x.
- HOFMANN, H.J., O'BRIEN, S.J., and KING, A.F., 2008, Ediacaran biota on Bonavista Peninsula, Newfoundland, Canada: *Journal of Paleontology*, v. 82, p. 1–36, doi: 10.1666/06-087.1.  
[https://www.cambridge.org/core/product/identifier/S0022336000054147/type/journal\\_article](https://www.cambridge.org/core/product/identifier/S0022336000054147/type/journal_article).
- HORODYSKI, R.J., 1977, Lyngbya Mats at Laguna Mormona, Baja California, Mexico: Comparison with Proterozoic Stromatolites: *SEPM Journal of Sedimentary Research*, v. Vol. 47, p. 1305–1320, doi: 10.1306/212F732E-2B24-11D7-8648000102C1865D.  
<https://pubs.geoscienceworld.org/jsedres/article/47/3/1305-1320/97045>.
- HORSTWOOD, M.S.A., KOŠLER, J., GEHRELS, G., JACKSON, S.E., MCLEAN, N.M., PATON, C., PEARSON, N.J., SIRCOMBE, K., SYLVESTER, P., VERMEESCH, P., BOWRING, J.F., CONDON, D.J., and SCHOENE, B., 2016, Community-Derived Standards for LA-ICP-MS U-(Th-)Pb Geochronology – Uncertainty Propagation, Age Interpretation and Data Reporting: *Geostandards and Geoanalytical Research*, v. 40, p. 311–332, doi: 10.1111/j.1751-908X.2016.00379.x.
- INGLEZ, L., WARREN, L.V., OKUBO, J., SIMÕES, M.G., QUAGLIO, F., ARROUY, M.J., and NETTO, R.G., 2019, Discs and discord: The paleontological record of Ediacaran

- discoidal structures in the south American continent: Journal of South American Earth Sciences, v. 89, p. 319–336, doi: 10.1016/j.jsames.2018.11.023.  
<https://linkinghub.elsevier.com/retrieve/pii/S0895981118302797>.
- VAN ITEN, H., MARQUES, A.C., LEME, J. de M., PACHECO, M.L.A.F., and SIMÕES, M.G., 2014, Origin and early diversification of the phylum Cnidaria Verrill: Major developments in the analysis of the taxon's proterozoic-cambrian history: Palaeontology, v. 57, p. 677–690, doi: 10.1111/pala.12116.
- IVANTSOV, A., NAGOVITSYN, A., and ZAKREVSKAYA, M., 2019, Traces of locomotion of ediacaran macroorganisms: Geosciences (Switzerland), v. 9, doi: 10.3390/geosciences9090395.
- JACKSON, S.E., PEARSON, N.J., GRIFFIN, W.L., and BELOUSOVA, E.A., 2004, The application of laser ablation-inductively coupled plasma-mass spectrometry to in situ U-Pb zircon geochronology: Chemical Geology, v. 211, p. 47–69, doi: 10.1016/j.chemgeo.2004.06.017.
- JAFFEY, A.H., FLYNN, K.F., GLENDEENIN, L.E., BENTLEY, W.C., and ESSLING, A.M., 1971, Precision measurement of half-lives and specific activities of U235 and U238: Physical Review C, v. 4, p. 1889–1906, doi: 10.1103/PhysRevC.4.1889.
- JAVAUX, E.J., and KNOLL, A.H., 2017, Micropaleontology of the lower Mesoproterozoic Roper Group, Australia, and implications for early eukaryotic evolution: Journal of Paleontology, v. 91, p. 199–229, doi: 10.1017/jpa.2016.124.
- JEFFERSON, T.H., 1982, The preservation of fossil leaves in Cretaceous volcanioclastic rocks from Alexander Island, Antarctica: Geological Magazine, v. 119, p. 291–300, doi: 10.1017/S0016756800026108.
- JENSEN, S., DROSER, M.L., and GEHLING, J.G., 2007, A Critical Look at the Ediacaran Trace Fossil Record: Neoproterozoic Geobiology and Paleobiology, p. 115–157, doi: 10.1007/1-4020-5202-2\_5.
- JENSEN, S., GEHLING, J.G., and DROSER, M.L., 1998, Ediacara-type fossils in Cambrian sediments: Nature, v. 393, p. 567–569, doi: 10.1038/31215.  
<http://www.nature.com/articles/31215>.
- JENSEN, S., PALACIOS, T., and MARTÍ Mus, M., 2005, Megascopic filamentous organisms preserved as grooves and ridges in Ediacaran siliciclastics, *in*

- Paleobios Volume 25, Supplement to Number 2: p. 65–66.
- JIANG, B., FÜRSICH, F.T., SHA, J., WANG, B., and NIU, Y., 2011, Early Cretaceous volcanism and its impact on fossil preservation in Western Liaoning, NE China: *Palaeogeography, Palaeoclimatology, Palaeoecology*, v. 302, p. 255–269, doi: 10.1016/j.palaeo.2011.01.016. <http://dx.doi.org/10.1016/j.palaeo.2011.01.016>.
- JØRGENSEN, B.B., 1977, Distribution of colorless sulfur bacteria (*Beggiatoa* spp.) in a coastal marine sediment: *Marine Biology*, v. 41, p. 19–28, doi: 10.1007/BF00390577.
- JØRGENSEN, B.B., and GALLARDO, V.A., 1999, *Thioploca* spp.: Filamentous sulfur bacteria with nitrate vacuoles: *FEMS Microbiology Ecology*, v. 28, p. 301–313, doi: 10.1016/S0168-6496(98)00122-6.
- JØRGENSEN, B.B., TESKE, A., and AHMAD, A., 2015, *Thioploca*: Bergey's Manual of Systematics of Archaea and Bacteria, p. 1–12, doi: 10.1002/9781118960608.gbm01227.
- KAWANO, M., and TOMITA, K., 1997, Experimental study on the formation of zeolites from obsidian by interaction with NaOH and KOH solutions at 150 and 200 °C: *Clays and Clay Minerals*, v. 45, p. 365–377, doi: 10.1346/CCMN.1997.0450307.
- KAWANO, M., and TOMITA, K., 1992, Formation of allophane and beidellite during hydrothermal alteration of volcanic glass below 200°C: *Clays and Clay Minerals*, v. 40, p. 666–674, doi: 10.1346/CCMN.1992.0400606.
- KAWANO, M., and TOMITA, K., 2002, Microbiotic formation of silicate minerals in the weathering environment of a pyroclastic deposit: *Clays and Clay Minerals*, v. 50, p. 99–110, doi: 10.1346/000986002761002865.
- KAWANO, M., TOMITA, K., and SHINOHARA, Y., 1997, Analytical electron microscopic study of the noncrystalline products formed at early weathering stages of volcanic glass: *Clays and Clay Minerals*, v. 45, p. 440–447, doi: 10.1346/CCMN.1997.0450313.
- KIM, J., 2012, Overviews of Biogenic Smectite-To-Illite Reaction: *Clay science*, v. 16, p. 9–13, doi: 10.11362/jcssjclayscience.16.1\_9.
- KNOLL, A.H., 1982, Microfossils from the Late Precambrian Draken Conglomerate ,

- Ny Friesland , Svalbard: Journal of Paleontology, v. 56, p. 755–790.
- KNOLL, A.H., SWETT, K., and MARK, J., 1991, Paleobiology of a Neoproterozoic tidal flat/lagoonal complex: the Draken Conglomerate Formation, Spitsbergen: Journal of Paleontology, v. 65, p. 531–570, doi: 10.1017/S0022336000030663.
- KOLESNIKOV, A. V., and BOBKOV, N.I., 2019, Revisiting the age of the Asha group in the South Urals: Estudios Geologicos, v. 75, p. 1–5, doi: 10.3989/EGEOL.43590.558.
- KOLESNIKOV, A. V., DANELIAN, T., GOMMEAUX, M., MASLOV, A. V., and GRAZHDANKIN, D. V., 2017, Arumberiamorph structure in modern microbial mats: Implications for Ediacaran paleobiology: Bulletin de la Societe Geologique de France, v. 188, p. 57–66, doi: 10.1051/bsgf/2017006.
- KOLESNIKOV, A. V., ROGOV, V.I., BYKOVA, N. V., DANELIAN, T., CLAUSEN, S., MASLOV, A. V., and GRAZHDANKIN, D. V., 2018, The oldest skeletal macroscopic organism *Palaeopascichnus linearis*: Precambrian Research, v. 316, p. 24–37, doi: 10.1016/j.precamres.2018.07.017.  
<https://doi.org/10.1016/j.precamres.2018.07.017>.
- KONHAUSER, K.O., FISHER, Q.J., FYFE, W.S., LONGSTAFFE, F.J., and POWELL, M.A., 1998, Authigenic mineralization and detrital clay binding by freshwater biofilms: The brahmani river, India: Geomicrobiology Journal, v. 15, p. 209–222, doi: 10.1080/01490459809378077.
- KONHAUSER, K.O., FYFE, W.S., FERRIS, F.G., and BEVERIDGE, T.J., 1993, Metal sorption and mineral precipitation by bacteria in two Amazonian river systems: Rio Solimões and Rio Negro, Brazil: Geology, v. 21, p. 1103, doi: 10.1130/0091-7613(1993)021<1103:MSAMPB>2.3.CO;2.  
<https://pubs.geoscienceworld.org/geology/article/21/12/1103-1106/197737>.
- KONHAUSER, K.O., SCHIFFMAN, P., and FISHER, Q.J., 2002, Microbial mediation of authigenic clays during hydrothermal alteration of basaltic tephra, Kilauea Volcano: Geochemistry, Geophysics, Geosystems, v. 3, p. 1–13, doi: 10.1029/2002gc000317.
- KONHAUSER, K.O., and URRUTIA, M.M., 1999, Bacterial clay authigenesis: A common biogeochemical process: Chemical Geology, v. 161, p. 399–413, doi:

10.1016/S0009-2541(99)00118-7.

KUMAR, S., and AHMAD, S., 2014, Microbially induced sedimentary structures (MISS) from the Ediacaran Jodhpur Sandstone, Marwar Supergroup, western Rajasthan: Journal of Asian Earth Sciences, v. 91, p. 352–361, doi:

10.1016/j.jseaes.2014.01.009. <http://dx.doi.org/10.1016/j.jseaes.2014.01.009>.

KUMAR, S., and PANDEY, S., 2008, Arumberia and associated fossils from the Neoproterozoic Maihar Sandstone, Vindhyan Supergroup, Central India: Journal of the Palaeontological Society of India, v. 53, p. 83–97.

KUNZMANN, M., BUI, T.H., CROCKFORD, P.W., HALVERSON, G.P., SCOTT, C., LYONS, T.W., and WING, B.A., 2017, Bacterial sulfur disproportionation constrains timing of Neoproterozoic oxygenation: Geology, v. 45, p. 207–210, doi: 10.1130/G38602.1. <https://pubs.geoscienceworld.org/geology/article/45/3/207-210/195246>.

DE LA FUENTE, S., CUADROS, J., FIORE, S., and LINARES, J., 2000, Electron microscopy study of volcanic tuff alteration to illite-smectite under hydrothermal conditions: Clays and Clay Minerals, v. 48, p. 339–350, doi: 10.1346/CCMN.2000.0480305. [http://www.clays.org/journal/archive/volume\\_48/48-3-339.pdf](http://www.clays.org/journal/archive/volume_48/48-3-339.pdf).

LAFLAMME, M., XIAO, S., and KOWALEWSKI, M., 2009, Osmotrophy in modular Ediacara organisms: Proceedings of the National Academy of Sciences, v. 106, p. 14438–14443, doi: 10.1073/pnas.0904836106. <http://www.pnas.org/cgi/doi/10.1073/pnas.0904836106>.

LARKIN, J.M., and HENK, M.C., 1996, Filamentous sulfide-oxidizing bacteria at hydrocarbon seeps of the Gulf of Mexico: Microscopy Research and Technique, v. 33, p. 23–31, doi: 10.1002/(SICI)1097-0029(199601)33:1<23::AID-JEMT4>3.0.CO;2-1.

LARKIN, J.M., and STROHL, W.R., 1983, Beggiatoa, Thiothrix, and Thioploca: Annual Review of Microbiology, v. 37, p. 341–367, doi: 10.1146/annurev.mi.37.100183.002013.

LEIPNITZ, I.I., PAIM, P.S.G., DA ROSA, A.A.S., ROSA, A.L.Z. da, and NOWATZKI, C.H., 1997, Primeira ocorrência de Chancelloriidae no Brasil, *in* Congresso Brasileiro

- de Paleontologia: São Pedro, p. 15.
- LIU, A.G., 2016, Framboidal pyrite shroud confirms the “death mask” model for moldic preservation of ediacaran soft-bodied organisms: *PALAIOS*, v. 31, p. 259–274, doi: 10.2110/palo.2015.095.  
<https://pubs.geoscienceworld.org/palaios/article/31/5/259-274/325574>.
- LIU, A.G., BRASIER, M.D., BOGOLEPOVA, O.K., RAEVSKAYA, E.G., and GUBANOV, A.P., 2013a, First report of a newly discovered ediacaran biota from the irkineeva uplift, East Siberia: *Newsletters on Stratigraphy*, v. 46, p. 95–110, doi: 10.1127/0078-0421/2013/0031.
- LIU, A.G., and DUNN, F.S., 2020, Filamentous Connections between Ediacaran Fronds: *Current Biology*, v. 30, p. 1322-1328.e3, doi: 10.1016/j.cub.2020.01.052.  
<https://linkinghub.elsevier.com/retrieve/pii/S0960982220300968>.
- LIU, A.G., KENCHINGTON, C.G., and MITCHELL, E.G., 2015, Remarkable insights into the paleoecology of the Avalonian Ediacaran macrobiota: *Gondwana Research*, v. 27, p. 1355–1380, doi: 10.1016/j.gr.2014.11.002.  
<http://dx.doi.org/10.1016/j.gr.2014.11.002>.
- LIU, A.G., MATTHEWS, J.J., and MCILROY, D., 2016a, The Beothukis/Culmofrons problem and its bearing on Ediacaran macrofossil taxonomy: Evidence from an exceptional new fossil locality: *Palaeontology*, v. 59, p. 45–58, doi: 10.1111/pala.12206.
- LIU, A.G., MATTHEWS, J.J., and MCILROY, D., 2016b, The Beothukis/Culmofrons problem and its bearing on Ediacaran macrofossil taxonomy: Evidence from an exceptional new fossil locality: *Palaeontology*, v. 59, p. 45–58, doi: 10.1111/pala.12206.
- LIU, A.G., MATTHEWS, J.J., MENON, L.R., MCILROY, D., and BRASIER, M.D., 2014, *Haootia quadriformis* n. gen., n. sp., interpreted as a muscular cnidarian impression from the Late Ediacaran period (approx. 560 Ma): *Proceedings of the Royal Society B: Biological Sciences*, v. 281, doi: 10.1098/rspb.2014.1202.
- LIU, A.G., MCILROY, D., and BRASIER, M.D., 2010, First evidence for locomotion in the Ediacara biota from the 565 Ma Mistaken Point Formation, Newfoundland: *Geology*, v. 38, p. 123–126, doi: 10.1130/G30368.1.

- LIU, A.G., McMAHON, S., MATTHEWS, J.J., STILL, J.W., and BRASIER, A.T., 2019, Petrological evidence supports the death mask model for the preservation of Ediacaran soft-bodied organisms in South Australia: *Geology*, v. 47, p. 215–218, doi: 10.1130/G45918.1.
- LIU, P., YIN, C., CHEN, S., TANG, F., and GAO, L., 2013b, The biostratigraphic succession of acanthomorphic acritarchs of the Ediacaran Doushantuo Formation in the Yangtze Gorges area, South China and its biostratigraphic correlation with Australia: *Precambrian Research*, v. 225, p. 29–43, doi: 10.1016/j.precamres.2011.07.009.  
<http://dx.doi.org/10.1016/j.precamres.2011.07.009>.
- LOKHORST, G.M., and TRASK, B.J., 1981, Taxonomic studies on Urospora (Acrosiphoniales, Chlorophyceae) in western Europe: *Acta Botanica Neerlandica*, v. 30, p. 353–431, doi: 10.1111/j.1438-8677.1981.tb01265.x.  
<http://doi.wiley.com/10.1111/j.1438-8677.1981.tb01265.x>.
- LUDWIG, K.R., 2003, User's Manual for Isoplot/Ex version 3.00—A Geochronology Toolkit for Microsoft Excel, N° 4: Berkeley Geochronology Center Special Publication, p. 71.
- LUTHER, G.W., FINDLAY, A.J., MACDONALD, D.J., OWINGS, S.M., HANSON, T.E., BEINART, R.A., and GIRGUIS, P.R., 2011, Thermodynamics and kinetics of sulfide oxidation by oxygen: A look at inorganically controlled reactions and biologically mediated processes in the environment: *Frontiers in Microbiology*, v. 2, p. 1–9, doi: 10.3389/fmicb.2011.00062.
- MADEJOVÁ, J., GATES, W.P., and PETIT, S., 2017, IR Spectra of Clay Minerals: 107–149 p.
- MASON, S.J., NARBONNE, G.M., DALRYMPLE, R.W., and O'BRIEN, S.J., 2013, Paleoenvironmental analysis of Ediacaran strata in the Catalina Dome, Bonavista Peninsula, Newfoundland: *Canadian Journal of Earth Sciences*, v. 50, p. 197–212, doi: 10.1139/cjes-2012-0099.
- MATHUR, V.K., and SRIVASTAVA, D.K., 2004, Record of tissue grade colonial eucaryote and microbial mat associated with Ediacaran fossils in Krol Group, Garhwal Syncline, lesser Himalaya, Uttarakhand: *Journal of the Geological*

- Society of India, v. 63, p. 100–102.
- McFADDEN, K.A., XIAO, S., ZHOU, C., and KOWALEWSKI, M., 2009, Quantitative evaluation of the biostratigraphic distribution of acanthomorphic acritarchs in the Ediacaran Doushantuo Formation in the Yangtze Gorges area, South China: Precambrian Research, v. 173, p. 170–190, doi: 10.1016/j.precamres.2009.03.009.
- MCILROY, D., CRIMES, T.P., and PAULEY, J.C., 2005, Fossils and matgrounds from the Neoproterozoic Longmyndian Supergroup, Shropshire, UK: Geological Magazine, v. 142, p. 441–455, doi: 10.1017/S0016756805000555.
- MCILROY, D., and WALTER, M.R., 1997, A reconsideration of the biogenicity of *Arumberia banksi* Glaessner & Walter: Alcheringa, v. 21, p. 79–80, doi: 10.1080/03115519708619187.
- MCMENAMIN, M.A.S., 1998, *The Garden of Ediacara: Discovering the First Complex Life*: Columbia University Press, New York, 295 p.
- MENDELOVICI, E., YARIV, S., and VILLALBA, R., 1979, Iron-bearing kaolinite in Venezuelan laterites: I. Infrared spectroscopy and chemical dissolution evidence: Clay Minerals, v. 14, p. 323–331, doi: 10.1180/claymin.1979.014.4.08. [https://www.cambridge.org/core/product/identifier/S0009855800023256/type/journal\\_article](https://www.cambridge.org/core/product/identifier/S0009855800023256/type/journal_article).
- MENON, L.R., MCILROY, D., LIU, A.G., and BRASIER, M.D., 2016, The dynamic influence of microbial mats on sediments: Fluid escape and pseudofossil formation in the Ediacaran Longmyndian Supergroup, UK: Journal of the Geological Society, v. 173, p. 177–185, doi: 10.1144/jgs2015-036.
- MEUNIER, A., 2005, *Clays*: Springer-Verlag, Berlin/Heidelberg, 1–472 p. <http://link.springer.com/10.1007/b138672>.
- MEYER, M., SCHIFFBAUER, J.D., XIAO, S., CAI, Y., and HUA, H., 2012, Taphonomy of the Upper Ediacaran Enigmatic Ribbonlike Fossil Shaanxilithes: Palaios, v. 27, p. 354–372, doi: 10.2110/palo.2011.p11-098r.
- MIRANDA, L.S., COLLINS, A.G., and MARQUES, A.C., 2015, Is *haootia quadriformis* related to extant staurozoa (cnidaria)? Evidence from the muscular system reconsidered: Proceedings of the Royal Society B: Biological Sciences, v. 282,

- p. 3–5, doi: 10.1098/rspb.2014.2396.
- MISRA, S.B., 1969, Late Precambrian (?) Fossils from Southeastern Newfoundland: GSA Bulletin, v. 80, p. 2133–2140, doi: [https://doi.org/10.1130/0016-7606\(1969\)80\[2133:LPFFSN\]2.0.CO;2](https://doi.org/10.1130/0016-7606(1969)80[2133:LPFFSN]2.0.CO;2).
- MUSCENTE, A.D., BOAG, T.H., BYKOVA, N., and SCHIFFBAUER, J.D., 2018, Environmental disturbance, resource availability, and biologic turnover at the dawn of animal life: Earth-Science Reviews, v. 177, p. 248–264, doi: 10.1016/j.earscirev.2017.11.019.  
<http://dx.doi.org/10.1016/j.earscirev.2017.11.019>.
- MUSCENTE, A.D., BYKOVA, N., BOAG, T.H., BUATOIS, L.A., MÁNGANO, M.G., ELEISH, A., PRABHU, A., PAN, F., MEYER, M.B., SCHIFFBAUER, J.D., FOX, P., HAZEN, R.M., and KNOLL, A.H., 2019, Ediacaran biozones identified with network analysis provide evidence for pulsed extinctions of early complex life: Nature Communications, v. 10, p. 1–15, doi: 10.1038/s41467-019-08837-3.  
<http://dx.doi.org/10.1038/s41467-019-08837-3>.
- NAGOVITSIN, K.E., GRAZHDANKIN, D. V., and KOCHNEV, B.B., 2008, Ediacaria in the Siberian hypostratotype of the Riphean: Doklady Earth Sciences, v. 419, p. 423–427, doi: 10.1134/S1028334X0803015X.
- NARBONNE, G.M., 2005, The Ediacara Biota: Neoproterozoic Origin of Animals and Their Ecosystems: Annual Review of Earth and Planetary Sciences, v. 33, p. 421–442, doi: 10.1146/annurev.earth.33.092203.122519.
- NARBONNE, G.M., and GEHLING, J.G., 2003, Life after snowball: The oldest complex Ediacaran fossils Figure 1. A: Map showing locations of upper Drook fossils (asterisks). B: Stratigraphic column showing Neoproterozoic stratigraphy of Avalon zone and stratigraphic position of new fossil discoveri: p. 27–30.
- NARBONNE, G.M., LAFLAMME, M., TRUSLER, P.W., DALRYMPLE, R.W., and GREENTREE, C., 2014, Deep-Water Ediacaran Fossils from Northwestern Canada: Taphonomy, Ecology, and Evolution: Journal of Paleontology, v. 88, p. 207–223, doi: 10.1666/13-053.
- NARBONNE, G.M., XIAO, S., SHIELDS, G.A., and GEHLING, J.G., 2012, The Ediacaran Period: Elsevier, 413–435 p. <http://dx.doi.org/10.1016/B978-0-444-59425>

9.00018-4.

- NAVARRETE, J.U., CAPPELLE, I.J., SCHNITTNER, K., and BORROK, D.M., 2013, Bioreaching of ilmenite and basalt in the presence of iron-oxidizing and iron-scavenging bacteria: International Journal of Astrobiology, v. 12, p. 123–134, doi: 10.1017/S1473550412000493.
- NELSON, D.C., REVSBECH, N.P., and JØRGENSEN, B.B., 1986, Microoxic-Anoxic Niche of Beggiatoa spp.: Microelectrode Survey of Marine and Freshwater Strains: Applied and Environmental Microbiology, v. 52, p. 161–168, doi: 10.1128/aem.52.1.161-168.1986.
- NETTO, R.G., 2012, Evidences of Life in Terminal Proterozoic Deposits of Southern Brazil : a Synthesis, *in* RG, N., NB, C., and FMW, T., eds., Ichnology of Latin America—Selected Papers: Sociedade Brasileira de Paleontologia, Porto Alegre, p. 15–26.
- NETTO, R.G., and ROSA, A.L.Z. da, 1997, Registro icnofossilífero da Bacia do Itajaí, SC: Uma primeira visão, *in* Congresso Brasileiro de Paleontologia: São Pedro, p. 15.
- NOBLE, S.R., CONDON, D.J., CARNEY, J.N., WILBY, P.R., PHARAOH, T.C., and FORD, T.D., 2015, U-Pb geochronology and global context of the charnian supergroup, UK: Constraints on the age of key Ediacaran fossil assemblages: Bulletin of the Geological Society of America, v. 127, p. 250–265, doi: 10.1130/B31013.1.
- NOFFKE, N., GERDES, G., KLENKE, T., and KRUMBEIN, W.E., 2001, Microbially Induced Sedimentary Structures: A New Category within the Classification of Primary Sedimentary Structures: Journal of Sedimentary Research, v. 71, p. 649–656, doi: 10.1306/2dc4095d-0e47-11d7-8643000102c1865d.
- NYBERG, A. V., and SCHOPF, J.W., 1984, Microfossils in stromatolitic cherts from the upper proterozoic Min'yar formation, southern Ural Mountains, USSR.: Journal of paleontology, v. 58, p. 738–72. <https://www.jstor.org/stable/1304915>.
- ORR, P.J., BRIGGS, D.E.G., SIVETER, D.J., and SIVETER, D.J., 2000, Three-dimensional preservation of a non-biomineralized arthropod in concretions in Silurian volcaniclastic rocks from Herefordshire, England: Journal of the Geological Society, v. 157, p. 173–186, doi: 10.1144/jgs.157.1.173.

- PACHECO, M.L.A.F., GALANTE, D., RODRIGUES, F., LEME, J.D.M., BIDOLA, P., HAGADORN, W., STOCKMAR, M., HERZEN, J., RUDNITZKI, I.D., PFEIFFER, F., and MARQUES, A.C., 2015, Insights into the skeletonization, lifestyle, and affinity of the unusual ediacaran fossil Corumbella: *PLoS ONE*, v. 10, p. 1–19, doi: 10.1371/journal.pone.0114219.
- PAIM, P.S.G., CHEMALE JR., F., and LOPES, R.C., 2000, A bacia do Camaquã, *in* Holz, M. and De Ros, L.F., eds., *Geologia Do Rio Grande Do Sul*: CIGO/UFRGS, Porto Alegre.
- PAIM, P.S.G., LEIPNITZ, I., ROSA, A.L.Z. da, and DA ROSA, A.A.S., 1997, Preliminary report on the occurrence of *Chancelloria* sp. in the Itajaí Basin, Southern Brazil: v. 27, p. 303–308.  
<http://www.ppegeo.igc.usp.br/index.php/rbg/article/view/11297>.
- PECKMANN, J., THIEL, V., REITNER, J., TAVIANI, M., AHARON, P., and MICHAELIS, W., 2004, A microbial mat of a large sulfur bacterium preserved in a miocene methane-seep limestone: *Geomicrobiology Journal*, v. 21, p. 247–255, doi: 10.1080/01490450490438757.
- PETIT, S., and DECARREAU, A., 1990, Hydrothermal (200°C) synthesis and crystal chemistry of iron-rich kaolinites: *Clay Minerals*, v. 25, p. 181–196, doi: 10.1180/claymin.1990.025.2.04.
- PETIT, S., MADEJOVÁ, J., DECARREAU, A., and MARTIN, F., 1999, Characterization of octahedral substitutions in kaolinites using near infrared spectroscopy: *Clays and Clay Minerals*, v. 47, p. 103–108, doi: 10.1346/CCMN.1999.0470111.
- PIERRE, F. Dela, NATALICCHIO, M., FERRANDO, S., GIUSTETTO, R., BIRGEL, D., CARNEVALE, G., GIER, S., LOZAR, F., MARABELLO, D., PECKMANN, J., and TORINO, U., 2015, Are the large filamentous microfossils preserved in Messinian gypsum colorless sulfide-oxidizing bacteria ? v. 43, p. 855–858, doi: 10.1130/G37018.1.
- PU, J.P., BOWRING, S.A., RAMEZANI, J., MYROW, P., RAUB, T.D., LANDING, E., MILLS, A., HODGIN, E., and MACDONALD, F.A., 2016, Dodging snowballs: Geochronology of the Gaskiers glaciation and the first appearance of the Ediacaran biota: *Geology*, v. 44, p. 955–958, doi: 10.1130/G38284.1.
- RETALLACK, G.J., 2016, Ediacaran sedimentology and paleoecology of Newfoundland

- reconsidered: *Sedimentary Geology*, v. 333, p. 15–31, doi: 10.1016/j.sedgeo.2015.12.001. <http://dx.doi.org/10.1016/j.sedgeo.2015.12.001>.
- ROSA, A.L.Z. da, 2005, Evidencias de vida no Ediacarano Inferior da Bacia do Itajaí, SC [meio eletronico]:Universidade do Vale do Rio dos Sinos - UNISINOS, 56 p. [http://aleph.cenpes.petrobras.com.br/LINKS/TESES/ROSA\\_ALZ\\_Evidencias\\_de\\_vida\\_no\\_edicarano...pdf](http://aleph.cenpes.petrobras.com.br/LINKS/TESES/ROSA_ALZ_Evidencias_de_vida_no_edicarano...pdf) Clique aqui para ver o texto.
- DA ROSA, A.A.S., PAIM, P.S.G., CHEMALE JR., F., ROSA, A.L.Z. da, and GIRARDI, R.V., 1997, The “state-of-art” of the Cambrian Itajaí Basin (Southern Brazil), *in* 18th IAS Regional European Meeting of Sedimentology: Heidelberg, p. 112.
- ROSTIROLLA, S.P., 1991, Tectônica e Sedimentação da Bacia do Itajaí – SC:UFOP.
- ROSTIROLLA, S.P., AHRENDT, A., SOARES, P.C., and CARMIGNANI, L., 1999, Basin analysis and mineral endowment of the Proterozoic Itajai Basin, south-east Brazil: *Basin Research*, v. 11, p. 127–142, doi: 10.1046/j.1365-2117.1999.00090.x.
- ROSTIROLLA, S.P., ALKMIM, F.F., and SOARES, P.C., 1992, O Grupo Itajaí, Estado de Santa Catarina, Brasil: Exemplo de sedimentação em uma bacia flexural de antepaís: *B. Geoci. PETROBRÁS*, v. 6, p. 109–122.
- RUNNEGAR, B.N., and FEDONKIN, MIKHAIL, A., 1992, Proterozoic metazoan body fossils, *in* Schopf, J.W., ed., *The Proterozoic Biosphere*: Cambridge University Press, p. 369–388.
- RUSSELL, J.D., and FRASER, A.R., 1994, Infrared methods, *in* Wilson, M.J., ed., *Clay Mineralogy: Spectroscopic and Chemical Determinative Methods*: Springer Netherlands, Dordrecht, p. 11–67. [http://link.springer.com/10.1007/978-94-011-0727-3\\_2](http://link.springer.com/10.1007/978-94-011-0727-3_2).
- SANTOS, M.M., LANA, C., SCHOLZ, R., BUICK, I., SCHMITZ, M.D., KAMO, S.L., GERDES, A., CORFU, F., TAPSTER, S., LANCASTER, P., STOREY, C.D., BASEI, M.A.S., TOHVER, E., ALKMIM, A., et al., 2017, A New Appraisal of Sri Lankan BB Zircon as a Reference Material for LA-ICP-MS U-Pb Geochronology and Lu-Hf Isotope Tracing: *Geostandards and Geoanalytical Research*, v. 41, p. 335–358, doi: 10.1111/ggr.12167. <http://doi.wiley.com/10.1111/ggr.12167>.
- SAPPENFIELD, A., DROSER, M.L., and GEHLING, J.G., 2011, Ediacaran Trace Fossil

- Record One Tube At a Time: Society, v. 85, p. 256–265.
- SAYAMA, M., 2001, Presence of Nitrate-Accumulating Sulfur Bacteria and Their Influence on Nitrogen Cycling in a Shallow Coastal Marine Sediment: Applied and Environmental Microbiology, v. 67, p. 3481–3487, doi: 10.1128/AEM.67.8.3481-3487.2001.
- SAYLOR, B.Z., GROTZINGER, J.P., and GERMS, G.J.B., 1995, Sequence stratigraphy and sedimentology of the Neoproterozoic Kuibis and Schwarzrand Subgroups (Nama Group), southwestern Namibia: Precambrian Research, v. 73, p. 153–171, doi: 10.1016/0301-9268(94)00076-4.
- SCHIEBER, J., BOSE, P., ERIKSSON, P.G., BANERJEE, S., SARKAR, S., ALTERMANN, W., and CATUNEANU, O., 2007, Atlas of Microbial Mat Features Preserved within the Siliciclastic Rock Record, Volume 2: Elsevier Science, 324 p.  
<https://www.elsevier.com/books/atlas-of-microbial-mat-features-preserved-within-the-siliciclastic-rock-record/schieber/978-0-444-52859-9>.
- SCHIFFBAUER, J.D., HUNTLEY, J.W., O'NEIL, G.R., DARROCH, S.A.F., LAFLAMME, M., and CAI, Y., 2016, The Latest Ediacaran Wormworld Fauna: Setting the Ecological Stage for the Cambrian Explosion: GSA Today, v. 26, p. 4–11, doi: 10.1130/GSATG265A.1.
- SCHMITZ, M.D., 2012, Radiometric ages used in GTS2012: Elsevier B.V., 1045–1082 p. <http://dx.doi.org/10.1016/B978-0-444-59425-9.15002-4>.
- SCHOPF, J.W., and KLEIN, C., 1992, The Proterozoic Biosphere (J. W. Schopf & C. Klein, Eds.): Cambridge University Press.  
<https://www.cambridge.org/core/product/identifier/9780511601064/type/book>.
- SCHULZ, H.N., 2006, The Genus *Thiomargarita*, in The Prokaryotes: Springer New York, p. 1156–1163. [http://link.springer.com/10.1007/0-387-30746-X\\_47](http://link.springer.com/10.1007/0-387-30746-X_47).
- SCHULZ, H.N., JØRGENSEN, B.B., FOSSING, H.A., and RAMSING, N.B., 1996, Community structure of filamentous, sheath-building sulfur bacteria, *Thioploca* spp., off the coast of Chile: Applied and Environmental Microbiology, v. 62, p. 1855–1862.
- SCOTT, A.C., 1990, in Lower Carboniferous volcanic sequences in Scotland: .

SEILACHER, A., 2001, Concretion morphologies reflecting diagenetic and epigenetic pathways: *Sedimentary Geology*, v. 143, p. 41–57, doi: 10.1016/S0037-0738(01)00092-6.

SEILACHER, A., 1992, Vendobionta and Psammocorallia: lost constructions of Precambrian evolution: *Journal - Geological Society (London)*, v. 149, p. 607–613, doi: 10.1144/gsjgs.149.4.0607.

SEILACHER, A., GRAZHDANKIN, D., and LEGOUTA, A., 2003, Ediacaran biota: The dawn of animal life in the shadow of giant protists: *Paleontological Research*, v. 7, p. 43–54, doi: 10.2517/prpsj.7.43.  
<http://www.bioone.org/doi/abs/10.2517/prpsj.7.43>.

SEILACHER, A., MESCHEDE, M., BOLTON, E.W., and LUGINSLAND, H., 2000, Precambrian “fossil” Vermiforma is a tectograph: *Geology*, v. 28, p. 235–238.

SEREZHNIKOVA, E.A., RAGOZINA, A.L., DORJNAMJAA, D., and ZAITSEVA, L. V., 2014, Fossil microbial communities in Neoproterozoic interglacial rocks, Maikhanuu Formation, Zavkhan basin, Western Mongolia: *Precambrian Research*, v. 245, p. 66–79, doi: 10.1016/j.precamres.2014.01.005.  
<http://dx.doi.org/10.1016/j.precamres.2014.01.005>.

SERGEEV, V.N., KNOLL, A.H., VOROB’EVA, N.G., and SERGEEVA, N.D., 2016, Microfossils from the lower Mesoproterozoic Kaltasy Formation, East European Platform: *Precambrian Research*, v. 278, p. 87–107, doi: 10.1016/j.precamres.2016.03.015.  
<http://dx.doi.org/10.1016/j.precamres.2016.03.015>.

SHEN, B., DONG, L., XIAO, S., and KOWALEWSKI, M., 2008, The Avalon explosion: Evolution of Ediacara morphospace: *Science*, v. 319, p. 81–84, doi: 10.1126/science.1150279.

SHEN, B., XIAO, S., DONG, L.I.N., ZHOU, C., LIU, J., and LIU, J., 2007, Problematic macrofossils from Ediacaran, North China.pdf: *Journal of Paleontology*, v. 81, p. 1396–1411.

SHEPARD, R.N., and SUMNER, D.Y., 2010, Undirected motility of filamentous cyanobacteria produces reticulate mats: *Geobiology*, v. 8, p. 179–190, doi: 10.1111/j.1472-4669.2010.00235.x.

- DA SILVA, L.C., ARMSTRONG, R., PIMENTEL, M.M., SCANDOLARA, J., RAMGRAB, G., WILDNER, W., ANGELIM, L.A. de A., VASCONCELOS, A.M., RIZZOTO, G., SANTO QUADROS, M.L.D.E., and SANDER, A., 2002, Reavaliação da evolução geológica em terrenos pré-cambrianos brasileiros com base em novos dados U-Pb SHRIMP, Parte III: Províncias Borborema, Mantiqueira Meridional e Rio Negro-Juruena: Revista Brasileira de Geociências, v. 32, p. 529–544.
- SIM, M.S., LIANG, B., PETROFF, A.P., EVANS, A., KLEPAC-CERAJ, V., FLANNERY, D.T., WALTER, M.R., and BOSAK, T., 2012, Oxygen-dependent morphogenesis of modern clumped photosynthetic mats and implications for the archean stromatolite record: Geosciences (Switzerland), v. 2, p. 235–259, doi: 10.3390/geosciences2040235.
- SLÁMA, J., KOŠLER, J., CONDON, D.J., CROWLEY, J.L., GERDES, A., HANCHAR, J.M., HORSTWOOD, M.S.A., MORRIS, G.A., NASDALA, L., NORBERG, N., SCHALTEGGER, U., SCHOENE, B., TUBRETT, M.N., and WHITEHOUSE, M.J., 2008, Plešovice zircon - A new natural reference material for U-Pb and Hf isotopic microanalysis: Chemical Geology, v. 249, p. 1–35, doi: 10.1016/j.chemgeo.2007.11.005.
- SOLIMAN, M.F., 2001, The Mineralogical and Geochemistry of the Paleocene Succession at Gabal El-Qreiya, Nile Valley, Egypt.pdf, *in* The Second International Conference on the Geology of Africa: Assiut, Egypt, p. 1.
- SOUTHAM, G., DONALD, R., RÖSTAD, A., and BROCK, C., 2001, Pyrite discs in coal: Evidence for fossilized bacterial colonies: Geology, v. 29, p. 47–50, doi: 10.1130/0091-7613(2001)029<0047:PDICEF>2.0.CO;2.
- SPERLING, E.A., PETERSON, K.J., and LAFLAMME, M., 2011, Rangeomorphs, Thectardis (Porifera?) and dissolved organic carbon in the Ediacaran oceans: Geobiology, v. 9, p. 24–33, doi: 10.1111/j.1472-4669.2010.00259.x.
- SPERLING, E.A., WOLOCK, C.J., MORGAN, A.S., GILL, B.C., KUNZMANN, M., HALVERSON, G.P., MACDONALD, F.A., KNOLL, A.H., and JOHNSTON, D.T., 2015, Statistical analysis of iron geochemical data suggests limited late Proterozoic oxygenation: Nature, v. 523, p. 451–454, doi: 10.1038/nature14589.
- STACEY, J.S., and KRAMERS, J.D., 1975, Approximation of terrestrial lead isotope evolution by a two-stage model: Earth and Planetary Science Letters, v. 26, p.

- 207–221, doi: 10.1016/0012-821X(75)90088-6.
- STROHL, W.R., 2015a, *Beggiatoa* : Bergey's Manual of Systematics of Archaea and Bacteria, p. 1–23, doi: 10.1002/9781118960608.gbm01223.
- STROHL, W.R., 2015b, *Beggiatoa*, in Bergey's Manual of Systematics of Archaea and Bacteria: John Wiley & Sons, Ltd, Chichester, UK, p. 1–23.  
<http://doi.wiley.com/10.1002/9781118960608.gbm01223>.
- SUTHERLAND, J.E., LINDSTROM, S.C., NELSON, W.A., BRODIE, J., LYNCH, M.D.J., HWANG, M.S., CHOI, H.-G., MIYATA, M., KIKUCHI, N., OLIVEIRA, M.C., FARR, T., NEEFUS, C., MOLS-MORTENSEN, A., MILSTEIN, D., et al., 2011, A new look at an ancient order: generic revision of the Bangiales (Rhodophyta): Journal of Phycology, v. 47, p. 1131–1151, doi: 10.1111/j.1529-8817.2011.01052.x.  
<http://doi.wiley.com/10.1111/j.1529-8817.2011.01052.x>.
- SUTTON, M.D., BRIGGS, D.E.G., SIVETER, D.J., and SIVETER, D.J., 2005, Silurian brachiopods with soft-tissue preservation: Nature, v. 436, p. 1013–1015, doi: 10.1038/nature03846.
- TANG, Q., PANG, K., YUAN, X., WAN, B., and XIAO, S., 2015, Organic-walled microfossils from the Tonian Gouhou Formation, Huabei region, North China Craton, and their biostratigraphic implications: Precambrian Research, v. 266, p. 296–318, doi: 10.1016/j.precamres.2015.05.025.  
<http://dx.doi.org/10.1016/j.precamres.2015.05.025>.
- TARHAN, L.G., DROSER, M.L., GEHLING, J.G., and DZAUGIS, M.P., 2015, Taphonomy and morphology of the Ediacara form genus Aspidella: Precambrian Research, v. 257, p. 124–136, doi: 10.1016/j.precamres.2014.11.026.  
<http://dx.doi.org/10.1016/j.precamres.2014.11.026>.
- TARHAN, L.G., HOOD, A. v. S., DROSER, M.L., GEHLING, J.G., and BRIGGS, D.E.G., 2017, Exceptional preservation of soft-bodied Ediacara Biota promoted by silica-rich oceans: REPLY: Geology, v. 45, p. e408–e408, doi: 10.1130/G38858Y.1.  
<https://pubs.geoscienceworld.org/geology/article/45/2/e408/195307>.
- TARHAN, L.G., HOOD, A.V.S., DROSER, M.L., GEHLING, J.G., and BRIGGS, D.E.G., 2016, Exceptional preservation of soft-bodied Ediacara Biota promoted by silica-rich oceans: Geology, v. 44, p. 951–954, doi: 10.1130/G38542.1.

- TAZAKI, K., 1997, Biomineralization of layer silicates and hydrated Fe/Mn oxides in microbial mats: An electron microscopical study: *Clays and Clay Minerals*, v. 45, p. 203–212, doi: 10.1346/CCMN.1997.0450208.
- TEIXEIRA, A.L., GAUCHER, C., PAIM, P.S.G., FONSECA, M.M., and FILHO, W.F.S., 2004, Bacias do estágio de Transição da Plataforma Sul-Americana, *in* Mantesso-Neto, V., Bartorelli, A., Carneiro, C., Dal, R., and Brito Neves, B.B., eds., *Geologia Do Continente Sul-American: Evolução Da Obra de Fernando Flávio de Almeida: Beca Produções Culturais Ltda*, São Paulo, p. 487–536.
- TESKE, A., and NELSON, D.C., 2006, The Genera *Beggiatoa* and *Thioploca*, *in* Prokaryotes: Springer New York, p. 784–810. [http://link.springer.com/10.1007/0-387-30746-X\\_27](http://link.springer.com/10.1007/0-387-30746-X_27).
- TOSTEVIN, R., WOOD, R.A., SHIELDS, G.A., POULTON, S.W., GUILBAUD, R., BOWYER, F., PENNY, A.M., HE, T., CURTIS, A., HOFFMANN, K.H., and CLARKSON, M.O., 2016, Low-oxygen waters limited habitable space for early animals: *Nature Communications*, v. 7, doi: 10.1038/ncomms12818.
- TYNNI, R., and DONNER, J., 1980, A microfossil and sedimentation study of the Late Precambrian formation of Hailuoto, Finland: Geological Survey of Finland, v. 311, p. 1–27. <http://pascal-francis.inist.fr/vibad/index.php?action=getRecordDetail&idt=PASCALGEOODEBRGM8220294319>.
- UESHIMA, M., and TAZAKI, K., 2001, Possible role of microbial polysaccharides in nontronite formation: *Clays and Clay Minerals*, v. 49, p. 292–299, doi: 10.1346/CCMN.2001.0490403.
- VAHEDI, V., and PASBAKHSH, P., 2015, Functionalization and compatibilization of halloysite nanotubes: *Natural Mineral Nanotubes Properties and Applications*, p. 283–306, doi: 10.1201/b18107.
- WADE, M., 1968, Preservation of soft-bodied animals in Precambrian sandstones at Ediacara, South Australia: *Lethaia*, v. 1, p. 238–267, doi: 10.1111/j.1502-3931.1968.tb01740.x. <http://doi.wiley.com/10.1111/j.1502-3931.1968.tb01740.x>.
- WAGGONER, B., 2003, The Ediacaran Biotas in Space and Time: Integrative and Comparative Biology, v. 43, p. 104–113, doi: 10.1093/icb/43.1.104.

[https://academic.oup.com/icb/article-lookup/doi/10.1093/icb/43.1.104.](https://academic.oup.com/icb/article-lookup/doi/10.1093/icb/43.1.104)

WALTER, M.R., BAULD, J., and BROCK, T.D., 1976, Chapter 6.2 Microbiology and Morphogenesis of Columnar Stromatolites (*Conophyton*, *Vacerrilla*) from Hot Springs in Yellowstone National Park: Developments in Sedimentology, v. 20, p. 273–310, doi: 10.1016/S0070-4571(08)71140-3.

WALTER, M.R., BAULD, J., and BROCK, T.D., 1972, Siliceous algal and bacterial stromatolites in hot spring and geyser effluents of Yellowstone National Park: Science, v. 178, p. 402–405, doi: 10.1126/science.178.4059.402.

WAN, B., YUAN, X., CHEN, Z., GUAN, C., PANG, K., TANG, Q., and XIAO, S., 2016, Systematic description of putative animal fossils from the early Ediacaran Lantian Formation of South China: Palaeontology, v. 59, p. 515–532, doi: 10.1111/pala.12242.

WARREN, L. V., FAIRCHILD, T.R., GAUCHER, C., BOGGIANI, P.C., POIRÉ, D.G., ANELLI, L.E., and INCHAUSTI, J.C.G., 2011, Corumbella and in situ Cloudina in association with thrombolites in the Ediacaran Itapucumi Group, Paraguay: Terra Nova, v. 23, p. 382–389, doi: 10.1111/j.1365-3121.2011.01023.x.

WARREN, L. V., QUAGLIO, F., RICCOMINI, C., SIMÕES, M.G., POIRÉ, D.G., STRIKIS, N.M., ANELLI, L.E., and STRIKIS, P.C., 2014, The puzzle assembled: Ediacaran guide fossil Cloudina reveals an old proto-Gondwana seaway: Geology, v. 42, p. 391–394, doi: 10.1130/G35304.1.

WARREN, L.V., QUAGLIO, F., SIMÕES, M.G., GAUCHER, C., RICCOMINI, C., POIRÉ, D.G., FREITAS, B.T., BOGGIANI, P.C., and SIAL, A.N., 2017, Cloudina-Corumbella-Namacalathus association from the Itapucumi Group, Paraguay: Increasing ecosystem complexity and tiering at the end of the Ediacaran: Precambrian Research, v. 298, p. 79–87, doi: 10.1016/j.precamres.2017.05.003.  
<http://dx.doi.org/10.1016/j.precamres.2017.05.003>.

WOOD, R., 2018, Exploring the drivers of early biomimetic mineralization: Emerging Topics in Life Sciences, v. 2, p. 201–212, doi: 10.1042/etls20170164.

XIAO, S., and LAFLAMME, M., 2009, On the eve of animal radiation: phylogeny, ecology and evolution of the Ediacara biota: Trends in Ecology and Evolution, v. 24, p. 31–40, doi: 10.1016/j.tree.2008.07.015.

- XIAO, S., YUAN, X., STEINER, M., and KNOLL, A.H., 2002, Macroscopic carbonaceous compressions in a terminal Proterozoic shale: A systematic reassessment of the Miaohe biota, south China: *Journal of Paleontology*, v. 76, p. 347–376, doi: 10.1017/S0022336000041743.  
[https://www.cambridge.org/core/product/identifier/S0022336000041743/type/journal\\_article](https://www.cambridge.org/core/product/identifier/S0022336000041743/type/journal_article).
- XIAO, S., ZHOU, C., LIU, P., WANG, D., and YUAN, X., 2014, Phosphatized acanthomorphic acritarchs and related microfossils from the Ediacaran Doushantuo Formation at Weng'an (South China) and their implications for biostratigraphic correlation: *Journal of Paleontology*, v. 88, p. 1–67, doi: 10.1666/12-157r.
- YIN, Z., ZHU, M., BOTTJER, D.J., ZHAO, F., and TAFFOREAU, P., 2016, Meroblastic cleavage identifies some Ediacaran Doushantuo (China) embryo-like fossils as metazoans: *Geology*, v. 44, p. 735–738, doi: 10.1130/G38262.1.
- YUAN, X., CHEN, Z., XIAO, S., ZHOU, C., and HUA, H., 2011, An early Ediacaran assemblage of macroscopic and morphologically differentiated eukaryotes: *Nature*, v. 470, p. 390–393, doi: 10.1038/nature09810.  
<http://dx.doi.org/10.1038/nature09810>.
- ZHANG, G., DONG, H., KIM, J., and EBERL, D.D., 2007, Microbial reduction of structural Fe<sup>3+</sup> in nontronite by a thermophilic bacterium and its role in promoting the smectite to illite reaction: *American Mineralogist*, v. 92, p. 1411–1419, doi: 10.2138/am.2007.2498.
- ZOPFI, J., KJAR, T., NIELSEN, L.P., and JORGENSEN, B.B., 2001, Ecology of *Thioploca* spp.: Nitrate and Sulfur Storage in Relation to Chemical Microgradients and Influence of *Thioploca* spp. on the Sedimentary Nitrogen Cycle: *Applied and Environmental Microbiology*, v. 67, p. 5530–5537, doi: 10.1128/AEM.67.12.5530-5537.2001.  
<http://aem.asm.org/cgi/doi/10.1128/AEM.67.12.5530-5537.2001>.
- ZVIAGINA, B.B., DRITS, V.A., ŠRODON', J., McCARTY, D.K., and DORZHIEVA, O. V., 2015, The illite aluminoceladonite series: Distinguishing features and identification criteria from X-ray diffraction and infrared spectroscopy data: *Clays and Clay Minerals*, v. 63, p. 378–394, doi: 10.1346/CCMN.2015.0630504.

## APPENDIX I - ARTICLE ONE

Supplementary Table 1. Investigated outcrops and respective geographic coordinates

<b>Outcrop</b>	<b>Coordinates</b>
AF1	27° 2'38.30"S 49°23'42.70"W
AF2	27° 4'56.00"S 49°30'42.60"W
AF4	27° 4'38.70"S 49°29'44.20"W
AF6	27° 5'46.00"S 49°27'34.80"W
AF7	27° 5'56.00"S 49°27'35.80"W
AF8	27° 5'46.11"S 49°27'49.91"W
AF9	27° 5'0.20"S 49°26'38.07"W
AF10	27° 6'11.70"S 49°25'27.20"W
AF11	27° 6'8.30"S 49°25'37.60"W
AF12	27° 5'56.70"S 49°25'45.20"W
AF13	27° 5'54.40"S 49°25'49.00"W
AF14	27° 5'49.40"S 49°25'51.20"W
AF15	27° 5'47.80"S 49°25'52.90"W
AF16	27° 5'43.70"S 49°26'0.60"W
AF17	27° 5'11.60"S 49°26'26.70"W
AF18	27° 2'23.80"S 49°23'27.20"W
AF19	27° 2'29.11"S 49°23'32.50"W
AF20	27° 2'16.00"S 49°23'16.60"W
AF21	27° 2'15.60"S 49°23'15.80"W
AF22	27° 2'20.00"S 49°22'53.70"W
AF23	27° 2'48.70"S 49°21'44.00"W
AF24	27° 3'7.07"S 49°21'33.30"W
AF25	27° 3'23.80"S 49°21'18.80"W
AF26	27° 3'26.00"S 49°21'5.70"W
AF27	27° 3'48.20"S 49°21'15.10"W
AF28	27° 4'22.60"S 49°20'17.10"W
AF29	27° 4'58.60"S 49°20'10.70"W
AF30	27° 5'17.70"S 49°19'56.60"W
AF31	27° 2'3.90"S 49°22'56.80"W
AF32	27° 7'56.80"S 49°19'31.00"W
AF33	27° 9'1.20"S 49°19'22.20"W
AF34	27° 9'2.80"S 49°19'13.30"W
AF36	27° 9'33.80"S 49°19'2.20"W
AF37	27° 9'48.10"S 49°18'59.40"W
AF38	26°59'7.80"S 49°22'13.20"W
AF39	26°59'10.50"S 49°22'10.70"W
AF40	26°59'21.70"S 49°22'9.90"W
AF41	26°59'24.60"S 49°21'56.60"W
AF42	26°59'36.80"S 49°21'30.40"W
AF43	26°59'52.50"S 49°21'12.30"W
AF44	27° 0'2.90"S 49°21'8.10"W
AF45	27° 0'9.30"S 49°20'56.00"W
AF46	27° 0'8.70"S 49°20'53.70"W
AF47	27° 0'7.70"S 49°20'50.70"W
AF48	27° 0'15.40"S 49°20'32.90"W
AF49	27° 0'18.80"S 49°20'28.50"W
AF50	27° 0'23.00"S 49°20'23.80"W
AF51	27° 0'15.00"S 49°20'37.00"W
AF52	27° 0'19.70"S 49°20'33.50"W

Appendix I - Supplementary Table 1. *Cont.*

AF53	27° 0'27.80"S 49°20'31.30"W
AF54	27° 0'41.00"S 49°20'25.00"W
AF55	27° 0'48.10"S 49°20'19.70"W
AF56	27° 1'9.90"S 49°20'24.70"W
AF57	27° 1'18.00"S 49°20'12.40"W
AF58	27° 0'46.90"S 49°22'12.20"W
AF59	27° 0'53.50"S 49°22'7.20"W
AF60	27° 1'8.90"S 49°21'50.00"W
AF61	27° 1'15.70"S 49°21'37.00"W
AF62	27° 1'25.73"S 49°21'16.11"W
AF63	27° 1'30.38"S 49°21'10.78"W
AF64	27° 1'31.70"S 49°21'3.10"W
AF65	27° 1'31.40"S 49°20'57.80"W
AF66	27° 1'33.90"S 49°20'52.20"W
AF67	27° 1'35.10"S 49°20'50.10"W
AF68	27° 1'39.30"S 49°20'45.00"W
AF69	27° 1'40.90"S 49°20'40.10"W
AF70	27° 1'50.60"S 49°20'34.20"W
AF71	27° 1'53.90"S 49°20'29.00"W
AF72	27° 1'59.50"S 49°20'18.80"W
AF73	27° 1'34.30"S 49°20'56.80"W
AF74	27° 1'34.90"S 49°20'54.40"W
AF75	27° 1'47.70"S 49°20'57.90"W
AF76	27° 2'22.00"S 49°20'33.40"W
AF77	27° 7'8.90"S 49°26'59.60"W
AF78	27° 7'26.00"S 49°26'51.40"W
AF79	27° 7'37.00"S 49°26'43.70"W
AF80	27° 7'38.50"S 49°26'43.80"W
AF81	27° 7'44.90"S 49°26'47.80"W
AF82	27° 7'48.70"S 49°26'48.20"W
AF83	27° 8'4.60"S 49°27'0.40"W
AF84	27° 8'25.30"S 49°27'23.20"W
AF85	27° 8'1.90"S 49°27'22.90"W
AF86	27° 7'7.50"S 49°25'52.60"W
AF87	27° 7'9.30"S 49°25'51.00"W
AF88	27° 7'11.80"S 49°25'41.90"W
AF89	27° 7'25.40"S 49°25'20.40"W
AF90	27° 7'29.60"S 49°25'15.30"W
AF91	27° 7'36.80"S 49°25'3.60"W
AF92	27° 7'25.70"S 49°24'42.10"W
AF93	27° 7'15.10"S 49°24'29.60"W
AF94	27° 2'1.00"S 49°23'35.80"W
AF95	27° 2'7.10"S 49°23'51.40"W
AF96	27° 1'58.10"S 49°24'4.50"W
AF97	27° 2'11.80"S 49°23'48.40"W
AF98	27° 2'9.60"S 49°24'7.50"W
AF99	27° 3'5.00"S 49°23'34.40"W
AF100	27° 3'12.09"S 49°23'34.20"W
AF101	27° 3'17.70"S 49°23'35.60"W
AF102	27° 1'41.02"S 49°23'21.80"W

Appendix I - Supplementary Table 1. *Cont.*

AF103	27° 1'19.40"S 49°22'55.40"W
AF104	27° 0'44.30"S 49°22'40.60"W
AF105	27° 0'36.70"S 49°22'42.70"W
AF106	27° 0'3.20"S 49°22'45.40"W
AF107	26°59'14.70"S 49°23'7.00"W
AF108	26°58'59.80"S 49°22'48.10"W
AF109	26°58'57.90"S 49°22'46.10"W
AF111	26°57'13.60"S 49°19'35.60"W
AF113	26°57'11.30"S 49°10'36.30"W
AF114	26°57'56.80"S 49°10'40.50"W
AF115	26°58'3.80"S 49°10'44.40"W
AF116	26°58'14.60"S 49°10'34.70"W
AF117	26°59'10.10"S 49°10'55.60"W
AF118	26°59'6.60"S 49°10'59.90"W
AF119	26°59'30.60"S 49°11'22.00"W
AF120	26°59'32.20"S 49°11'19.60"W
AF121	26°59'38.50"S 49°11'20.60"W
AF122	26°59'54.60"S 49°11'33.30"W
AF123	26°59'53.40"S 49°11'35.30"W
AF124	26°59'48.80"S 49°11'44.60"W
AF125	26°59'49.50"S 49°11'46.80"W
AF126	26°59'50.50"S 49°11'51.80"W
AF127	26°59'56.60"S 49°12'2.30"W
AF128	27° 7'14.60"S 49°26'3.95"W
AF129	27° 7'43.40"S 49°25'45.40"W
AF130	27° 7'55.80"S 49°25'37.50"W
AF131	27° 8'0.20"S 49°25'37.30"W
AF132	27° 8'3.20"S 49°25'35.60"W
AF133	27° 8'17.60"S 49°25'22.50"W
AF134	27° 8'20.10"S 49°25'24.50"W
AF135	27° 8'31.80"S 49°25'26.60"W
AF136	27° 8'41.70"S 49°25'22.50"W
AF137	27° 9'1.00"S 49°25'1.70"W
AF138	27° 9'11.40"S 49°24'55.20"W
AF139	27° 9'16.60"S 49°25'1.70"W
AF143	27° 8'30.80"S 49°20'24.30"W
AF144	27° 8'24.20"S 49°20'0.70"W
AF145	27° 8'10.70"S 49°19'38.40"W
AF146	27° 7'59.10"S 49°19'32.30"W
AF147	26°53'26.50"S 48°53'9.70"W
AF148	26°53'36.30"S 48°53'49.40"W
AF149	26°49'5.40"S 48°47'5.50"W
AF150	26°48'58.80"S 48°47'23.90"W
AF151	26°57'47.50"S 49°21'29.20"W
AF152	26°57'53.70"S 49°20'52.30"W
AF153	26°58'0.70"S 49°20'10.80"W
AF154	26°57'34.00"S 49°18'48.70"W
AF155	26°57'18.50"S 49°18'50.40"W
AF156	26°58'25.50"S 49°15'40.70"W
AF157	26°58'26.20"S 49°15'0.90"W

Appendix I - Supplementary Table 1. *Cont.*

AF158	26°57'55.40"S 49°14'6.60"W
AF159	26°57'53.70"S 49°14'3.30"W
AF161	27° 4'36.00"S 49°24'38.10"W
AF162	27° 8'1.70"S 49°26'16.90"W
AF163	27° 2'36.60"S 49°22'17.50"W
AF164	27° 2'37.40"S 49°22'25.40"W
AF165	27° 4'42.00"S 49°21'21.80"W
AF166	27° 4'54.50"S 49°21'18.60"W
AF167	27° 5'7.90"S 49°21'24.90"W
AF168	27° 5'35.10"S 49°21'46.50"W
AF169	27° 5'42.90"S 49°21'51.50"W
AF170	27° 6'6.80"S 49°22'26.30"W
AF171	27° 6'30.90"S 49°23'4.00"W
AF172	27° 6'38.30"S 49°23'5.00"W
AF173	27° 6'57.80"S 49°23'4.20"W
AF174	27° 7'16.20"S 49°22'59.60"W
AF175	26°58'59.90"S 49°24'34.10"W
AF176	26°59'38.80"S 49°26'4.60"W
AF177	26°59'39.40"S 49°26'8.10"W
AF178	26°59'46.90"S 49°27'12.30"W
AF179	26°59'48.10"S 49°27'31.70"W
AF180	26°56'4.30"S 49° 3'39.40"W
AF181	27° 0'19.80"S 49° 4'5.50"W
AF183	26°58'22.60"S 49°16'53.00"W
AF184	26°59'31.40"S 49°16'5.00"W
AF189	27° 4'36.30"S 49°19'26.60"W
AF190	27° 4'40.30"S 49°19'23.30"W
AF191	27° 4'44.50"S 49°19'11.70"W
AF192	27° 4'49.20"S 49°19'3.60"W
AF193	27° 4'44.60"S 49°18'40.70"W
AF194	27° 4'45.80"S 49°18'33.30"W
AF195	27° 5'5.80"S 49°18'8.90"W
AF196	27° 5'38.70"S 49°18'3.20"W
AF197	27° 5'57.90"S 49°17'56.60"W
AF198	27° 6'17.20"S 49°17'39.20"W
AF199	27° 6'19.00"S 49°17'36.90"W
AF200	27° 6'20.40"S 49°17'37.40"W
AF201	27° 6'23.40"S 49°17'34.10"W
AF202	27° 6'31.30"S 49°17'29.10"W
AF203	27° 6'48.80"S 49°17'17.50"W
AF204	27° 6'48.40"S 49°17'13.20"W
AF205	27° 4'28.50"S 49°25'23.90"W
AF206	27° 4'40.90"S 49°25'17.10"W
AF207	27° 4'56.40"S 49°25'11.40"W
AF208	27° 4'57.70"S 49°24'57.00"W
AF209	27° 4'59.90"S 49°24'44.10"W
AF210	27° 5'1.00"S 49°24'39.60"W
AF211	27° 5'5.10"S 49°24'36.10"W
AF212	27° 5'13.50"S 49°24'25.20"W
AF213	27° 5'16.90"S 49°24'22.60"W

Appendix I - Supplementary Table 1. *Cont.*

AF214	27° 5'21.00"S 49°24'21.30"W
AF215	27° 5'23.40"S 49°24'19.00"W
AF216	27° 5'35.10"S 49°24'6.60"W
AF217	26°57'50.40"S 49°19'3.70"W
AF218	27° 5'35.60"S 49°26'10.60"W
AF219	27° 5'45.50"S 49°25'54.60"W
AF220	26°52'44.30"S 48°50'35.90"W
AF221	26°52'18.90"S 48°50'19.80"W
AF222	26°52'15.10"S 48°50'29.50"W
AF223	26°51'52.00"S 48°50'33.40"W
AF224	26°51'23.30"S 48°50'51.80"W
AF225	26°50'58.90"S 48°51'57.00"W
AF226	26°51'0.00"S 48°54'19.70"W
AF227	26°50'54.00"S 48°54'52.50"W
AF228	26°50'28.50"S 48°54'48.30"W
AF229	26°50'23.00"S 48°55'8.10"W
AF231	26°59'22.10"S 49°25'9.30"W
AF232	27° 3'7.00"S 49°24'12.60"W
AF233	27° 3'8.60"S 49°24'25.90"W
AF234	27° 2'39.50"S 49°24'57.20"W
AF235	27° 2'34.20"S 49°24'58.20"W
AF236	27° 2'29.10"S 49°25'7.40"W
AF237	27° 2'25.70"S 49°25'20.30"W
AF238	27° 2'24.10"S 49°25'24.60"W
AF239	27° 2'21.60"S 49°25'33.40"W
AF240	27° 3'6.80"S 49°24'11.70"W
AF241	27° 3'13.50"S 49°25'25.10"W
AF242	27° 3'14.00"S 49°25'31.20"W
BERG	27° 4'6.81"S 49°25'8.98"W
AF Z	27° 9'27.08"S 49°19'2.54"W
AF H	27° 2'34.62"S 49°21'54.00"W
M9	26°54'52.05"S 48°58'7.15"W
M11	26°54'54.75"S 48°58'11.27"W
M12	26°55'1.20"S 48°58'8.90"W
A16	27° 5'46.62"S 49°25'51.43"W

## APPENDIX II - ARTICLE TWO

**Supplementary Table 1.** Database of the size ranges of modern unbranched filamentous organisms

phylum	class	order	family	spp	fil_width_min	fil_width_max	trich_width_min	trich_width_max	cell_width_min	cell_width_max	cell_length_min	cell_length_max	fil_length_in	fil_length_max	ref	
PROTEOBACTERIA	Gammaproteobacteria	Thiotrichales	Thiotrichaceae	"Candidatus Marinbeggiaota vulgaris" (Attached filaments)	4	112	4	112	4	112					[1]	
PROTEOBACTERIA	Gammaproteobacteria	Thiotrichales	Thiotrichaceae	Beggiatoaceae	18	28									[2]	
PROTEOBACTERIA	Gammaproteobacteria	Thiotrichales	Thiotrichaceae	Beggiatoa sp.	116	122	116	122	116	122					[3]	
PROTEOBACTERIA	Gammaproteobacteria	Thiotrichales	Thiotrichaceae	Beggiatoa sp.	6	200	6	200	6	200					20,000.0 [4]	
PROTEOBACTERIA	Gammaproteobacteria	Thiotrichales	Thiotrichaceae	Beggiatoa sp.		6.3	6.3	6.3							[5]	
PROTEOBACTERIA	Gammaproteobacteria	Thiotrichales	Thiotrichaceae	Beggiatoa sp.	5	35	5	35	5	35					[5]	
PROTEOBACTERIA	Gammaproteobacteria	Thiotrichales	Thiotrichaceae	Beggiatoa sp.	8	10	8	10	8	10					[5]	
PROTEOBACTERIA	Gammaproteobacteria	Thiotrichales	Thiotrichaceae	Beggiatoa sp.	3	4	3	4	3	4					[6]	
PROTEOBACTERIA	Gammaproteobacteria	Thiotrichales	Thiotrichaceae	Beggiatoa sp.	40	45	40	45	40	45					[7]	
PROTEOBACTERIA	Gammaproteobacteria	Thiotrichales	Thiotrichaceae	Beggiatoa sp.		120		120						2,000.0, 10,000.0 [7]		
PROTEOBACTERIA	Gammaproteobacteria	Thiotrichales	Thiotrichaceae	Beggiatoa sp.	35	40	35	40	35	40					[8]	
PROTEOBACTERIA	Gammaproteobacteria	Thiotrichales	Thiotrichaceae	Beggiatoa sp.	30	50	30	50	30	50					[9]	
PROTEOBACTERIA	Gammaproteobacteria	Thiotrichales	Thiotrichaceae	Beggiatoa sp.	88	108	88	108	88	108					[9]	
PROTEOBACTERIA	Gammaproteobacteria	Thiotrichales	Thiotrichaceae	Beggiatoa sp.		200		200						Several cms [10]		
PROTEOBACTERIA	Gammaproteobacteria	Thiotrichales	Thiotrichaceae	Beggiatoa sp.	20	30	20	30	20	30					[11]	
PROTEOBACTERIA	Gammaproteobacteria	Thiotrichales	Thiotrichaceae	Beggiatoa sp.	32.5	50	32.5	50	32.5	50					[11]	
PROTEOBACTERIA	Gammaproteobacteria	Thiotrichales	Thiotrichaceae	Beggiatoa sp.	80	160	80	160	80	160					[11]	
PROTEOBACTERIA	Gammaproteobacteria	Thiotrichales	Thiotrichaceae	Beggiatoa sp.	22.5	40	22.5	40	22.5	40					[11]	
PROTEOBACTERIA	Gammaproteobacteria	Thiotrichales	Thiotrichaceae	Beggiatoa sp.	65	85	65	85	65	85	5	36	10,000.0	100,000.0 [12]		
PROTEOBACTERIA	Gammaproteobacteria	Thiotrichales	Thiotrichaceae	Beggiatoa sp.	88	140	88	140	88	140					[12]	
PROTEOBACTERIA	Gammaproteobacteria	Thiotrichales	Thiotrichaceae	Beggiatoa sp.	20	35	20	35	20	35					[11]	
PROTEOBACTERIA	Gammaproteobacteria	Thiotrichales	Thiotrichaceae	Beggiatoa sp.	80	160	80	160	80	160					[11]	
PROTEOBACTERIA	Gammaproteobacteria	Thiotrichales	Thiotrichaceae	Beggiatoa sp.	3	5	3	5	3	5				800.0 [13]		
PROTEOBACTERIA	Gammaproteobacteria	Thiotrichales	Thiotrichaceae	Beggiatoa sp.	5	23	5	23	5	23				1,000.0 [13]		
PROTEOBACTERIA	Gammaproteobacteria	Thiotrichales	Thiotrichaceae	Beggiatoa sp.	23	35	23	35	23	35				1,900.0 [13]		
PROTEOBACTERIA	Gammaproteobacteria	Thiotrichales	Thiotrichaceae	Beggiatoa sp.	20	76	20	76	20	76				[1]		
PROTEOBACTERIA	Gammaproteobacteria	Thiotrichales	Thiotrichaceae	Beggiatoa sp.	20	95	20	95	20	95				[14]		
PROTEOBACTERIA	Gammaproteobacteria	Thiotrichales	Thiotrichaceae	Beggiatoa sp.	1	40	1	40	1	40			100.0	10,000.0 [15]		
PROTEOBACTERIA	Gammaproteobacteria	Thiotrichales	Thiotrichaceae	"Candidatus Maribeggiaota vulgaris" (Beggiatoa sp.)	65	85	65	85	65	85					[16]	
PROTEOBACTERIA	Gammaproteobacteria	Thiotrichales	Thiotrichaceae	"Candidatus Isobeggiaota divulgata" (Beggiatoa sp.)	9	11	9	11	9	11					[17]	
PROTEOBACTERIA	Gammaproteobacteria	Thiotrichales	Thiotrichaceae	Beggiatoa sp.	5.3	31	5.3	31	5.3	31					[18]	
PROTEOBACTERIA	Gammaproteobacteria	Thiotrichales	Thiotrichaceae	"Candidatus Parabeggiaota" (Beggiatoa spp.)	5	30	5	30	5	30					[17]	
PROTEOBACTERIA	Gammaproteobacteria	Thiotrichales	Thiotrichaceae	Beggiatoa spp.	5	8	5	8	5	8					[19]	
PROTEOBACTERIA	Gammaproteobacteria	Thiotrichales	Thiotrichaceae	"Candidatus Isobeggiaota divulgata" (Beggiatoa spp.)	2	5					3.7		5.4	250.0 [20]		
PROTEOBACTERIA	Gammaproteobacteria	Thiotrichales	Thiotrichaceae	"Candidatus Isobeggiaota divulgata" (Beggiatoa spp.)	11	22					19		9		[20]	
PROTEOBACTERIA	Gammaproteobacteria	Thiotrichales	Thiotrichaceae	"Candidatus Isobeggiaota divulgata" Beggiatoa spp.	23	50									1,500.0 [20]	
PROTEOBACTERIA	Gammaproteobacteria	Thiotrichales	Thiotrichaceae	"Candidatus Isobeggiaota divulgata" (Beggiatoa spp.)	10	30	10	30	10	30					[21]	
PROTEOBACTERIA	Gammaproteobacteria	Thiotrichales	Thiotrichaceae	Beggiatoa spp.	6	8	6	8	6	8				1,000.0	10,000.0 [22]	
PROTEOBACTERIA	Gammaproteobacteria	Thiotrichales	Thiotrichaceae	"Candidatus Marinithrix sp."	110		110		110						[23]	
PROTEOBACTERIA	Gammaproteobacteria	Thiotrichales	Thiotrichaceae	Large filamentous bacteria	20	30	20	30	20	30					[24]	
PROTEOBACTERIA	Gammaproteobacteria	Thiotrichales	Thiotrichaceae	Large filamentous bacteria	40	60	40	60	40	60					[24]	
PROTEOBACTERIA	Gammaproteobacteria	Thiotrichales	Thiotrichaceae	Large filamentous bacteria	135		135		135						[24]	
PROTEOBACTERIA	Gammaproteobacteria	Thiotrichales	Thiotrichaceae	Microphototype 1	60		60		60					18.6	30,000.0 [25]	
PROTEOBACTERIA	Gammaproteobacteria	Thiotrichales	Thiotrichaceae	Microphototype 2	30		30		30					3.8		[25]
PROTEOBACTERIA	Gammaproteobacteria	Thiotrichales	Thiotrichaceae	Sheathless Thiotricha		50		60								[26]
PROTEOBACTERIA	Gammaproteobacteria	Thiotrichales	Thiotrichaceae	Thioploca	21.5	89.1	1.5	4.2			1			5.7		[27]
PROTEOBACTERIA	Gammaproteobacteria	Thiotrichales	Thiotrichaceae	Thioploca	10.4	65.3	2.2	10.7			1.37			11.1		[27]
PROTEOBACTERIA	Gammaproteobacteria	Thiotrichales	Thiotrichaceae	Thioploca	10.8	124.6	1.6	7.4			1.2			8.9		[27]
PROTEOBACTERIA	Gammaproteobacteria	Thiotrichales	Thiotrichaceae	Thioploca	233.4	234	1.4	9.4			1			11.9		[27]
PROTEOBACTERIA	Gammaproteobacteria	Thiotrichales	Thiotrichaceae	Thioploca		6.5	10.5									[27]
PROTEOBACTERIA	Gammaproteobacteria	Thiotrichales	Thiotrichaceae	Thioploca	100	200										[27]
PROTEOBACTERIA	Gammaproteobacteria	Thiotrichales	Thiotrichaceae	Thioploca	17	28	2	4.3								[27]
PROTEOBACTERIA	Gammaproteobacteria	Thiotrichales	Thiotrichaceae	Thioploca		2.6	5.8									[28]
PROTEOBACTERIA	Gammaproteobacteria	Thiotrichales	Thiotrichaceae	Thioploca		3	4									[29]
PROTEOBACTERIA	Gammaproteobacteria	Thiotrichales	Thiotrichaceae	Thioploca	28.5	42.5	12	15						4,000.0	8,000.0 [151]	
PROTEOBACTERIA	Gammaproteobacteria	Thiotrichales	Thiotrichaceae	Thioploca	50	400	3	75						22,000.0	56,000.0 [30]	
PROTEOBACTERIA	Gammaproteobacteria	Thiotrichales	Thiotrichaceae	Thioploca inrica	30	90	3	6	3	6					30,000.0 [32]	
PROTEOBACTERIA	Gammaproteobacteria	Thiotrichales	Thiotrichaceae	"Candidatus Maritiphloca" (Thioploca spp.)	100	500	2.5	40	2.5	40						[33]
PROTEOBACTERIA	Gammaproteobacteria	Thiotrichales	Thiotrichaceae	Thioploca schmidlei	1	8										[36]
PROTEOBACTERIA	Gammaproteobacteria	Thiotrichales	Thiotrichaceae	Thioploca spp.	15	80	4	4							50,000.0 [37]	
PROTEOBACTERIA	Gammaproteobacteria	Thiotrichales	Thiotrichaceae	Thioploca sp.		60		125								[38]
PROTEOBACTERIA	Gammaproteobacteria	Thiotrichales	Thiotrichaceae	Thioploca sheaths	50	500									100,000.0 [39]	
PROTEOBACTERIA	Gammaproteobacteria	Thiotrichales	Thiotrichaceae	Thiodixis nivea							1.5	3	1.5	3		[39]
PROTEOBACTERIA	Gammaproteobacteria	Thiotrichales	Thiotrichaceae	Thiodixis sp.		1.5									[40]	
CYANOBACTERIA	Cyanophyceae	Oscillatoriaceae	Anagnostidina acutissimum		1.5	2.5					3		7		[41][42][43]	
CYANOBACTERIA	Cyanophyceae	Oscillatoriaceae	Anagnostidina amphibium					1.5	3	3	9				[41][44]	
CYANOBACTERIA	Cyanophyceae	Oscillatoriaceae	Anagnostidina ionicum					1	1.3	2	5.5				[41][42][43]	
CYANOBACTERIA	Cyanophyceae	Oscillatoriaceae	Anagnostidina lemmermannii					2	2.5	4	6				[41][42][43]	
CYANOBACTERIA	Cyanophyceae	Oscillatoriaceae	Geitlerinema aculeiforme		0.7	0.9					3.5		6.5		[41][42][43]	
CYANOBACTERIA	Cyanophyceae	Oscillatoriaceae	Geitlerinema numidicum		2.3	4					2.8		6.5		[41][42][43]	
CYANOBACTERIA	Cyanophyceae	Oscillatoriaceae	Geitlerinema splenditum		1.8	3.1					3		9		1,000.0 [41][42][44]	
CYANOBACTERIA	Cyanophyceae	Oscillatoriaceae	Jaegnema pseudogenitatum		1.3	2.2					2		2.6		[41][42][43]	
CYANOBACTERIA	Cyanophyceae	Oscillatoriaceae	Kamptoneima animale		1.3	4					1.5		5		[41][42][46]	
CYANOBACTERIA	Cyanophyceae	Oscillatoriaceae	Kamptoneima chlorinum		3.5	4					3.7		8		[41][42][46]	
CYANOBACTERIA	Cyanophyceae	Oscillatoriaceae	Arthrosira jenneri		4	6					2		6		[41][42][47]	
CYANOBACTERIA	Cyanophyceae	Oscillatoriaceae	Arthrosira khaniae								1.7				[41][42][43]	
CYANOBACTERIA	Cyanophyceae	Oscillatoriaceae	Arthrosira platensis		6	7					2		6		[41][42][43]	
CYANOBACTERIA	Cyanophyceae	Oscillatoriaceae	Kamptoneima formosum		4	5.5					3		4.5		[41][42][49]	
CYANOBACTERIA	Cyanophyceae	Oscillatoriaceae	Microcoleus amoenus		2.5	5					2.5		4.2		[41][50][43]	
CYANOBACTERIA	Cyanophyceae	Oscillatoriaceae	Microcoleus setchellianus		4	6.5			3.4	4.4	1.9		3.8		[41][42][43]	
CYANOBACTERIA	Cyanophyceae	Oscillatoriaceae	Microcoleus subtrifoliosus	13.2	20	6	8	6	10	3	10				[41][42][43]	
CYANOBACTERIA	Cyanophyceae	Oscillatoriaceae	Planktothrix rubescens					2.8	3.2	2	4				[41][43]	
CYANOBACTERIA	Cyanophyceae	Oscillatoriaceae	Porphyrioniphon versicolor												[41][43]	
CYANOBACTERIA	Cyanophyceae	Oscillatoriaceae	Symploca elegans		1.3	2					2		4		[41][43]	
CYANOBACTERIA	Cyanophyceae	Oscillatoriaceae	Symploca flaccida		4	5					1.3		2.5		[45]	
CYANOBACTERIA	Cyanophyceae	Oscillatoriaceae	Symploca muralis					3.4	4	2.5	5.5			2,500.0 [41][42]		
CYANOBACTERIA	Cyanophyceae	Oscillatoriaceae	Symploca muscorum	9		4.5	8	5	11	3.5	9.2				[41][42][43]	
CYANOBACTERIA	Cyanophyceae	Oscillatoriaceae	Symploca parietina					1.5	3	3.5	15.4				[41][42][43]	
CYANOBACTERIA	Cyanophyceae	Oscillatoriaceae	Trichodessium clevei	6.3	7.7					6.3	15.4			2,000.0		[41][43]
CYANOBACTERIA	Cyanophyceae															

Appendix II - Supplementary Table 1. Cont.

CYANOBACTERIA	Cyanophyceae	Oscillatoriaceae	Oscillatoriaceae	<i>Phormidium irriguum</i>		6	11.2	4	11	[41][43]							
CYANOBACTERIA	Cyanophyceae	Oscillatoriaceae	Oscillatoriaceae	<i>Phormidium lucidum</i>		6	8	2	2.5	[41][43]							
CYANOBACTERIA	Cyanophyceae	Oscillatoriaceae	Oscillatoriaceae	<i>Phormidium nigrum</i>				1.8	2.8	[41][43][66]							
CYANOBACTERIA	Cyanophyceae	Oscillatoriaceae	Oscillatoriaceae	<i>Phormidium retzii</i>			4.5	12	3.2	[41][43][60]							
CYANOBACTERIA	Cyanophyceae	Oscillatoriaceae	Oscillatoriaceae	<i>Phormidium rubidum</i>	6	7	4	4.5	7.5	[41][45][43]							
CYANOBACTERIA	Cyanophyceae	Oscillatoriaceae	Oscillatoriaceae	<i>Phormidium schultzii</i>			1	2.6	1.5	[57]							
CYANOBACTERIA	Cyanophyceae	Oscillatoriaceae	Oscillatoriaceae	<i>Phormidium stagninum</i>	8	12	7	10	2	[41][43][58]							
CYANOBACTERIA	Cyanophyceae	Oscillatoriaceae	Oscillatoriaceae	<i>Phormidium subincrustatum</i>	6.2	7.7			8	[41][43]							
CYANOBACTERIA	Cyanophyceae	Oscillatoriaceae	Oscillatoriaceae	<i>Phormidium terebriforme</i>			4.3	4.6	1.5	[41][59][45]							
CYANOBACTERIA	Cyanophyceae	Oscillatoriaceae	Oscillatoriaceae	<i>Phormidium tergestinum</i>			4	6.5	2.4	[41][43]							
CYANOBACTERIA	Cyanophyceae	Oscillatoriaceae	Oscillatoriaceae	<i>Phormidium uncinatum</i>			4	10	2.4	[41][43]							
CYANOBACTERIA	Cyanophyceae	Oscillatoriaceae	Oscillatoriaceae	<i>Phormidium uncinatum</i>			5.5	9	2	[41][43]							
CYANOBACTERIA	Cyanophyceae	Spirulinaceae	Spirulinaceae	<i>Glaucospira laxissima</i>			0.5	0.6	2.7	[41][60][43]							
CYANOBACTERIA	Cyanophyceae	Spirulinaceae	Spirulinaceae	<i>Spirulina corakiana</i>			0.7	0.8		[41][43]							
CYANOBACTERIA	Cyanophyceae	Spirulinaceae	Spirulinaceae	<i>Spirulina major</i>			1	2		[41][43]							
CYANOBACTERIA	Cyanophyceae	Spirulinaceae	Spirulinaceae	<i>Spirulina menegehiniana</i>			1.2	1.8		[41][43]							
CYANOBACTERIA	Cyanophyceae	Spirulinaceae	Spirulinaceae	<i>Spirulina spiruloides</i>			5	6	4	[41][43]							
CYANOBACTERIA	Cyanophyceae	Spirulinaceae	Spirulinaceae	<i>Spirulina subtilissima</i>			0.5	1		[41][43]							
CYANOBACTERIA	Cyanophyceae	Spirulinaceae	Spirulinaceae	<i>Spirulina tenerima</i>			0.3	0.6		[41][43]							
CYANOBACTERIA	Cyanophyceae	Nostocales	Aphanizomenonaceae	<i>Anabaenopsis elenkinii</i>			4	6	4	[41][43]							
CYANOBACTERIA	Cyanophyceae	Nostocales	Aphanizomenonaceae	<i>Aphanizomenon flos-aquae</i>			5	6	5	2.000.0							
CYANOBACTERIA	Cyanophyceae	Nostocales	Aphanizomenonaceae	<i>Nodularia harveyana</i>	4	7.5		3.5	7.2	[41][51]							
CYANOBACTERIA	Cyanophyceae	Nostocales	Aphanizomenonaceae	<i>Nodularia spumigena</i>	8	16		7.5	16	[41][62][51]							
CYANOBACTERIA	Cyanophyceae	Nostocales	Nostocaceae	<i>Anabaena inaequalis</i>			4	5.3	4.0	[41][51][63]							
CYANOBACTERIA	Cyanophyceae	Nostocales	Nostocaceae	<i>Anabaena catenula</i>			5	8		[41][51]							
CYANOBACTERIA	Cyanophyceae	Nostocales	Nostocaceae	<i>Anabaena cylindrica</i>			3	4	5	[41][51]							
CYANOBACTERIA	Cyanophyceae	Nostocales	Nostocaceae	<i>Anabaena felsii</i>			5.8	7	6	[41][42]							
CYANOBACTERIA	Cyanophyceae	Nostocales	Nostocaceae	<i>Anabaena oscillarioides</i>			3	6	4	[41][64]							
CYANOBACTERIA	Cyanophyceae	Nostocales	Nostocaceae	<i>Anabaena saaremaensis</i>			4.8	5.5	4.6	[41][42]							
CYANOBACTERIA	Cyanophyceae	Nostocales	Nostocaceae	<i>Anabaena sphaerica</i>			5	6.2	5	[41][42]							
CYANOBACTERIA	Cyanophyceae	Nostocales	Nostocaceae	<i>Cylirostpermum licheniforme</i>			2.5	4.2	4	[41][45]							
CYANOBACTERIA	Cyanophyceae	Nostocales	Nostocaceae	<i>Cylirostpermum majus</i>			4	5	5	[41][45]							
CYANOBACTERIA	Cyanophyceae	Nostocales	Nostocaceae	<i>Cylirostpermum stagnale</i>			4	4.8	4	[41][42]							
CYANOBACTERIA	Cyanophyceae	Nostocales	Rivulariaceae	<i>Calothrix atricha</i>			6	8		[41][42]							
CYANOBACTERIA	Cyanophyceae	Nostocales	Rivulariaceae	<i>Calothrix brevirostrata</i>	15	16		5.5	7.5	1.3	3.8	380.0	[41][45]				
CYANOBACTERIA	Cyanophyceae	Nostocales	Rivulariaceae	<i>Calothrix brevisima</i>			6.5	8	5	7.5	53.0	94.0	[41][57][45]				
CYANOBACTERIA	Cyanophyceae	Nostocales	Rivulariaceae	<i>Calothrix clavata</i>			4	6	3	7		100.0	[41][64][45]				
CYANOBACTERIA	Cyanophyceae	Nostocales	Rivulariaceae	<i>Calothrix ephippifera</i>	5	7.5		3	3.6	6	8.4	250.0	350.0	[41][55][45][66]			
CYANOBACTERIA	Cyanophyceae	Nostocales	Rivulariaceae	<i>Calothrix kossinskiae</i>			3.5	6				160.0	[41][42]				
CYANOBACTERIA	Cyanophyceae	Nostocales	Rivulariaceae	<i>Calothrix linearis</i>	4	12		3	9.5	2.5	5		450.0	[41][67]			
CYANOBACTERIA	Cyanophyceae	Nostocales	Rivulariaceae	<i>Calothrix marchia</i>			9	10	6	9			[41][49]				
CYANOBACTERIA	Cyanophyceae	Nostocales	Rivulariaceae	<i>Calothrix paretina</i>			4.5	10.5	5	12.5		250.0	1.000.0	[41][64][45]			
CYANOBACTERIA	Cyanophyceae	Nostocales	Rivulariaceae	<i>Calothrix pulvinata</i>	7	12		5	10	3	6	2.000.0	3.000.0	[41][68][51]			
CYANOBACTERIA	Cyanophyceae	Nostocales	Rivulariaceae	<i>Calothrix stagnalis</i>	8	10		5	9	5	7		1.000.0	[41][69][51]			
CYANOBACTERIA	Cyanophyceae	Nostocales	Rivulariaceae	<i>Microchaete elongata</i>			11	14	33	42			[42]				
CYANOBACTERIA	Cyanophyceae	Nostocales	Rivulariaceae	<i>Microchaete investiens</i>	8.5	9	5.0	5.6						[41][70]			
CYANOBACTERIA	Cyanophyceae	Nostocales	Rivulariaceae	<i>Microchaete tenera</i>	6	7	4.5	5		5	10		1.000.0	[41][51][45]			
CYANOBACTERIA	Cyanophyceae	Nostocales	Rivulariaceae	<i>Rivularia aquatica</i>			8.4	9.6		0.8	1.2		3.500.0	[41][45][71]			
CYANOBACTERIA	Cyanophyceae	Nostocales	Rivulariaceae	<i>Rivularia beccariana</i>	7	9	4.8	6		12	18			[41][45][71]			
CYANOBACTERIA	Cyanophyceae	Nostocales	Rivulariaceae	<i>Rivularia bullata</i>			5	8		10	16			[41][51]			
CYANOBACTERIA	Cyanophyceae	Nostocales	Rivulariaceae	<i>Rivularia dura</i>			4	9						[41][72]			
CYANOBACTERIA	Cyanophyceae	Nostocales	Rivulariaceae	<i>Rivularia hanggiri</i>			2.8	3.5		3.7	5			[41][45][73]			
CYANOBACTERIA	Cyanophyceae	Nostocales	Rivulariaceae	<i>Rivularia manginii</i>	10	30	3	5		1	1.5			[41][45]			
CYANOBACTERIA	Cyanophyceae	Nostocales	Tolyphothriaceae	<i>Tolyphothrix lanata</i>			9	11	4.5	8				[41][74]			
CYANOBACTERIA	Cyanophyceae	Nostocales	Scytonemataceae	<i>Heteroscytonema crispum</i>	22.8	27.8		17.7	22.8	3.8	6.3		4.000.0	[41][58]			
CYANOBACTERIA	Cyanophyceae	Synechococcaceae	Pseudanabaenaceae	<i>Pseudanabaena catenata</i>			1.2	2	2	6	40.0	200.0	[41][43]				
CYANOBACTERIA	Cyanophyceae	Synechococcaceae	Pseudanabaenaceae	<i>Pseudanabaena coccularis</i>			1	1.5	8	12	20.0	75.0	[41][43]				
CYANOBACTERIA	Cyanophyceae	Synechococcaceae	Pseudanabaenaceae	<i>Pseudanabaena arcuata</i>			5	7		2	14	10.0	20.0	[41][43]			
CYANOBACTERIA	Cyanophyceae	Synechococcaceae	Pseudanabaenaceae	<i>Pseudanabaena batrachospermorum</i>			0.6	1.5		3	8			[41][43]			
CYANOBACTERIA	Cyanophyceae	Synechococcaceae	Pseudanabaenaceae	<i>Pseudanabaena limmetica</i>			1.2	1.5		4	12			[41][43]			
CYANOBACTERIA	Cyanophyceae	Synechococcaceae	Pseudanabaenaceae	<i>Pseudanabaena ionchoidea</i>			0.6	1		2	8	200.0	300.0	[41][43]			
CYANOBACTERIA	Cyanophyceae	Synechococcaceae	Pseudanabaenaceae	<i>Pseudanabaena minima</i>			1.3	2.5		1.5	4			[41][43]			
CYANOBACTERIA	Cyanophyceae	Synechococcaceae	Pseudanabaenaceae	<i>Pseudanabaena mucicola</i>				1.3	2	1.3	4	10.0	50.0	[41][43]			
CYANOBACTERIA	Cyanophyceae	Synechococcaceae	Pseudanabaenaceae	<i>Pseudanabaena persicina</i>			1.7	2		2	7			[41][43]			
CYANOBACTERIA	Cyanophyceae	Synechococcaceae	Pseudanabaenaceae	<i>Pseudanabaena skujae</i>			2.3	2.5		2.3	7.5			[41][43]			
CYANOBACTERIA	Cyanophyceae	Synechococcaceae	Pseudanabaenaceae	<i>Pseudanabaena spelea</i>			0.8	1.2		0.8	2.4			[41][43]			
CYANOBACTERIA	Cyanophyceae	Synechococcaceae	Leptolyngbyaceae	<i>Heteroleibnia chaetomorpha</i>								27.0		[41][43]			
CYANOBACTERIA	Cyanophyceae	Synechococcaceae	Leptolyngbyaceae	<i>Heteroleibnia kuetzingii</i>	2	3.5	1.2	2		1.3	1.5		30.0	80.0	[41][43]		
CYANOBACTERIA	Cyanophyceae	Synechococcaceae	Leptolyngbyaceae	<i>Heteroleibnia mesotricha</i>				3	5	4	8		1.000.0	[41][43]			
CYANOBACTERIA	Cyanophyceae	Synechococcaceae	Leptolyngbyaceae	<i>Schizothrix fragilis</i>	20	1.4	2.5		1.5	2.5	2	3		1.000.0	[41][43]		
CYANOBACTERIA	Cyanophyceae	Synechococcaceae	Leptolyngbyaceae	<i>Schizothrix porphyromelana</i>				0.8	1.8	2	6.5				[41][45]		
CYANOBACTERIA	Cyanophyceae	Synechococcaceae	Leptolyngbyaceae	<i>Schizothrix tenuis</i>	2	4	0.8	1.5		3	4	2		3.000.0	[41][45]		
CYANOBACTERIA	Cyanophyceae	Synechococcaceae	Leptolyngbyaceae	<i>Leptothrix epiphytis</i>	1.5	2			1	1.5	1	2				[41][45]	
CYANOBACTERIA	Cyanophyceae	Synechococcaceae	Leptolyngbyaceae	<i>Leptolyngbya oligranulata</i>	0.8	1			0.5	0.9	9	13				[41][43]	
CYANOBACTERIA	Cyanophyceae	Synechococcaceae	Leptolyngbyaceae	<i>Leptolyngbya granulifera</i>					0.8	1.5	2.5	8.5				[41][43]	
CYANOBACTERIA	Cyanophyceae	Synechococcaceae	Leptolyngbyaceae	<i>Leptolyngbya legerimii</i>	2	2.5			1.5	2.5	2	3				[41][43]	
CYANOBACTERIA	Cyanophyceae	Synechococcaceae	Leptolyngbyaceae	<i>Leptolyngbya lamellosa</i>					0.8	1.8	2	6.5				[41][43]	
CYANOBACTERIA	Cyanophyceae	Synechococcaceae	Leptolyngbyaceae	<i>Leptolyngbya mucosa</i>	3.2	3.8	2.5	3		1.1	2	1.5		25		[41][51]	
CYANOBACTERIA	Cyanophyceae	Synechococcaceae	Leptolyngbyaceae	<i>Leptolyngbya perlelagens</i>	1.5	3	1	1.6			2	8				[41][43]	
CYANOBACTERIA	Cyanophyceae	Synechococcaceae	Leptolyngbyaceae	<i>Leptolyngbya polypiphoniae</i>	3	4	2	2.5			0.5	1.7		200.0		[41][43]	
CYANOBACTERIA	Cyanophyceae	Synechococcaceae	Leptolyngbyaceae	<i>Leptolyngbya purpurens</i>					1.5	2.5						[41][43]	
CYANOBACTERIA	Cyanophyceae	Synechococcaceae	Leptolyngbyaceae	<i>Leptolyngbya valderiana</i>	3						2.5	7.5				[41][43]	
CYANOBACTERIA	Cyanophyceae	Synechococcaceae	Leptolyngbyaceae	<i>Planktolyngbya bipunctata</i>	1.5	2				1	1.5	3.5	5.5				[41][43]
CYANOBACTERIA	Cyanophyceae	Synechococcaceae	Leptolyngbyaceae	<i>Planktolyngbya limnetica</i>	1	2				0.5	1.8	1	5	100.0	600.0	[41][43]	
CYANOBACTERIA	Cyanophyceae	Synechococcaceae	Leptolyngbyaceae	<i>Tapinothrix janthina</i>					1.5	2.3		1.5	2.3		500.0	[41][75]	
CYANOBACTERIA	Cyanophyceae	Synechococcaceae	Leptolyngbyaceae	<i>Tapinothrix varians</i>					2.2	2.5		1.1	1.3		3.000.0	[41][75]	

Appendix II - Supplementary Table 1. Cont.

kingdom	phylum	class	order	fam	spp	fil_width_min	fil_width_max	cell_width_min	cell_width_max	fil_length_m	fil_length_in	cell_length_min	cell_length_max	ref
CHROMALVEOLATA	OCHROPHYTA	Phaeophyceae	Laminariales	Chordaceae	<i>Chorda asiatica</i>	1500	3000	1000000	2000000					[76]
CHROMALVEOLATA	OCHROPHYTA	Phaeophyceae	Laminariales	Chordaceae	<i>C. filum</i>	5000	5000	6000000	6000000					[77]
CHROMALVEOLATA	OCHROPHYTA	Phaeophyceae	Laminariales	Chordaceae	<i>C. concreta</i>	2500	2500	400000	500000					[76]
CHROMALVEOLATA	OCHROPHYTA	Phaeophyceae	Laminariales	Chordaceae	<i>C. concreta</i>	3500	3500	300000	500000					[76]
CHROMALVEOLATA	OCHROPHYTA	Phaeophyceae	Pseudochordales	Pseudochordaceae	<i>Pseudochorda gracilis</i>	1400	1400	800000	800000					[79]
CHROMALVEOLATA	OCHROPHYTA	Phaeophyceae	Laminariales	Pseudochordaceae	<i>Pseudochorda nagaia</i>	1500	1500	600000	600000					[152]
CHROMALVEOLATA	OCHROPHYTA	Phaeophyceae	Stichopeltidae	Stichopeltidae	<i>Stichopeltis flabellaris</i>	400	1000	20000	200000	170000				[30][41]
CHROMALVEOLATA	OCHROPHYTA	Phaeophyceae	Ectocarpales	Scytosiphonaceae	<i>Melanosiphon intestinalis</i>	200	2000			50000	150000			[81]
CHROMALVEOLATA	OCHROPHYTA	Phaeophyceae	Ectocarpales	Scytosiphonaceae	<i>Myelophycus cavus</i>	1000	1500			300000				[82]
CHROMALVEOLATA	OCHROPHYTA	Phaeophyceae	Ectocarpales	Scytosiphonaceae	<i>Myelophycus simplex</i>	4000	4000			300000				[82]
CHROMALVEOLATA	OCHROPHYTA	Phaeophyceae	Ectocarpales	Scytosiphonaceae	<i>Scytosiphon lomentaria</i>	2300	2300			330000				[83]
CHROMALVEOLATA	OCHROPHYTA	Xanthophyceae	Tribonematales	Tribonemataceae	<i>Bumilleria</i> sp. 1			5	5.6			4	6.4	[42]
CHROMALVEOLATA	OCHROPHYTA	Xanthophyceae	Tribonematales	Tribonemataceae	<i>Tribonema affine</i>			4.6	6.5					[84]
CHROMALVEOLATA	OCHROPHYTA	Xanthophyceae	Tribonematales	Tribonemataceae	<i>Tribonema delitescens</i>			15	30			15	30	[42]
CHROMALVEOLATA	OCHROPHYTA	Xanthophyceae	Tribonematales	Tribonemataceae	<i>Tribonema elegans</i>			19	37					[84]
CHROMALVEOLATA	OCHROPHYTA	Xanthophyceae	Tribonematales	Tribonemataceae	<i>Tribonema intermedium</i>			8.4	11.2					[84]
CHROMALVEOLATA	OCHROPHYTA	Xanthophyceae	Tribonematales	Tribonemataceae	<i>Tribonema microchloron</i>			2.8	3.7					[84]
CHROMALVEOLATA	OCHROPHYTA	Xanthophyceae	Tribonematales	Tribonemataceae	<i>Tribonema minus</i>			4.6	6.5					[84]
CHROMALVEOLATA	OCHROPHYTA	Xanthophyceae	Tribonematales	Tribonemataceae	<i>Tribonema monochloron</i>			2	3			18		[42]
CHROMALVEOLATA	OCHROPHYTA	Xanthophyceae	Tribonematales	Tribonemataceae	<i>Tribonema regulara</i>			5.6	7.4					[84]
CHROMALVEOLATA	OCHROPHYTA	Xanthophyceae	Tribonematales	Tribonemataceae	<i>Tribonema utriculosum</i>			12.1	25					[84]
CHROMALVEOLATA	OCHROPHYTA	Xanthophyceae	Tribonematales	Tribonemataceae	<i>Tribonema viride</i>			10.2	13.1					[84]
CHROMALVEOLATA	OCHROPHYTA	Xanthophyceae	Tribonematales	Tribonemataceae	<i>Tribonema viride</i>			8	10					[85]
CHROMALVEOLATA	OCHROPHYTA	Xanthophyceae	Tribonematales	Tribonemataceae	<i>Tribonema vulgare</i>			7.4	9.3					[84]
CHROMALVEOLATA	OCHROPHYTA	Xanthophyceae	Tribonematales	Tribonemataceae	<i>Xanthophora</i>			3.5	10					[86]
CHROMALVEOLATA	OCHROPHYTA	Xanthophyceae	Tribonematales	Tribonemataceae	<i>Xanthophora debilis</i>			6	8					[86]
CHROMALVEOLATA	OCHROPHYTA	Xanthophyceae	Tribonematales	Tribonemataceae	<i>Xanthophora horridula</i>			3.6	4.6					[84]
CHROMALVEOLATA	OCHROPHYTA	Xanthophyceae	Tribonematales	Tribonemataceae	<i>Xanthophora montanum</i>			0	5					[86]
CHROMALVEOLATA	OCHROPHYTA	Xanthophyceae	Tribonematales	Tribonemataceae	<i>Xanthophora solidum</i>			4	7.5					[86]
CHROMALVEOLATA	OCHROPHYTA	Xanthophyceae	Tribonematales	Tribonemataceae	<i>Xanthophora sessile</i>			4	5.5					[86]
CHROMALVEOLATA	OCHROPHYTA	Xanthophyceae	Tribonematales	Tribonemataceae	<i>Xanthophora exilis</i>			3.5	4.5			6	13	[42]
ARCHEAELPLASTIDA	RHODOPHYTA	Stylonematophyceae	Stylonematales	Stylonemataceae	<i>Purpureofilum apyrenoidigerum</i>	10	25	10	14	1000	6	12		[87]
ARCHEAELPLASTIDA	RHODOPHYTA	Compsopogonophyceae	Erythritales	Erythritaceae	<i>Erythritrichia biserata</i>	10	27			1000				[88]
ARCHEAELPLASTIDA	RHODOPHYTA	Compsopogonophyceae	Erythritales	Erythritaceae	<i>Erythritrichia carneae</i>	12	33.5	12	27	500	2000	14	30	[88][89]
ARCHEAELPLASTIDA	RHODOPHYTA	Compsopogonophyceae	Erythritales	Erythritaceae	<i>Erythritrichia carnea tenuis</i>	9	22	9	12	1000	4000	9	20	[90]
ARCHEAELPLASTIDA	RHODOPHYTA	Compsopogonophyceae	Erythritales	Erythritaceae	<i>Erythritrichia pseudotenuis</i>	12	40			5000				[90]
ARCHEAELPLASTIDA	RHODOPHYTA	Compsopogonophyceae	Erythritales	Erythritaceae	<i>Porphyroneura japonicum</i>	7.0	260	7.9	10.7	5000	7.3	20		[91][93]
ARCHEAELPLASTIDA	RHODOPHYTA	Banjiales	Banjiales	Banjiales	<i>Banisia atropurpurea</i>	15	360							[94][95][96]
ARCHEAELPLASTIDA	RHODOPHYTA	Banjiales	Banjiales	Banjiales	<i>Banisia atropurpurea subsp. <i>Brevisegmenta</i></i>	16	75			10000	30000	8	20	
ARCHEAELPLASTIDA	RHODOPHYTA	Banjiales	Banjiales	Banjiales	" <i>Banisia fuscorubra</i> "	15	50							[97]
ARCHEAELPLASTIDA	RHODOPHYTA	Banjiales	Banjiales	Banjiales	<i>Banisia vermicularis?</i>	40	60			30000				[90]
ARCHEAELPLASTIDA	RHODOPHYTA	Banjiales	Banjiales	Banjiales	<i>Dione arcuata</i>	47	80	47	60	15000				[98]
ARCHEAELPLASTIDA	RHODOPHYTA	Banjiales	Banjiales	Banjiales	<i>Minerva aenigmata</i>	13	77	17	40	100000				[98]
ARCHEAELPLASTIDA	RHODOPHYTA	Banjiales	Banjiales	Banjiales	<i>Pseudobanisia kavoleana</i>	29.4	83.3	29.4	49	10000				[99]
ARCHEAELPLASTIDA	RHODOPHYTA	Cladophorales	Cladophorales	Cladophoraceae	<i>Chaetomorpha aerea</i>			87.5	350	150000	70	270		[100]
ARCHEAELPLASTIDA	RHODOPHYTA	Cladophorales	Cladophorales	Cladophoraceae	<i>Chaetomorpha antennina</i>			150	250		300	900		[101]
ARCHEAELPLASTIDA	RHODOPHYTA	Cladophorales	Cladophorales	Cladophoraceae	<i>Chaetomorpha billardieri</i>			220	350					[97]
ARCHEAELPLASTIDA	RHODOPHYTA	Cladophorales	Cladophorales	Cladophoraceae	<i>Chaetomorpha brachycarpa</i>			50	187					[100]
ARCHEAELPLASTIDA	RHODOPHYTA	Cladophorales	Cladophorales	Cladophoraceae	<i>Chaetomorpha californica</i>			320	680	20000	210	840		[100]
ARCHEAELPLASTIDA	RHODOPHYTA	Cladophorales	Cladophorales	Cladophoraceae	<i>Chaetomorpha icca</i>			1500	5000	100000	400000			[97]
ARCHEAELPLASTIDA	RHODOPHYTA	Cladophorales	Cladophorales	Cladophoraceae	<i>Chaetomorpha leucostoma</i>			250	300			250	300	[102]
ARCHEAELPLASTIDA	RHODOPHYTA	Cladophorales	Cladophorales	Cladophoraceae	<i>Chaetomorpha lirum ("C. crassa")</i>			200	750			170	630	[100]
ARCHEAELPLASTIDA	RHODOPHYTA	Cladophorales	Cladophorales	Cladophoraceae	<i>Chaetomorpha meleagrum</i>			400	600	20000	50000			[97]
ARCHEAELPLASTIDA	RHODOPHYTA	Cladophorales	Cladophorales	Cladophoraceae	<i>Chaetomorpha minima</i>			20	42.5					[100]
ARCHEAELPLASTIDA	RHODOPHYTA	Cladophorales	Cladophorales	Cladophoraceae	<i>Chaetomorpha nodosa</i>			32.5	82.5	120000	30	95		[100]
ARCHEAELPLASTIDA	RHODOPHYTA	Cladophorales	Cladophorales	Cladophoraceae	<i>Chaetomorpha philippinensis</i>			9	14	300	15			[103]
ARCHEAELPLASTIDA	RHODOPHYTA	Cladophorales	Cladophorales	Cladophoraceae	<i>Chaetomorpha valida</i>			200	475	150	1000			[104][105][106][107]
ARCHEAELPLASTIDA	RHODOPHYTA	Cladophorales	Cladophorales	Cladophoraceae	<i>Chaetomorpha viellardi</i>			486	534			730	890	[108]
ARCHEAELPLASTIDA	RHODOPHYTA	Cladophorales	Cladophorales	Cladophoraceae	<i>Rhizoclonium hieroglyphicum</i>			10	37			2x	6x	[42]
ARCHEAELPLASTIDA	RHODOPHYTA	Cladophorales	Cladophorales	Cladophoraceae	<i>Rhizoclonium rupinum</i>			20	32					[109]
ARCHEAELPLASTIDA	RHODOPHYTA	Cladophorales	Cladophorales	Cladophoraceae	<i>Rhizoclonium ruppelianum</i>			3.5	10	100	200		21	[110]
ARCHEAELPLASTIDA	RHODOPHYTA	Cladophorales	Cladophorales	Cladophoraceae	<i>Kraftiomema allantoides</i>			6	8	1500	402	10	18	[111]
ARCHEAELPLASTIDA	RHODOPHYTA	Cladophorales	Cladophorales	Cladophoraceae	<i>Gloetoclospis sterilis</i>			4.5	5.7			6.1	13.4	[112]
ARCHEAELPLASTIDA	RHODOPHYTA	Cladophorales	Cladophorales	Cladophoraceae	<i>Hormidiosiphon crenulata</i>			9	25			0.5	2x	[42]
ARCHEAELPLASTIDA	RHODOPHYTA	Cladophorales	Cladophorales	Cladophoraceae	<i>Pearsonella variabilis</i>			22	40			20	90	[113]
ARCHEAELPLASTIDA	RHODOPHYTA	Cladophorales	Cladophorales	Cladophoraceae	<i>Ulothrix aequalis</i>			13	15			18	30	[114]
ARCHEAELPLASTIDA	RHODOPHYTA	Cladophorales	Cladophorales	Cladophoraceae	<i>Ulothrix albicans</i>			7.7	12.6			1/2x	2x	[115]
ARCHEAELPLASTIDA	RHODOPHYTA	Cladophorales	Cladophorales	Cladophoraceae	<i>Ulothrix ciliata</i>			10	21.25			8.2	22	[116][117]
ARCHEAELPLASTIDA	RHODOPHYTA	Cladophorales	Cladophorales	Cladophoraceae	<i>Ulothrix ciliata</i>			9.8	15.4	50000	110000	9	450	[120]
ARCHEAELPLASTIDA	RHODOPHYTA	Cladophorales	Cladophorales	Cladophoraceae	<i>Schizomeria leibnizii</i>	20	54	10	30			10	55	[119][142]
ARCHEAELPLASTIDA	RHODOPHYTA	Cladophorales	Cladophorales	Cladophoraceae	<i>Ulothrix subfalcata</i>			4	5			12	32	[119]
ARCHEAELPLASTIDA	RHODOPHYTA	Cladophorales	Cladophorales	Cladophoraceae	<i>Ulothrix tenerimma</i>			7	10			10	15	[119]
ARCHEAELPLASTIDA	RHODOPHYTA	Cladophorales	Cladophorales	Cladophoraceae	<i>Ulothrix tenerissima</i>			15	20					[102]
ARCHEAELPLASTIDA	RHODOPHYTA	Cladophorales	Cladophorales	Cladophoraceae	<i>Urospora bengalensis</i>			20	40			20	60	[120]
ARCHEAELPLASTIDA	RHODOPHYTA	Cladophorales	Cladophorales	Cladophoraceae	<i>Urospora neglecta</i>			14	180	80000	9	220		[120]
ARCHEAELPLASTIDA	RHODOPHYTA	Cladophorales	Cladophorales	Cladophoraceae	<i>Urospora penicillifloris</i>			9	90	50000				[120]
ARCHEAELPLASTIDA	RHODOPHYTA	Cladophorales	Cladophorales	Cladophoraceae	<i>Urospora warnstorfii</i>			18	1500	110000	9	450		[120]
ARCHEAELPLASTIDA	RHODOPHYTA	Cladophorales	Cladophorales	Cladophoraceae	<i>Oedogonium cinnatum</i>			7	34	50				[122]
ARCHEAELPLASTIDA	RHODOPHYTA	Cladophorales	Cladophorales	Cladophoraceae	<i>Oedogonium peplinense</i>			19	28			21	49	[122]
ARCHEAELPLASTIDA	RHODOPHYTA	Cladophorales	Cladophorales	Cladophoraceae	<i>Oedogonium echinostermum</i>			18	30			2x	5x	[42]
ARCHEAELPLASTIDA	RHODOPHYTA	Cladophorales	Cladophorales	Cladophoraceae	<i>Oedogonium gracilis</i>			20	29			29	76	[122]
ARCHEAELPLASTIDA	RHODOPHYTA	Cladophorales	Cladophorales	Cladophoraceae	<i>Oedogonium grae</i>			24	34	130				[123]
ARCHEAELPLASTIDA	RHODOPHYTA	Cladophorales	Cladophorales	Cladophoraceae	<i>Oedogonium hastanense</i>			15	25					[102]
ARCHEAELPLASTIDA	RHODOPHYTA	Cladophorales	Cladophorales	Cladophoraceae	<i>Oedogonium itzahonii</i>			5	11			2x	6x	[42]
ARCHEAELPLASTIDA	RHODOPHYTA	Cladophorales	Cladophorales	Cladophoraceae	<i>Oedogonium laeve</i>									

Appendix II - Supplementary Table 1. Cont.

ARCHAELPLASTIDA	CHLOROPHYTA	Chlorophyceae	Sphaeropleales	Microsporaceae	<i>Microspora williana</i>	10	15	10	20	[102]
ARCHAELPLASTIDA	CHLOROPHYTA	Chlorophyceae	Sphaeropleales	Microsporaceae	<i>Microspora wittrockii</i>	14	17	11	21	[132]
ARCHAELPLASTIDA	CHLOROPHYTA	Chlorophyceae	Sphaeropleales	Microsporaceae	<i>Microspora zhoui</i>	8	11	6	20	[132]
ARCHAELPLASTIDA	CHLOROPHYTA	Chlorophyceae	Sphaeropleales	Cylircapsaceae	<i>Cylircapsa geminella</i>	13	28.7	14	55	[133][149][117]
ARCHAELPLASTIDA	CHLOROPHYTA	Trebouxiophyceae	Trebouxiophyceae	Klebsomidiaceae	<i>Klebsiella inuita</i>	2.7	3.8	3x	8x	[134]
ARCHAELPLASTIDA	CHLOROPHYTA	Trebouxiophyceae	Prasiolales	Prasiolaceae	<i>Rosenvinella polvizia</i>	12	40			[97]
ARCHAELPLASTIDA	CHLOROPHYTA	Trebouxiophyceae	Prasiolales	Prasiolaceae	<i>Rosenvinella tasmanica</i>	20	26			[135]
ARCHAELPLASTIDA	CHLOROPHYTA	Trebouxiophyceae	Chlorellales	Chlorellaceae	<i>Gemmella ellipsoidea</i>	10	15	4.2	7.3	[42]
ARCHAELPLASTIDA	CHLOROPHYTA	Trebouxiophyceae	Chlorellales	Chlorellaceae	<i>Gemmella interrupta</i>	15	30	6	9	[42]
ARCHAELPLASTIDA	CHLOROPHYTA	Trebouxiophyceae	Chlorellales	Chlorellaceae	<i>Gemmella minor</i>	6	15	2	8	[42]
ARCHAELPLASTIDA	CHLOROPHYTA	Trebouxiophyceae	Chlorellales	Chlorellaceae	<i>Gemmella planonica</i>	20	50	4	7	5000
ARCHAELPLASTIDA	CHLOROPHYTA	Trebouxiophyceae	Chlorellales	Chlorellaceae	<i>Gemmella ordinata</i>	15	20	5	9	5
ARCHAELPLASTIDA	CHLOROPHYTA	Trebouxiophyceae	Chlorellales	Chlorellaceae	<i>Gloeoella subconstricta</i>					12
ARCHAELPLASTIDA	CHLOROPHYTA	Klebsomidiophyceae	Klebsomidiates	Klebsomidiaceae	<i>Klebsomidium acidophilum</i>	6	8			[138]
ARCHAELPLASTIDA	CHLOROPHYTA	Klebsomidiophyceae	Klebsomidiates	Klebsomidiaceae	<i>Klebsomidium kuetzingianum</i>	3	5			[137]
ARCHAELPLASTIDA	CHLOROPHYTA	Klebsomidiophyceae	Klebsomidiates	Klebsomidiaceae	<i>Klebsomidium elegans</i>	11	15			[137]
ARCHAELPLASTIDA	CHLOROPHYTA	Klebsomidiophyceae	Klebsomidiates	Klebsomidiaceae	<i>Klebsomidium flaccidum</i>	6	8			[138]
ARCHAELPLASTIDA	CHLOROPHYTA	Klebsomidiophyceae	Klebsomidiates	Klebsomidiaceae	<i>Klebsomidium fulvans</i>	7	8.5			[138]
ARCHAELPLASTIDA	CHLOROPHYTA	Klebsomidiophyceae	Klebsomidiates	Klebsomidiaceae	<i>Klebsomidium mucosum</i>	15	20			[138]
ARCHAELPLASTIDA	CHLOROPHYTA	Klebsomidiophyceae	Klebsomidiates	Klebsomidiaceae	<i>Klebsomidium nitens</i>	6.5	6.5			[138]
ARCHAELPLASTIDA	CHLOROPHYTA	Klebsomidiophyceae	Klebsomidiates	Klebsomidiaceae	<i>Klebsomidium rivulare</i>	5	11			[138]
ARCHAELPLASTIDA	CHLOROPHYTA	Klebsomidiophyceae	Klebsomidiates	Klebsomidiaceae	<i>Klebsomidium sp.</i>	6.5	9.84			[139]
ARCHAELPLASTIDA	CHLOROPHYTA	Klebsomidiophyceae	Klebsomidiates	Klebsomidiaceae	<i>Klebsomidium sp.</i>	4.75	4920			[139]
ARCHAELPLASTIDA	CHLOROPHYTA	Klebsomidiophyceae	Klebsomidiates	Klebsomidiaceae	<i>Klebsomidium sp.</i>	5.25	3150			[139]
ARCHAELPLASTIDA	CHLOROPHYTA	Klebsomidiophyceae	Klebsomidiates	Klebsomidiaceae	<i>Klebsomidium sp.</i>	5.5	625			[139]
ARCHAELPLASTIDA	CHLOROPHYTA	Klebsomidiophyceae	Klebsomidiates	Klebsomidiaceae	<i>Klebsomidium sp.</i>	5.5	665			[139]
ARCHAELPLASTIDA	CHLOROPHYTA	Klebsomidiophyceae	Klebsomidiates	Klebsomidiaceae	<i>Klebsomidium sp.</i>	8	11900			[139]
ARCHAELPLASTIDA	CHLOROPHYTA	Zygnematophyceae	Zygnematales	Zygnemataceae	<i>Mougeotia quanahacibensis</i>	4	7			[42]
ARCHAELPLASTIDA	CHLOROPHYTA	Zygnematophyceae	Zygnematales	Zygnemataceae	<i>Mougeotia abnormis</i>	43	53			[127]
ARCHAELPLASTIDA	CHLOROPHYTA	Zygnematophyceae	Zygnematales	Zygnemataceae	<i>Mougeotia aculeata</i>	25	29			[140]
ARCHAELPLASTIDA	CHLOROPHYTA	Zygnematophyceae	Zygnematales	Zygnemataceae	<i>Mougeotia angulensis</i>	9	13			[140]
ARCHAELPLASTIDA	CHLOROPHYTA	Zygnematophyceae	Zygnematales	Zygnemataceae	<i>Mougeotia calcarea</i>	18	23			[140]
ARCHAELPLASTIDA	CHLOROPHYTA	Zygnematophyceae	Zygnematales	Zygnemataceae	<i>Mougeotia capucina</i>	12.5	14			[140]
ARCHAELPLASTIDA	CHLOROPHYTA	Zygnematophyceae	Zygnematales	Zygnemataceae	<i>Mougeotia disjuncta</i>	26	35.5			[140]
ARCHAELPLASTIDA	CHLOROPHYTA	Zygnematophyceae	Zygnematales	Zygnemataceae	<i>Mougeotia hupenensis</i>	27	30			[140]
ARCHAELPLASTIDA	CHLOROPHYTA	Zygnematophyceae	Zygnematales	Zygnemataceae	<i>Mougeotia laevis</i>	25	31			[42]
ARCHAELPLASTIDA	CHLOROPHYTA	Zygnematophyceae	Zygnematales	Zygnemataceae	<i>Mougeotia latifolia</i>	23	30			[140]
ARCHAELPLASTIDA	CHLOROPHYTA	Zygnematophyceae	Zygnematales	Zygnemataceae	<i>Mougeotia mesocyclista</i>	11	16			[140]
ARCHAELPLASTIDA	CHLOROPHYTA	Zygnematophyceae	Zygnematales	Zygnemataceae	<i>Mougeotia mesocarpiana</i>	16	17.5			[141]
ARCHAELPLASTIDA	CHLOROPHYTA	Zygnematophyceae	Zygnematales	Zygnemataceae	<i>Mougeotia nummuloides</i>	10	12			[140]
ARCHAELPLASTIDA	CHLOROPHYTA	Zygnematophyceae	Zygnematales	Zygnemataceae	<i>Mougeotia oblongata</i>	19	22			[140]
ARCHAELPLASTIDA	CHLOROPHYTA	Zygnematophyceae	Zygnematales	Zygnemataceae	<i>Mougeotia oedopionoides</i>	16	18			[140]
ARCHAELPLASTIDA	CHLOROPHYTA	Zygnematophyceae	Zygnematales	Zygnemataceae	<i>Mougeotia oeloussensis</i>	25	30			[140]
ARCHAELPLASTIDA	CHLOROPHYTA	Zygnematophyceae	Zygnematales	Zygnemataceae	<i>Mougeotia producta</i>	7	8			[140]
ARCHAELPLASTIDA	CHLOROPHYTA	Zygnematophyceae	Zygnematales	Zygnemataceae	<i>Mougeotia pseudo-oeloussensis</i>	27	29			[140]
ARCHAELPLASTIDA	CHLOROPHYTA	Zygnematophyceae	Zygnematales	Zygnemataceae	<i>Mougeotia punctata</i>	8	12			[140]
ARCHAELPLASTIDA	CHLOROPHYTA	Zygnematophyceae	Zygnematales	Zygnemataceae	<i>Mougeotia subhastata</i>	25	33			220
ARCHAELPLASTIDA	CHLOROPHYTA	Zygnematophyceae	Zygnematales	Zygnemataceae	<i>Mougeotia subspicata</i>	5	6.5			[140]
ARCHAELPLASTIDA	CHLOROPHYTA	Zygnematophyceae	Zygnematales	Zygnemataceae	<i>Mougeotia transseai</i>	14	17			[140]
ARCHAELPLASTIDA	CHLOROPHYTA	Zygnematophyceae	Zygnematales	Zygnemataceae	<i>Mougeotia trapeziformis</i>	4.5	5.5			41
ARCHAELPLASTIDA	CHLOROPHYTA	Zygnematophyceae	Zygnematales	Zygnemataceae	<i>Mougeotia tumidula</i>	11	14			[140]
ARCHAELPLASTIDA	CHLOROPHYTA	Zygnematophyceae	Zygnematales	Zygnemataceae	<i>Mougeotia varana</i>	25	27			[140]
ARCHAELPLASTIDA	CHLOROPHYTA	Zygnematophyceae	Zygnematales	Zygnemataceae	<i>Mougeotia viscosa</i>	14	18			[140]
ARCHAELPLASTIDA	CHLOROPHYTA	Zygnematophyceae	Zygnematales	Zygnemataceae	<i>Mougeotia violacea</i>	6	9			[140]
ARCHAELPLASTIDA	CHLOROPHYTA	Zygnematophyceae	Zygnematales	Zygnemataceae	<i>Spirogyra australica</i>	27	30			[42]
ARCHAELPLASTIDA	CHLOROPHYTA	Zygnematophyceae	Zygnematales	Zygnemataceae	<i>Spirogyra bellis</i>	65	80			[42]
ARCHAELPLASTIDA	CHLOROPHYTA	Zygnematophyceae	Zygnematales	Zygnemataceae	<i>Spirogyra boreana</i>	30	35			[42]
ARCHAELPLASTIDA	CHLOROPHYTA	Zygnematophyceae	Zygnematales	Zygnemataceae	<i>Spirogyra brunnescens</i>	51	60			[42]
ARCHAELPLASTIDA	CHLOROPHYTA	Zygnematophyceae	Zygnematales	Zygnemataceae	<i>Spirogyra cateniformis</i>	24.4	33			[42]
ARCHAELPLASTIDA	CHLOROPHYTA	Zygnematophyceae	Zygnematales	Zygnemataceae	<i>Spirogyra elongata</i>	51.2	58.5			[143]
ARCHAELPLASTIDA	CHLOROPHYTA	Zygnematophyceae	Zygnematales	Zygnemataceae	<i>Spirogyra flosca</i>	21	38			[143]
ARCHAELPLASTIDA	CHLOROPHYTA	Zygnematophyceae	Zygnematales	Zygnemataceae	<i>Spirogyra emilianensis</i>	50	53			[145][42]
ARCHAELPLASTIDA	CHLOROPHYTA	Zygnematophyceae	Zygnematales	Zygnemataceae	<i>Spirogyra fenicis</i>	15.5	18			[146]
ARCHAELPLASTIDA	CHLOROPHYTA	Zygnematophyceae	Zygnematales	Zygnemataceae	<i>Spirogyra fluviatilis</i>	30	56			[127]
ARCHAELPLASTIDA	CHLOROPHYTA	Zygnematophyceae	Zygnematales	Zygnemataceae	<i>Spirogyra hassallii</i>	24	35			[145]
ARCHAELPLASTIDA	CHLOROPHYTA	Zygnematophyceae	Zygnematales	Zygnemataceae	<i>Spirogyra hirsutula</i>	45	65			[145]
ARCHAELPLASTIDA	CHLOROPHYTA	Zygnematophyceae	Zygnematales	Zygnemataceae	<i>Spirogyra inflata</i>	17	19			[145]
ARCHAELPLASTIDA	CHLOROPHYTA	Zygnematophyceae	Zygnematales	Zygnemataceae	<i>Spirogyra juliana</i>	52	64			[42]
ARCHAELPLASTIDA	CHLOROPHYTA	Zygnematophyceae	Zygnematales	Zygnemataceae	<i>Spirogyra koreana</i>	51.2	56.9			[143]
ARCHAELPLASTIDA	CHLOROPHYTA	Zygnematophyceae	Zygnematales	Zygnemataceae	<i>Spirogyra laevis</i>	50	55			[146]
ARCHAELPLASTIDA	CHLOROPHYTA	Zygnematophyceae	Zygnematales	Zygnemataceae	<i>Spirogyra lunalis</i>	83.2	89.6			[143]
ARCHAELPLASTIDA	CHLOROPHYTA	Zygnematophyceae	Zygnematales	Zygnemataceae	<i>Spirogyra kusamoensis</i>	15	16			[42]
ARCHAELPLASTIDA	CHLOROPHYTA	Zygnematophyceae	Zygnematales	Zygnemataceae	<i>Spirogyra miquelianum</i>	35	41			[42]
ARCHAELPLASTIDA	CHLOROPHYTA	Zygnematophyceae	Zygnematales	Zygnemataceae	<i>Spirogyra marilandica</i>	50	100			[145][42]
ARCHAELPLASTIDA	CHLOROPHYTA	Zygnematophyceae	Zygnematales	Zygnemataceae	<i>Spirogyra minivillosa</i>	20	30			[102]
ARCHAELPLASTIDA	CHLOROPHYTA	Zygnematophyceae	Zygnematales	Zygnemataceae	<i>Spirogyra maxima</i>	120	150			[147]
ARCHAELPLASTIDA	CHLOROPHYTA	Zygnematophyceae	Zygnematales	Zygnemataceae	<i>Spirogyra minutiflora</i>	13	16			[127]
ARCHAELPLASTIDA	CHLOROPHYTA	Zygnematophyceae	Zygnematales	Zygnemataceae	<i>Spirogyra multiconiata</i>	23	32			[147]
ARCHAELPLASTIDA	CHLOROPHYTA	Zygnematophyceae	Zygnematales	Zygnemataceae	<i>Spirogyra neglecta</i>	55	68			[145]
ARCHAELPLASTIDA	CHLOROPHYTA	Zygnematophyceae	Zygnematales	Zygnemataceae	<i>Spirogyra setiformis</i>	90	120			[102]
ARCHAELPLASTIDA	CHLOROPHYTA	Zygnematophyceae	Zygnematales	Zygnemataceae	<i>Spirogyra sphaerulata</i>	33	35			[42]
ARCHAELPLASTIDA	CHLOROPHYTA	Zygnematophyceae	Zygnematales	Zygnemataceae	<i>Spirogyra paschiana</i>	17	20			[146]
ARCHAELPLASTIDA	CHLOROPHYTA	Zygnematophyceae	Zygnematales	Zygnemataceae	<i>Spirogyra parvula</i>	20	24			[42]
ARCHAELPLASTIDA	CHLOROPHYTA	Zygnematophyceae	Zygnematales	Zygnemataceae	<i>Spirogyra plena</i>	35	45			[142]
ARCHAELPLASTIDA	CHLOROPHYTA	Zygnematophyceae	Zygnematales	Zygnemataceae	<i>Spirogyra portulaca</i>	39	55			[145]
ARCHAELPLASTIDA	CHLOROPHYTA	Zygnematophyceae	Zygnematales	Zygnemataceae	<i>Spirogyra recta</i>	29	42			[142]
ARCHAELPLASTIDA	CHLOROPHYTA	Zygnematophyceae	Zygnematales	Zygnemataceae	<i>Spirogyra rodens</i>	40	85			[147]
ARCHAELPLASTIDA	CHLOROPHYTA	Zygnematophyceae	Zygnematales	Zygnemataceae	<i>Spirogyra rodenscula</i>	32	38			[42]
ARCHAELPLASTIDA	CHLOROPHYTA	Zygnematophyceae	Zygnematales	Zygnemataceae	<i>Spirogyra seminervata</i>	25	46			[145]
ARCHAELPLASTIDA	CHLOROPHYTA	Zygnematophyceae	Zygnematales	Zygnemataceae	<i>Spirogyra setiformis</i>	90	120			[102]
ARCHAELPLASTIDA	CHLOROPHYTA	Zygnematophyceae	Zygnematales	Zygnemataceae	<i>Spirogyra silesiaca</i>	43	52			[144]
ARCHAELPLASTIDA	CHLOROPHYTA	Zygnematophyceae	Zygnematales	Zygnemataceae	<i>Spirogyra sphaerulata</i>	18	23			[42]
ARCHAELPLASTIDA	CHLOROPHYTA	Zygnematophyceae	Zygnematales	Zygnemataceae	<i>Spirogyra varians</i>	37	41			[144]
ARCHAELPLASTIDA	CHLOROPHYTA	Zygnematophyceae	Zygnematales	Zygnemataceae	<i>Spirogyra variana</i>	35	40			[42]
ARCHAELPLASTIDA	CHLOROPHYTA	Zygnematophyceae	Zygnematales	Zygnemataceae	<i>Spirogyra velata</i>	29	44			[145]
ARCHAELPLASTIDA	CHLOROPHYTA	Zygnematophyceae	Zygnematales	Zygnemataceae	<i>Spirogyra weberi</i>	20	25			[146]
ARCHAELPLASTIDA	CHLOROPHYTA	Zygnematophyceae	Zygnematales	Zygnemataceae	<i>Spirogyra vuin</i>	45	55			[144]
ARCHAELPLASTIDA	CHLOROPHYTA	Zygnematophyceae	Zygnematales	Zygnemataceae	<i>Spiromeria apianosporum</i>	24.1	33.2			[42]
ARCHAELPLASTIDA	CHLOROPHYTA	Zygnematophyceae	Zygnematales	Zygnemataceae	<i>Spiromeria californicum</i>	23	29			[148]
ARCHAELPLASTIDA	CHLOROPHYTA	Zygnematophyceae	Zygnematales	Zygnemataceae	<i>Spiromeria collisianum</i>	26	28			[148]
ARCHAELPLASTIDA	CHLOROPHYTA	Zygnematophyceae	Zygnematales	Zygnemataceae	<i>Spiromeria cruciatum</i>	18	25			[102]
ARCHAELPLASTIDA	CHLOROPHYTA	Zygnematophyceae	Zygnematales	Zygnemataceae	<i>Spiromeria obtuseum</i>	32	39			[149]
ARCHAELPLASTIDA	CHLOROPHYTA	Zygnematophyceae	Zygnematales							

## Appendix II - Supplementary Table 1. Cont.

- | Nº | Reference  |
|----|--|
| 1  | Kalantra KM, Huston SL, Nelson DC. 2004 Novel, Attached, Sulfur-Oxidizing Bacteria at Shallow Hydrothermal Vents Possess Vacuoles Not Involved in Respiratory Nitrate Accumulation. <i>Appl. Environ. Microbiol.</i> 70, 7487–7496. (doi:10.1128/AEM.70.12.7487)   |
| 2  | Aranda CP, Valenzuela C, Matamala Y, Godoy FA, Aranda N. 2015 Sulphur-cycling bacteria and ciliated protozoans in a Beggiatoaceae mat covering organically enriched sediments beneath a salmon farm in a southern Chilean fjord. <i>Mar. Pollut. Bull.</i> 100, 270–278. (doi:10.1016/j.marpolbul.2015.08.040)       |
| 3  | Jannasch HW, Nelson DC, Wirsén CO. 1989 Massive natural occurrence of unusually large bacteria ( <i>Beggiatoa</i> sp.) at a hydrothermal deep-sea vent site. <i>Nature</i> 342, 834–836. (doi:10.1038/340301a0)  |
| 4  | Larkin J, Henk MC, Aharon P. 1994 Beggiatoa in microbial mats at hydrocarbon vents in the Gulf of Mexico and Warm Mineral Springs, Florida. <i>Geo-Marine Lett.</i> 14, 97–103. (doi:10.1007/BF01203720)   |
| 5  | Dunker R, Rey H, Jørgensen BB. 2010 Temperature regulation of gliding motility in filamentous sulfur bacteria, <i>Beggiatoa</i> spp. <i>FEMS Microbiol. Ecol.</i> 73, no-no. (doi:10.1111/j.1574-6941.2010.00887.x)  |
| 6  | Sweerts J-PRA, Beer D De, Nielsen LP, Verdouw H, den Heuvel JC Van, Cohen Y, Cappenberg TE. 1990 Denitrification by sulphur oxidizing <i>Beggiatoa</i> spp. mats on freshwater sediments. <i>Nature</i> 344, 762–763. (doi:10.1038/344762a0)   |
| 7  | Gundersen JK, Jørgensen BB, Larsen E, Jannasch HW. 1992 Mats of giant sulphur bacteria on deep-sea sediments due to fluctuating hydrothermal flow. <i>Nature</i> 360, 454–456. (doi:10.1038/360454a0)  |
| 8  | Teske A, Sojiri ML, Nielsen LP, Jannasch HW. 1999 Phylogenetic Relationships of a Large Marine <i>Beggiatoa</i> . <i>Syst. Appl. Microbiol.</i> 22, 39–44. (doi:10.1016/S0723-2020(99)80026-5)   |
| 9  | Wirsén CO, Jannasch HW, Molneux SJ. 1992 Results of studies concerning microbiota. In: Chemosynthetic Ecosystems Study Interim Report, Appendix A (eds IR MacDonald, W Schroeder), pp. A1–A14. New Orleans, US: US Dept. Interior, Minerals Management Service, Gulf of Mexico OCS Region.                           |
| 10 | Sassen R, Roberts HH, Aharon P, Larkin J, Chinne EW, Carney R. 1993 Chemosynthetic bacterial mats at cold hydrocarbon seeps, Gulf of Mexico continental slope. <i>Org. Geochem.</i> 20, 77–89. (doi:10.1016/0146-6380(93)90083-N)  |
| 11 | Nelson DC, Wirsén CO, Jannasch HW. 1989 Characterization of Large, Autotrophic <i>Beggiatoa</i> spp. Abundant at Hydrothermal Vents of the Guaymas Basin. <i>Appl. Environ. Microbiol.</i> 55, 2909–2917. (doi:10.1128/AEM.55.11.2909-2917.1989)   |
| 12 | McHatton SC, Barry JP, Jannasch HW, Nelson DC. 1996 High Nitrate Concentrations in Vacuolate, Autotrophic Marine <i>Beggiatoa</i> spp. <i>Appl. Environ. Microbiol.</i> 62, 954–958. (doi:10.1128/AEM.62.3.954-958.1996)   |
| 13 | Jørgensen BB. 1977 Distribution of colorless sulfur bacteria ( <i>Beggiatoa</i> spp.) in a coastal marine sediment. <i>Mar. Biol.</i> 41, 19–28. (doi:10.1007/BF00390577)  |
| 14 | Nikolaus R, Ammerman J, MacDonald I. 2003 Distinct pigmentation and trophic modes in <i>Beggiatoa</i> from hydrocarbon seeps in the Gulf of Mexico. <i>Aquat. Microb. Ecol.</i> 32, 85–93. (doi:10.3354/ame032085)   |
| 15 | Möller MM, Nielsen LP, Jørgensen BB. 1985 Oxygen Responses and Mat Formation by <i>Beggiatoa</i> spp. <i>Appl. Environ. Microbiol.</i> 50, 373–382.  |
| 16 | Ahmad A, Barry JP, Nelson DC. 1999 Phylogenetic affinity of a wide, vacuolate, nitrate-accumulating <i>Beggiatoa</i> sp. from Monterey Canyon, California, with <i>Thioploca</i> spp. <i>Appl. Environ. Microbiol.</i> 65, 270–277. (doi:0099-2240/99/\$04.00+0)   |
| 17 | Mussmann M, Schulz HN, Strommann B, Kjaer T, Nielsen LP, Rossello-Mora RA, Amann RI, Jørgensen BB. 2003 Phylogeny and distribution of nitrate-storing <i>Beggiatoa</i> spp. in coastal marine sediments. <i>Environ. Microbiol.</i> 5, 523–533. (doi:10.1046/j.1462-2920.2003.00440.x)                               |
| 18 | Dunker R, Rey H, Kamp A, Jørgensen BB. 2011 Motility patterns of filamentous sulfur bacteria, <i>Beggiatoa</i> spp. <i>FEMS Microbiol. Ecol.</i> 77, 176–185. (doi:10.1111/j.1574-6941.2011.01099.x)   |
| 19 | Macalady JL, Dattagupta S, Schaperdoh I, Jones DS, Druschel GK, Eastman D. 2008 Niche differentiation among sulfur-oxidizing bacterial populations in cave waters. <i>ISME J.</i> 2, 590–601. (doi:10.1038/ismej.2008.25)  |
| 20 | Jørgensen BB, Dunker R, Rey H. 2010 Filamentous sulfur bacteria, <i>Beggiatoa</i> spp., in arctic marine sediments (Svalbard, 79°N). <i>FEMS Microbiol. Ecol.</i> 73, no-no. (doi:10.1111/j.1574-6941.2010.00918.x)  |
| 21 | Kojima H, Fukui M. 2003 Phylogenetic analysis of <i>Beggiatoa</i> spp. from organic rich sediment of Tokyo Bay, Japan. <i>Water Res.</i> 37, 3216–3223. (doi:10.1016/S0043-1354(03)00206-9)  |
| 22 | Hinck S, Neu TR, Lavik G, Mussmann M, De Beer D, Jonkers HM. 2007 Physiological adaptation of a nitrate-storing <i>Beggiatoa</i> sp. to diel cycling in a phototrophic hypersaline mat. <i>Appl. Environ. Microbiol.</i> 73, 7013–7022. (doi:10.1128/AEM.00548-07)   |
| 23 | Salman-Carvalho F, Vadee E, Joye SB, Teske A. 2016 How clonal is clonal? Genome plasticity across multicellular segments of a ‘ <i>candidatus marithrix</i> sp.’ filament from sulfidic, briny seafloor sediments in the Gulf of Mexico. <i>Front. Microbiol.</i> 7, 1–14. (doi:10.3389/fmicb.2016.01173)            |
| 24 | Grönke S, Felden J, Lütschglaub A, Girecht AC, De Beer D, Wenzhöfer F, Boetius A. 2011 Niche differentiation among mat-forming, sulfide-oxidizing bacteria at cold seeps of the Nile Deep Sea Fan (Eastern Mediterranean Sea). <i>Geobiology</i> 9, 330–348. (doi:10.1111/j.1472-4669.2011.00281.x)                  |
| 25 | Jean MRN, Gonzalez-Rizzo S, Gaufré-Autelin P, Lengger SK, Schouten S, Gros O. 2015 Two new <i>Beggiatoa</i> species inhabiting marine mangrove sediments in the Caribbean. <i>PLoS One</i> 10, 1–16. (doi:10.1371/journal.pone.0171832)  |
| 26 | Schulz HN, Jørgensen BB, Fossing HA, Ramsing NB. 1996 Community structure of filamentous, sheath-building sulfur bacteria, <i>Thioploca</i> spp., off the coast of Chile. <i>Appl. Environ. Microbiol.</i> 62, 1855–1862.  |
| 27 | Zemskaya TI, Chernysh SM, Dul'Tseva NM, Sergeeva VN, Pogodaeva TB V. 2009 Colorless sulfur bacteria <i>Thioploca</i> from different sites in Lake Baikal. <i>Microbiology</i> 78, 117–124. (doi:10.1134/S0026261709010159)   |
| 28 | Nemoto F, Kojima H, Ohtaka A, Fukui M. 2012 Filamentous sulfur-oxidizing bacteria of the genus <i>Thioploca</i> from Lake Tonle Sap in Cambodia. <i>Aquat. Microb. Ecol.</i> 66, 295–300. (doi:10.3354/ame01578)   |
| 29 | Kojima H, Koizumi Y, Fukui M. 2006 Community structure of bacteria associated with sheaths of freshwater and brackish <i>Thioploca</i> species. <i>Microb. Ecol.</i> 52, 765–773. (doi:10.1007/s00248-006-9127-8)  |
| 30 | Schmaljohann R, Drews M, Walter S, Linke P, von Rad U, Imhoff J. 2001 Oxygen-minimum zone sediments in the northeastern Arabian Sea off Pakistan: a habitat for the bacterium <i>Thioploca</i> . <i>Mar. Ecol. Prog. Ser.</i> 211, 27–42. (doi:10.3354/meps211027)   |
| 31 | Dermott R, Legner M. 2002 Dense mat-forming bacterium <i>Thioploca ingrica</i> (Beggiatoaceae) in eastern Lake Ontario: Implications to the benthic food web. <i>J. Great Lakes Res.</i> 28, 688–697. (doi:10.1016/S0380-1330(02)70614-X)  |
| 32 | Danovaro R et al. 2017 A submarine volcano eruption leads to a novel microbial habitat. <i>Nat. Ecol. Evol.</i> 1, 0144. (doi:10.1038/s41559-017-0144)   |
| 33 | Fossing H et al. 1995 Concentration and transport of nitrate by the mat-forming sulphur bacterium <i>Thioploca</i> . <i>Nature</i> 374, 713–715. (doi:10.1038/374713a0)  |
| 34 | Maier S, Gallardo VA. 1984 <i>Thioploca araucae</i> sp. nov. and <i>Thioploca chilensis</i> sp. nov. <i>Int. J. Syst. Bacteriol.</i> 34, 414–418. (doi:10.1099/00207113-34-4-414)  |
| 35 | Gallardo VA. 1977 Large benthic microbial communities in sulphide biota under Peru–Chile Subsurface Countercurrent. <i>Nature</i> 268, 331–332. (doi:10.1038/268331a0)   |
| 36 | Larkin JM, Strohl WR. 1983 <i>Beggiatoa</i> , <i>Thiotricha</i> , and <i>Thioploca</i> . <i>Annu. Rev. Microbiol.</i> 37, 341–367. (doi:10.1146/annurev.mi.37.100183.002013)   |
| 37 | Nishino M, Fukui M, Nakajima T. 1998 Dense mats of <i>thioploca</i> , gliding filamentous sulfur-oxidizing bacteria in lake Biwa, central Japan. <i>Water Res.</i> 32, 953–957. (doi:10.1016/S0043-1354(97)00227-3)  |
| 38 | Jørgensen BB, Gallardo VA. 1999 <i>Thioploca</i> spp.: filamentous sulfur bacteria with nitrate vacuoles. <i>FEMS Microbiol. Ecol.</i> 28, 301–313. (doi:10.1016/S0168-6496(98)00122-6)  |
| 39 | Brock TD. 1974 Genus II. <i>Thiotricha</i> Winogradsky. In: Bergey's manual of determinative bacteriology (eds RE Buchanan, NC Gibbons), p. 119. The Williams & Wilkins Co. Baltimore.   |
| 40 | Kalantra KM, Nelson DC. 2010 Vacuolate-attached filaments: Highly productive <i>Ridgeia piscesea</i> epibionts at the Juan de Fuca hydrothermal vents. <i>Mar. Biol.</i> 157, 791–800. (doi:10.1007/s00227-009-1362-3)   |
| 41 | Guiry MD, Guiry GM. 2019 AlgaeBase. World-wide Electron. Publ. Natl. Univ. Ireland. Galw. See <a href="http://www.algaebase.org">http://www.algaebase.org</a>  |
| 42 | Stanchev R, Fuller C, Sheath RG. 2013 Soft-Bodied Stream Algae of California. See <a href="http://dbmuseblade.colorado.edu/DiatomTwobssac_site/">http://dbmuseblade.colorado.edu/DiatomTwobssac_site/</a> (accessed on 20 August 2019)   |
| 43 | Komárek J, Anagnostidis K. 2005 Süßwasserflora von Mitteleuropa: Cyanoprokaryota: 2. Teil/2nd Part: Oscillatoriaceae. München: Elsevier Spektrum Akademischer Verlag.  |
| 44 | Struncky O, Bohumicka M, Johansen JR, Capkova K, Raabova L, Dvorak P, Komárek J. 2017 A revision of the genus <i>Geltterinema</i> and a description of the genus <i>Anagnostidinema</i> gen. nov. (Oscillatoriophycidae, Cyanobactera). <i>Fottea</i> 17, 114–126. (doi:10.5507/fot.2016.025)                        |
| 45 | Desikachary TV. 1959 Cyanophyta. New Delhi: Indian Council of Agricultural Research  |
| 46 | Struncky O, Komárek J, Šmrádka J. 2014 Kamptoneia ( <i>Microcoleaceae</i> , Cyanobacteria), a new genus derived from the polyphyletic <i>Phormidium</i> on the basis of combined molecular and cytomorphological markers. <i>Preslia</i> 86, 193–207   |
| 47 | Santosh MCM, Barupur GK. 2017 Floristic Composition and Periodical Analysis of Cyanobacteria of Some Freshwater Aquatic Bodies of Bikaner (Rajasthan), India. <i>J. Algal Biomass Util.</i> 8, 30–33.  |
| 48 | Wu H, Gao K, Villafane VE, Watanabe T, Helbling EW. 2005 Effects of Solar UV Radiation on Morphology and Photosynthesis of Filamentous Cyanobacterium <i>Arthrospira platensis</i> . <i>Appl. Environ. Microbiol.</i> 71, 5004–5013. (doi:10.1128/AEM.71.9.5004-5013.2005)   |
| 49 | Bhakta S, Das SK, Adhikary SP. 2016 Algal Diversity in Hot Springs of Odisha. <i>Nelumbo</i> 58, 157–173. (doi:10.20324/nelumbo/v58/2016/105914)   |
| 50 | Auricchio MR, Lambrecht RW, Peres CK. 2019 Stream macroalgae flora from Paraiaba River Basin, Brazil: Reducing Wallacean shortfall. <i>Biota Neotrop.</i> 19, 1–19. (doi:10.1590/1676-0611-BN-2018-0685)   |
| 51 | John DM, Whittton BA, Brook AJ. 2002 The Freshwater Algal Flora of the British Isles: An Identification Guide to Freshwater and Terrestrial Algae. Cambridge, UK: Cambridge University Press.  |
| 52 | Sikdar J, Keshri JP. 2014 The Genus Oscillatoria Vaucher (Oscillatoriaceae, Cyanoprokaryota) in West Bengal, India. <i>Int. J. Curr. Res. Rev.</i> 6, 47–59.   |
| 53 | Komárek J et al. 2013 Polyphasic evaluation of <i>Limnorphis robusta</i> , a water-bloom forming cyanobacterium from Lake Atitlán, Guatemala, with a description of <i>Limnorphis</i> gen. nov. <i>Fottea</i> 13, 39–52. (doi:10.5507/fot.2013.004)  |
| 54 | Dennison WC, O'Neil JM. 1999 Blooms of the cyanobacterium <i>Lyngbya majuscula</i> in coastal waters of Queensland, Australia. In: <i>Marine Cyanobacteria - Bulletin de l'Institut océanographique</i> , Monaco, n° spécial 19, pp. 501–506   |
| 55 | Ulçay S, Taşkin E, Kurt O, Özürk M. 2015 Marine benthic Cyanobacteria in Northern Cyprus (Eastern Mediterranean Sea). <i>Turk. J. Botany</i> 39, 173–188. (doi:10.3906/bot-1311-52)  |
| 56 | Roy S, Keshri JP. 2014 On the Occurrence of the Members of <i>Nostocales</i> (Cyanophyta) from Burdwan , West Bengal , India. <i>Int. J. Life Sci. Biotechnol. Pharma Res.</i> 3, 126–149  |
| 57 | Turkey J, Adhikary SP. 2006 Blue green algae in the biological soil crusts of different regions of India. <i>Feddes Report.</i> 117, 280–306. (doi:10.1002/fdr.200511095)  |
| 58 | Vitányé I, Kasperoviciene J. 2018 Phylogenetic diversity of cyanobacteria from Lithuania. <i>Biosyst. Bot.</i> 21, 99–118. (doi:10.1515/botlit-2015-0013)  |
| 59 | Datta S, Keshri JP. 2014 Soil and sub aerial blue green algae (Cyanoprokaryotes) of Burdwan, West Bengal, India. <i>Vegetos</i> 27, 112–126. (doi:10.5958/2229-4473.2014.00021.4)  |
| 60 | Simic SB, Keshri J, Đorđević NB. 2014 The Confirmation of the genus <i>Glaucospirula</i> (Cyanobacteria) and the Occurrence of <i>Glaucospirula laxissima</i> (G. S. West) comb. nova in Serbia. <i>Cryptogam. Algol.</i> 35, 259–267. (doi:10.7872/crya.v35.iss3.2014.259)  |
| 61 | Turicchia S, Ventura S, Komárek J, Komárek J. 2009 Taxonomic evaluation of cyanobacterial microflora from alkaline marshes of northern Belize: 2. Diversity of oscillatorialean genera. <i>Nov. Hedwigia</i> 89, 165–200. (doi:10.1127/0029-5035/2009/0089-0165)   |
| 62 | Nordin RN, Stein JR. 1980 Taxonomic revision of <i>Nodularia</i> (Cyanophyceae/Cyanobacteria). <i>Can. J. Bot.</i> 45, 1212–1224   |
| 63 | Gupta P. 2017 New record of Cyanoprokaryotes from West Bengal in Maldah district. <i>Triv. Plant. Res.</i> 4, 421–432. (doi:10.22271/tpr.2017.v4.i3.056)   |
| 64 | Dash PK, Mohapatra PK, Kar M. 2011 Diversity of cyanobacteria from freshwater bodies of Simlipal biosphere reserve, Odisha, India. <i>E-Planet</i> 9, 1–14   |
| 65 | Saha SK, Das R, Bora KN, Uma L. 2007 Biodiversity of epilithic cyanobacteria from freshwater streams of Kakoijana reserve forest, Assam, India. <i>Indian J. Microbiol.</i> 47, 219–232. (doi:10.1007/s12088-007-0043-5)   |
| 66 | Sikdar J, Keshri JP. 2015 The genera <i>Calothrix</i> Agardh ex Boret et Flahault, <i>Gloeotrichia</i> J. Agardh ex Boret et Flahault and <i>Rivularia</i> (Roth) C. Agardh ex Boret et Flahault (Cyanoprokaryota: Nostocales) in West Bengal, India. <i>Vegetos</i> 28, 25–35. (doi:10.5958/2229-4473.2015.00033.6) |
| 67 | Rao CB. 1937 The Myxophyceae of the United Provinces, India.-III. <i>Proc. Indian Acad. Sci. - Sect. B</i> 6, 339–375. (doi:10.1007/BF03051432)  |
| 68 | Barberousse H, Tell G, Yerémian C, Couté A. 2006 Diversity of algae and cyanobacteria growing on building façades in France. <i>Arch. Hydrobiol. Suppl. Algol. Stud.</i> 120, 81–105. (doi:10.1127/1864-1318/2006/0120-0081)   |
| 69 | Reddy M, Chaturvedi A. 2018 Study of Cyanobacterial diversity from the major rivers of Chandrapur district , Maharashtra. <i>Phycologia</i> 48, 36–45.   |
| 70 | D'Hollander E, Caljon A. 1979 Le Phytoplankton De L'adriatique à L'exclusion Des Diatomées. <i>Bull. Soc. Roy. Bot. Belgique</i> 112, 203–216  |
| 71 | Skinner S, Entwistle T. 2001 Non-marine algae of Australia: 1. Survey of colonial gelatinous blue-green macroalgae (Cyanobacteria). <i>Telopea</i> 9, 573–599. (doi:10.7751/telopea20024003)   |
| 72 | Bose R, Nandi C, Roy AS, Gorai PC, Pal R. 2016 Floristic Survey of Microplanktonic Cyanobacteria and Chlorophyta from Different Ecological Niches of West Bengal , India. <i>Phytomorphology</i> 66, 77–93   |
| 73 | Ram AT, Shamina M. 2015 New report of cyanobacterial association on the roots of epiphytic orchid, <i>Dendrobium crumenatum</i> Sw. <i>Ijcs</i> 1, 19–21.  |
| 74 | Broady PA. 1978 The terrestrial algae of Glérardalur Akureyri, Iceland. <i>Acta Bot. Islandica</i> 5, 3–60.  |
| 75 | Johansen JR, Rehakova K, Acker F. 2011 <i>Tapinothrix ozarkiana</i> sp. nov., with notes on distribution for the genus in North America. <i>Fottea</i> 11, 141–148. (doi:10.5507/fot.2011.014)   |
| 76 | Sasaki H, Kawai H. 2007 Taxonomic revision of the genus <i>Chorda</i> (Chordaceae, Laminariales) on the basis of sporophyte anatomy and molecular phylogeny. <i>Phycologia</i> 46, 10–21. (doi:10.2216/06-06-1)  |
| 77 | South GR, Burrows EM. 1967 Studies on marine algae of the British Isles. 5. <i>Chorda filum</i> (L.) stackh. Br. <i>Phycol. Bull.</i> 3, 379–402. (doi:10.1080/07161700650261)   |
| 78 | Kawai H, Sasaki H, Maeda Y, Ariai S. 2000 Morphology, life history, and molecular phylogeny of <i>Chorda rigida</i> , sp. nov. (Laminariales, Phaeophyceae) from the Sea of Japan and the genetic diversity of <i>Chorda filum</i> . <i>J. Phycol.</i> 37, 130–142. (doi:10.1046/j.1529-8817.1999.014012130.x)       |
| 79 | Kawai H, Nabata S. 1990 Life history and systematic position of <i>Pseudochorda gracilis</i> sp. nov. (Laminariales, Phaeophyceae). <i>J. Phycol.</i> 26, 721–727. (doi:10.1111/j.1529-8817.1990.00721.x)  |
| 80 | Kawai H, Sasaki H. 2004 Morphology, life history, and molecular phylogeny of <i>Stichospira flagellaris</i> (Tilioporidales, Phaeophyceae) and the erection of the <i>stichosporiaceae</i> fam. nov. <i>J. Phycol.</i> 40, 1156–1169. (doi:10.1111/j.1529-8817.2004.01513.x)   |
| 81 | Edelstein T, Wynne MJ, McLachlan J. 1970 <i>Melanosiphon intestinalis</i> (Saund.) Wynne, a new record for the Atlantic. <i>Phycologia</i> 9, 5–9. (doi:10.2216/i0031-8884-9-1-5.1)  |
| 82 | Cho TO, Cho YG, Yoon HS, Boo SM, Lee WJ. 2003 New records of <i>Myelophycus cavus</i> (Scytiophyceae, Phaeophyceae) in Korea and the taxonomic position of the genus on the basis of a plastid DNA phylogeny. <i>Nov. Hedwigia</i> 76, 381–397. (doi:10.1127/0029-5035/2003/0076-0381)                               |
| 83 | Parente MI, Neto AI, Fletcher RL. 2003 Morphology and life history of <i>Scytiophyton lomentaria</i> (Scytiophyceae, Phaeophyceae) from the Azores. <i>J. Phycol.</i> 39, 353–359. (doi:10.1046/j.1529-8817.2003.02032.x)  |
| 84 | Zuccarello GC, Lokhorst GM. 2005 Molecular phylogeny of the genus <i>Tribonema</i> (Xanthophyceae) using rbcL gene sequence data: monophly of morphologically simple algal species. <i>Phycologia</i> 44, 384–392.   |
| 85 | Gudlieffson BE. 1984 <i>Tribonema viride</i> (Xanthophyta) on cultivated grassland during winter and spring. <i>Acta Bot. Islandica</i> 7, 27–30.  |
| 86 | Broady PA, Ohtani S, Ingerfeld M. 1997 A comparison of strains of <i>Xanthonema</i> (= <i>Heterothrix</i> , <i>Tribonematales</i> , Xanthophyceae) from Antarctica, Europe, and New Zealand. <i>Phycologia</i> 36, 164–171. (doi:10.2216/i0031-8884-36-2-164.1)  |

## Appendix II - Supplementary Table 1. Cont.

- 87 West JA, Zuccarello GC, Scott J, Pickett-Heaps J, Gwang HK. 2005 Observations on *Purpureofilum apyrenoidigerum* gen. et sp. nov. from Australia and *Bangiopsis subsimplex* from India (Stylonematales, Bangiophyceae, Rhodophyta). *Phycol. Res.* 53, 49–66. (doi:10.1111/j.1440-1835.2005.tb00357.x)
- 88 Tanaka T. 1951 The Species of Erythrocitharia from Japan (I). *Acta Phytotaxon. Geobot.* 14, 96–100. (doi:10.18942/bunruichir.KJ00001077629)
- 89 Ugadim Y. 1974 Algas Marinhas Bentônicas do Litoral Sul do Estado de São Paulo e do Litoral do Estado do Paraná, III – Divisão Rhodophyta (1): Goniotrichales, Bangiales, Nemalionales e Gelidiales. *Bol. Botânica* 2, 93–137. (doi:10.1106/lssn.2316-9052.v2i0p93-137)
- 90 Norris JN. 2014 Marine Algae of the Northern Gulf of California II: Rhodophyta. Smithsonian Institution Scholarly Press. (doi:10.5479/si.19382812.96)
- 91 Kikuchi N, Shin JA. 2011 *Porphyrostromium japonicum* (Tokida) Kikuchi comb. nov. (Erythrolitidales, Rhodophyta) from Japan. *Phycologia* 50, 122–131. (doi:10.2216/10-06.1)
- 92 Sheath RG, Cole KM. 1984 Systematics of Bangia (Rhodophyta) in North America. I. Biogeographic trends in morphology. *Phycologia* 23, 383–396. (doi:10.2216/0031-8884-23-3-383.1)
- 93 Lowe RL, Rosen BH, Kingston JC. 1982 A Comparison of Epiphytes On Bangia atropurpurea (Rhodophyta) and Cladophora glomerata (Chlorophyta) from Northern Lake Michigan. *J. Great Lakes Res.* 8, 164–168. (doi:10.1016/S0380-1330(82)71954-9)
- 94 Edwards WM, Harold LL. 1970 Bangia Atropurpurea (Roth) A. in Western Lake Erie. *Ohio J. Sci.* 70, 56–57.
- 95 Woolcott GW, King RJ. 1998 Porphyra and Bangia (Bangiaceae, Rhodophyta) in warm temperate waters of eastern Australia: Morphological and molecular analyses. *Phycol. Res.* 46, 111–123.
- 96 Gargiulo GM, Genovese G, Morabito M, Culoso F, De Masi F. 2001 Sexual and asexual reproduction in a freshwater population of Bangia atropurpurea (Bangiales, Rhodophyta) from eastern Sicily (Italy). *Phycologia* 40, 88–96. (doi:10.2216/0031-8884-40-1-88.1)
- 97 Womersley HBS. 1984 The marine benthic flora of Southern Australia. Part 1. University of Adelaide, South Australia.
- 98 Nelson WA, Farr TJ, Broome JES. 2005 Dionia and Minerva, two new genera from New Zealand circumscribed for basal taxa in the Bangiales (Rhodophyta). *Phycologia* 44, 139–145.
- 99 Müller KM, Cannone JJ, Sheath RG. 2005 A molecular phylogenetic analysis of the Bangiales (Rhodophyta) and description of a new genus and species, *Pseudobangia kaycolea*. *Phycologia* 44, 146–155.
- 100 Alves AM, Moura CW do N, Alves GL, Gestinari LM de S. 2009 Os gêneros chaetomorpha Kütz. nom. cons. e *Rhizoclonium* Kütz. (Chlorophyta) do litoral do Estado da Bahia, Brasil. *Rev. Bras. Bot.* 32, 545–570. (doi:10.1590/s0100-8404200900300014)
- 101 Leliaert F, D'Hondt S, Tyberghein L, Verbruggen H, De Clerck O. 2011 Atypical development of Chaetomorpha antennina in culture (Cladophorales, Chlorophyta). *Phycol. Res.* 59, 91–97. (doi:10.1111/j.1440-1835.2010.00604.x)
- 102 Satpathi GG, Pal R. 2016 New and rare records of filamentous green algae from Indian Sundarbans Biosphere Reserve. *J. Algal Biomass Util.* 7, 159–175.
- 103 Leliaert F, Payo DA, Calumpang HP, De Clerck O. 2011 *Chaetomorpha philippinensis* (cladophorales, chlorophyta), a new marine microfilamentous green alga from tropical waters. *Phycologia* 50, 384–391. (doi:10.2216/10-76.1)
- 104 Chi Y, Wang L, Luan R, Wang H. 2009 *Cheatomorpha valida*-a new recorded green alga species in genus *Chaetomorpha* Kuetzing in China. *Fish. Sci.* 28, 162–163.
- 105 Dong Y, Tang X, Huang B, Ding L. 2011 Life history of *Chaetomorpha valida* (Cladophoraceae, Chlorophyta) in culture. *Bot. Mar.* 54, 551–556. (doi:10.1515/BOT.2011.066)
- 106 Deng Y, Tang X, Zhan Z, Teng L, Ding L, Huang B. 2013 Culture observation and molecular phylogenetic analysis on the blooming green alga *Chaetomorpha valida* (Cladophorales, Chlorophyta) from China. *Chinese J. Oceanol. Limnol.* 31, 552–558. (doi:10.1007/s00343-013-2216-x)
- 107 Ding LP, Luan RX. 2013 Flora Algarum Marinorum Sinicarum Tomus IV. Chlorophyta No. I. Sci. Press. Beijing, China
- 108 Wynne MJ. 2011 Proposal on the Name *Chaetomorpha viellardii* (Kütz.), n. Comb., for a Large-Celled Tropical Chaetomorpha (Chlorophyta). *Pacific Sci.* 65, 109–115. (doi:10.2984/65.1.109)
- 109 Skinner S, Entwistle TJ. 2014 Non-marine algae of Australia : 6. Cladophoraceae (Chlorophyta). *Teopela* 10, 731–748.
- 110 Leliaert F, Ruennen J, Boedecker C, Maggs CA, Coquy E, Verbruggen H, de Clerck O. 2009 Systematics of the marine microfilamentous green algae *Uronema curvatum* and *Urosora microscopica* (Chlorophyta). *Eur. J. Phycol.* 44, 487–496. (doi:10.1080/00670260903229540)
- 111 Wetherbee R, Verbruggen H. 2016 *Kraftionema allantoides*, a new genus and family of Ulotrichales (Chlorophyta) adapted for survival in high intertidal pools. *J. Phycol.* 52, 704–715. (doi:10.1111/jpy.12447)
- 112 Deason TR. 1969 Filamentous and Colonial Soil Algae from Dauphin Island, Alabama. *Trans. Am. Microsc. Soc.* 88, 240. (doi:10.2307/3224496)
- 113 Sarma P, Keshri JP. 1995 The genus *Pearsoniella* Fritsch & Rich 1924 (Order Ulotrichales, Chlorophyceae) in India. *J. Indian bot Soc* 74, 313–314.
- 114 Akhtar N, Rehman SR. 2009 Some Members of Ulotrichales From Jalala, District Mardan, Pakistan. *Pak. J. Pl. Sci.* 15, 19–30.
- 115 Lokhorst GM, Vromen M. 1972 Taxonomic Study on Three Freshwater Ulothrix Species. *Acta Bot. Neerl.* 21, 449–480.
- 116 Sophia M da G, Dias ICA, De Araújo AM. 2005 Chlorophyceae and zygnematiophyceae from the turvo state forest park, state of Rio Grande do Sul, Brazil. *Iheringia - Ser. Bot.* 60, 25–47.
- 117 Sikdar J, Mustafa G, Keshri JP. 2012 Some Fresh Water Green Algae of West Bengal, India. *J. Appl. Biosci.* 38, 179–186.
- 118 Lokhorst GM, Vromen M. 1974 Taxonomic Studies on the Genus *Ulothrix* (Ulotrichales, Chlorophyceae) III. *Acta Bot. Neerl.* 23, 561–602. (doi:10.1111/j.1438-8677.1974.tb00971.x)
- 119 Keshri JP. 2010 Contribution to our knowledge of Ulotrichales (Chlorophyta) of West Bengal, India. *Arch. Hydrobiol. Suppl. Algal. Stud.* 133, 29–41. (doi:10.1127/1864-1318/2010/0133-0029)
- 120 Lokhorst GM, Trask BJ. 1981 Taxonomic Studies on *Urosora* (Acrosiphoniales, Chlorophyceae) In Western Europe. *Acta Bot. Neerl.* 30, 353–431. (doi:10.1111/j.1438-8677.1981.tb01265.x)
- 121 Lee KW. 1978 *Uronema trentonense* sp. nov. (Chlorophyceae, Ulotrichales): a new edaphic alga from New Jersey. *Phycologia* 17, 191–195. (doi:10.2216/0031-8884-17-2-191.1)
- 122 Novis PM. 2003 A taxonomic survey of oedogonium (Oedogoniales, chlorophyta) in the South Island and Chatham Islands, New Zealand. *New Zeal. J. Bot.* 41, 335–358. (doi:10.1080/0028825X.2003.9512853)
- 123 Shukla HM, Tiwari GL, Pandey UC, Habib I. 1988 Oedogoniales of Uttar Pradesh, India-Oedogonium Link. *Proc. Plant Sci.* 98, 465–470. (doi:10.1007/BF03053402)
- 124 Marta P, Beata M. 2015 New data on distribution, morphology and ecology of *Oedogonium capillare* Kützing ex Hirn (Oedogoniales, Chlorophyta) in Poland. *Biodivers. Res. Conserv.* 40, 21–26. (doi:10.1515/birc-2015-0032)
- 125 Rai SK. 2012 Five new species of Oedogonium Link (Chlorophyta), a freshwater filamentous algae from Nepal. *Nepal. J. Biosci.* 2, 17–23. (doi:10.3126/njbs.v2i0.7485)
- 126 Liu G, Hu Z. 2004 Predominant occurrence of apical cell divisions in Oedogonium pakistaniense and its phylogenetic significance. *Phycologia* 43, 669–671. (doi:10.2216/0031-8884-43-6-669.1)
- 127 Dias ICA. 1989 Chlorophyta filamentosas do município de Cáceres e arredores, Mato Grosso, Brasil: uma contribuição ao seu conhecimento. *Acta Bot. Brasileira* 3, 03–12. (doi:10.1590/s0102-33061989000200001)
- 128 Mahato AK. 1999 A new species of Oedogonium (Chlorophyceae, Oedogoniales) from Bihar, India. *Feddes Repert.* 110, 173–176.
- 129 Buchheim MA, Hoffman LR. 1987 Structure and reproduction of *Sphaeropelea fragilis* sp.nov., a new member of the Sphaeropleaceae (Chlorophyceae) from California. *Can. J. Bot.* 65, 2330–2337. (doi:10.1139/b87-317)
- 130 Buchheim MA, Hoffman LR. 1985 *Sphaeropelea robusta* n. sp., a New Member of the Sphaeropleaceae (Chlorophyceae) from Texas. *Trans. Am. Microsc. Soc.* 104, 178–187. (doi:10.2307/3226425)
- 131 Hoffman LR. 1986 Zygotes of *Sphaeropelea tenuis* (Chlorophyceae). *Br. Phycol. J.* 21, 115–123. (doi:10.1080/00071618600650111)
- 132 Novis PM. 2004 A taxonomic survey of microspora (Chlorophyceae, Chlorophyta) in New Zealand. *New Zeal. J. Bot.* 42, 153–165. (doi:10.1080/0028825X.2004.9512896)
- 133 Kamat ND. 1963 The Algae of Kolhapur, India. *Hydrobiologia* XXII, 209–305.
- 134 Lokhorst GM, Star W, Zuccarello GC. 2004 New genus *Kolellopsis* (Trebouxiophyceae, Chlorophyta): Its phylogenetic position inferred from ultrastructure and nuclear ribosomal DNA sequences. *Phycol. Res.* 52, 235–243. (doi:10.1111/j.1440-1835.2004.tb00333.x)
- 135 Moniz MBJ, Rindi F, Guiry MD. 2012 Phylogeny and taxonomy of Prasiolales (Trebouxiophyceae, Chlorophyta) from Tasmania, including *Rosenvingiella tasmanica* sp. nov. *Phycologia* 51, 86–97. (doi:10.2216/10-103.1)
- 136 Tiwari GL, Pandey DC. 1972 On a new variety of *Geminella planctonica* (Balachonzew) comb. nov. (Chlorophyceae, Ulotrichales). *Phycologia* 11, 193–196. (doi:10.2216/0031-8884-11-2-193.1)
- 137 Novis PM. 2006 Taxonomy of Klebsormidium (Klebsormidiales, Charophyceae) in New Zealand streams and the significance of low-pH habitats. *Phycologia* 45, 293–301. (doi:10.2216/04-70.1)
- 138 Rindi F, Mikhailyuk TI, Sluitman HJ, Friedl T, López-Bautista JM. 2011 Phylogenetic relationships in *Interfilum* and *Klebsormidium* (Klebsormidiophyceae, Streptophyta). *Mol. Phylogenet. Evol.* 58, 218–231. (doi:10.1016/j.mpev.2010.11.030)
- 139 Skaloud P. 2006 Variation and taxonomic significance of some morphological features in European strains of Klebsormidium (Klebsormidiophyceae, Streptophyta). *Nov. Hedwigia* 83, 533–550. (doi:10.1127/0029-5035/2006/0083-0533)
- 140 Skinner S, Entwistle TJ. 2015 Mougeotia (Zygnemataceae, Streptophyta) in Australia. *Telopea* 18, 481–494.
- 141 Ferrer NC, Cáceres EJ. 2005 Mougeotia mesocarpiana (Zygnemataceae, Chlorophyta), a new freshwater species of the Mesocarpus Section from Argentina. *Iheringia - Ser. Bot.* 60, 63–68.
- 142 Faghri M, Shafii S. 2013 Floristic study on the algae of Siah Darvishan River in Gilan Province, North Iran. *Casp. J. Environ. Sci.* 11, 111–126.
- 143 Kim GH, Youn M, Klochko TA. 2005 A moving mat: Phototaxis in the filamentous green alga *Spirogyra* (Chlorophyta, Zygnemataceae). *J. Phycol.* 41, 232–237. (doi:10.1111/j.1529-8817.2005.03234.x)
- 144 Sviridenko BF, Sviridenko TV, Yevzhenko KS. 2015 Discovery of *Spirogyra* subcolligata Bl (Spirogyraceae, Zygnematales) in Russia. *Int. J. Water Biol.* 8, 218–221. (doi:10.1134/S199508291503013X)
- 145 Schagerl M, Zwirn M. 2015 A brief introduction to the morphological species concept of Spirogyra and emanating problems. *Arch. Hydrobiol. Suppl. Algal. Stud.* 148, 67–86.
- 146 Kim JH. 2015 New records of the genus *Spirogyra* (Zygnemataceae, Conjugatophyceae) in Korea. *J. Ecol. Environ.* 38, 611–618. (doi:10.5141/econv.2015.061)
- 147 Ferrer NC. 2008 *Spirogyra multiconjugata* sp. nov. (Zygnemataceae, Chlorophyta), a new species of the Punctata group found in Argentina. *Arch. Hydrobiol. Suppl. Algal. Stud.* 128, 1–10. (doi:10.1127/1864-1318/2008/0128-0001)
- 148 Stancheva R, Sheath RG, Hall JD. 2012 Systematics of the genus *Zygnema* (zygnemataceae, charophyta) from californian watersheds. *J. Phycol.* 48, 409–422. (doi:10.1111/j.1529-8817.2012.01127.x)
- 149 Kim J-H, Kim Y-H. 2009 Morphological Note of *Zygnema cruciatum* (Zygnemataceae, Chlorophyta) in Korea. *ALGAE* 24, 57–60. (doi:10.4490/algae.2009.24.2.057)
- 150 Kim J-H, Boo SM, Kim YH. 2012 Morphology and plastid psbA phylogeny of *Zygnema* (Zygnemataceae, Chlorophyta) from Korea: *Z. insigne* and *Z. leiospermum*. *ALGAE* 27, 225–234. (doi:10.4490/algae.2012.27.4.225)
- 151 Gallardo VA, Klingelhoeffer E, Arntz W, Graco M. 1998 First Report of the Bacterium *Thioploca* in the Benguela Ecosystem off Namibia . *J. Mar. Biol. Assoc. United Kingdom* 78, 1007–1010. (doi:10.1017/s0025315400044945)
- 152 Kawai H, Kurogi M. 1985 On the life history of *Pseudochordia nagaii* (Pseudochordaceae fam. nov.) and its transfer from the Chordariales to the Laminariales (Phaeophyta). *Phycologia* (doi:10.2216/0031-8884-24-3-289.1)

### APPENDIX III - ARTICLE THREE

Appendix III - Supplementary Table 1. Infrared absorption bands of the selected samples (clay fraction)

Sample code	Outcrop	Dep Seq	Material	Si-O bend		
IB7	AF222	DS1	Fine silicilasts (mud and silt)	418sh		<b>429</b>
IB1	AF151	DS1	Fine silicilasts	416sh	425sh	<b>430</b>
IB2	AF153	DS1	Fine silicilasts	416sh	425sh	<b>428</b>
IB5	AF236	DS1 (Arumberia level)	Fossiliferous beds (Arumberia)	416sh	423sh	<b>430</b>
IB6	AF236	DS1	Fine silicilasts			<b>426</b>
IB8	M9	DS1	Fine silicilasts			<b>428</b>
IB9	M11	DS1	Fine silicilasts	421sh	<b>426</b>	436
IB10	M12	DS1	Fine silicilasts	417sh	422sh	<b>430</b>
IB12	AF103	DS2	Fine silicilasts			<b>428</b>
IB13	AP1	DS2	Fine silicilasts	415sh	423sh	<b>430</b>
IB14	AF19	DS2	Fine silicilasts	416sh	426sh	<b>431</b>
IB15	AF9	DS2	Fine silicilasts	423sh	426	<b>431</b>
A16	A16	DS2	Fossiliferous beds	416sh	426sh	<b>430</b>
IB20	AF14	DS2-DS3	Fine silicilasts	415sh		<b>431</b>
IB17	AF57	DS3	Fine silicilasts		420sh	<b>429</b>
IB22	AF80	DS3	Fine silicilasts			<b>429</b>
IB23	B16	DS4 (Similar to A16)	Fossiliferous beds	420sh	<b>426</b>	431sh
IB24	AF172	DS4	Fine silicilasts			
IB3	AF236	DS1	Silicified tuffite (chert)			<b>426</b>
IB4	AF236	DS1	Silicified tuffite (chert)	416		
IB29	AFZ	DS5?	Vitric tuffite (chert)			<b>426</b>
IB11	M12	DS1	Argillaceous tuff		423	
04 (MM)	A16	DS2	Fossil clays	429		
05 (CL)	A16	DS2	Coarse-grained volcanioclastic laminae	430		

Appendix III - Supplementary Table 1. Cont.

	Si–O–Si bend			Si–O–Al			Alb	Feldspars	Si–O	Feldspars		
463sh	<b>470</b>		520sh <b>531</b>			649w <b>695</b>		~725?				
	<b>469</b>	474sh	<b>520</b> 529sh			649 <b>695</b>		~724				
	<b>469</b>	474sh	<b>522</b> 529sh			648 <b>695</b>		~725?				
463sh	<b>471</b>	475sh	<b>518</b>	531sh		589sh	648	<b>696</b>	~724			
464sh	<b>469</b> 475sh		<b>525</b>			589sh	649	<b>695</b>	~725			
	<b>470</b>		520sh <b>532</b>				644	<b>696</b>	~725?			
	<b>470</b>		<b>521</b>	530sh	589sh		649	<b>695</b>	~725			
462sh	<b>468</b>	473sh	523sh 529sh <b>533</b>				643	<b>696</b>				
443sh	<b>469</b> 474sh		<b>520</b>	528sh	590sh		649	<b>696</b>	~725			
	<b>470</b>		515sh	<b>523</b>	528sh	533sh	649	<b>696</b>	~725?			
	<b>470</b>		<b>518</b>	529sh			648	<b>696</b>	~725?			
445	<b>470</b>	474sh	516sh	<b>527</b>	533sh		646	<b>695</b>	~725			
<b>470</b>			<b>525</b>					<b>696</b>				
457sh	463sh	<b>468</b>	<b>471</b>	<b>518</b>	<b>535</b>	589sh	<b>646</b>	<b>696</b>	725			
468sh	<b>472</b>		522sh <b>529</b>			534sh		<b>695</b>				
	<b>472</b>		<b>526</b>					<b>696</b>				
<b>471</b>			<b>521</b>			589sh	~643	~695	~725?			
							~653	<b>695</b>				
464sh	<b>470</b>	474sh	<b>515</b>				591sh	647	<b>695</b>			
464sh	<b>468</b>	<b>474</b>	478	<b>515</b>				647	<b>695</b>			
464sh	<b>468</b>	472	480sh	<b>516</b>				645	<b>695</b>			
	472		<b>524</b>									
<b>471</b> ~475sh			<b>528</b>					<b>697</b>				
<b>471</b>			<b>526</b>					<b>696</b>				

### Appendix III - Supplementary Table 1. *Cont.*

Albite	Al-O-Si in plane	Qz	Qz	Al-O out-of-plane		AlOHAl bend	Si-O-Si stretching	Si-O-Si stretchin	SiOap stretch
746	~761	779	797	830	~878	911	1007	1028	1079
746	~761	779	798	827	~878	912	1012sh	1028	1086
746	~761	779	798	827	~878	911	1012sh	1027	1085
746	~761	779	799	827	~878	915	1012	1033	1062sh 1090
746	~761	779	798	827	~878	912	1012	1029	1062sh? 1085
	~752	779	799	827	~878	912	1008	1030	1082
746	~761	779	799	827	~878	911	1007	1029	1085
	~752	779	799	827	~878	911	1007	1031	1084
~747	~760	779	798	828	~878	911	~935	1008	1029 1087
~746	~760	779	798	828	~878	911	~935	1008	1029 1081
	~760	779	799	828	~878	912	1008	1029	1087
~746	760	779	798	828	~878	912	1008	1029	1087sh
	~755	779	799	825	~878	913	1012	1032	1084
		779	799		~878	913	~940	1010	1033 ~1060 1082
~755	~778	798		828	~878	912	~1008	1030	1076
		779	797			912	1011	1030	
~746	~755	798	778	828	~878	912	~1008	1030	~1060 1084
	~755	798	~778	828	~878	912	1008	1030	1082
		779	799	828	~878	910		1034	~1061 1090
		779	799	828	~878	912		1034	~1062 1087
		779	799	828	~878	913		1034	1090
~750	779	800		827	~878	911	~1012	1028	~1080
~754	779	800		~830	~874	913	~1011	1032	1085
~754	779	799		~828	~878	913	~1012	1033	1083

Appendix III - Supplementary Table 1. *Cont.*

<b>SiOap stretch</b>	<b>Qz</b>	<b>Aliphatic compounds</b>			<b>OH-stretch</b>						
1110sh	1162	2855	2926	2963		3599sh	<b>3620</b>	3628sh?		<b>3698</b>	
1110sh	1163	2855	2926		3568	3599sh	<b>3620</b>	3628sh	3652?	3669?	<b>3698</b>
1110sh	1163	2855	2926	2966		3599sh	<b>3620</b>	3628sh?		<b>3698</b>	
	1164	2855	2926		3568		<b>3622</b>	3628sh	3652?	3669?	<b>3700</b>
	1163	2855	2926		3568?		<b>3620</b>	3628sh		<b>3700</b>	
1112sh	1163	2855	2926			3599sh	<b>3620</b>		3652	3669	<b>3698</b>
1112sh	1164	2855	2926			3599sh	<b>3620</b>	3628sh?		<b>3698</b>	
1112sh	1164	2855	2926			3599sh	<b>3620</b>		3652	3669	<b>3698</b>
~1164	2856w	2926w			3568sh	3599sh	<b>3620</b>	3628sh		<b>3700</b>	
~1112	~1163	2856w	2926w		3568sh	3599sh	<b>3620</b>	3628sh	~3652	~3669	<b>3700</b>
~1112	~1164	2856w	2926w		3568sh	3599sh	<b>3620</b>	3628sh	~3652	~3669	<b>3699</b>
~1112	~1162	2856w	2926w		3568sh	3599sh	<b>3620</b>	3628sh	~3652	~3669	<b>3700</b>
~1112	~1164	2856	2926	2960	3568sh		<b>3621</b>	3628sh	~3652	~3669	<b>3701</b>
~1112	~1163	2856	2928	2975	3568sh	3599sh	<b>3620</b>	3628sh	~3652	~3670	<b>3696</b>
~1112	~1163	2856	2928	2975?	3568sh	3599sh	<b>3622</b>	3628sh	~3652	~3670	<b>3701</b>
	~1164	2856	2928			3599sh	<b>3622</b>	3628sh		~3670	<b>3701</b>
	~1164	2856	2928		3568sh	3599sh	<b>3620</b>	3628sh	~3653	~3670	<b>3700</b>
~1112	~1165	2856	2928	2962	3568sh	3599sh	<b>3620</b>	3628sh	~3654	~3670	<b>3698</b>
	~1165	2856	2926	2961			<b>3622</b>	3629sh			
	~1164	2856	2928	2970	3568sh		<b>3622</b>	3629sh			
	~1165	2856	2928		3568sh		<b>3622</b>	3629sh		<b>3696</b>	
		2856	2928	2961	3568sh		<b>3620</b>	3629sh			
~1112	1164	2855	2927	2960		~3604sh	<b>3623</b>		~3656		<b>3702</b>
~1112	1164	2855	2927	2960		~3604sh	<b>3622</b>		~3656		<b>3702</b>

Appendix III - Supplementary Table 1. *Cont.*

(ν+δ)AlMgOH?	AlFe <sup>3+</sup> OH?	Illite	H <sub>2</sub> O
~4088 ~4181w 4240w ~4364		~4466sh <b>4524</b> 4621sh	<b>5216</b> 6812sh 7020sh
~4088 ~4190w 4241w ~4364		~4466sh ~4503sh <b>4524</b> 4621sh	<b>5221</b> 7020sh
~4088 ~4190w 4241w	4449sh	~4503sh <b>4522</b>	<b>5222</b>
~4083 ~4190w 4247w	4446	~4503sh <b>4528</b>	<b>5227</b>
~4088 ~4190w 4246w	4446		<b>4522</b> <b>5221</b>
~4088 ~4190 4239w		~4466sh <b>4526</b> 4621sh	<b>5222</b> 7020sh
~4088 ~4190w 4241w	4446	~4503sh <b>4522</b>	<b>5214</b> 7020sh
~4088 ~4190 4240w		~4466sh <b>4526</b> 4621sh	<b>5220</b> 7020sh
~4088 ~4190 ~4246	~4442		<b>4520</b> <b>5221</b>
~4088 ~4190 ~4247	~4442		<b>4525</b> <b>5232</b>
~4088 ~4190 ~4248	~4442		<b>4525</b> <b>5228</b>
~4090 ~4190 ~4249	~4442		<b>4526</b> <b>5232</b>
~4083 ~4190 ~4250	~4442	~4503sh <b>4529</b>	<b>5221</b>
~4088 ~4192 4240		<b>4527</b> ~4622	<b>5222</b> ~7018sh
~4088 ~4190 4246		<b>4527</b>	<b>5228</b>
~4088 ~4190 4246		<b>4527</b>	<b>5228</b>
~4083 ~4192 4250	4440	~4506sh <b>4523</b>	<b>5225</b>
~4088 ~4190 4243		<b>4526</b>	<b>5222</b> ~7018sh
~4090 4249	~4439		<b>4528</b> <b>5229</b>
~4090 4251	~4440		<b>4532</b> <b>5229</b>
~4090 4247	~4441		<b>4529</b> <b>5213</b>
~4083 4249	~4442	<b>4509</b>	4700 <b>5229</b> ~6830
~4083 4189 4249	~4442		<b>4529</b> <b>5238</b> ~6830
~4083 4189 4247	~4442		<b>4529</b> <b>5224</b>

Appendix III - Supplementary Table 1. *Cont.*

**2v(OH)  
overtone**

<b>7065</b>	~7170sh	
<b>7065</b>		
<b>7065</b>		
<b>7071</b>		
<b>7067</b>		
<b>7065</b>	7170sh	
<b>7065</b>		
<b>7065</b>	7170sh	
<b>7062</b>		
<b>7066</b>		
<b>7066</b>		
<b>7068</b>		
<b>7070</b>	~7215	
<b>7066</b>	7170sh	
<b>7070</b>		
<b>7070</b>		
<b>7066</b>	~7215?	
<b>7067</b>		
<b>7075</b>		
<b>7075</b>		
<b>7071</b>		
<b>7065</b>		
<b>7072</b>	~7082	~7215
<b>7070</b>		~7215

Appendix III - Supplementary Table 2. Oxide wt% results and calculated structural formula of illite crystals from fossils

Oxides wt%	1	2	3	4	5	6	7	8	9	10	11	12
SiO <sub>2</sub>	56,20	55,33	56,61	60,34	56,59	62,43	56,82	56,75	56,09	54,60	55,60	58,66
Al <sub>2</sub> O <sub>3</sub>	29,56	30,24	31,15	27,06	30,22	25,16	30,27	30,30	31,19	32,01	31,02	27,52
FeO	-	-	-	-	-	-	-	-	-	-	-	-
Fe <sub>2</sub> O <sub>3</sub>	5,05	4,94	3,58	4,00	4,40	4,25	3,96	4,46	4,03	3,94	4,02	4,62
MgO	1,22	1,34	1,11	1,25	1,24	1,08	0,97	1,18	1,40	1,25	1,14	1,37
TiO <sub>2</sub>	0,19	0,25	0,16	0,34	0,17	0,31	0,09	0,09	0,00	0,26	0,34	0,34
MnO	0,00	0,00	0,07	0,00	0,03	0,02	0,00	0,00	0,00	0,06	0,06	0,02
CaO	0,13	0,10	0,08	0,10	0,11	0,09	0,07	0,04	0,03	0,07	0,10	0,18
Na <sub>2</sub> O	0,09	0,09	0,08	0,04	0,09	0,13	0,00	0,12	0,11	0,08	0,10	0,13
K <sub>2</sub> O	8,06	8,19	7,40	7,17	7,55	6,95	8,20	7,52	7,55	8,07	8,00	7,39
Total	101	100	100	100	100	100	100	100	100	100	100	100
Numbers of cations on the basis of 11 oxygens												
Si	3,47	3,42	3,47	3,68	3,48	3,79	3,50	3,49	3,45	3,37	3,43	3,60
Al <sup>IV</sup>	0,53	0,58	0,53	0,32	0,52	0,21	0,50	0,51	0,55	0,63	0,57	0,40
ΣTet	4,00	4,00	4,00	4,00	4,00	4,00	4,00	4,00	4,00	4,00	4,00	4,00
Al <sup>VI</sup>	1,63	1,63	1,72	1,62	1,67	1,59	1,70	1,68	1,71	1,70	1,68	1,59
Fe <sup>+3</sup>	0,23	0,23	0,17	0,18	0,20	0,19	0,18	0,21	0,19	0,18	0,19	0,21
Fe <sup>+2</sup>	-	-	-	-	-	-	-	-	-	-	-	-
Mg	0,11	0,12	0,10	0,11	0,11	0,10	0,09	0,11	0,13	0,12	0,10	0,13
Ti	0,01	0,02	0,01	0,03	0,01	0,02	0,01	0,01	0,00	0,02	0,03	0,03
Mn	0,00	0,00	0,00	0,00	0,00	0,00	0,00	0,00	0,00	0,00	0,00	0,00
ΣOct	1,99	2,00	2,01	1,94	2,00	1,91	1,98	2,00	2,02	2,02	2,00	1,96
Ca	0,01	0,01	0,01	0,01	0,01	0,01	0,00	0,00	0,00	0,00	0,01	0,01
Na	0,01	0,01	0,01	0,00	0,01	0,01	0,00	0,01	0,01	0,01	0,01	0,02
K	0,64	0,65	0,58	0,56	0,59	0,54	0,64	0,59	0,59	0,64	0,63	0,58
ΣInt.	0,66	0,66	0,59	0,57	0,61	0,56	0,65	0,61	0,61	0,65	0,65	0,61

All Fe has been considered as Fe<sup>3+</sup>. Tet = tetrahedral occupancy; Oct = octahedral

Appendix III - Supplementary Table 2. *Cont.*

13	14	15	16	17	18	19	20	21	22	23	24	25	26
53,23	61,66	66,43	56,30	58,24	59,32	56,56	59,33	54,17	56,01	62,62	60,03	57,38	55,08
31,83	25,88	22,37	29,61	28,67	27,06	29,22	26,05	30,95	29,11	23,79	26,46	26,66	29,33
-	-	-	-	-	-	-	-	-	-	-	-	-	-
4,82	4,01	3,48	4,09	3,71	3,51	4,15	4,90	4,01	4,75	4,52	4,03	5,40	5,19
1,36	1,03	0,98	1,21	1,33	1,30	1,02	1,17	1,34	1,49	1,20	1,05	1,59	1,27
0,18	0,24	0,37	0,17	0,23	0,32	0,34	0,29	0,26	0,41	0,16	0,25	0,40	0,33
0,00	0,02	0,05	0,00	0,02	0,00	0,00	0,00	0,02	0,01	0,03	0,04	0,00	0,00
0,00	0,00	0,06	0,08	0,00	0,00	0,02	0,03	0,00	0,01	0,07	0,01	0,00	0,02
0,13	0,08	0,12	0,06	0,09	0,07	0,10	0,10	0,07	0,10	0,06	0,11	0,08	0,10
8,46	7,09	6,14	8,49	7,70	8,42	8,60	8,13	9,18	8,12	7,55	8,03	8,49	8,67
100	100	100	100	100	100	100	100	100	100	100	100	100	100
3,32	3,76	4,00	3,49	3,58	3,65	3,51	3,67	3,38	3,47	3,84	3,69	3,57	3,44
0,68	0,24	0,00	0,51	0,42	0,35	0,49	0,33	0,62	0,53	0,16	0,31	0,43	0,56
4,00	4,00	4,00	4,00	4,00	4,00	4,00	4,00	4,00	4,00	4,00	4,00	4,00	4,00
1,67	1,62	1,58	1,66	1,66	1,62	1,64	1,56	1,66	1,60	1,55	1,61	1,52	1,60
0,23	0,18	0,16	0,19	0,17	0,16	0,19	0,23	0,19	0,22	0,21	0,19	0,25	0,24
-	-	-	-	-	-	-	-	-	-	-	-	-	-
0,13	0,09	0,09	0,11	0,12	0,12	0,09	0,11	0,12	0,14	0,11	0,10	0,15	0,12
0,01	0,02	0,03	0,01	0,02	0,02	0,03	0,02	0,02	0,03	0,01	0,02	0,03	0,03
0,00	0,00	0,00	0,00	0,00	0,00	0,00	0,00	0,00	0,00	0,00	0,00	0,00	0,00
2,03	1,92	1,86	1,97	1,97	1,92	1,96	1,92	1,99	1,99	1,89	1,91	1,95	1,98
0,00	0,00	0,00	0,01	0,00	0,00	0,00	0,00	0,00	0,00	0,00	0,00	0,00	0,00
0,02	0,01	0,01	0,01	0,01	0,01	0,01	0,01	0,01	0,01	0,01	0,01	0,01	0,01
0,67	0,55	0,47	0,67	0,60	0,66	0,68	0,64	0,73	0,64	0,59	0,63	0,67	0,69
0,69	0,56	0,49	0,68	0,61	0,67	0,69	0,65	0,74	0,66	0,60	0,64	0,68	0,70

Appendix III - Supplementary Table 2. *Cont.*

27	28	29	30
57,29	61,72	55,86	59,36
28,54	24,70	29,24	29,74
-	-	-	-
5,22	4,62	4,35	2,93
1,20	1,38	1,52	1,08
0,52	0,16	0,16	0,11
0,04	0,00	0,00	0,01
0,06	0,07	0,05	0,03
0,07	0,05	0,06	0,64
7,07	7,30	8,76	6,11
100	100	100	100
<hr/>			
3,53	3,78	3,48	3,61
0,47	0,22	0,52	0,39
4,00	4,00	4,00	4,00
1,60	1,56	1,62	1,74
0,24	0,21	0,20	0,13
-	-	-	-
0,11	0,13	0,14	0,10
0,04	0,01	0,01	0,01
0,00	0,00	0,00	0,00
1,99	1,92	1,98	1,98
0,00	0,00	0,00	0,00
0,01	0,01	0,01	0,07
0,55	0,57	0,70	0,47
0,57	0,58	0,71	0,55

Appendix III - Supplementary Table 3. Raman fitting results for the fossil and cement/matrix (C/M) clay minerals, and detrital micas

Mineral/Structure	Centre	Width	Area	Centre	Width	Area	Centre	Width	Area	Centre	Width
C/M	129,386	7,97508	952719				149,663	22,1699	941262		
C/M	129,104	6,31943	783621	146,224	7,43827	164051				154,649	14,3316
C/M	127,676	8,554	1,44E+06				151,829	20,6853	315809		
C/M	129,159	6,28984	684786	144,769	5,43862	118825	149,667	10,3926	141230		
C/M	129,203	6,74691	1,64E+06	148,093	19,6143	629523					
C/M	129,292	7,25242	1,39E+06	145,237	21,1994	3,24E+06					
C/M	129,495	6,63278	1,26E+06	147,534	8,38337	124347					
C/M	129,336	6,18041	508175	144,773	6,85297	134649	152,517	12,8342	177612		
C/M	129,163	7,91477	1,28E+06	147,527	9,59184	215956				157,022	9,59184
C/M	129,693	6,50796	898010	144,796	8,4336	433761	149,526	15,2699	261519		
C/M				144,983	8,98975	771373	153,238	13,2126	304251		
C/M	128,858	5,28012	166049	145,839	10,607	2,57E+06					
C/M	129,498	6,39541	819102	145,047	8,87969	978005					
C/M	129,574	6,67476	1,75E+06								
C/M	129,214	6,74589	1,28E+06								
C/M	129,546	7,02453	1,22E+06	144,632	9,72427	1,87E+06					
C/M	129,301	6,7904	1,16E+06	149,154	9,33432	105090					
C/M	128,71	6,43878	511166	145,961	7,69446	374926	152,708	12,1833	242972		
C/M	128,861	6,64692	676934	146,68	9,72464	781383				157,42	12,8934
C/M	129,566	7,90206	1,18E+06	145,412	10,7551	1,62E+07					
C/M	128,709	7,39782	980836	146,179	11,5853	2,20E+06					
C/M	129,412	5,05224	199583	146,405	10,9618	8,95E+06					
C/M	129,348	7,04772	1,20E+06	146,066	10,3627	7,43E+06					
C/M	129,221	6,91541	722762	145,587	9,9584	2,64E+06					
C/M	129,787	7,62905	321987	146,214	13,2876	1,58E+06					
C/M	129,967	6,32857	263331	146,431	5,5925	27508,2				154,331	10,6933
C/M	129,757	5,62866	42812	146,862	8,71827	118003				155,958	14,0511
C/M	129,961	5,49947	114779	146,724	10,1025	922236					
C/M	129,852	6,18981	192128	146,751	7,76327	75965,9				155,746	10,9328
C/M	129,694	6,32842	218836	146,322	7,68103	90975,6				154,055	12,5254
C/M	129,694	5,6709	126276	145,505	7,19097	108443	152,548	12,6567	119131		
C/M				146,662	10,8679	1,12E+06					
C/M	129,761	4,62238	47130,8	146,164	9,87262	1,08E+06					
C/M	128,916	6,5703	112763	146,203	8,14737	107533	153,226	12,3607	78574,2		
C/M				145,374	10,8479	5,38E+06					
C/M	129,759	5,59982	86765,1	147,089	11,2848	599267					
C/M	129,773	6,26316	195939	146,146	7,84083	156358	153,902	10,5144	69402,1		
C/M	129,814	5,71142	108980	146,813	11,281	1,26E+06					
C/M	129,529	6,05063	199803	146,391	7,70953	128800	154,979	12,0575	119289		
C/M	129,522	6,27029	142411	146,193	7,84923	107805	153,184	12,8826	118794		
C/M	129,151	7,50969	233918				153,664	14,2401	166645		
C/M	129,408	5,68092	71438,4				151,556	17,0172	295774		
C/M	129,286	6,81552	314241								
C/M	129,58	6,02224	114844	145,642	8,68336	321960				154,052	10,5142
C/M	129,78	5,83179	100072	145,571	8,5516	411179				153,29	14,0185
C/M	129,283	6,38666	152535	146,197	8,1254	110531				154,346	13,4958
C/M	129,697	5,12219	72921,9	145,709	8,6519	475848				154,205	12,8919
C/M	129,086	6,97068	187769				151,719	14,324	88940,1		
C/M	129,77	6,3518	342712				152,867	12,9592	93272		
C/M	128,68	4,5899	55715,5	147,368	10,8071	744460					
C/M	129,234	4,9173	74311,6	146,931	11,6376	786950					

Appendix III - Supplementary Table 3. Cont.

C/M				146,151	11,6355	2,99E+06					
C/M	129,618	5,59928	108481	145,802	10,3068	833871					
C/M				145,726	10,797	1,00E+07					
C/M				145,516	10,7202	1,69E+07					
C/M	129,363	6,29426	185494				151,063	13,7892	110264		
C/M	128,916	6,54677	256432	146,42	7,37895	95642,4	153,967	11,3371	104512		
C/M	129,302	6,4682	169058				152,997	16,3033	336710		
C/M	129,071	6,14589	75875,9	145,447	7,97111	119118				154,641	14,3559
C/M	129,736	5,87057	124061	145,316	7,80162	138661	153,155	13,3014	180097		
C/M	128,992	6,62715	140168	147,044	9,09668	108660				155,742	11,0883
C/M	129,983	5,45274	67796	146,19	8,45124	103395				155,071	13,2586
C/M	129,489	5,79998	148195	145,583	7,87253	199851	153,028	13,3651	175014		
C/M	129,382	6,4496	302174							155,17	13,86
C/M	129,765	4,97152	87516	145,308	7,84894	246515	153,271	14,1441	233082		
C/M	129,656	5,72743	130690	145,54	7,69071	165643	153,112	12,6614	131104		
C/M	129,316	6,32229	82861,5				152,252	17,1302	218147		
C/M				146,226	9,24894	579049				155,981	11,99
C/M				146,028	8,95294	648332				155,154	14,0278
C/M				145,993	10,2193	2,20E+06					
C/M				147,603	11,9917	1,19E+06					
C/M				147,974	12,1456	944742					
C/M				146,566	9,61069	677582				155,059	13,7269
C/M				149,101	15,1026	838002				159,256	7,40642
C/M				145,943	10,0456	4,28E+06					
C/M				146,317	10,3285	2,42E+06					
C/M				147,009	11,4723	3,89E+06					
C/M				145,789	10,3283	9,94E+06					
C/M	129,864	5,86095	98573,5	145,835	7,82479	256270				154,77	14,5648
C/M				146,118	10,2639	3,24E+06					
C/M	128,999	6,46085	84155,1	146,156	8,35749	302431				154,484	14,6428
C/M	129,954	6,00195	141650	146,051	8,23056	195435				154,816	14,2708
C/M				146,413	10,5205	2,20E+06					
C/M				145,656	8,46159	482267				154,422	14,4958
C/M				146,364	8,80254	678439				155,395	13,0172
C/M				146,431	9,26368	282958				155,535	13,444
Fossil				147,706	12,6714	1,21E+08					
Fossil	127,83	7,3457	683607	146,421	12,6497	7,49E+06					
Fossil				148,615	13,1089	1,30E+07					
Fossil				148,892	13,6585	1,03E+07					
Fossil				148,763	13,0783	3,22E+07					
Fossil				149,218	14,1319	5,48E+06					
Fossil				147,806	12,791	2,49E+07					
Fossil				148,901	13,8391	7,13E+06					
Fossil				148,444	13,5484	4,15E+07					
Fossil				148,769	13,3454	1,40E+07					
Fossil				148,532	13,2999	1,19E+07					
Fossil				148,017	12,4945	1,26E+07					
Fossil	127,372	9,34272	1,01E+06	147,567	12,8541	6,26E+06					
Fossil				149,258	13,8485	2,04E+07					
Fossil				149,631	13,905	3,78E+07					
Fossil	127,947	6,91114	783502	147,04	11,5526	7,67E+06					
Fossil				148,241	13,4788	1,65E+07					

Appendix III - Supplementary Table 3. *Cont.*

Fossil				147,86	12,5082	7,12E+06					
Fossil				147,542	12,1683	4,96E+07					
Fossil				147,938	13,0232	1,41E+07					
Fossil				147,638	12,5072	1,84E+07					
Fossil				147,655	12,6328	1,25E+08					
Fossil				148,324	13,2264	7,64E+06					
Fossil				147,646	13,2451	2,33E+07					
Fossil	128,393	6,12363	329812	146,972	12,2083	7,35E+06					
Fossil				147,736	12,6652	1,82E+07					
Fossil				144,768	11,3537	1,52E+06					
Fossil				143,946	9,13886	336299	151,062	15,99	202608		
Fossil				144,056	10,9045	3,38E+06					
Fossil				143,964	8,78305	295571	152,098	15,0099	172732		
Fossil				145,021	11,0908	2,59E+06					
Fossil				143,769	8,16879	252939	152,008	14,2293	98465		
Fossil				144,183	10,6878	1,45E+06					
Fossil				145,159	10,9685	1,97E+06					
Fossil				145,467	11,7954	701738					
Fossil				144,42	9,36299	623559	152,723	13,76	211657		
Fossil				144,9	10892	7,19E+06					
Fossil	127,812	4,47556	53262,5	144,728	10,6631	2,81E+06					
Fossil				145,08	11,3789	3,58E+06					
Fossil				145,121	11,2145	3,05E+06					
Fossil				148,216	13,4249	1,58E+06					
Fossil				147,849	12,1212	2,61E+06					
Fossil				147,122	11,6961	2,12E+06					
Fossil				147,849	12,0049	2,52E+06					
Fossil				147,562	12,389	3,41E+06					
Fossil				147,983	12,995	5,65E+06					
Fossil				147,651	12,1895	8,75E+06					
Fossil				147,79	12,1298	2,86E+06					
Fossil				147,788	12,6523	3,28E+06					
Fossil				147,616	12,0732	2,63E+06					
Fossil				148,214	13,1858	1,49E+06					
Fossil				147,546	12,1994	5,55E+06					
Fossil				147,904	12,5621	1,79E+06					
Fossil				147,447	11,7926	6,65E+06					
Fossil				148,199	12,9601	3,57E+06					
Fossil				147,823	12,5943	2,14E+06					
Fossil				146,896	12,028	2,22E+06					
Fossil				147,083	12,1146	2,89E+06					
Fossil				147,113	11,8607	1,95E+06					
Fossil				147,645	13,1702	4,66E+06					
Fossil				146,519	12,074	3,34E+06					
Fossil				146,36	9,9252	800702				154,731	14,0264
Fossil				146,774	11,9863	4,74E+06					
Fossil				148,169	12,4547	6,72E+06					
Fossil				146,867	11,6595	8,04E+06					
Fossil				146,868	11,6776	8,03E+06					
Fossil				146,751	11,5009	2,72E+06					
Fossil				147,413	12,0608	1,43E+06					
Fossil				147,412	12,0584	1,43E+06					

Appendix III - Supplementary Table 3. *Cont.*

Fossil		147,424	12,1579	3,02E+06				
Fossil		147,542	12,1892	2,93E+06				
Fossil		147,306	12,103	3,81E+06				
Fossil		147,345	11,6679	2,39E+06				
Fossil		147,345	11,667	2,40E+06				
Fossil		147,698	12,3435	2,62E+06				
Fossil		148,216	13,0601	1,05E+07				
Fossil		148,064	12,862	1,86E+06				
Fossil		147,924	12,1069	1,36E+06				
Fossil		149,01	13,3615	808676				
Fossil		147,692	11,2304	1,09E+06				
Fossil		147,724	112479	1,25E+06				
Fossil		147,924	12,2787	9,70E+06				
Fossil		147,917	12,0997	2,03E+06				
Fossil		147,507	12,1735	3,74E+06				
Fossil		147,645	11,8443	1,46E+06				
Fossil		147,212	11,1336	3,43E+06				
Fossil		147,891	12,2979	2,20E+06				
Fossil		147,982	12,3151	1,41E+06				
Fossil		148,284	12,8794	1,46E+06				
Fossil		149,137	13,5574	1,42E+06				
Fossil		148,259	12,4964	2,19E+06				
Fossil		148,113	12,675	1,46E+06				
Fossil		147,525	11,3744	2,26E+06				
Fossil		147,563	11,4947	1,80E+06				
Fossil		147,622	11,7108	1,91E+06				
Mica clast					150,733	17,8309	105184	
Mica clast					149,767	16,2107	80313,2	
Mica clast					152,682	17,9995	92517,7	
Mica clast		143,987	9,26545	482470				155,298 16,2715
Mica clast					152,112	18,3915	305673	
Mica clast		143,896	11,1251	2,74E+06				
Mica clast								
Mica clast					149,892	16,2581	125263	
Mica clast					151,578	17,3694	141005	
Mica clast					149,008	17,0228	129583	
Mica clast		143,636	8,51843	133815	152,744	15,8381	147644	
Mica clast		144,655	8,02256	71458,8	152,844	142161	178976	
Mica clast					151,162	18,5717	269572	
Mica clast		144,06	7,62159	99767,7	152,266	14,1953	78292,8	
Mica clast		144,349	8,08032	189069	152,277	14,4594	83180	
Mica clast					151,572	17,4123	71062,3	
Mica clast		144,633	7,01784	40892,1	151,354	12,2784	44516,3	
Mica clast		145,406	7,41524	38546,1	153,923	13,8271	32693,7	
Mica clast		145,766	9,17852	62785,8				156,532 18,376
Mica clast		145,581	9,36284	123152				154,969 13,8707

### Appendix III - Supplementary Table 3. *Cont.*

Appendix III - Supplementary Table 3. *Cont.*

221276					204,152
78208,3					204,272
155088					203,38
568346					199,033
206407					203,986
422688					204,426
237863					203,834
59852					202,205
423238					204,457
315178					202,234
267556					202,472
356412					204,451
358886					204,926
341388					203,366
					203,997
					202,01
					203,481
					201,802
					202,889
					196,188
					201,165
					202,387
					202,577
					202563
					202,68
					202,597
					198,025
					203,584
					203,777
					202,388
					204,155
					203,164
					201,927
					201,932
					200,366
			194,677	16,003	1,30E+06
			195,83	17,9532	1,74E+06
					199,509
					201,69
			192,752	14,2648	568099
					205,252
					200,7
					201,308
					200,449
					200,133
					199,814
					199,689
			195,704	17,573	1,71E+06
					200,462
					201,795
					200,937
					199,759

Appendix III - Supplementary Table 3. *Cont.*

428908				194,768	15,6372	997517	199,523
							197,89
							201,932
							200,333
				195,499	14,6122	838113	206,989
							199,169
							196,408
							198,022
							200,162
							199,539
							196,39
							199,581
							198,955
							201,491
							200,135
							199,086
				193,63	15,2577	231814	206,892
							198,971
							197,124
							201,775
							197,136
							199,012
							198,861
							200,441
							196,116
				195,673	16,6932	406028	
				195,239	15,2435	357349	206,913
							200,878
							198,345
				196,192	17,0799	491065	
							200,753
				195,731	16,8904	463123	
							199,105
							201,344
				194,801	15,725	292789	206,55
							198,17
							200,221
							201,297
							199,448
							200,801
							199,573
							200,15
							199,931
							200,487
							200,796
							200,59
							201,358
							201,362
							201,72
				194,61	15,6909	250919	206,914
				194,614	15,6936	251172	206,926

### Appendix III - Supplementary Table 3. *Cont.*

### Appendix III - Supplementary Table 3. *Cont.*

Appendix III - Supplementary Table 3. *Cont.*

23,7015	595672					
26,6242	863007					
25,3653	1,92E+06					
7,67064	181133	207,971	13,8523	257286		
27,6476	1,23E+06					
29,7951	1,33E+06					
27,4871	1,39E+06					
26,9451	1,00E+06					
28,541	1,03E+06					
27,3712	898626					
27,2789	882731					
27,7892	1,25E+06					
26,562	1,15E+06					248,853 6,87918
27,2996	1,14E+06					
280545	1,02E+06					
28105	896602					
27,6338	1,17E+06					
26,3041	971591					
26,3309	1,00E+06					
17,7122	457998	207,93	24,5244	773341		
25,1787	1,17E+06					
26,9366	1,04E+06					
26,0854	1,23E+06					
25,3568	1,16E+06					
25,3227	1,06E+06					
24,4774	917625					
15,0941	495691	210,312	22,8186	483433		
27,2824	1,38E+06					
26,4551	1,27E+06					
28,1033	1,10E+06					
28,198	1,29E+06					
27,1942	1,53E+06					
27,9663	1,06437E+11					
26,3425	1,36E+06					
26,3758	1,07E+06					
6,86192	1,00E+06					
22,2767	1,60E+06					
21,65	1,54E+06	210,24	21,3422	953066		
18,6666	2,29E+06					
20,1044	1,10E+06					
17,8326	1,69E+06					
10,5115	1,39E+06					
11,1296	999136					
18,5282	1,33E+06					
20,3926	1,41E+06					
20,309	1,66E+06					
18,0398	1,63E+06	211,37	24,379	1,11E+06		
12,5576	1,10E+06					
25,5405	3,69E+06					
18,8818	1,45E+06					

Appendix III - Supplementary Table 3. *Cont.*

8,59094	831439	207,637	20,2425	735868			
13,6043	857127	209,009	13,7992	343324			
20,3729	1,75E+06	211,066	14,941	288571			
6,39844	876240						
17,7573	455309						
16808	1,62E+06						
15,9033	1,03E+06	209,091	21296	1,13E+06			
14,2192	1,25521E+11	213,364	14,1415	369142			
22,1542	167605						
25,7335	337891						
13,974	163831	209,179	16,3619	93116			
25,1609	307254						
22,3408	420930						
28,09	481870						
23,6903	258142						
24,3792	450757						
20,456	235883						
25,2173	600505						
131354	311564	209,391	159434	191320			
24,955	779715						
15,6501	330590	212,192	16,1625	149239			
22,3379	503151						
23,4882	614630						
22,8278	594269						
17,2967	411541	210,895	21,277	258878			
		209,268	20,4684	247632			
21,2118	444311						
18,6032	520605						
14,3767	463762	210,185	19,6523	293021			
		208,357	22,8675	447447			
23,2041	774445						
		209,449	22,132	357233			
22,9592	607650						
20,71	629281						
20,4217	306245						
15,4156	447922	210,116	21,1843	307515			
22,2956	798466						
11,707	477016						
24,2873	666398						
25,2013	1,21E+06						
24,7884	722637						
21,9453	727475						
21,2323	526621						
25,7282	867552						
20,1635	470148						
19,6079	684695						
19,5135	569016						
19,6213	571603						
23,6311	613287						
21,5916	232242						
21,5834	231962						

Appendix III - Supplementary Table 3. *Cont.*

22,2648	557536						
21,9997	174283	Supplementary Table 3. <i>Cont.</i>					
19,15	339058						
23,0246	296487						
22,8881	291058						
22,7004	635812						
11,4518	252449						
20,4718	334552						
26,3282	998225						
26,1357	948693						
27,2936	1,07E+06						
28,1942	1,32E+06						
14,5217	505252	209,916	20,6487	420263			
17,6056	489100	208,656	25,2359	596714			
17,6015	540470	210,447	24,903	452301			
17,3111	423220	208,106	25,6013	716131			
18,6817	561608	211,337	25,7693	483183			
17,5865	429892	207,49	24,6612	574781			
19,5168	533359	210,098	25,0247	373535			
25,4134	940716						
26,3827	1,10E+06						
17,0901	554017	207,394	24,8661	882368			
25,4133	1,17E+06						
17,7274	573787	208,747	25,9422	928866			
17,6628	444755	207,799	24,86	718371			
25,9501	1,12E+06						
18,2675	160687				214,725	10,9533	46688,3
		208,37	17,6206	122405			
		208,821	16,9517	41884			
					213,823	15,2889	185963
26,8719	741794						
19,0467	717765						
19,3825	797649						
18,5652	161098						
20,5955	219127						
		207,634	21,3382	69981,4			
		206,923	21,3558	145536			
25538	368321						
25,139	302189						
17,9605	131215				215,95	12,4967	54320,7
18,503	251433						
19,0323	206236				213,674	15,3909	101133
					216,416	14,1181	61221,1
					215,132	13,7382	43684,9
24,0655	195055						
16,873	137431						
13,3402	73743,3	211,806	16,5194	47156,5			
19,9734	245310						
17,1961	205042						
					213,087	16,3098	78678,2
					216,727	10,9123	57943,9

### Appendix III - Supplementary Table 3. *Cont.*

Appendix III - Supplementary Table 3. Cont.

	265,412	12,7868	310121					335,141	15,6045	32498,3
	264,946	13,2371	487300					335,476	23,215	137914
	264,749	10,9894	236232					333,614	19,3198	69031,4
	264,954	14,1911	359981					337,157	15,1413	33546,3
	264,503	12,5568	724732					332,593	24,1487	75584,9
	264,526	12,1684	320446	292,946	14,215	90829		334,411	26,4247	96109,6
	264,223	12,6456	595628					326,506	19,4612	208675
	264,394	13,542	764248					334,791	25,7842	105643
	264,89	12,7378	371506					338,234	20,3795	46184
	264,07	13,2508	549271					333,296	27,2531	79429,7
	264,34	13,5641	839266					337,151	28,9479	247986
	264,5	12,1883	351084					335,314	25,3101	259184
48568,7	264,186	12,415	479179					335,367	27,0433	211627
	264,328	13,0695	694401					335,523	25,0583	245515
	264,922	12,8448	382987					335,858	24,8548	182859
	264,559	13,6816	646670					337,415	24,1366	174093
	266,186	12,8096	350332					335,859	25,548	264846
	265,674	12,9506	370852					336,224	27,6572	269469
	265,81	13,3503	339323					335,357	23,4098	233928
	265,846	13,5259	423862					336,075	28,2393	208873
	265,219	13,7703	785347					336,229	26,9248	218878
	265,602	12,6034	273982					334,812	24,2735	243409
	265,563	13,3521	525588					336,193	27,8559	269824
	265,839	13,9439	491489					335,342	28,0491	238443
	265,956	12,4966	399185					336,451	25,9432	187618
	265,655	12,6491	382407					335,777	25,5413	232074
	265,76	13,4369	431163					336,668	24,6039	186904
	266,271	12,497	301748					336,652	22,1745	266627
	265,734	11,9221	267020					336,416	22,4907	181429
	265,693	13,6664	361710							
	265,727	11,5064	321202							
	265,892	12,8097	402441							
	265,912	13,554	285277							
	265,669	13,7905	636733							
	265,661	14,3544	526592							
	263,821	15,9306	2,28E+06							
	262,729	13,5881	2,08E+06	274,084	28,9776	532500				
	262,774	15,8782	3,29E+06							
	262,579	15,9885	2,49454E+06	286,172	20,2367	377134	332,733	19,0847	216538	
	262,952	14,9529	1,85E+06	286,353	19,5884	395927	332,757	18,1749	248056	
	262,65	16,54	2,03E+06	286,245	21,3008	435190	333,012	16,7325	136516	
	263,279	14,9117	2,55E+06							
	262,744	14,4939	2,55E+06							
	263,197	15,9327	3,13E+06							
	263,274	15,7649	2,68E+06					333,617	19,9779	294221
	262,897	16,4839	2,74E+06	287,632	19,6602	494171	331,476	10,9017	97301,6	
	263,149	15,3097	2,79E+06							
	263,128	14,2941	2,53E+06	291,64	12,0634	462634	328,807	14,827	157344	
	262,97	15,6462	3,07E+06							
	263,169	16,4352	2,50E+06							
	263,725	14,4813	2,46E+06	289,293	16,0648	548490				
	262,942	16,8703	2,93E+06	287,279	18,5794	386701	331,448	9,02867	70404,7	

Appendix III - Supplementary Table 3. *Cont.*

262,837	15,1142	2,79E+06		275,359	30,8961	598696	332,198	15,2752	144795
263,772	14,6592	3,39E+06		286,692	18,9246	261584			
263,398	15,502	3,00E+06							
263,373	14,4515	1,47E+06		283,681	19,0219	534597			
263,824	15,5917	2,21E+06		287,949	14,6095	37767			
263,112	16,0175	3,76E+06					333,231	14,9565	164459
263,255	15,8953	3,51E+06							
263,556	14,1321	1,94E+06							
263,418	15,1449	3,51E+06							
263,232	15,0221	172177							
263,798	15,1178	266701					336,347	12,5235	24524,3
263,925	14,6055	273386					332,371	22,5262	58652,1
263,919	13,2795	230520							
263,315	14,1314	522214							
263,447	12,6128	172026							
263,909	14,0567	312410					333,159	19,8767	46013,4
263,453	15,7487	494501		289,339	12,7638	100002	331,463	12,0149	33576,1
263,738	14,4997	703119							
263,136	14,6422	543012		283,629	17,3276	112931	331,812	23,9132	90593,2
263,122	15,0842	510284							
263,45	12,9922	417006							
262,987	14,0406	559386							
263,361	14,9016	718062							
263,774	15,183	669074							
264,458	14,574	715312							
264,263	15,1154	662148							
263,919	15,1199	742464							
264,633	14,1726	645059							
264,382	16,0441	564164							
264,485	15,808	554264							
264,599	14,8232	643892							
264,916	14,733	583092							
264,111	14,5708	624860							
263,976	15,1372	756067							
264,502	14,4467	498153							
264,831	14,8868	625051							
264,363	14,007	526961							
264,392	15,9305	696922							
264,981	14,5628	446348							
263,186	15,2099	690121							
263,584	14,1231	451165					336,101	28,9858	224281
263,614	15,0805	723185							
264,288	15,0713	624633					335,522	18,797	82131,2
264,184	15,0934	737911							
264,087	14,9721	468880					335,938	26,5568	187407
264,353	13,9734	523318							
263,911	14,7742	631188							
264,133	14,8852	604493							
264,134	15,0457	599808							
264,727	15,4245	485930							
263,871	15,6302	736114							
263,871	15,63	736182							

Appendix III - Supplementary Table 3. *Cont.*

	264,359	14,84	632640					333,697	18,8017	81240,4
	264,702	14,4468	535243					332,379	15,3212	61402,2
	264,318	15,3557	514133					332,195	15,8242	64732
	263,515	19,091	337012	292,009	10,9952	82233,4		334,654	21,1887	166268
	263,528	19,2049	349375	292,052	11,1602	96529,1				
	264,621	14,7725	512857							
	264,533	15,8714	336414							
	264,121	15,2076	576902							
	265,261	13,7935	367250					335,847	29,5284	275650
	265,291	14,2319	430196					336,798	29,8178	228455
	265,383	13,201	347271					336,761	25,5609	181126
	265,194	12,5667	357824					336,003	25,0681	171668
	265,337	14,6894	353894					333,777	22,4846	156166
	265,417	14,8149	498018					334,923	25,4455	206694
	265,215	14,6254	362782					336,12	26,9985	247874
	265,81	14,865	347518					336,92	28,2517	246593
	265,804	13,2903	250143					338,078	29,6671	388921
	265,428	14,6037	416761					335,508	27,6364	203908
	265,223	13,4252	443038					337,687	27,2741	146893
	265,745	14,3055	326492					337,296	28,7692	270035
	265,573	14,3836	394499					336,621	29,048	315875
	265,079	14,8503	485980					338,391	33,0761	327495
	265,136	14,2134	497559					335,681	29,8789	324906
	265,538	13,7774	404167					335,68	25,3994	238242
	265,208	13,8146	427687					336,032	25,28	190854
	265,158	14,2746	459275					335,493	28,2154	267989
	264,102	13,2507	296954							
	261,138	18,801	865957							
	262,516	13,9018	320697							
	262,541	14,3652	1,86E+06							
	263,545	14,018	1,54E+06							
	263,65	13,8108	1,94E+06							
	264,072	14,0012	1,78E+06							
	263,748	13,4748	508709							
	263,478	13,4887	479977							
	263,602	14,003	279302							
	264,231	13,2718	397422							
	264,023	13,6773	327641							
	263,801	13,4623	425099							
	264,047	13,3957	463603							
	263,574	12,3827	435576							
	264,823	13,4297	616335							
	262,761	15,2648	780756							
	264,794	13,6474	608281							
	263,641	14,0036	579100							
	264,065	13,601	571053							
	264,444	14,4523	446146							
	264,906	13,177	558117							

Appendix III - Supplementary Table 3. Cont.

Centre	Width	Area	Centre	Width	Area	Centre	Width	Area	Centre	Width	Area	Centre
355,889	3,49353	51915										409,509
355,914	4,52351	176453							399,728	16,896	346458	
355,411	4,31725	181407				393,751	5,34719	203710	401,916	7,80401	214042	
355,695	5,04445	143014				393,846	4,33454	31420,4	400,444	19,361	427124	
355,488	5,13557	434421				394,07	4,98878	140382	402,148	6,66006	154726	
355,955	5,10676	443393				394,665	6,74515	167368	402,462	6,0507	105429	
355,965	5,02415	274322				394,41	4,98655	110460	401,873	8,66913	154587	
355,942	4,50716	92218,9							405,597	26,6549	519066	
356,07	4,38841	180108				397,829	12,0513	350156				
356,041	4,76587	175787							401,39	19,3673	390103	
355,81	2,96101	37020,6										
355,89	4,56834	258829							399,444	18,7382	468033	
355,753	5,17038	653831				394,246	4,72609	262724	402,25	4,98703	114101	
355,535	5,48499	304636				393,981	5,58235	137555	402,416	7,51174	178929	
355,871	5,12673	231191				394,561	7,1528	228967	402,841	7,70912	171210	
355,903	4,75401	245188				394,137	3,83197	56814,2	400,036	13,2033	243706	
356,218	5,03573	93428,8							398,604	29,7799	2,35E+06	
356,131	4,71558	214193							398,432	19,8882	670852	
355,965	5,41636	244343				396,68	18,6402	940376				
356,034	5,40554	159496							398,235	18,1789	480381	
356,066	4,94383	64459,5							398,233	25,8332	1,03E+06	
356,019	5,25519	203533				393,56	10,1019	364546	401,465	11,7928	312464	
356,069	5,01472	149714				393,998	7,95347	306508	402,293	10,7703	229659	
356,621	5,07934	38240,1							398,294	14,0625	98100,7	
356,58	5,58166	84886,2				396,455	7,441	36669,4	404,104	4,8689	21975,2	
									398,948	14,2742	63045	
356,816	5,39939	52559,8							398,489	12,6555	53819,2	
356,732	6,1443	79549,1							398,822	11,7422	49255,1	
356,579	6,15047	79752,6							398,822	16,4678	74210,6	
356,251	11,5599	95143,1							398,103	21,9506	185455	
									398,567	20,1211	149482	
356,155	3,71682	25117,1							399,138	15,254	76595,8	
356,805	5,24432	29782,5							397,618	18,8559	179948	
356,859	4,57764	25892,2							398,239	17,8153	110764	
356,723	5,54879	32906,3							397,888	14,2322	92659,9	
356,093	10,5524	84308,4							397,227	17,7144	128528	
356,933	4,73663	29281,7							398,354	14,6096	87278,6	
357,199	5,7023	64735,6							397,952	13,2134	60907,7	
356,659	5,32206	73822,2							399,422	14,6777	54365,5	
356,346	6,56266	42665,8							403,83	22,1886	99741	
357,529	4,861	24014,8										
356,679	7,84245	138169				395,039	9,08374	90315,5	403,241	5,89657	26226,4	
356,563	4,99627	55929,7							397,164	11,7298	58123,9	
356,638	4,62176	28214							398,969	18,601	105262	
356,718	5,04061	38008,3							398,871	15,3735	77804,2	
356,711	3,74527	26984,7							398,205	16,0815	99503,5	
356,92	5,58297	45575,1										
356,728	6,09629	117087							396,537	12,5416	82210,6	
357,022	4,95143	27140,1							397,657	15,5597	115158	
356,68	5,359	47593,1							398,877	17,1759	122034	

Appendix III - Supplementary Table 3. Cont.

357,035	4,83082	19112					396,195	19,1009	227504				
356,834	5,1544	40977,3					399,199	15,067	76656,7				
356,962	5,13838	27503,9					396,42	22,9779	756228				
356,543	5,24531	62974,5					400,399	15,0546	55763,2				
357,051	5,45727	58635,1					401,655	17,0169	92184,5				
357,029	5,82307	42418,3					398,705	12,9674	82831,7				
357,251	3,74974	17207,3					403,103	22,9325	84996,4				
356,432	5,0904	69015,8					401,758	11,2894	54292,9				
356,935	4,7608	29787,6					399,411	13,6182	71188,8				
357,245	4,90393	25450,1					404,587	24,3554	89589,3				
356,659	5,35908	69169					396,415	14,2266	82153,9				
356,418	5,92292	68158,6	368,338	11,9132	85862,1		399,296	19,5339	139363				
356,799	4,52891	23632,6					398,235	15,0278	93213,6				
356,672	4,91375	49533,4					397,596	14,195	75639,6				
356,647	5,94936	24000,4					399,149	14,6049	48520				
							396,721	14,9408	113919				
							396,235	16,0869	96193,6				
357,56	5,25614	24521,9					396,544	16,9973	150540				
357,527	5,80503	38119,7					395,611	15,001	90503,5				
							396,959	15,6631	91641,8				
357,687	4,91545	28449,8					396,886	15,0231	103871				
358	4,83318	32751,4					396,447	14,5027	97162				
357,536	5,73723	32837,7					395,891	18,8113	321571				
358,028	4,07532	18810,9					396,797	18,1548	205137				
							395,515	18,2624	250309				
							396,055	19,611	475932				
357,666	6,37816	79239,4					395,264	16,1052	118508				
359,147	20,2535	213502					395,368	21,359	343919				
357,74	6,50294	49231,7					394,929	17,7274	102631				
357,111	5,37095	52818,5					396,153	12,0458	70962				
357,035	4,30099	34961,2					396,153	18,0691	230698				
357,59	5,61324	2263,7					395,704	14,4761	95105,3				
358,066	4,65532	23029,6					396,469	13,537	106416				
358,081	4,75838	23913,4					397,58	14,4219	81860,7				
							395,378	28,9054	6,23E+06				
355,756	5,57802	151514	383,412	6,74617	24273		394,628	4,79157	41998,1	399,217	19,0038	532500	
356,334	4,8066	48154,2					396,102	26,7119	1,53E+06		398,55	25,837	791370
							395,795	23,7574	1,56E+06		398,674	25,1461	473197
							396,429	23,611	1,51E+06				
							395,63	28,3018	5,35E+06				
							395,47	25,5513	2,15E+06				
										399,646	27,6822	1,31E+06	
										398,749	33,5691	1,39E+06	
356,791	4,86017	56945,7								397,183	20,5013	538158	
356,605	4,88473	93150,3								402,264	23,1848	887277	
							397,082	28,811	1,94E+06				
							396,143	28,665	2,80E+06				
356,193	5,41441	201089								398,937	18,6546	615198	
							397,643	31,0336	1,70E+06				

Appendix III - Supplementary Table 3. *Cont.*

356,192	5,4995	102988		397,018	28,9493	3,83E+06	404,634	38,9512	1,32E+06
				396,209	22,059	1,04E+06	404,587	44,4859	2,06607
356,097	5,51839	111966		395,37	29,0534	6,07E+06			
				396,515	27,4164	2,07E+06			
355,375	4,51118	33733,2		397,606	24,7608	800824			
				398,139	27,4118	1,15E+06			
355,375	4,51118	33733,2		396,183	24,8303	189823			
				398,771	20,2741	53332,8			
355,375	4,51118	33733,2		395,311	21,9236	192143			
				395,593	20,9421	211213			
355,375	4,51118	33733,2		395,474	17,1567	60449,2			
				398,174	25,352	151270			
355,375	4,51118	33733,2		397,558	24,5831	242338			
							401,946	23,0556	95987,9
355,375	4,51118	33733,2					398,588	17,3042	69531,4
				395,739	19951	528944			
355,375	4,51118	33733,2		395,772	20,6283	237081			
							398,275	27,2164	399039
355,375	4,51118	33733,2		396,14	24,6953	311739			
				397,911	19,0289	122542			
355,375	4,51118	33733,2		397,88	23,3038	257571			
				397,562	22,4799	206460			
355,375	4,51118	33733,2		397,261	21,8096	193652			
				397,154	20,1485	387117			
355,375	4,51118	33733,2		396,586	20,4397	314623			
				396,314	22,0991	431727			
355,375	4,51118	33733,2		397,201	16,0867	178456			
				396,746	17,848	221760			
355,375	4,51118	33733,2		396,931	20,1091	182898			
				399,728	26,5095	213151			
355,375	4,51118	33733,2		396,256	21,488	309343			
				399,061	16,6951	108630			
355,375	4,51118	33733,2		397,518	21,1519	390510			
				395,87	18,8116	305970			
355,375	4,51118	33733,2		395,911	25,5928	1,93E+06			
							396,514	20,6881	205712
355,375	4,51118	33733,2		395,069	18,6319	276505			
							400,529	30,1144	371872
355,375	4,51118	33733,2					395,914	21,9243	315328
							397,809	23,4934	419105
355,375	4,51118	33733,2					396,931	13,1337	65627,3
							396,572	21,8837	298028
355,375	4,51118	33733,2					396,081	18,6539	307692
							396,395	22,9945	720527
355,375	4,51118	33733,2					396,396	22,8137	730427
							397,408	19,6754	162203
355,375	4,51118	33733,2					398,343	24,7933	157194
							398,354	24,8083	157115

### Appendix III - Supplementary Table 3. *Cont.*

Appendix III - Supplementary Table 3. Cont.

Width	Area	Centre	Width	Area	Centre	Width	Area	Centre	Width	Area	Centre	Width
31,9514	946554										464,479	8,62327
		415,68	3,9553	21742,8							464,682	8,89728
		412,032	7,80401	99554,7							464,56	9,12906
		415,935	0,315133	72879,9							464,738	9,07281
											464,913	8,83434
											465,002	8,9255
											465,223	9,00141
											464,982	8,97221
		414,525	12,0513	194057							464,977	9,81016
		413,778	47,1382	2,55E+06							465,206	8,89985
		411,341	44,2076	1,96E+06							464,719	10,0053
											464,787	9,62975
											465,125	8,96922
											465,164	8,52029
		412,565	9,81497	92705,4							464,918	8,89892
		412,444	9,23122	78552,1							465,085	9,04868
											465,056	9,05219
											464,704	9,94781
											464,645	9,31386
											464,835	9,55204
											464,319	9,63952
		417,159	7,32105	64726,6							464,588	9,93165
		413,494	8,28161	55037,3							464,978	9,40589
											464,945	9,31457
											465,723	9,8279
											465,993	9,31123
											465,819	9,5294
											465,996	9,49659
											465,94	9,25714
											465,826	9,57434
											465,902	9,35867
											465,744	10,4713
											465,835	9,7227
		414,915	8,08561	16259,8							465,54	10,3368
		411,524	3,40319	28894,1							465,968	9,68822
											465,672	9,65639
											465,667	9,25352
											465,811	9,92538
											465,988	9,58306
											465,841	9,73749
											465,988	9,19026
											465,901	9,45372
											465,649	9,48915
											465,623	9,8657
											465,529	9,56521
											465,709	9,76732
											465,963	9,57098
											465,484	10,1432
											466,021	9,18216
											465,296	10,3977
											465,583	10,0747

Appendix III - Supplementary Table 3. *Cont.*

				465,876	10,3408	
				465,701	10,2472	
				465,417	10,3069	
				465,659	9,772	
				465,899	9,37688	
				465,544	9,86933	
				465,812	9,68059	
				465,946	9,43789	
				465,914	9,95013	
				465,372	10,0983	
				466,149	9,25376	
				465,726	9,71185	
				465,711	9,80136	
				465,827	9,45926	
				465,798	9,59705	
				465,456	9,79717	
				465,979	9,84981	
				465,846	11,1683	
				465,872	10,1144	
				465,55	10,6115	
				465,801	10,228	
				465,659	10,5326	
				465,93	9,49574	
				465,738	9,67809	
				466,191	10,1291	
				466,016	10,1615	
				465,878	10,8145	
				465,958	9,85783	
				465,975	9,5005	
				465,872	9,66967	
				465,864	9,67719	
				465,942	10,0497	
				465,836	10,0649	
				466	9,55227	
				465,811	10,4932	
				463,587	10,9631	
				463,401	11,1777	
				462,975	12,5986	
		436,269	41,5968	2,58E+06	462,778	12,122
					462,86	11,6857
					462,564	13,273
					463,335	12,2357
					462,836	12,3969
					462,829	12,4273
					462,784	14,2141
					463,182	11,8856
					463,246	11,9426
		434,187	45,2047	1,41E+06	463,634	11,8134
					462,976	12,9354
					463,012	11,1541
					464,216	10,5454
					463,166	11,5633

Appendix III - Supplementary Table 3. *Cont.*

				463,535	11,8711
				463,806	9,68871
				463,317	12,5046
				463,459	11,0581
				463,591	10,9631
	423,446	61,107	3,54E+06	462,984	14,7846
	437,306	40,0207	2,07E+06	463,434	11,5886
				464,064	10,0988
				463,54	11,4696
				464,52	10,4475
				463,61	9,23315
				463,674	9,64856
				463,927	11,0844
				463,834	10,1056
				464,219	9,53409
	445,137	38,1169	471526	464,015	9,75338
				463,673	10,6371
				464,143	10,0131
				463,414	10,0542
	448,045	37,5322	208158	463,93	9,81997
				464,016	10,1102
				463,368	11,3994
				464,026	10,2334
				463,243	14,9177
				464,9	11,1144
				464,713	11,4137
				464,59	11,1396
				464,24	13,7022
				464,456	12,3675
				464,263	12,5286
				464,688	12,3324
				464,062	12,6936
				464,463	11,831
				464,427	11,9918
				464,392	12,2897
				464,286	11,2842
	444,545	34,5268	558453	464,741	10,9253
				464,1	12,5539
				465,402	11,0983
				463,832	12,8257
				463,544	12,1457
				463,896	11,1186
				464,216	13,725
				464,629	11,3426
				464,085	11,9751
				464,508	11,689
				463,086	13,1535
				464,887	11,5215
				464,882	11,4625
				464,685	11,1793
	431,654	49,1742	241655	464,626	13,1883
	431,847	49,5397	244466	464,634	13,2286

Appendix III - Supplementary Table 3. *Cont.*

					464,958	12,107			
					464,514	13,695			
					464,917	11,6239			
					464,159	12,121			
					464,129	12,6619			
					463,828	14,0743			
					464,135	10,2795			
			439,292	42,8162	968432	464,452	15,7025		
			444,749	19,1645	81321,6	465,304	11,7653		
					453,742	35,991	170262	465,546	10,5907
						465,522	10,5374		
						465,151	10,8099		
						464,052	12,5086		
						464,919	13,7998		
						465,307	11,6487		
						464,822	12,5947		
						464,748	12,751		
						465,284	11,6533		
						465,46	12,9664		
						464,892	15,188		
						464,517	14,321		
						464,866	12,6472		
			448,521	31,9404	509787	465,074	11,7181		
						465,225	11,3288		
						465,327	10,6731		
						464,809	12,0987		
						464,284	8,33084		
37,1431	119611					464,057	10,2562		
31,6316	1,50E+06	412,729	22,5373	344399		464,609	8,78708		
26,2933	890193					464,388	8,98039		
36,9721	1,35E+06					464,615	9,98227		
39,601	242090					464,474	10,6276		
31,6812	116598	412,563	37,1739	237234		464,055	12,82		
						463,854	8,44389		
						464,575	9,47502		
						464,551	9,14715		
35,6341	154099					464,372	9,80142		
37,3196	406816					464,47	9,88845		
46,6493	368197	412,555	42,0783	139593		464,648	9,12042		
45,4773	537680					465,477	11,177		
39,0578	477965					465,475	9,34829		
33,4075	107047					465,283	9,61069		
40,3331	641282					465,331	9,59011		

Appendix III - Supplementary Table 3. Cont.

Area				Centre	Width	Area	Centre	Width	Area	Centre	Width	Area
3,32E+06												
7,19E+06	477,065	13,3325	675987				508,925	11,168	646611			
6,92E+06	478,082	11,7374	619575				507,472	7,91711	577667			
6,25E+06	477,576	11,3121	778257									
1,07E+07												
1,33E+07							509,176	10,3621	566086			
1,19E+07							509,873	12,5587	219308			
4,74E+06							509,494	11,2474	667868			
8,00E+06												
7,05E+06												
1,77E+06												
3,02E+06							509,573	10,2361	336333			
8,43E+06												
1,78E+07							509,336	11,6823	182260			
8,97E+06							509,604	9,93471	301420			
9,35E+06												
1,03E+07							509,775	3,76665	13239,7			
5,29E+06										510,971	12,9794	845727
7,36E+06	476,18	12,8965	891407									
1,04E+07												
6,73E+06	474,054	14,3493	587523									
3,16E+06	478,704	10,1045	714837				508,233	8,75707	714900			
1,04E+07										511,504	13,748	523553
7,34E+06												
2,01E+06												
2,40E+06												
662354												
1,85E+06												
1,99E+06												
2,21E+06												
1,36E+06												
730319												
1,10E+06										510,927	9,05095	32211,4
1,21E+06												
1,51E+06												
1,20E+06	479,509	13,7717	171815									
2,29E+06	477,782	17,9658	266456									
1,61E+06												
1,75E+06												
1,85E+06												
1,28E+06												
1,08E+06												
2,39E+06												
1,81E+06												
1,35E+06	478,522	13,628	156180							511,234	14,6632	289977
1,50E+06												
1,50E+06												
1,85E+06												
2,71E+06												
1,46E+06												
1,37E+06												

Appendix III - Supplementary Table 3. *Cont.*

1,33E+06								
1,77E+06								
2,09E+06								
1,44E+06								
1,94E+06								
2,42E+06								
1,91E+06								
1,14E+06								
1,95E+06								
1,51E+06								
990412								
2,23E+06								
2,14E+06								
1,52E+06								
1,75E+06								
991567								
1,05E+06								
693782								
873414								
1,02E+06								
766664								
1,27E+06								
1,01E+06								
867301								
845189								
602042								
502795								
1,59E+06								
1,11E+06								
1,05E+06								
1,62E+06								
1,46E+06								
751356								
1,06E+06								
942943								
3,56E+06								
5,87E+06	476,053	10,4403	406015		508,886	7,99887	141123	510,172    14,8883    1,41E+06
2,93E+06								510,095    13,651    411018
1,47E+06	476,134	8,69238	92501,6		509,69	13,3209	419759	
1,86E+06	475,858	8,1921	129964		509,241	13,7352	723607	
1,08E+06	477,026	8,1907	220173		508,519	11,2447	436567	
4,99E+06								510,702    12,3213    406808
2,96E+06								
1,22E+06								511,412    19,4684    1,11E+06
1,68E+06								
1,03E+06	476,3	7,93874	129099		509,353	12,6412	501231	
2,41E+06								
6,56E+06								
1,06E+06								511,322    17,6728    734025
658188					509,915	16,836	1,18E+06	
8,28E+06								
943169	476,364	8,40452	126378		509,899	14,9364	780838	510,08    11,3411    812262

### Appendix III - Supplementary Table 3. *Cont.*

Appendix III - Supplementary Table 3. *Cont.*

384097						
594947						
110998						
113715	479,195	6,91007	24955,9			510,193
116343	479,311	7,22473	27965,5			509,976
408063						11,7376
103049						11,5529
231623						189272
732191						186424
628931						
965862						
1,57E+06						
474798						
626473						
455403						
662790						
517482						
521475						
532289						
632022						
745902						
863892						
490674						
1,06E+06						
1,05E+06						
740168						
102241						
160543	478,808	7,66628	73377,7			508,231
884470						9,79608
536653						189093
608616						
122230						
70670,5						
33092,4						
122797						
339658						
103659						
100530						
305963						
157983						
30346,5						
131321	478,102	8,51421	13799,8			509,813
160032						8,11831
						20814,2
						509,452
						9,62617
						43746,3
						508,864
						6,4196
						10574,9

### Appendix III - Supplementary Table 3. *Cont.*

515,2	17,5401	495203					
514,94	10,0627	377930					
			519,487	23,66	659096		
			517,27	20,1192	430540		
			516,12	13,9272	99009,7		
			524,66	15,2208	61217,3		
			522,329	21,2302	91195,4		
513,241	14,7452	331951					
			523,626	20,5683	67919,6		
			521,663	21,6068	108175		
514,087	13,8751	81326,2					
			523,254	19,7641	110921		
			520,527	23,4349	236559		
			522,247	28,8464	322248		
			523,337	24,4865	263012		
			521,245	23,4054	237137		
			519,095	20,9229	209202		
			522,937	21,5667	174688		
			520,683	25,8429	490875		
			521,662	28,2049	454533		
			520,151	24,6888	397881		
513,576	14,2118	313396	525,603	20,1221	302567		
			521,988	23,782	203545		
519,742	22,4767	292111					
			522,714	22,8085	126509		
			521,798	20,9897	116848		
			520,19	26,1212	382225		
			522,455	22,6457	171438		
			522,274	21,676	193639		
			520,86	22,4631	209965		
517,328	14,9607	108439	522,177	23,8419	1,48E+06		
			522,414	21,0234	467146		601,799
			527,107	31,3882	777413		609,075
			522,162	24,183	956127		
			524,14	28,4459	524065		
			522,055	20,3739	404160		
515,264	27,9261	4,07E+06	529,326	34,5752	1,30E+06		
			523,238	37,5897	1,35E+06		
			526,625	33,2881	1,01E+06		
516,394	24,5628	791768				548,342	51,7255
							1,90E+06
			528,126	31,0846	1,42E+06		
			524,698	33,0801	1,80E+06		
			527,851	37,6848	1,14E+06		

Appendix III - Supplementary Table 3. Cont.

			533,188	43,5923	703226						
			521,16	22,6832	889284						
			525,153	25,4951	289883						
517,627	24,8055	547214	522,423	24,0005	1,48E+06						612,479
			528,622	27,8559	588371						
			525,149	24,6735	663344						
513,156	13,8834	815115									
515,293	22,6182	648246				545,222	49,6118	1,30E+06			
			520,033	24,2152	108229						
			521,642	23,1007	47279,2						
512,601	16,6214	131473	529,142	16,8696	79016,3						
516,417	24,8557	228002				546,352	49,6868	292437			
514,489	18,4758	64947,2									
			525,713	25,1273	102144						
			521,55	22,6651	149473						
			518,951	18,3957	53659,5						
513,618	14,678	123724									
			524,141	239609	265123						
			523,157	19,9958	107678						
			517,742	21,8683	126678						
			516,291	24,1582	275955	547,145	48,8624	397162			
			522,185	26,8537	168792						
			523,656	38,7733	696674						
			522,321	33,0238	433320						
512,341	14,6657	107621	527,695	27,037	168600						
			525,93	25,4867	278961						
			520,491	28,8295	551480						
			518,334	25,5634	479728						
521,849	28,6415	329497									
			518,449	26,1518	378276						
			519,874	25,3826	238309						
			520,947	28,1074	253280						
			519,665	28,2616	418859						
			522,002	27,4138	220203						
			518,91	25,1279	375739						
			520,111	28,3482	482655						
516,509	27,2678	1,52E+06									
			516,331	22,3016	185958						
			519,726	24,3101	335916						
			519,095	23,718	144880						
			518,783	26,1438	391414						
			519,281	26,7334	291200						
			519,893	24,8926	209560						
			517,907	26,5665	409564						
			517,179	26,0281	508308						
			516,683	23,3549	696717						
			516,639	23,1323	706983						
512,436	16,8817	305089									
			520,844	28,9745	192140						
			520,847	29,0704	191867						

Appendix III - Supplementary Table 3. *Cont.*

512,183	13,0368	190777	521,231	30,7469	353060	546,418	43,2666	193530	
			526,064	21,1353	139908				
			519,34	29,2514	380123				
			524,896	25,8519	342264				
			523,951	23,5176	283409				
			518,901	25,0949	330499				
			517,714	30,0763	1,07E+06				
			518,629	26,2294	195002				
			521,13	24,7629	245530				
			521,638	25,6638	216324				
512,096	17,6269	382419	521,929	24,2884	173145				
			520,686	24,5266	240022				
			524,905	26,0597	550347				
			521,447	26,7581	325345				
			519,632	26,5731	478066				
			522,348	24,3157	234567				
			520,854	28,9398	404188				
			520,832	25,5777	289333				
			529,452	11,5585	108193				
			521,165	25,5428	263501				
514,703	13,433	211194	522,278	25,5875	264826				
			521,468	26,7763	350387				
			522,895	26,5866	304749				
			521,215	26,8074	359573				
			519,938	24,2897	252531				
			519,745	23,7821	292368				
516,781	20,7812	195952				549,34	49,3832	296858	
			527,13	34,0343	52785,5				
			523,981	32,9371	110157				
516,053	207481	69137,6				548,851	68,8367	456277	
			526,847	20,5371	38443,2				
			523,073	22,838	39654,2				
			530,065	44,4796	116701				

Appendix III - Supplementary Table 3. Cont.

Width	Area	Centre	Width	Area	Centre	Width	Area	Centre	Width	Area
	642,419	22,6514	310982					703,387	16,2969	2,38E+06
	644,606	26,8147	543167					703,163	15,8292	962352
	639,327	11,0479	247555	655,025	15,6341	139434		702,95	15,6341	1,06E+06
	638,984	7,24279	165875	648,125	25,3152	371981		702,923	16,4343	724484
	643,861	21,6694	202389					702,646	17,0406	1,18E+06
	638,827	6,19155	162153	647,614	15,0298	119972		702,816	17,0965	615719
	642,723	26,2307	351731					702,798	16,2647	699014
	640,97	25,8246	280006					703,696	16,6032	1,45E+06
	641,721	16,2507	340165					703,45	16,2507	1,44E+06
	639,929	25,8382	294509					703,116	17,5936	822466
	639,581	25,2696	507437					703,48	16,615	2,61E+06
	638,597	24,8214	652907					703,486	16,7496	2,47E+06
	640,5	24,0931	651280					703,131	16,3709	1,40E+06
	642,865	20,751	232262					699,6	15,1432	302681
	640,522	17,9196	283153					702,76	17,0832	1,22E+06
	639,535	23,2628	815404					702,873	16,339	1,16E+06
	641,886	22,3988	291647					702,84	16,6698	863265
	639,722	5,77075	273091	645,195	28,0287	598235		702,573	14,3568	725341
	646,358	33,2931	1,48E+06					703,406	14,8171	884101
	638,609	25,7161	3,51E+06					702,892	14,0336	446716
	639,14	31,2755	654639					702,599	16,1047	820931
	638,646	26,6794	1,69E+06					703,134	15,4903	447919
	639,414	26,4692	1,10E+06					702,754	16,3503	623669
	638,16	31,6711	828715					703,059	16,1863	966520
	642,228	26,2958	224048					704,317	15,9729	166986
	644,856	29,7496	164194					703,929	15,2006	137459
	647	27,7501	178223					705,441	14,591	263585
	642,965	30,1761	301565					704,538	14,5207	143765
	644,83	31,6785	154084					704,075	16,1589	192640
	646,68	33,7129	199790					703,859	15,2718	101925
	646,051	32,9784	196681					704,746	14,9854	228151
	642,06	25,0054	303163					704,107	14,2947	125004
	643,765	30,9884	328533					704,285	14,7429	178214
	643,838	28,2531	121459					703,985	14,7981	169742
	639,195	27,2874	1,25E+06					704,468	12,7366	103006
	643,53	32,332	291274					704,414	13,2576	65029,6
	644,96	34,9566	189781					704,144	14,3984	74492,7
	642,384	31,0979	335086					705,082	13,918	91276,5
	647,128	32,9981	241110					704,852	14,6689	132849
	645,692	31,8225	187291					704,53	14,3945	153377
	650,253	31,8279	190169					705,095	14,5226	236036
	646,489	32,1205	385547					704,71	15,3994	301080
								703,936	17,5493	86278,4
								704,653	18,0119	260243
	644,812	31,5174	309130					704,47	14,4349	118263
	647,686	33,4939	249898					704,116	15,2048	201229
	645,278	33,9021	413457					704,535	14,7755	208482
								704,248	16,517	160747
	647,679	33,9747	207996					703,853	15,4563	135672
	645,154	33,3557	358358					704,322	13,5503	145409
	643,818	32,433	278956					704,382	14,6789	174836

Appendix III - Supplementary Table 3. Cont.

		641,726	28,585	834396		704,756	10,8073	41147,7		
		644,261	32,1423	337044		705,078	14,7912	130156		
		643,115	30,6702	2,53E+06		705,245	10,8431	157043		
		639,801	24,9839	2,91E+06		705,081	12,2415	102344		
		643,632	31,0579	154220		703,889	15,4636	219921		
		651,517	29,0928	139114		704,149	16,5703	125324		
		647,791	34,0436	362033		705,103	14,9939	213099		
		646,968	33,4293	319570		704,848	14,5192	285719		
		646,147	34,6975	284460		703,944	13,5184	98351		
						704,281	16,4533	252401		
		645,532	28,7366	211063		704,618	14,4598	316057		
		646,628	31,0072	240649		704,707	14,0345	119356		
		645,489	32,1423	309960		704,379	15,2409	174432		
		646,621	36,1228	405746		704,398	15,1352	285632		
		644,726	28,765	279460		704,156	14,2035	125733		
		646,512	31,5567	260540		704,737	14,4413	250279		
					648,793	34,9949	589002	706,148	12,4693	106822
					648,104	34,9383	636261	706,093	12,8382	131215
					645,802	34,3099	815881	705,209	14,0179	195818
					648,618	35,7153	641112	705,988	14,8032	183611
					647,242	36,218	625037	704,971	14,8757	251273
					648,263	38,1241	707124	705,551	11,7501	82829
					650,15	37,8136	742514	706,154	13,0412	191510
		642,396	25,8067	1,12E+06		705,54	13,9778	162627		
					646,054	34,4366	917162	706,241	13,752	179949
					644,205	31,6171	1,17E+06	705,91	11,8466	131168
		641,315	26,63	2,64E+06		705,909	11,0104	129906		
					649,366	38,6754	925993	706,409	11,4308	97287,1
		639,071	21,1956	514568	657,185	32,678	508298	706,13	14,1246	174420
		640,035	17,2431	304602	658,747	26,6467	304051	705,482	12,9481	131958
					649,452	38,1285	608244	705,965	12,8619	85943,5
		639,469	21,0809	547024	659,275	28,4054	507743	705,511	13,3714	154647
					648,102	36,1021	643449	706,787	9,35717	53100,1
					649,56	36,5732	719645	705,558	14,8864	265182
					649,241	36,3243	719489	705,535	13,7828	188360
		636,629	28,3823	1,66E+07		703,262	13,5782	614064		
		636,998	26,2243	811168		701,977	18,8654	1,04E+06		
17,8056	25199.5	636,247	36,3524	3,39E+06		701,547	13,8571	558504		
18,6495	186408	633,75	21,5689	630288		702,156	24,5441	1,89E+06		
		637,141	32,7475	6,29E+06		702,21	12,0287	348169		
		639,631	31,0942	879355		701,618	18,1063	760261		
		636,597	28,3363	3,52E+06		701,856	16,4365	742766		
		635,396	30,7567	1,08E+07		702,574	14,9094	603447		
		635,392	27,5609	4,88E+06		702,436	19,597	1,38E+06		
		637,227	24,2247	1,63E+06		702,439	18,908	1,03E+06		
		636,298	27,7774	1,39E+06		702,051	18,7244	1,08E+06		
		635,845	17,4244	501380		702,292	26,6537	2,90E+06		
25,7853	666573	635,497	32,0728	1,25E+06		701,751	16,5232	845409		
		637,009	30,3842	3,04E+06		702,034	16,7332	792274		
		635,688	29,4735	4,55E+06		702,725	17,0456	766514		
		638,473	25,7832	1,85E+06		702,185	16,4503	838178		
		636,794	27,0555	2,19E+06		702,038	18,0861	1,05E+06		

Appendix III - Supplementary Table 3. Cont.

23,3371	253424	638,161	19,9321	1,07E+06		702,007	18,4674	1,35E+06		
		637,153	27,9743	8,54E+06		702,742	13,9261	790646		
		635,677	27,1867	1,72E+06		702,105	18,4056	993686		
		636,717	28,7069	3,04E+06		702,117	15,5522	422080		
		636,638	28,4677	1,66E+07		703,202	13,4001	597656		
		637,083	20,3796	604060		701,841	20,2701	1,64E+06		
		633,5	31,2443	3,34E+06		702,565	19,5151	1,48E+06		
		638,228	28,5423	1,40E+06		702,401	15,9899	663896		
		636,217	23,1975	1,35E+06		702,266	20,9382	1,91E+06		
		639,357	27,9553	327197		703,932	12,4146	42915		
		643,877	33,6694	208949		702,915	14,3843	89588,7		
		636,87	22,9543	619221	655,953	22,186	115525	703,798	12,9897	70763,8
		644,469	29,1625	248426		703,257	13,165	80407		
		639,382	23,8053	399825		703,044	16,6464	263410		
		637,386	19,1681	104569	655,74	25,5635	91198,3	703,27	13,3177	53692,6
		638,295	17,9779	204204		703,747	16,9327	142259		
		639,034	25,2235	363460		703,134	16,7246	201390		
		640,814	24,3918	195984		703,156	16,3668	281124		
		637,702	25,061	1,34E+06		703,216	20,2954	415210		
		637,078	23,167	585820	656,217	21,4481	98631,3	703,09	14,4593	143829
		638,004	29,1643	791308		703,085	13,8737	111310		
		638,938	23,8005	447491		702,315	14,72285	153061		
		643,567	32,7973	371919		703,075	17,1465	303848		
		641,007	27,331	425593		703,984	15,8265	159750		
		640,542	27,7796	405908		703,892	14,9646	245625		
		640,198	31,1604	566858		703,686	15,8665	226534		
		642,213	32,4674	622651		703,544	14,686	192986		
		640,207	26,5737	717629		703,774	16,1394	226775		
		640,107	31,5988	1,97E+06		704,443	16,3411	164499		
		644,234	33,6017	694860		703,768	12,0771	106124		
		643,425	33,1989	671739		704,193	13,9331	190803		
		641,842	32,4255	597041		705,14	14,7303	155611		
		641,747	30,7099	332438		703,448	14,5953	176630		
		640,618	29,6217	1,07E+06		703,9	16,5857	233418		
		643,178	31,4702	346193		704,853	14,2197	139687		
		638,502	27,3405	1,48E+06		704,22	15,4421	196436		
		643,912	34,3905	866544		704,993	13,9964	147990		
		638,824	30,5369	4,32E+06		704,186	13,2432	151402		
		640,922	28,4329	377032		704,549	9,72333	74807,8		
		644,783	37,2009	1,03E+06		702,868	16,3695	232731		
		640,778	28,675	391330		704,511	12,8663	124514		
		641,659	34,8321	1,11E+06		703,194	15,2865	248670		
		639,226	23,9178	348619		704,16	13,6566	159166		
		644,387	27,6368	217529		703,789	17,4738	387065		
		639,362	26,1278	729945		704,629	15,9142	171200		
		638,402	23,3947	594034		704,711	16,1305	194232		
		639,682	28,1026	1,69E+06		704,635	19,8493	380232		
		639,679	28,0378	1,69E+06		704,277	12,7413	112856		
		640,492	30,8006	594482		704,282	12,757	112558		
		640,67	28,2855	275297		704,141	11,3832	76085,7		
		640,67	28,2914	275390		703,022	15,8167	217934		
						703,022	15,8176	217955		

Appendix III - Supplementary Table 3. Cont.

	640,775	25,4713	530596		704,233	14,7618	188971		
	639,229	24,8946	572686		704,396	15,3721	135755		
	639,573	22,6281	442309		704,509	17,8323	246187		
	639,269	19,9499	240193		704,266	19,992	183548		
	639,341	20,23	243190		704,282	19,6522	175709		
	640,726	19,5998	267637		705,108	17,4348	247169		
	637,885	26,2114	1,36E+06		705,547	17,316	155132		
	636,826	25,1704	324954		703,927	18,5708	246240		
				648,519	38,4451	702696	705,768	14,8901	173137
				652,271	40,6505	596403	705,905	14,9727	180749
	646,889	37,9295	562216		705,863	13,2048	110194		
	640,511	32,8211	2,08E+06	647,876	37,5215	623681	705,306	12,33	84412,8
				647,732	38,0729	771153	706,225	9,65633	81607,5
				644,12	37,1366	1,09E+06	704,864	12,1459	95350,6
				648,981	38,1533	738624	705,479	10,86	85822,1
	637,012	21,1455	454904	656,16	31,3044	585116	706,216	8,87	116983
	636,536	21,8926	356795	655,533	27,4994	464953	705,908	11,5964	111120
				647,16	38,2599	567963	705,364	13,5248	145981
				650,091	39,4557	718719	705,837	13,6471	87778,8
				650,208	39,387	712942	705,563	12,7227	144268
				647,277	37,4323	815819	705,394	12,1203	143698
				648,016	33,5944	292007	705,767	15,357	224032
				646,78	39,2955	1,05E+06	705,594	12,531	110799
				645,873	39,532	915460	705,45	11,9676	106297
				648,321	39,5429	852871	704,803	14,2282	152219
	641,397	31,5941	102219		702,739	15,5949	110334		
	642,059	26,8572	108554		700,834	18,4608	233869		
	644,842	29,0308	60348,7		702,168	14,0674	129047		
	638,22	15,3056	320571	650,635	5,97176	16349,8	701,182	16,8161	773499
	639,361	10,9786	192830		701,946	15,9546	799741		
	638,032	26,0442	1,09E+06		701,931	15,9984	711123		
	639,681	24,7712	449498		702,469	15,8912	708406		
	640,813	28,1334	118348		702,676	15,1473	183032		
	645,101	31,2358	106331		703,082	15,3217	164365		
	643,229	25,2838	78975,9		702,939	14,738	98988,8		
	643,992	31,203	120177		703,418	16,0763	227930		
	646,336	302869	152494		703,639	14,973	116306		
	646,335	32,6513	132540		703,307	15,1793	177501		
	639,174	29,3056	122191		703,141	16,3401	236292		
	640,196	26,2046	110536		703,206	15,8615	176633		
	641,823	28,0437	160821		703,904	15,7078	252073		
	639,763	24,9976	61832,2		703,363	16,0867	226059		
	638,6	21,8103	95710,8		703,381	16,7874	225419		
	639,727	27,1999	140404		702,602	15,8474	230866		
	638,287	26,1858	102584		703,226	16,5721	304047		
	643,145	16,7459	27177,2		703,767	16,3573	269663		
	638,699	25,5687	102467		703,591	16,8859	288178		

Appendix III - Supplementary Table 4. Raman spectroscopy polymorph identification in randomly chosen TiO<sub>2</sub> crystals from fossils (3D Arumberia mats) and sedimentary matrix

Date of analysis	Series	Point	Static center	Pot	Mineral/Structure	Identified polymorph
2018_08	Af236-2-Region1	1	750	5%	TiO <sub>2</sub> Fossil	Anatase
2018_08	Af236-2-Region1	2	750	5%	TiO <sub>2</sub> Fossil	Anatase
2018_08	Af236-2-Region1	3	750	5%	TiO <sub>2</sub> Fossil	Anatase
2018_08	Af236-2-Region1	4	750	5%	TiO <sub>2</sub> Fossil	Anatase
2018_08	Af236-2-Region1	5	750	5%	TiO <sub>2</sub> Fossil	Anatase
2018_08	Af236-2-Region1	6	750	5%	TiO <sub>2</sub> Fossil	Anatase
2018_08	Af236-2-Region1	7	750	5%	TiO <sub>2</sub> Fossil	Anatase
2018_08	Af236-2-Region1	8	750	5%	TiO <sub>2</sub> Fossil	Anatase
2018_08	Af236-2-Region1	9	750	5%	TiO <sub>2</sub> Fossil	Anatase
2018_08	Af236-2-Region1	10	750	5%	TiO <sub>2</sub> Fossil	Anatase
2018_08	Af236-2-Region1	11	750	5%	TiO <sub>2</sub> Fossil	Anatase
2018_08	Af236-2-Region1	12	750	5%	TiO <sub>2</sub> Fossil	Anatase
2018_08	Af236-2-Region1	13	750	5%	TiO <sub>2</sub> Fossil	Anatase
2018_08	Af236-2-Region1	14	750	5%	TiO <sub>2</sub> Fossil	Anatase
2018_08	Af236-2-Region1	15	750	5%	TiO <sub>2</sub> Fossil	Anatase
2018_08	Af236-2-Region1	16	750	5%	TiO <sub>2</sub> Fossil	Anatase
2018_08	Af236-2-Region1	17	750	5%	TiO <sub>2</sub> Fossil	Anatase
2018_08	Af236-2-Region1	18	750	5%	TiO <sub>2</sub> Fossil	Anatase
2018_08	Af236-2-Region1	19	750	5%	TiO <sub>2</sub> Fossil	Anatase
2018_08	Af236-2-Region1	20	750	5%	TiO <sub>2</sub> Fossil	Anatase
2018_08	Af236-2-Region1	1	750	5%	TiO <sub>2</sub> Matrix	Anatase
2018_08	Af236-2-Region1	2	750	5%	TiO <sub>2</sub> Matrix	Anatase
2018_08	Af236-2-Region1	3	750	5%	TiO <sub>2</sub> Matrix	Anatase
2018_08	Af236-2-Region1	4	750	5%	TiO <sub>2</sub> Matrix	Anatase
2018_08	Af236-2-Region1	5	750	5%	TiO <sub>2</sub> Matrix	Anatase
2018_08	Af236-2-Region1	6	750	5%	TiO <sub>2</sub> Matrix	Anatase
2018_08	Af236-2-Region1	7	750	5%	TiO <sub>2</sub> Matrix	Anatase
2018_08	Af236-2-Region1	8	750	5%	TiO <sub>2</sub> Matrix	Anatase
2018_08	Af236-2-Region1	9	750	5%	TiO <sub>2</sub> Matrix	Anatase
2018_08	Af236-2-Region1	10	750	5%	TiO <sub>2</sub> Matrix	Anatase
2018_08	Af236-2-Region1	11	750	5%	TiO <sub>2</sub> Matrix	Anatase
2018_08	Af236-2-Region1	12	750	5%	TiO <sub>2</sub> Matrix	Anatase
2018_08	Af236-2-Region1	13	750	5%	TiO <sub>2</sub> Matrix	Anatase
2018_08	Af236-2-Region1	14	750	5%	TiO <sub>2</sub> Matrix	Anatase
2018_08	Af236-2-Region1	15	750	5%	TiO <sub>2</sub> Matrix	Anatase
2018_08	Af236-2-Region1	16	750	5%	TiO <sub>2</sub> Matrix	Anatase
2018_08	Af236-2-Region1	17	750	5%	TiO <sub>2</sub> Matrix	Anatase
2018_08	Af236-2-Region1	18	750	5%	TiO <sub>2</sub> Matrix	Anatase
2018_08	Af236-2-Region1	19	750	5%	TiO <sub>2</sub> Matrix	Anatase
2018_08	Af236-2-Region1	20	750	5%	TiO <sub>2</sub> Matrix	Anatase
2018_08	Af236-2-Region2	1	750	5%	TiO <sub>2</sub> Fossil	Anatase
2018_08	Af236-2-Region2	2	750	5%	TiO <sub>2</sub> Fossil	Anatase
2018_08	Af236-2-Region2	3	750	5%	TiO <sub>2</sub> Fossil	Anatase
2018_08	Af236-2-Region2	4	750	5%	TiO <sub>2</sub> Fossil	Anatase
2018_08	Af236-2-Region2	5	750	5%	TiO <sub>2</sub> Fossil	Anatase
2018_08	Af236-2-Region2	6	750	5%	TiO <sub>2</sub> Fossil	Anatase
2018_08	Af236-2-Region2	7	750	5%	TiO <sub>2</sub> Fossil	Anatase
2018_08	Af236-2-Region2	8	750	5%	TiO <sub>2</sub> Fossil	Anatase
2018_08	Af236-2-Region2	9	750	5%	TiO <sub>2</sub> Fossil	Rutile
2018_08	Af236-2-Region2	10	750	5%	TiO <sub>2</sub> Fossil	Anatase
2018_08	Af236-2-Region2	11	750	5%	TiO <sub>2</sub> Fossil	Anatase
2018_08	Af236-2-Region2	12	750	5%	TiO <sub>2</sub> Fossil	Anatase
2018_08	Af236-2-Region2	13	750	5%	TiO <sub>2</sub> Fossil	Anatase
2018_08	Af236-2-Region2	14	750	5%	TiO <sub>2</sub> Fossil	Anatase
2018_08	Af236-2-Region2	15	750	5%	TiO <sub>2</sub> Fossil	Anatase
2018_08	Af236-2-Region2	16	750	5%	TiO <sub>2</sub> Fossil	Anatase
2018_08	Af236-2-Region2	17	750	5%	TiO <sub>2</sub> Fossil	Anatase
2018_08	Af236-2-Region2	18	750	5%	TiO <sub>2</sub> Fossil	Anatase
2018_08	Af236-2-Region2	19	750	5%	TiO <sub>2</sub> Fossil	Anatase

Appendix III - Supplementary Table 4. Cont.

2018_08	Af236-2-Region2	20	750	5%	TiO <sub>2</sub> Fossil	Anatase
2018_08	Af236-2-Region2	21	750	5%	TiO <sub>2</sub> Fossil	Anatase
2018_08	Af236-2-Region2	22	750	5%	TiO <sub>2</sub> Fossil	Anatase
2018_08	Af236-2-Region2	23	750	5%	TiO <sub>2</sub> Fossil	Anatase
2018_08	Af236-2-Region2	24	750	5%	TiO <sub>2</sub> Fossil	Rutile
2018_08	Af236-2-Region2	25	750	5%	TiO <sub>2</sub> Fossil	Anatase
2018_08	Af236-2-Region2	26	750	5%	TiO <sub>2</sub> Fossil	Anatase
2018_08	Af236-2-Region2	27	750	5%	TiO <sub>2</sub> Fossil	Rutile
2018_08	Af236-2-Region2	28	750	5%	TiO <sub>2</sub> Fossil	Anatase
2018_08	Af236-2-Region2	29	750	5%	TiO <sub>2</sub> Fossil	Anatase
2018_08	Af236-2-Region2	30	750	5%	TiO <sub>2</sub> Fossil	Rutile
2018_08	Af236-2-Region2	1	750	5%	TiO <sub>2</sub> Matrix	Anatase
2018_08	Af236-2-Region2	2	750	5%	TiO <sub>2</sub> Matrix	Rutile
2018_08	Af236-2-Region2	3	750	5%	TiO <sub>2</sub> Matrix	Anatase
2018_08	Af236-2-Region2	4	750	5%	TiO <sub>2</sub> Matrix	Anatase
2018_08	Af236-2-Region2	5	750	5%	TiO <sub>2</sub> Matrix	Anatase
2018_08	Af236-2-Region2	6	750	5%	TiO <sub>2</sub> Matrix	Anatase
2018_08	Af236-2-Region2	7	750	5%	TiO <sub>2</sub> Matrix	Anatase
2018_08	Af236-2-Region2	8	750	5%	TiO <sub>2</sub> Matrix	Rutile
2018_08	Af236-2-Region2	9	750	5%	TiO <sub>2</sub> Matrix	Rutile
2018_08	Af236-2-Region2	10	750	5%	TiO <sub>2</sub> Matrix	Anatase
2018_08	Af236-2-Region2	11	750	5%	TiO <sub>2</sub> Matrix	Rutile
2018_08	Af236-2-Region2	12	750	5%	TiO <sub>2</sub> Matrix	Rutile
2018_08	Af236-2-Region2	14	750	5%	TiO <sub>2</sub> Matrix	Anatase
2018_08	Af236-2-Region2	15	750	5%	TiO <sub>2</sub> Matrix	Anatase
2018_08	Af236-2-Region2	16	750	5%	TiO <sub>2</sub> Matrix	Anatase
2018_08	Af236-2-Region2	17	750	5%	TiO <sub>2</sub> Matrix	Rutile
2018_08	Af236-2-Region2	18	750	5%	TiO <sub>2</sub> Matrix	Rutile
2018_08	Af236-2-Region2	19	750	5%	TiO <sub>2</sub> Matrix	Rutile
2018_08	Af236-2-Region2	20	750	5%	TiO <sub>2</sub> Matrix	Anatase
2018_08	Af236-2-Region2	21	750	5%	TiO <sub>2</sub> Matrix	Anatase
2018_08	Af236-2-Region2	22	750	5%	TiO <sub>2</sub> Matrix	Rutile
2018_08	Af236-2-Region2	23	750	5%	TiO <sub>2</sub> Matrix	Rutile
2018_08	Af236-2-Region2	24	750	5%	TiO <sub>2</sub> Matrix	Rutile
2018_08	Af236-2-Region2	25	750	5%	TiO <sub>2</sub> Matrix	Rutile
2018_08	Af236-2-Region2	26	750	5%	TiO <sub>2</sub> Matrix	Rutile
2018_08	Af236-2-Region2	27	750	5%	TiO <sub>2</sub> Matrix	Rutile
2018_08	Af236-2-Region2	28	750	5%	TiO <sub>2</sub> Matrix	Rutile
2018_08	Af236-2-Region2	29	750	5%	TiO <sub>2</sub> Matrix	Rutile
2018_08	Af236-2-Region2	30	750	5%	TiO <sub>2</sub> Matrix	Anatase
2018_08	Af236-2-Region3	1	750	5%	TiO <sub>2</sub> Fossil	Anatase
2018_08	Af236-2-Region3	2	750	5%	TiO <sub>2</sub> Fossil	Anatase
2018_08	Af236-2-Region3	3	750	5%	TiO <sub>2</sub> Fossil	Anatase
2018_08	Af236-2-Region3	4	750	5%	TiO <sub>2</sub> Fossil	Anatase
2018_08	Af236-2-Region3	5	750	5%	TiO <sub>2</sub> Fossil	Anatase and rutile
2018_08	Af236-2-Region3	6	750	5%	TiO <sub>2</sub> Fossil	Anatase
2018_08	Af236-2-Region3	7	750	5%	TiO <sub>2</sub> Fossil	Anatase
2018_08	Af236-2-Region3	8	750	5%	TiO <sub>2</sub> Fossil	Anatase
2018_08	Af236-2-Region3	9	750	5%	TiO <sub>2</sub> Fossil	Rutile
2018_08	Af236-2-Region3	10	750	5%	TiO <sub>2</sub> Fossil	Anatase
2018_08	Af236-2-Region3	11	750	5%	TiO <sub>2</sub> Fossil	Anatase
2018_08	Af236-2-Region3	12	750	5%	TiO <sub>2</sub> Fossil	Anatase
2018_08	Af236-2-Region3	13	750	5%	TiO <sub>2</sub> Fossil	Anatase
2018_08	Af236-2-Region3	14	750	5%	TiO <sub>2</sub> Fossil	Anatase and rutile
2018_08	Af236-2-Region3	15	750	5%	TiO <sub>2</sub> Fossil	Anatase
2018_08	Af236-2-Region3	16	750	5%	TiO <sub>2</sub> Fossil	Anatase and rutile
2018_08	Af236-2-Region3	1	750	5%	TiO <sub>2</sub> Matrix	Rutile
2018_08	Af236-2-Region3	2	750	5%	TiO <sub>2</sub> Matrix	Anatase
2018_08	Af236-2-Region3	3	750	5%	TiO <sub>2</sub> Matrix	Anatase
2018_08	Af236-2-Region3	4	750	5%	TiO <sub>2</sub> Matrix	Rutile

Appendix III - Supplementary Table 4. *Cont.*

2018_08	Af236-2-Region3	5	750	5%	TiO <sub>2</sub> Matrix	Anatase
2018_08	Af236-2-Region3	6	750	5%	TiO <sub>2</sub> Matrix	Anatase
2018_08	Af236-2-Region3	7	750	5%	TiO <sub>2</sub> Matrix	Anatase
2018_08	Af236-2-Region3	8	750	5%	TiO <sub>2</sub> Matrix	Anatase
2018_08	Af236-2-Region3	9	750	5%	TiO <sub>2</sub> Matrix	Anatase
2018_08	Af236-2-Region3	10	750	5%	TiO <sub>2</sub> Matrix	Anatase
2018_08	Af236-2-Region3	11	750	5%	TiO <sub>2</sub> Matrix	Anatase
2018_08	Af236-2-Region3	12	750	5%	TiO <sub>2</sub> Matrix	Anatase
2018_08	Af236-2-Region3	13	750	5%	TiO <sub>2</sub> Matrix	Rutile
2018_08	Af236-2-Region3	14	750	5%	TiO <sub>2</sub> Matrix	Rutile
2018_08	Af236-2-Region3	15	750	5%	TiO <sub>2</sub> Matrix	Rutile
2018_08	Af236-2-Region3	16	750	5%	TiO <sub>2</sub> Matrix	Rutile

Randomly chosen grains of TiO <sub>2</sub>			
	Anatase	Rutile	Both
Fossil	58	5	3
Matrix/Cement	43	22	0
			Total
			66
			65

TiO <sub>2</sub> disseminated in clays (based on data presented in the Supplementary Table 3)				
	Matrix		Fossils	
	Anatase	Total points	Anatase	Total points
2017_06B	Region 1	6	18	21
2018_08	Region 2	5	6	5
2018_08	Region 1	9	20	16
2018_08	Region 2	8	30	21
2018_08	SDSL	9	19	17
	Total	37	93	80
				81